IOWA STATE UNIVERSITY
Digital Repository

2015

Permeability and lateral earth pressure in granular backfill against bridge abutments

Lance David Keltner
Iowa State University

Follow this and additional works at: https://lib.dr.iastate.edu/etd

Part of the Civil Engineering Commons, and the Geotechnical Engineering Commons

www.manaraa.com

Permeability and lateral earth pressure in granular backfill against bridge abutments

by

Lance David Keltner

A thesis submitted to the graduate faculty

In partial fulfillment of the requirements for the degree of

MASTER OF SCIENCE

Major: Civil Engineering (Geotechnical Engineering)

Program of Study Committee:
David J. White, Co-Major Professor
Pavana Vennapusa, Co-Major Professor
Terry Wipf

Iowa State University

Ames, Iowa

2015

For my parents, Larry and Patty Keltner

TABLE OF CONTENTS

LIST OF TABLES

LIST OF FIGURES

LIST OF SYMBOLS

Symbol	Description	Unit
a	Fredlund and Xing Soil Suction Coefficient	kPa
c_c	Coefficient of curvature	—
c_u	Coefficient of uniformity	—
D_{10}	Diameter corresponding to 10% finer	mm
D_{30}	Diameter corresponding to 30% finer	mm
D_{60}	Diameter corresponding to 60% finer	mm
G_s	Specific gravity	—
I_c	Vertical collapse	%
k	Hydraulic conductivity	cm/s
m	Fredlund and Xing soil suction coefficient	—
m_v	Coefficient of volumetric compressibility	1/kPa
n	Fredlund and Xing soil suction coefficient	—

ABSTRACT

In bridge abutment design, Wisconsin DOT assumes the granular backfill material used behind bridge abutments as free-draining and no hydrostatic pressures are applied on the wall. This research study was undertaken to investigate if backfill materials meet the assumption of a freely-drained condition through a detailed laboratory and field study. Also, the viability of using recycled asphalt pavement (RAP) and shingles (RAS) for granular backfill was investigated.

Laboratory testing involved characterizing the materials in terms of gradation/classification, erodibility, permeability, shear strength, volume change (i.e., water induced collapse). Laboratory tests revealed bulking moisture content for natural materials and collapse upon wetting. RAP and RAS materials exhibited collapse upon wetting and creep under constant loading. Scaled abutment model testing was performed to assess pore pressure dissipation rates for the different materials and calibrate input parameters to predict drainage using finite element analysis (FEA). Abutment model testing indicated that addition of geocomposite vertical drain can substantially increase pore pressure dissipation rates and avoid material erosion.

Field testing involved in situ permeability, shear strength and moisture content testing, and monitoring lateral earth pressures and pore pressures behind abutment walls at four bridge sites. Results indicated that field conditions are more complex than the simple linear stress distributions typically assumed in the design for lateral earth pressures. Lateral earth pressures were greater than assumed in design over a majority of the monitoring period of this study. Pore pressures behind abutment wall were observed at one site following flooding. Predicted pore pressure dissipations using numerical analysis matched well with the measured values.

CHAPTER 1. INTRODUCTION

This chapter discusses the industry and technical problems addressed in this project. The research goal, specific objectives, and the significance of this research are presented in the following discussion.

Industry Problem

The Wisconsin DOT Bridge Design Manual (WisDOT 2014) states, *"Semi-retaining and full-retaining abutments generally will be overstressed or may slide if subject to large hydrostatic or frost pressures unless accounted for in the design"*. Current bridge abutment design addresses this problem by specifying granular backfill that is presumably "free-draining". If this assumption does not hold true, the abutment wall can be subjected to unwanted hydrostatic pressures. This increase in pressure can cause abutments to move, a problem that is compounded by temperature-related movements, resulting in gaps developing behind the abutment followed by settlement of the backfill.

The drainage capacity of the backfill material is primarily based on the hydraulic conductivity of the backfill material and the overall effectiveness of the drainage design, i.e., the underdrain systems. However, the current "free-draining" assumption in WisDOT design does not properly consider:

- properties of the granular backfill material in terms of its water infiltration capacity, permeability, and water retention characteristics,
- effects of undrained water on the lateral earth pressures exerted on the abutments, and
- short- and long-term effectiveness of the drainage system.

Technical Problem

Inadequate water management around bridges is a common problem reported in studies conducted recently in Iowa, Wisconsin, Colorado, and Texas (Abu-Hejleh et al. 2006; Helwany et al. 2007; Puppala et al. 2009; White et al. 2005) Although research into the effects of undrained water on erosion and settlement of granular backfill have been documented (Helwany et al. 2007; Phares et al. 2011; White et al. 2005), there is limited research on understanding how long does water take to drain behind the abutment wall for a given material, and how does undrained water affect stresses applied on abutment walls.

Goals of the Research

There are two main goals of this research. The first goal of this research is to develop a better understanding of the current state of the practice in bridge abutment backfill design, construction, and quality control/quality assurance (QC/QA) testing during construction. The second goal of this research is to identify parameters that can help designer's select appropriate granular backfill materials that can provide adequate drainage and improve long-term performance of the abutment systems.

Research Objectives

The following research objectives were established to achieve the goals of this research:

- Conduct a comprehensive review of current state of practice of abutment materials and construction practice, and drainage design
- Review previous studies documenting problems of backfill and underdrain systems on bridge performance
- Conduct field investigation to measure in situ lateral earth and pore water pressure at four locations with various backfill materials
- Conduct laboratory study to classify backfill materials and asses drainage, shear strength, and collapse characteristics.
- Asses the viability of recycled materials as backfill material
- Conduct a laboratory scaled bridge abutment model study to assess drainage capacity of backfill and performance of underdrain systems
- Conduct a numerical analysis for transient flow behind abutment walls and compare with measured values.

Significance of the Research

State departments of transportation, taxpayers, and researchers will benefit from this research because it will indicate ways to prevent damage and increase the service life of bridge abutment systems. Designers will also have a better understanding of drainage characteristics of granular backfill and be able to design better subsurface drainage systems to remove excess water behind bridge abutments and avoid unwanted lateral earth pressures from developing. In addition, this research will provide information on the viability of using recycled materials that agencies have limited experience with in using as backfill material.

Organization of the Document

    This report is organized into 6 chapters. Following this introduction chapter, Chapter 2 provides a review of previous studies that documented the performance of abutment backfill and drainage systems, methods to improve performance of abutment systems, potential for using recycled materials as backfill, an overview of the backfill material specifications and drainage design followed by various government agencies in the U.S and Canada, a review of drainage analysis and testing methods for backfill materials, and an overview of theories used for estimating lateral stresses behind the abutment wall. Chapter 3 describes the laboratory, field, and numerical analysis methods used in this study. Chapter 4 summarizes the laboratory test results from this study characterizing the index properties, shear strength properties, collapse characteristics, permeability properties of the materials collected from four field bridge sites and two alternative materials (recycled asphalt pavement (RAP) and recycled asphalt shingles (RAS)), and results of scaled abutment modeling testing and numerical analysis. Chapter 5 presents the results and analysis from field testing and instrumentation at the four bridge sites describing lateral earth pressures and pore water pressures behind abutment walls. Chapter 6 summarizes the key findings derived from this study, and provides recommendations to the current abutment backfill design and construction practices followed by Wisconsin DOT. Supporting material are included as appendices that follow the list of references.

CHAPTER 2. LITERATURE REVIEW

To ensure long-term performance of abutment systems, the backfill material must have good drainage characteristics with less susceptibility to erosion and post-construction volume changes, and the abutments must have good drainage features that are properly designed and constructed. This chapter provides background information related to these aspects and is organized into four sections. The first section provides a review of previous studies that documented the performance of abutment backfill and drainage systems, methods to improve performance of abutment systems, and potential for using recycled materials as backfill. The second section provides an overview of the abutment backfill material specifications and drainage design followed by various government agencies in the U.S and Canada. The third section provides a review of drainage analysis and testing methods for backfill materials. The fourth section provides an overview of classical and modified theories used for estimating lateral stresses behind the abutment wall.

Performance of Abutment Backfill and Drainage Systems

Previous Field Studies

Various studies in the states of Wisconsin, Iowa, Colorado, Texas, and Virginia have documented that poor drainage of backfill and water management around bridges (i.e., ineffectiveness of redirecting surface runoff and infiltrated water into abutments) are primary contributors to poor performance of bridge abutments (Abu-Hejleh et al. 2006; Ardani 1987; Briaud et al. 1997; Helwany et al. 2007; Jayawickrama et al. 2005; Wahls 1990; White et al. 2005; White et al. 2007a; White et al. 2007b). Puppala et al. (2009) provided a review of some of these studies.

White et al. (2007a) reported results of inspection on 74 bridges in Iowa and indicated that about 60% showed poor water management with clogged subdrains and end drains, and unsealed expansion joints (Figure 1). The authors inspected the subdrain outlets of six bridge sites which showed that the subdrains were either dry (despite wet field conditions), collapsed, or plugged with soil. They also reported that surface drainage features suffered from similar problems while bridge end drains were often blocked by debris or showed erosion outside of the tile.

Water that is not properly drained, seeps down between the abutment and the bridge approach through joints, cracks, or flows around the bridge resulting in erosion of the backfill

(Figure 2). Erosion can lead to voids developing underneath the bridge due to backfill moving to fill in eroded slopes, or slope failures due to the soil being removed away from abutment walls (Helwany et al. 2007; Jayawickrama et al. 2005). Based on field observations in Texas, Jayawickrama et al. (2005) noted that poor compaction of abutment backfill material, poor construction of joint sealants, and poor surface and subsurface drainage systems were the primary causes of erosion in backfill materials.

A schematic diagram summarizing frequent problems observed at several bridge sites is provided in Figure 3. White et al. (2007a) indicated that erosion on bridge sites was observed in many forms including erosion under the approach pavement, erosion of the embankment under the bridge, and at the abutment sides. Lateral movements of the abutment wall because of temperature fluctuations can aggregate the problem with erosion leading to larger size voids (Horvath 2005). One of the main causes of erosion is the use of erodible backfill materials, which is a function of soil gradation and classification, and is discussed further in the following section of this chapter. Asphalt overlays and underseal pressure grouting are generally not long-term solutions to prevent erosion or further settlement (White et al. 2007a). This finding from White et al. (2007a) was based on field observations at several sites where the repairs bridges were severely deteriorated within 3 years of placement, indicating the progressive nature of the problem.

In addition to the drainage problems, poor approach pavement and abutment notch construction, not using the specified backfill materials, and placing granular backfill in too thick of lifts and within the bulking moisture content range, are also contributors to poor performance of the backfill. Field test results reported by Whit et al. (2005) indicated that majority of the backfill material was placed within the bulking moisture range, which lead to post-saturation collapse of the backfill materials. Collapse potential was verified through laboratory testing, which indicated that some materials can undergo up to 18% collapse if placed within the bulking moisture range and saturated after construction. White et al. (2007a) indicated that porous backfill material (that is open-graded and have larger aggregate particles) are less susceptible to collapse and more resistant to erosion.

Figure 1. Examples of clogged end drains at I-80 bridge over McPearson Avenue (left) and the bridge on US 218 over South Skunk River (right) (White et al. 2005)

Figure 2. Examples of (left) severe damage of concrete slope protection due to erosion on I-380 bridge over Hwy 6 in Iowa (White et al. 2005), and (right) slope instability on West Beloit Road Bridge over Root River in Wisconsin (Helwany et al. 2007)
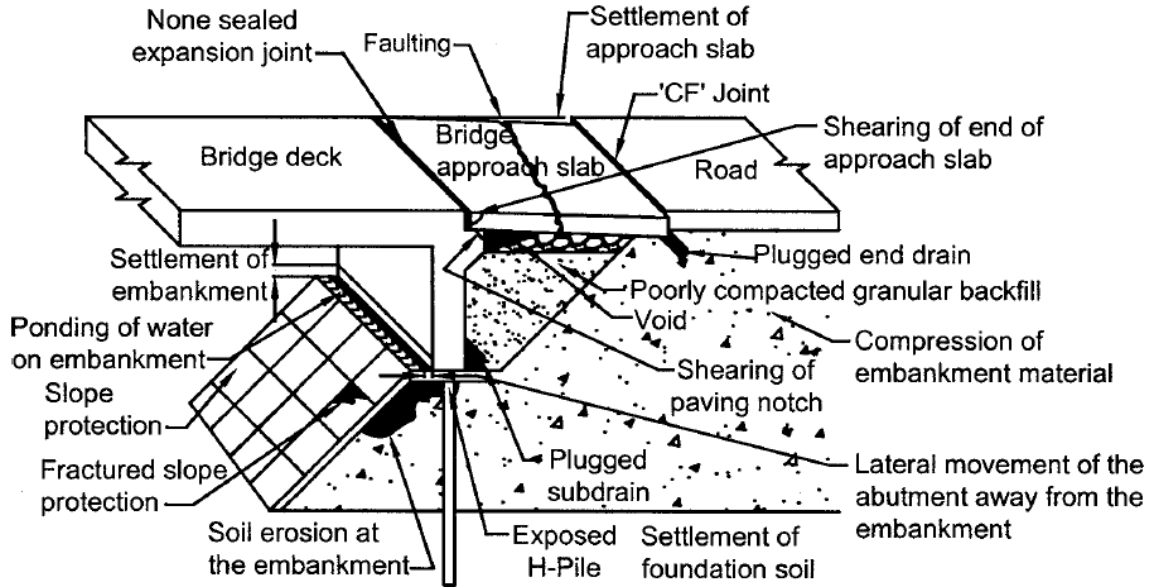
Figure 3. Shematic diagram summarizing frequent problems observed at several bridge sites (White et al. 2007a)

Methods to Improve Drainage and Performance

White et al. (2007b) reported laboratory test results using a one-fourth scale bridge abutment model (details of the model are provided in the Methods chapter of this report). The tests were used to evaluate the performance of horizontal layers of geotextile reinforcement and vertical geocomposite drainage systems. Figure 4 summarizes the various drainage design configurations tested in that study to improve drainage and performance of backfill.

Tests with Iowa DOT design setup (Figure 4a) indicated that the water migrates laterally before reaching the subdrain. The water took 10 minutes to reach a steady state flow rate of 32 cm^3/s. Collapse-induced voids and settlement of the approach slab was observed during the test. Tests with addition of Stripdrain 75 as a geocomposite vertical drain (Figure 4c) increased the steady state flow rate to 383 cm^3/s. Use of tire chips as backfill increased the steady state flow rate to 552 cm^3/s. The addition of these systems reduced lateral migration of water into the backfill and reduced the time for the water to reach the drain from 10 minutes to 1 minute. The use of open-graded gravel and pea gravel as backfill (Figure 7f) also increased the steady-state drainage to 366 cm^3/s for limestone and 92 cm^3/s for pea gravel.
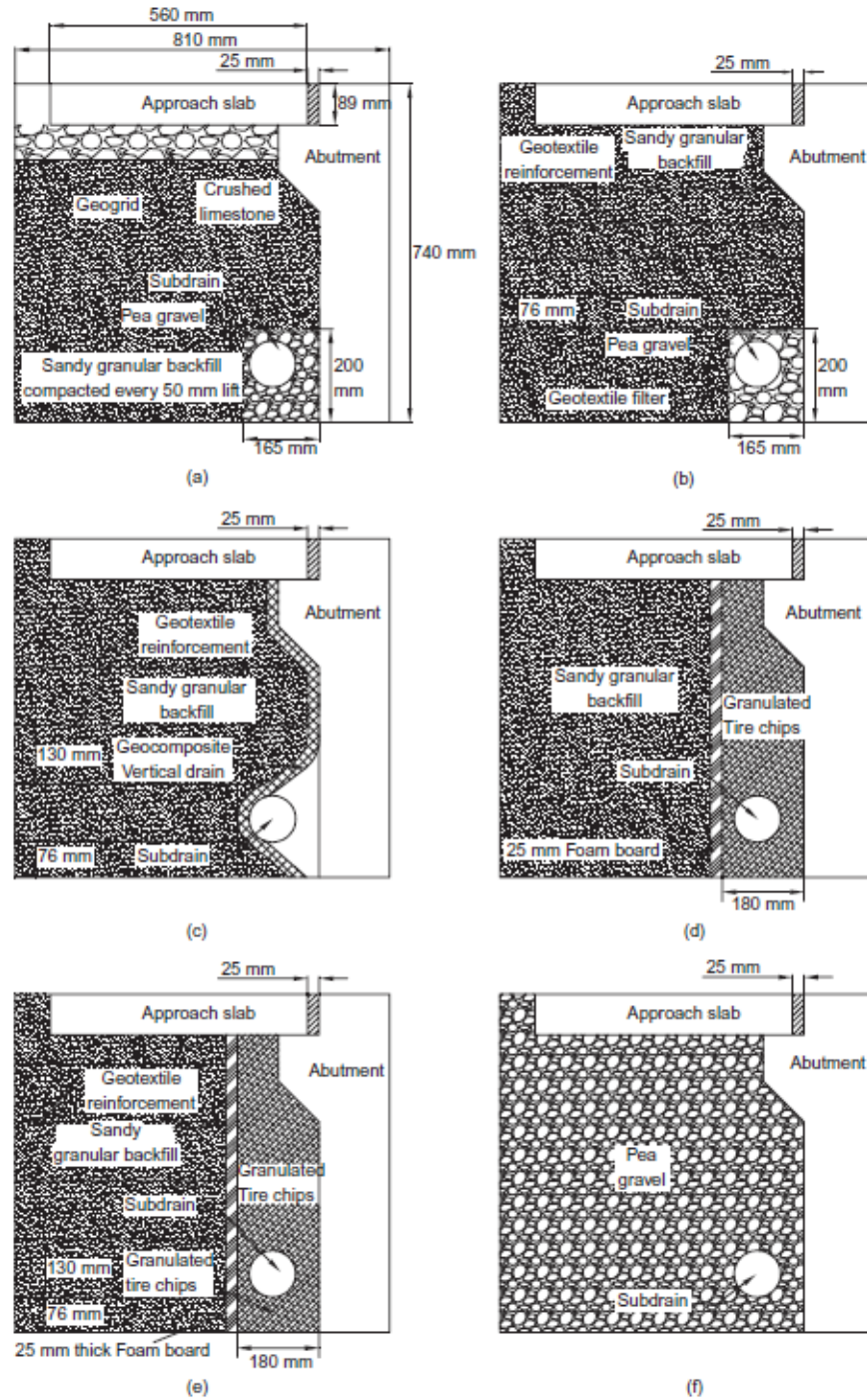
Figure 4. Schematic of various drainage model tests representing; (a) Iowa DOT design; (b) mechanically stabilized backfill; (c) geocomposite vertical drain attached to abutment face; (d) tire chips behind abutment; (e) tire chips with soil reinforcement; (f) porous backfill behind abutment (from White et al. 2007b)

White et al. (2007b) recommended the following based on this testing and field observations:

- Place and compact the granular backfill material at non-bulking moisture contents, preferably at wet of optimum moisture conditions by flooding.
- Use geotextile around porous backfill to prevent infiltration of fine granular particles into the subdrain and ensure more efficient drainage for longer durations.
- Use geocomposite vertical drain along the abutment wall-backfill interface to significantly improve overall drainage.
- Use open-graded gravel in place of for sandy granular backfills to avoid erosion and post-construction volume changes (collapse), while improving subsurface drainage.

Recycled Materials as Abutment Backfill

There is increased interest among highway agencies in exploring uses for recycled materials in construction. Approximately 73 million tons of recycled asphalt pavement (RAP) and 12 million tons of recycled asphalt shingles (RAS) are produced in the U.S. each year (Rathje et al. 2006; Soleimanbeigi et al. 2011). The use of these materials as an alternative to natural materials can potential help reduce transportation and disposal costs for the materials. A summary of properties of RAP and RAS materials from previous studies is provided in Table 1.

A 2006 study evaluated the use of RAP as backfill for mechanically stabilized earth (MSE) walls in Texas (Rathje et al. 2006). They reported that RAP met the gradation requirements for MSE walls per Texas DOT specifications and the falling head tests showed that the material was free-draining (Figure 5). They also reported that the properties of RAP are influenced by the properties of the parent hot mix asphalt material and that the secondary compressibility behavior of RAP, also known as creep, is a major concern. Rathje et al. (2006) recommended not to use RAP material as backfill because of the creep behavior.

Soleimanbeigi et al. (2011) investigated the viability of using RAS as structure fill in highway embankments or backfill material behind retaining structures. They also conducted permeability and triaxial tests on RAS and RAS mixtures with fly ash to investigate ways to minimize creep (Soleimanbeigi et al. 2013). They reported that the hydraulic conductivity of RAS depends on the consolidation pressure applied and addition of 10 to 20% class C fly ash reduced the hydraulic conductivity by about an order of one magnitude (Figure 6). The stabilized RAS material showed lower dry unit weight than natural materials (11.3 kN/m^3 for RAS, 12.5

kN/m^3 for 10% fly ash stabilized RAS, and 13.8 kN/m^3 for 20% fly ash stabilized RAS), which contributes to lower lateral earth pressures.

Table 1. Properties of RAP and RAS materials from previous studies

	Rathje et al. (2006)	Soleimanbeigi et al. (2011)	
Parameters	**RAP**	**RAS**	**RAS with 20% fly ash**
D_{10}, mm	1.2	0.17	
D_{30}, mm	4.2	—*	
D_{50}, mm	—*	1.1	
D_{60}, mm	9.6	—*	
C_c	1.53	7.6	
C_u	8	1.6	
% Fines (< 0.074 mm)	0	3.8	
USCS Classification	Well-Graded Gravel (GW)	Well-Graded Sand (SW)	
Std. Proctor Maximum Dry Unit Weight, kN/m^3	18.4	11.4	13.8
Std. Proctor Optimum Moisture Content, %	3	9	11
ϕ' (drained triaxial test), degree	37	36	37
c' (drained triaxial test), kPa	55.2	20.0	102.0
Creep, %	30% at 206 kPa	17.5% at 200 kPa	3% at 200 kPa

* not indicated

Soleimanbeigi et al. (2013) reported the unstabilized RAS exhibited 17.5% vertical strain under constant applied stress of 200 kPa. This extreme vertical strain was attributed to three mechanisms: 1) compression of cellulose felt voids within RAS; 2) piercing of the sand particles on RAS surfaces into the asphalt coatings; and 3) compression of RAS matrix because of viscous nature of the asphalt cement (Soleimanbeigi et al. 2013). Fly ash was added to the samples which lowered the vertical strain to 3.0%, which was similar to tests performed on glacial outwash sand in their study. Based on these findings, Soleimanbeigi et al. (2011) indicated that stabilized RAS

materials could potentially be a viable material for structural backfill. However, with the reduction in hydraulic conductivity of RAS by adding fly ash by nearly one order of magnitude (see Figure 6), it was unclear whether this can be considered "free-draining".
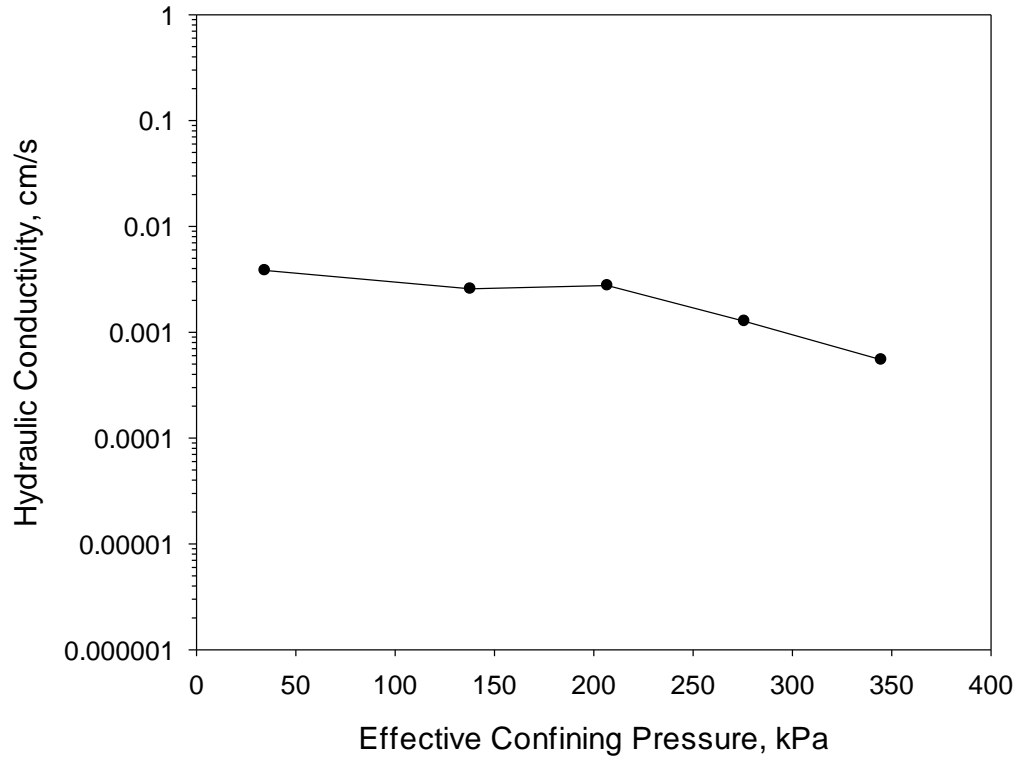
Figure 5. Hydraulic Conductivity of RAP (Reproduced from Rathje et al. 2006)
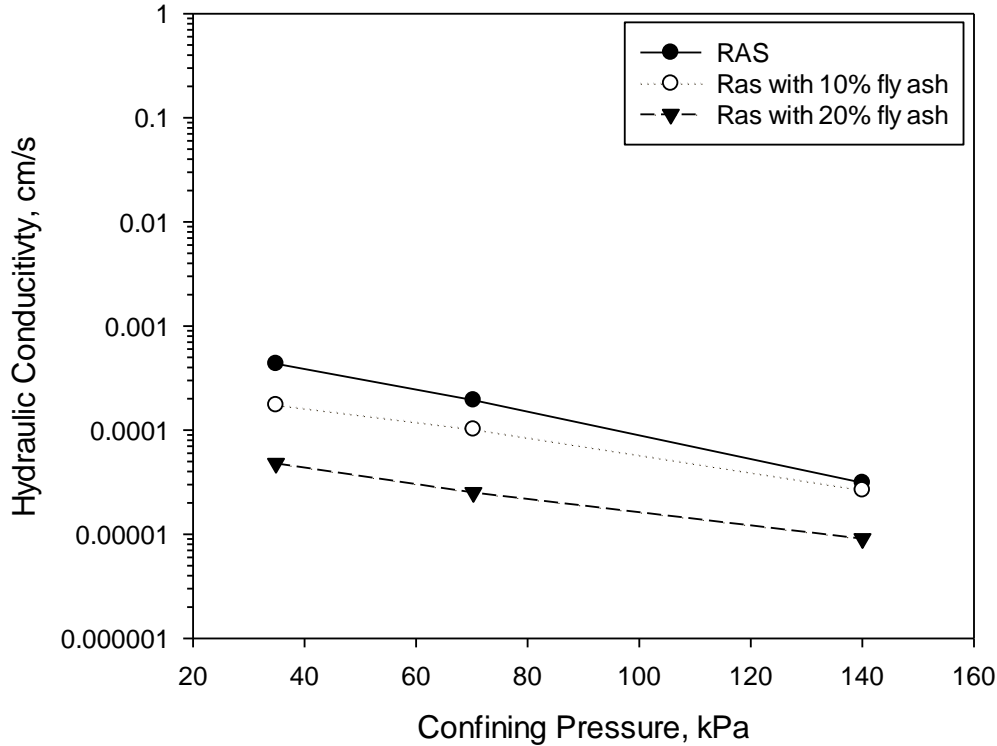
Figure 6. Hydraulic conductivity of RAS and RAS fly ash mixtures (Reproduced from Soleimanbeigi et al. 2011)

Bridge Abutment Backfill and Drainage Design Specifications

This section summarizes a review of specifications for bridge abutment backfill materials from 48 U.S. DOTs and 3 Ministries of Transportation in Canada. Critical parameters in the backfill specifications included material gradation properties, backfill placement and compaction properties (i.e., lift thickness, target compaction percentage, moisture control), quality control/quality assurance (QC/QA) testing requirements, and drainage design (i.e., drain tile location and specifications, and other drainage features).

Gradation limits, compaction assessment, and QC/QA specifications followed by different agencies are summarized in tables in Appendix A. The results from specification review are summarized as bar charts in Figure 7.
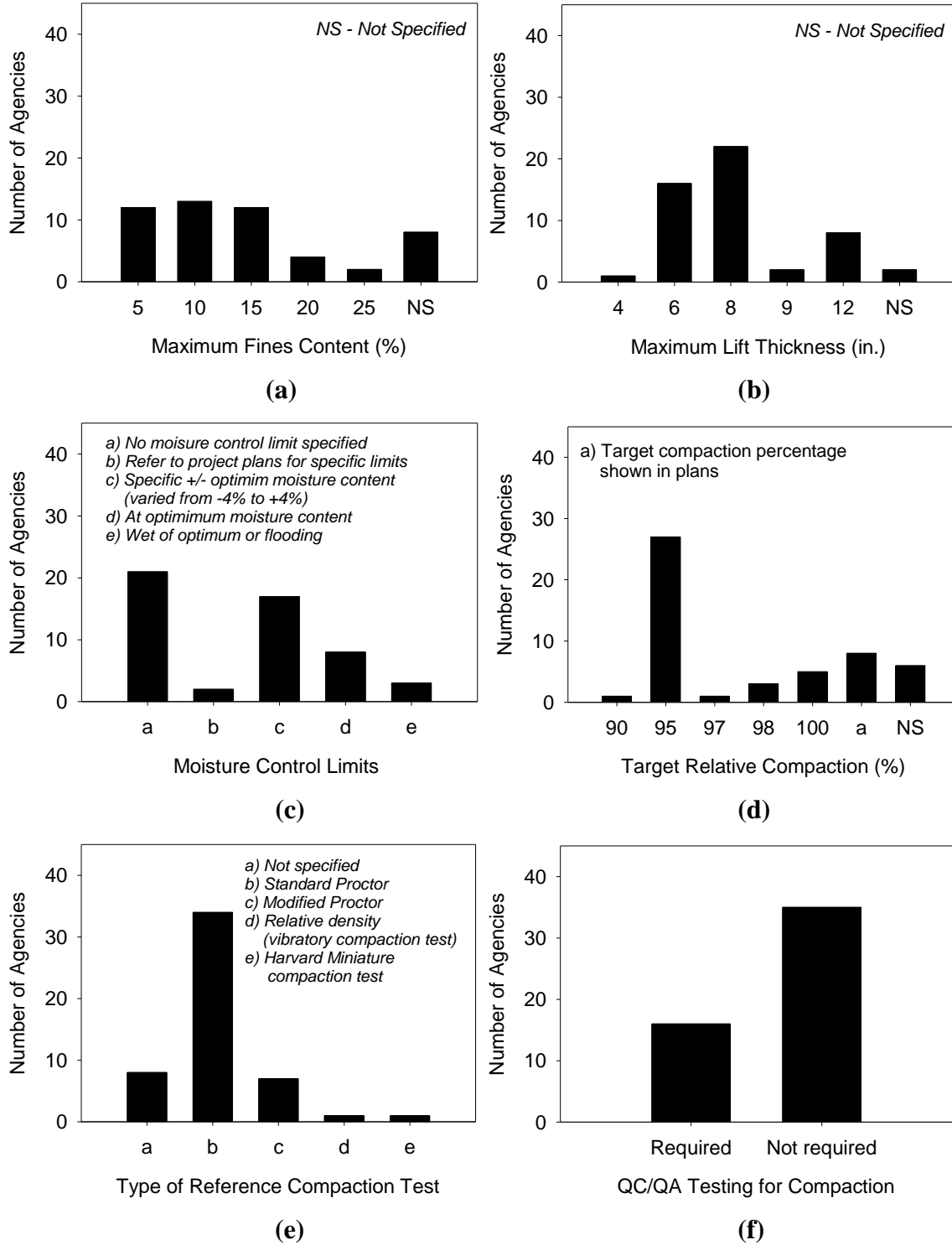
Figure 7. Bar charts of backfill specifications for: (a) maximum fines content, (b) maximum lift thickness, (c) moisture content limits, (d) target relative compaction, (e) type of reference compaction test, and (e) QC/QA testing for compaction

In the following sub sections, key findings from the specifications review and how the different parameters impact the abutment backfill and drainage performance are discussed. Further, how the current WisDOT specifications and methods are compared with the current practices by the different agencies is also discussed.

Gradation Properties of Backfill Materials

Influence of gradation on drainability

The drainability of backfill materials is influenced by the hydraulic conductivity properties of the material, which defines the quantity of water that flows through the material (Barksdale 1996). Of the various parameters that influence the hydraulic conductivity of the material, material gradation is the most critical one (Das 1990).

Cedergren (1994) indicated that the hydraulic conductivity of a material can increase by about 40,000 times if the material is composed of open-graded aggregate of 0.5-1.0 in size compared to sand size material. Many researchers have proposed empirical relationships to estimate hydraulic conductivity using material gradation parameters and are summarized in Table 2. The gradation parameters that have been commonly used to estimate hydraulic conductivity include: particle diameter at 5% and 10% passing (D_5 and D_{10}), void ratio (e), porosity (n), effective porosity (η), and percent fines passing the No. 200 sieve (P_{200}).

Previous studies have indicated that fines content (P_{200}) is one of the critical parameters that can significantly affect the hydraulic conductivity (Cedergren 1994). Based on laboratory and field testing conducted on crushed aggregate materials, Vennapusa (2004) reported that hydraulic conductivity decreases exponentially as fines content increases (Figure 8). Gomez (2013) reported hydraulic conductivity for fines content ranging from $0 - 10\%$ were close to each other, however there was a substantial drop in hydraulic conductivity between $10 - 15\%$ fines.

Table 2. Empirical relationships to determine hydraulic conductivity (from Vennapusa 2004)

No.	K (units)	Equation	Proposed By	Suitability
1	K (cm/sec)	$K = cD_{10}^2$ (c varies from 1 to 1.5)	Hazen (1930)	loose sand and clean filter sands
2	K (mm²)	$K = cD_5^2$ (c varies from 0.05 to 1)	Kenny *et al.* (1984)	Coarse sand
3	K (cm/sec)	$K = 1.2 C_u^{0.735} D_{10}^{0.89} \left(\dfrac{e^3}{1+e} \right)$	Shahabi *et al.* (1984)	Medium to fine sands
4	K (ft/day)	$K = \dfrac{6.214 \times 10^5 D_{10}^{1.478} n^{6.654}}{P_{200}^{0.597}}$	Moulton (1980)	Aggregates
5	K (cm/sec)	$K = \dfrac{D_s^2 \gamma e^3 C}{\mu(1+e)}$	Taylor (1948)	Soils
6	K (cm/sec)	$k = 7.137 + 12.521\eta + 0.411 D_{10}$ $- 0.192 P_{3/8}$ $K = \dfrac{\gamma e^3}{k_o S^2 \mu(1+e)}$	Kozeny-Carman	Soils
7	K (m/sec)	$K = 0.001 (d_{100})^{1.4}$	Cedergren (1974)	Crushed aggregate
8	K (m/sec)	$K = 0.001 (d_{100})^{1.5}$	Cedergren (1974)	Round Aggregate
9	K (cm/sec)	$K = 1.4 e^2 k_{0.85}$	Casagrande	Clean sands
10	K (cm/sec)	$\log K = 3.062 + 6.4 \log \eta + 1.905 \log D_{10}$	Richardson (1997)	For k = 10^{-5} to 10^1 cm/sec
11	K (cm/sec)	$K = -2.873 + 23.923\eta + 1.005 D_{10}$ $- 0.107 P_{3/8} - 0.214 P_{50} + 0.218 P_{16}$	Richardson (1997)	For $k > 0.1$ cm/sec open-graded materials
12	K (cm/sec)	$K = -0.024 + 5.573\eta - 0.024 P_{3/8}$ $+ 0.004 P_8$	Richardson (1997)	For k = 0.1 to 1 cm/sec
13	K (cm/sec)	$K = 7.137 + 12.521\eta + 0.411 D_{10}$ $- 0.192 P_{3/8}$	Richardson (1997)	For $k > 1$ cm/sec

Notes: K = hydraulic conductivity or coefficient of permeability, $k_{0.85}$ = hydraulic conductivity at a void ratio of 0.85, D_{10} = particle diameter at 10% passing (mm), c & C = constants, C_u = coefficient of uniformity, e = void ratio, γ = unit weight of permeant, η = effective porosity, n = porosity, μ = viscosity of Water, S = specific surface area, k_o = factor depending on pore shape and ratio of length of actual flow path to soil bed thickness, D_s = effective particle diameter, P_{200} = % passing #200 sieve, $P_{3/8}$ = % passing 3/8" sieve, P_8 = % passing #8 sieve, P_{16} = % passing #16 sieve, d_{100} = nominal size of aggregate in mm
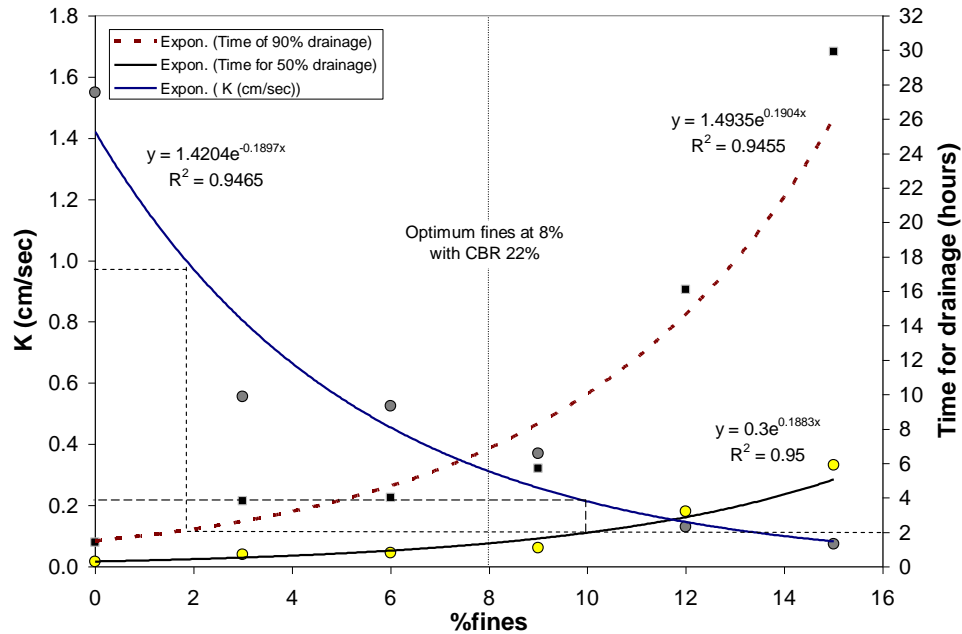
Figure 8. Influence of fines content on hydraulic conductivity of recycled portland cement concrete material (Vennapusa 2004)

The maximum allowable fines content varied between 5% and 25% among the various agencies (see Figure 7a). Currently, WisDOT specifies use of structure backfill (Section 210) or grade 1 granular backfill (Section 209), as backfill material in abutments. Gradation limits for these materials are provided Table 2. According to the gradation limits, the maximum allowable fines content for WisDOT materials can range between 3.75% and 15%.

Table 3. WisDOT specifications for bridge backfill

Sieve size	Structure Backfill (% passing)	Grade 1 Granular Backfill (% passing)
3"	100	—
No. 4	25-100	0-100
No. 40	—	0-75
No. 100	—	0-15
No. 200	0-3.75* 0-15*	0-8

Notes: — not specified, * percent passing is based on material passing No. 4 sieve (i.e., if percent passing No. 4 is 25%, the maximum percent passing No. 200 will be 3.75%; similarly, if percent passing No. 4 is 100%, the maximum percent passing No. 200 will be 15%)

Influence of gradation on erodability

Briaud et al. (1997) provided guidance on typical gradation limits of soils that are susceptible to erosion (Figure 9). According to these limits, materials that have silt to sand size particles are

more susceptible to erosion than other materials. Briaud (2008) proposed a graph that shows erodability of soils in relation to soil classifications, which also indicate that sandy and silty soils are more susceptible to erosion than other material types (Figure 10).
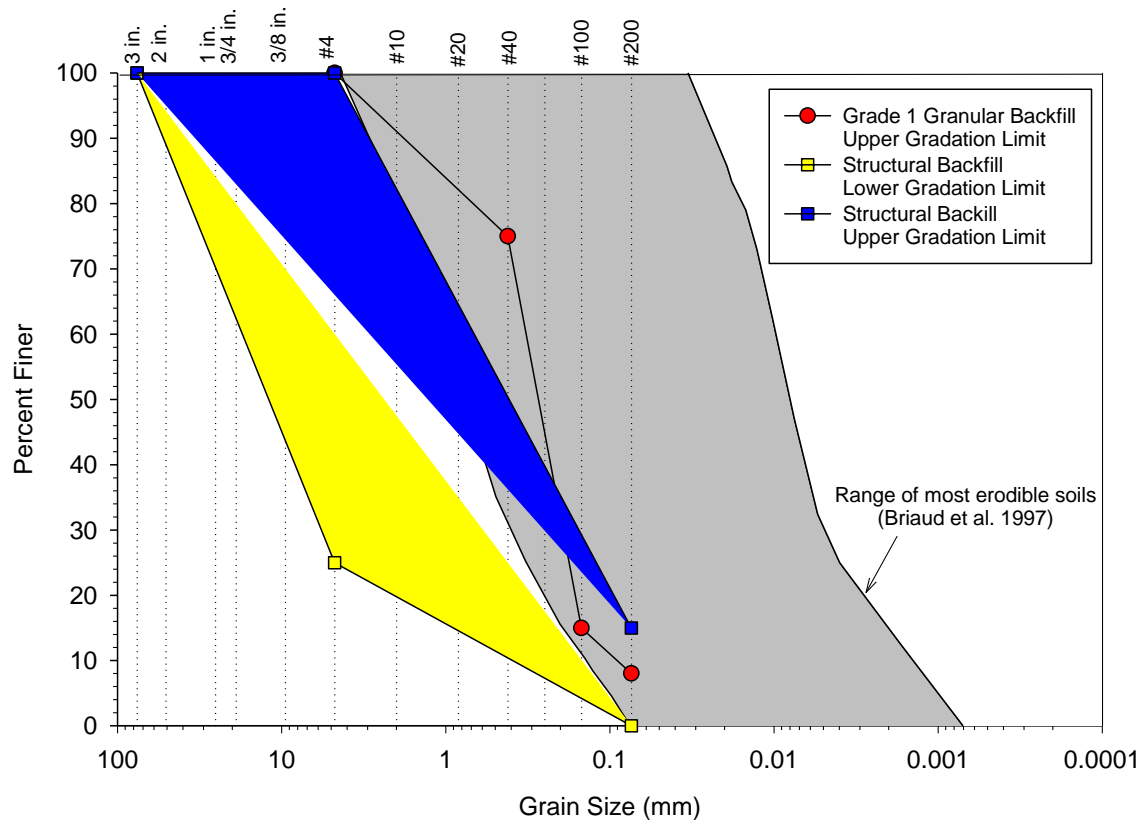
Figure 9. Range of most erodible soils per Briaud et al. (1997) and comparison with WisDOT specification for backfill materials

Also included in Figure 9 are the upper gradation limits for granular backfill and the upper and lower gradation limits for structure backfill, per WisDOT specifications as summarized in Table 3. This comparison indicates that the WisDOT materials that are close to their specified upper limits are susceptible to erosion.

Based on tests conducted on multiple bridge sites in Iowa and Ohio, White et al. (2005) (2005) and Phares et al.(2011) reported that most materials used in backfill were granular materials classified as poorly graded sand (SP), which fall in the gradation range for soils susceptible to erosion.
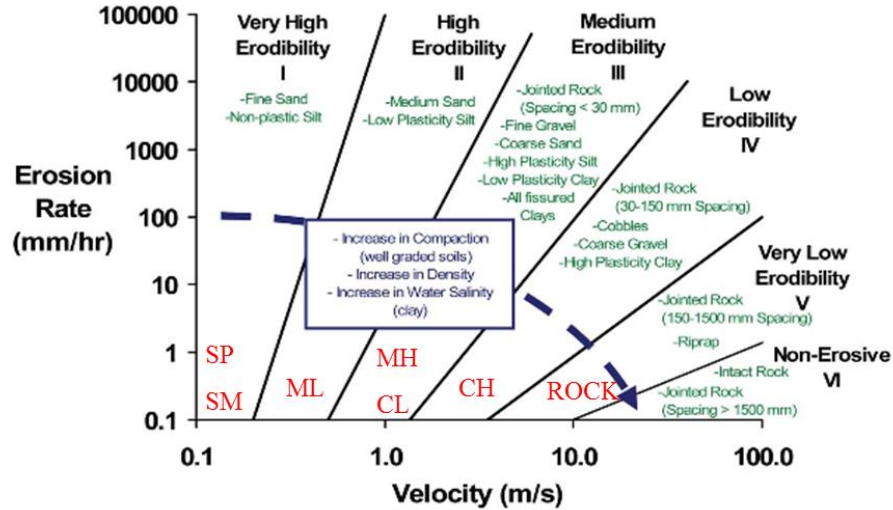
Figure 10. Proposed erosion categories for soils and rocks based on velocity (Briaud 2008)

Backfill Placement and Compaction

Lift thickness

Lift thickness plays a critical role in achieving proper compaction. Maximum lift thickness allowed by agencies varied from 4 in. to 12 in (Figure 7b). The WisDOT Bridge Manual indicates that backfill be placed in 4 in. to 6 in. thick layers (WisDOT 2014), and the WisDOT Standard Specifications indicate a maximum allowable lift thickness of 8 in. during compaction (WisDOT 2015).

Although most agencies specify the maximum allowable lift thickness, none of the agencies specify QC/QA guidelines for lift thickness control during construction. Field observations indicated that some contractors follow laser based methods to control lift thickness as part of the QC (Phares et al. 2011; Vennapusa et al. 2012).

Moisture control

Based on field testing in Iowa, White et al. (2007a) found that granular backfill placed at the "bulking" moisture content can undergo up to 18% collapse when it becomes saturated. Based on tests conducted on materials used in Ohio, Phares et al. (2011) reported a collapse potential of up to 14% when placed at the "bulking: moisture content. By flooding the material during compaction can help reduce the collapse potential of backfill (White et al. 2005).

As summarized in Figure 7c, moisture control specifications varied significantly among the specifications reviewed. 21 agencies did not require any moisture control, while the remaining had some moisture control limits in their specifications with a reference to the optimum moisture

content determined from Proctor test. Wisconsin DOT Bridge Manual (WisDOT 2014) states that strict moisture control be followed during construction, but does not elaborate on what the criteria is. The Wisconsin DOT Standard Specifications (WisDOT 2015) do not provide any guidelines on moisture control.

Based on laboratory testing, White et al. (2005) recommended moisture content be maintained wet of optimum or to flood the material during placement and compaction to avoid post-construction volume change due to collapse. Currently, only 3 agencies out of the 51 reviewed recommend flooding or wet of optimum conditions during backfill placement and compaction.

Compaction control

The compaction assessment practice varied significantly among the specifications reviewed. As summarized in Figure 7d, the target compaction percentage varied between 90 to 100% of a reference laboratory determined maximum dry unit weight. As summarized in Figure 7e, the reference laboratory test method specified was mostly either standard or modified Proctor, but a few agencies specified different methods (vibratory compaction test or Harvard miniature compaction test). Some agencies did not specify what method to use.

Wisconsin DOT Bridge Manual (WisDOT 2014) states that strict control of density is required during construction, but does not elaborate on what method to use or how to control compaction in situ. The Wisconsin DOT Specification (WisDOT 2015) states as follows: "*compact each layer, before placing the next layer, by using engineer approved rollers or portable mechanical or pneumatic tampers or vibrators*", but the document does not refer to laboratory and field test methods for QC/QA.

QC/QA Testing

QC/QA testing during backfill material placement and compaction is critical to ensure desired properties are being achieved in situ. A review of specifications of 48 states and 3 Canadian transportation agencies indicated that a majority of agencies (35 out of the 51 agencies reviewed) do not specify any QC/QA testing requirements during backfill placement or compaction (Figure 7e). The 15 agencies that do provide QC/QA focus on moisture and density testing. Testing for lift thickness control or permeability of the granular backfill materials is not specified in any of the 51 specifications reviewed.

Drainage Design

The review of literature and specifications revealed that 3 drainage designs are typically used for abutment backfill materials as illustrated in Figure 11 (White et al. 2005). Type a drainage design involves placing the drain in a porous backfill and placing the granular backfill material above it. Type b drainage involves wrapping a geotextile around the porous fill to reduce erosion and infiltration of fine particles into the drain. Type c drainage involves the addition of a vertical geocomposite drainage system at the backfill-abutment wall interface.

The review of specifications indicated that 39 agencies allow Type a drainage system, while 20 agencies allow Type b and 8 agencies allow Type c design (Figure 12). Some agencies (15) use a combination of two or more of these designs to increase drainage efficiency. Currently, WisDOT specifies using either Type a or Type b drainage systems. All bridges in Wisconsin are required to use a 6" perforated drain tile with a sock.
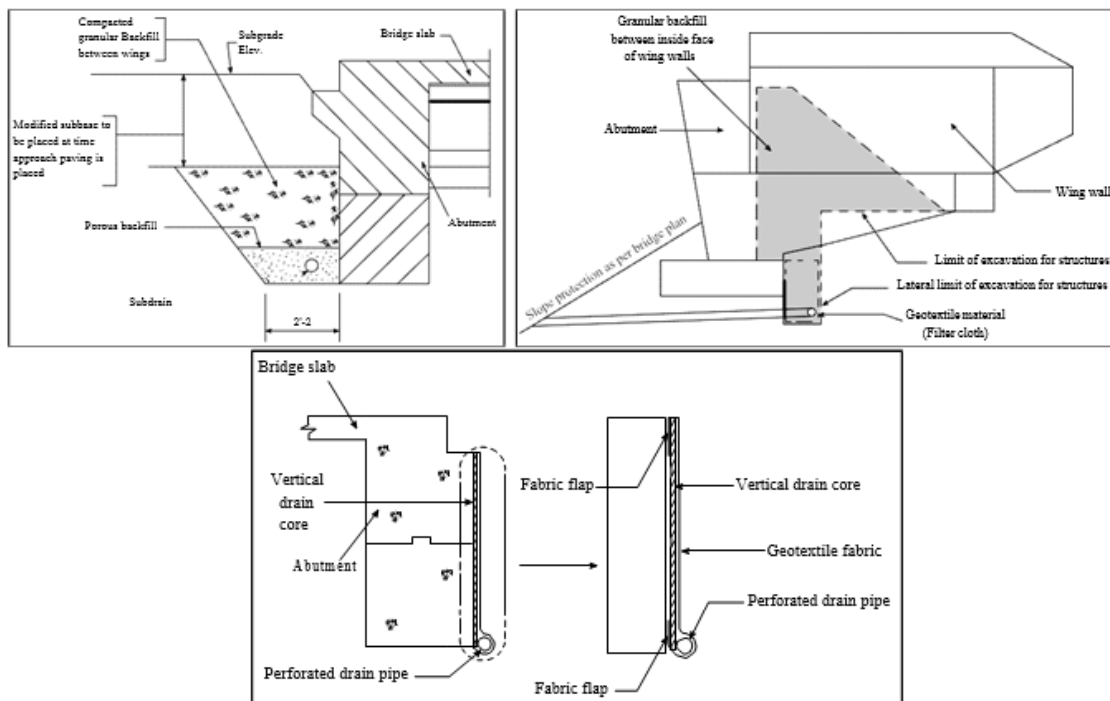
Figure 11. Porous backfill surrounding subdrain (Type a, top left); granular backfill wrapped with geotextile filter material (Type b, top right); and geocomposite vertical drain wrapped with filter fabric (Type c, bottom) (from White et al. 2005)
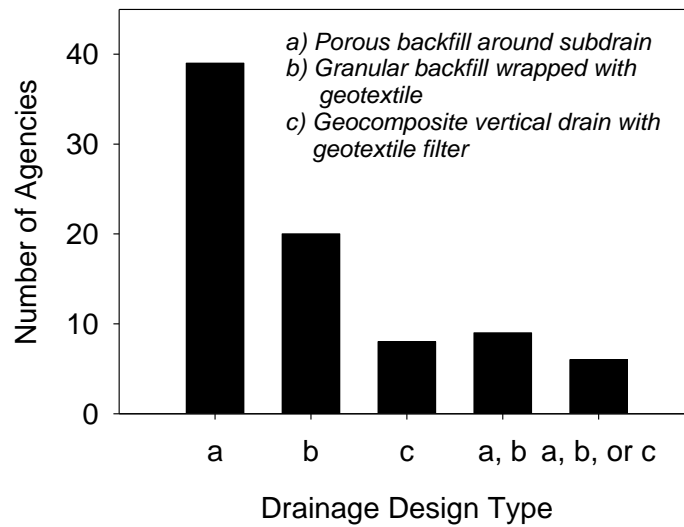
Figure 12. The number of agencies allowing each type of drainage design

Assessment of Abutment Backfill Drainage Characteristics

Drainage Analysis Methods

The primary goal of drainage analysis in abutment systems is to determine the time it takes for the water to drain out of the backfill material. The lesser the time it takes for a majority of the water to drain, the better it is to qualify as a "free-draining" material. There is no quantitative guidance in the literature, however, as to what amount of drainage is needed and in what time to qualify as a "free-draining" material. Drainage in pavement systems can be taken as a reference here (AASHTO 1993), where excellent drainage under pavement is considered when 90% of drainage occurs within 1 hour.

Casagrande and Shannon (1952) proposed a simple theoretical method for calculating drainage times for pavement base course materials. The drainage layer was modeled as a rectangle with a drain in the lower right corner. Initially, the drainage layer is assumed to be saturated, and the right lower corner is opened for free drainage (Figure 13). At that time, water begins dropping from position 1-4 to position 1-3, for which case the drainage is represented as:

$$dq = \frac{H n_e}{2} dx \qquad (1)$$

where: dq is the discharged quantity of water within time element dt per unit width (equal to the area of the shaded triangle 1-5-6 multiple by n_e), H = height of the drainage layer, and n_e = effective porosity, which is a function of the degree of interconnectivity of pores with in a

mixture. Typically, for open-graded materials porosity is considered equal to effective porosity (Vennapusa 2004).

Flow through the volume of 1-5-7 is calculated using Darcy's law. It is assumed that H/2 is the average area per unit width through which flow takes place and the average effective hydraulic gradient is H/x. These assumptions lead to a rate of flow by:

$$\frac{dq}{dt} = k\frac{H^2}{2x} \qquad (2)$$

where: dq/dt = flow rate,

k = hydraulic conductivity; and

x = horizontal distance.

The hydraulic gradient can be assumed to be equal to $H/c_1 x$ and an average area per unit width of H/c_2, in which c_1 and c_2 are quantities based on the shape and are assumed constant during the entire drainage process. Equation 3 can be found by substituting $c = c_1 c_2$ into Equation 2:

$$\frac{dq}{dt} = k\frac{H^2}{cx} \qquad (3)$$
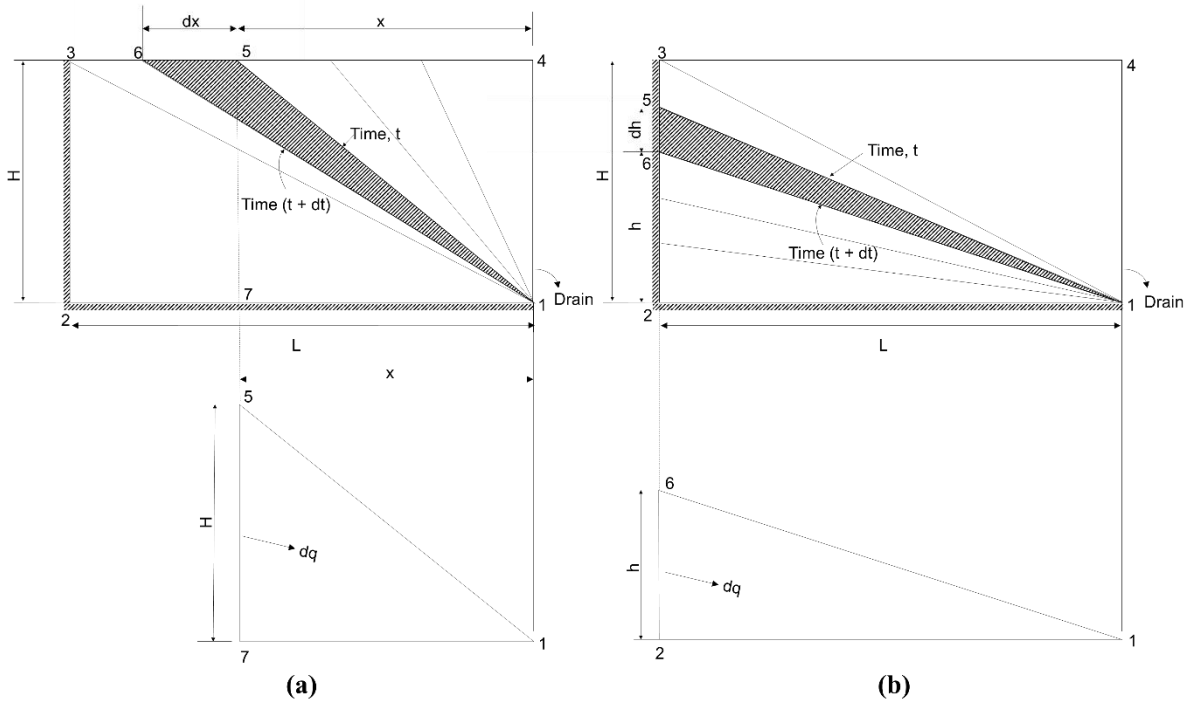
Figure 13. Assumed progress of free water surface: (a) drainage equal to or greater than 50% and (b) drainage equal to or less than 50%(reproduced from Casagrande and Shannon 1952)

The second half of drainage occurs as the surface water changes from position 1-3 to position 1-2. The calculation follows a similar derivation to drainage less than 50% and the variable triangle 1-5-6 has a constant base length *L* and a variable height *h*.

Combining Equations 1 and 3, a simple differential equation can be derived and solved to the following equation:

$$t = \frac{cn_e x^2}{4kH} \tag{4}$$

where: c = shape factor,

n_e = effective porosity,

x = horizontal distance,

k = hydraulic conductivity, and

H = height.

A dimensionless quantity T can be used to calculate the drainage percentage of the material:

$$T = \frac{2tkH}{cn_eL^2} \tag{5}$$

where: t = time,

k = hydraulic conductivity,

H = height of base course,

c = shape factor to be determined based on laboratory experiments,

n_e = effective porosity; and

L = length of base course.

The time factor T is then used to calculate the percent drainage by Equation 5 if the degree of drainage (U) is less than 50% and by Equation 6 if the U is greater than 50%.

$$T = 2U^2 \tag{6}$$

$$T = \frac{U}{2-2U} \tag{7}$$

where: U = drained area/total area.

While Casagrande and Shannon's method is simple and only requires geometry and hydraulic conductivity measurements, it does not fully consider the complexity involved in a true transient flow with soil transitioning from a saturated to a partially saturated state as water is drained away. The shape factor c must be determined based on laboratory calibrations to obtain appropriate results. Further, the method assumes the full vertical face on the right side of the drainage layer (i.e., 1-4), is open for drainage. This holds true for pavement base layers that are daylighted, but not for abutment backfill materials where the water exists through the drain tile or the underlying foundation layers.

Finite element programs, such as Geostudio Seep/W™, incorporate unsaturated soil mechanical parameters in analyzing transient flow conditions. Finite element analysis can take into account the complex boundary conditions and geometrics to better understand the stress state in the soil and better simulate the transient flow conditions (Fredlund et al. 1987). The analysis requires soil suction parameters, saturated hydraulic conductivity, volumetric moisture content, and coefficient of volume compressibility of the backfill material. Obtaining these parameters through laboratory testing is an expensive and elaborative process, but can be estimated using well-documented empirical relationships in the literature. These relationships are explained in more detail in Chapter 3. These model parameters however requires proper laboratory calibration to ensure reasonable results. In this study, measured results from a

laboratory scaled abutment model testing are compared with numerical analysis results and are discussed in Chapters 3 and 5.

Field and Laboratory Testing Methods for Assessment of Drainage

One of the key parameters in drainage assessment is the saturated hydraulic conductivity of the backfill material. Traditionally, the hydraulic conductivity is estimated using empirical relationships as summarized earlier in Table 1 or using laboratory test methods. Laboratory tests can be performed in accordance with ASTM D2434, *"Standard method for permeability of granular soils (constant head),"* or ASTM D5856, *"Standard test measurement of hydraulic conductivity of porous material using a rigid-wall, compaction-mold permeameter".* Both these tests provide appropriate results only if the porous stones used in the tests have higher permeability that the material being tested. For larger particle size materials, larger diameter compaction molds permeameter with larger porous stones must be used (for e.g., see Vennapusa 2004).

Although seldom used in practice, there are several devices that can be used in the field to determine in situ saturated hydraulic conductivity. Infiltrometer tests in accordance with ASTM D5093, *"Standard test method for field measurement of infiltration rate using a double-ring infiltrometers with a sealed-inner ring"* can be performed, but the device requires large quantities of water and is typically used to measure materials with hydraulic conductivities in the range of 10^{-7} to 10^{-10} cm/s (silts and clay soils). Corehole permeameter (CHP) and air permeameter test (APT) have been recently developed at Iowa State University to determine in situ saturated hydraulic conductivity of pavement base layers. APT has the advantage of being a rapid test (< 30 sec), over all other test methods and is applicable for materials with hydraulic conductivity in the range of 0.08 to 13 cm/s (White et al. 2013). CHP and APT test methods are discussed in detail in the Methods chapter.

Lateral Stresses on Bridge Abutments

Lateral earth pressures on bridge abutments can be calculated using multiple methods. Rankine and Coulomb theories are the two classical methods used for calculating active and passive earth pressures acting on the wall. These two methods are based primarily on the assumption of a linear plane failure surfaces. These two methods give reasonable estimates for active earth pressure, but tend to overestimate the passive earth pressures. Terzaghi proposed

another method for calculating passive earth pressure based on a curved failure surface. Experimental studies have been documented measuring lateral earth pressures accounting for compaction induced stresses and wall movements. Brief overview of those studies are provided below. Further, the analysis methods followed by WisDOT in determining lateral stress are also provided below.

Classical Lateral Earth Pressure Theories

Rankine's Theory

In 1857, Rankine proposed equations for calculating earth pressures. Rankine's method assumes a frictionless wall-soil interaction and a linear variation of stress as depth increases:

$$\sigma_a = K_a \gamma z \tag{8}$$

$$\sigma_p = K_p \gamma z \tag{9}$$

where: σ_a = active lateral earth pressure;

σ_p = passive lateral earth pressure;

γ = unit weight of the soil; and

z = depth.

K_a and K_p are the Rankine active and passive earth pressure coefficients defined by as:

$$K_a = cos\alpha(\frac{cos\alpha - \sqrt{cos^2(\alpha) - cos^2(\phi')}}{cos\alpha + \sqrt{cos^2(\alpha) - cos^2(\phi')}}) \tag{10}$$

$$K_p = cos\alpha(\frac{cos\alpha + \sqrt{cos^2(\alpha) - cos^2(\phi')}}{cos\alpha - \sqrt{cos^2(\alpha) - cos^2(\phi')}}) \tag{11}$$

where: α = the inclination of the granular backfill; and

ϕ' = the angle of internal friction.

If the angle of inclination of the backfill is zero, these coefficients simplify to:

$$K_a = \frac{1 - sin(\phi')}{1 + sin(\phi')} = tan^2(45° - \phi') \tag{12}$$

$$K_p = \frac{1 + sin(\phi')}{1 - sin(\phi')} = tan^2(45° + \phi') \tag{13}$$

Coulomb's Theory

In 1776, Coulomb proposed a theory for calculating active and passive earth pressures against retaining walls. This method is generally considered to be the first theory to predict the passive earth pressure coefficient. In this theory, Coulomb assumed the failure surface to be a

plane. Coulomb's Theory assumes a linear variation of stress as depth increases and uses Equation 8 and 9 to calculate the active and passive earth pressures. K_a and K_p are the Coulomb active and passive earth pressure coefficients and are calculated with Equations 14 and 15:

$$K_a = \frac{cos^2(\phi'-\theta)}{cos^2(\theta)cos(\delta'+\theta)\left[1+\sqrt{\frac{(sin(\phi'+\delta'))(sin(\phi'-\alpha))}{(cos(\delta'+\phi'))(cos(\theta-\alpha))}}\right]^2} \tag{14}$$

$$K_p = \frac{cos^2(\phi'+\theta)}{cos^2(\theta)cos(\delta'-\theta)\left[1-\sqrt{\frac{(sin(\phi'+\delta'))(sin(\phi'+\alpha))}{(cos(\delta'-\phi'))(cos(\theta-\alpha))}}\right]^2} \tag{15}$$

where: ϕ' = internal soil friction angle;

θ = angle of wall face (90° for vertical wall);

δ' = angle of wall friction; and

α = angle of backfill (0° for horizontal backfill)

In the case of $\delta' = 0$, the Coulomb coefficients simply to the Rankine coefficients. For granular material, δ' is typically in the range of $\phi'/2$ to $2\phi'/3$.

Log Spiral Method

Terzaghi proposed a theory to calculate passive earth pressures based on a failure surface in the shape of a log-spiral (Terzaghi 1943) The log spiral theory is less widely used due to its complexity, but provides better predictions for passive conditions and shows a more probable failure mechanism for values of $\delta > 0.4\phi'$ (Duncan and Mokwa 2001).

The theoretical failure surface consists of two zones: the Prandtl zone and the Rankine zone (Figure 14). The Prandtl zone is bounded by a logarithmic spiral. The shape of this logarithmic spiral is shown in Figure 15.
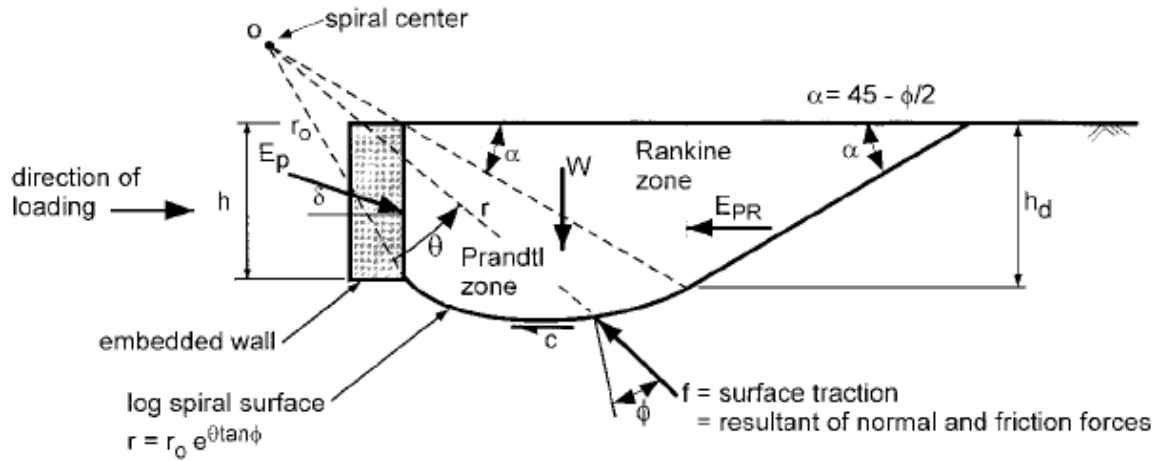
Figure 14. Terzaghi's Log-Spiral Failure Mechanism (Duncan and Mokwa 2001)
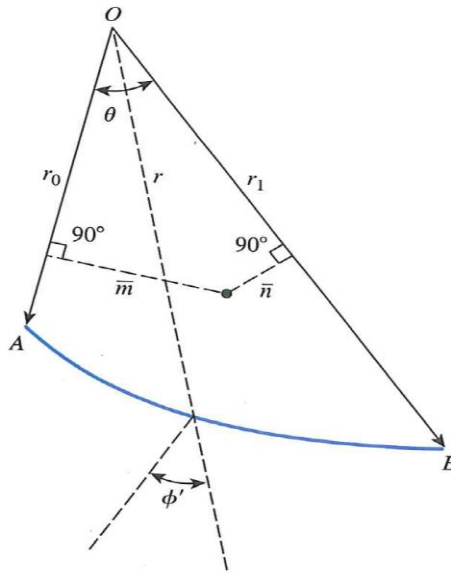
Figure 15. Logarithmic spiral shape (Das 2010)

The theory is primarily based on the theory that force factors acting on the logarithmic spiral make an angle of ϕ' with the tangent of the spiral, and the lines of action of the force vectors cross the center of the spiral.

The log spiral method can be implemented in three ways. The easiest way is to use tables or charts of passive pressure coefficients based on the log spiral theory, found in Caquot and Kerisel (1948) or NAVFAC (1986). The graphical method is explained in Terzaghi (1943) and Terzaghi et al. (1996), but requires considerable time and effort. Numerical analyses can also be

performed. These analyses can account for 3D effects, making them applicable for short and long structures (Duncan and Mokwa 2001).

Table 4 summarizes the advantages and limitations of all these methods in calculating passive earth pressures. Duncan and Mokwa (2001) calculated theoretical maximum earth pressures of a reinforced block in the ground and compared them to maximum loads applied to the concrete block. They concluded the log spiral passive theory with 3D corrections provided the most accurate predictions for computing ultimate passive soil resistance.

Experimental Results of Lateral Stresses on Bridge Abutments

All classical theories explained above assume that the pressure distribution is linear with depth, however experiments performed by Broms and Ingleson (1971) indicate that this is not the case. They reported that a pressure envelope develops behind the wall and earth pressure coefficients transition between passive and active states, because of compaction induced lateral pressures and wall rotation due to temperature induced movements particularly in integral abutments.

In 2001, England and Tsang performed experiments on a model simulating seasonal and daily temperature related movements. The experiment simulated thermal loading by rotating a model abutment around its vertical axis. They reported an increase in soil stress acting on the wall as it rotates inward toward the fill due to densification and proposed Equation 16 for calculating the earth pressure coefficient, which requires measurement of lateral movement:

$$K = K_o + (\frac{d}{0.03H})^{0.6}K_P \qquad (16)$$

where: K = earth pressure coefficient;

K_o = at-rest earth pressure coefficient (1-sin(φ'));

d = maximum lateral movement at the top of the abutment during a seasonal cycle;

H = height of the backfill; and

K_p = passive earth pressure coefficient.

Table 4. Advantages and limitations of passive earth pressure theories (from Duncan and Mokwa, 2001)

Theory	Advantages	Limitations
Rankine	Simplest method	It is assumed that δ = i, where i = inclination of ground surface; applies only to simple conditions (planar ground surface, uniform surcharge, homogeneous soil)
Coulomb	Applicable for any value of wall friction $0 \leq \delta \geq \phi$; easy to apply through charts, tables or formulas; can account for more complex conditions (irregular ground surface, nonuniform surcharge, nonhomogeneous soil conditions) through graphical analysis	Passive pressures are too high for values $\delta > .4\phi$; complex conditions require graphical analyses
Log spiral charts and tables	Accurate for any value of δ; easy to apply	Applicable only to simple conditions; does not accommodate cohesive component of shear strength
Log spiral graphical solution	Accurate for any value of δ; can accommodate cohesive as well as frictional soil strength; is applicable to complex conditions	Requires complex graphical analyses
Log spiral numerical solution	Accurate for any value of δ; can accommodate cohesive as well as frictional strength; with Ovesen's correction, accounts for 3D effects	Computer program is needed

Broms and Ingleson (1971) and England and Tsang (2001) both documented that the rotation of the abutment can be caused by temperature related movements. Integral bridges expand when temperatures increase and contract when they decrease (Figure 16). When temperatures increase, abutments move toward the backfill resulting in increasing lateral earth pressures. When temperatures decrease, abutments move away from the backfill and the applied pressures transition into active earth pressures (Horvath 2005). Repeated movements can also lead to void development as illustrated in Figure 17.
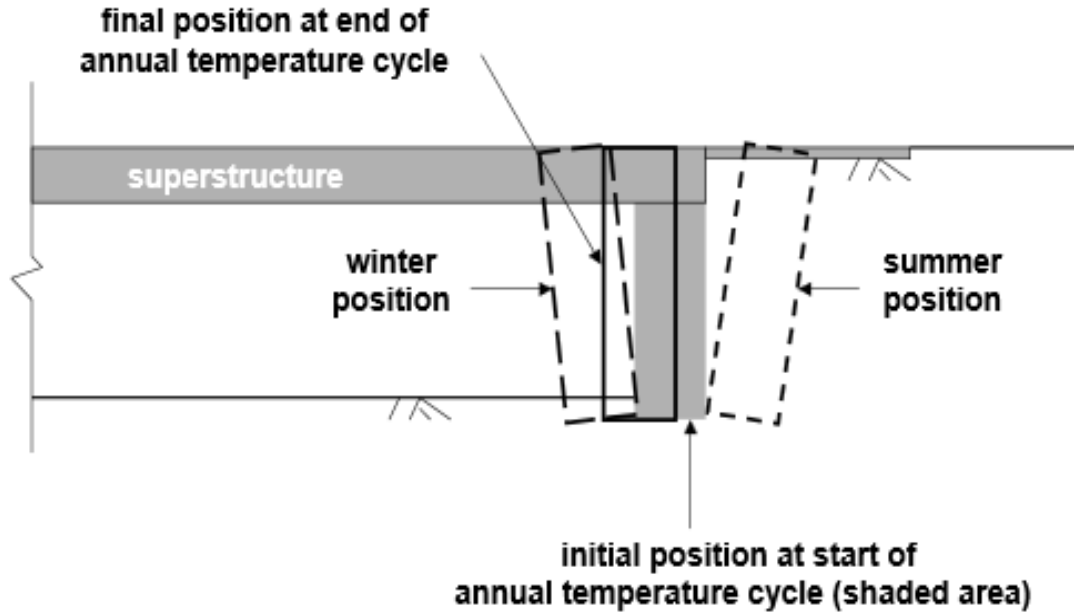
Figure 16. Thermally Induced Integral Bridge Abutment Movement (Horvath 2005)
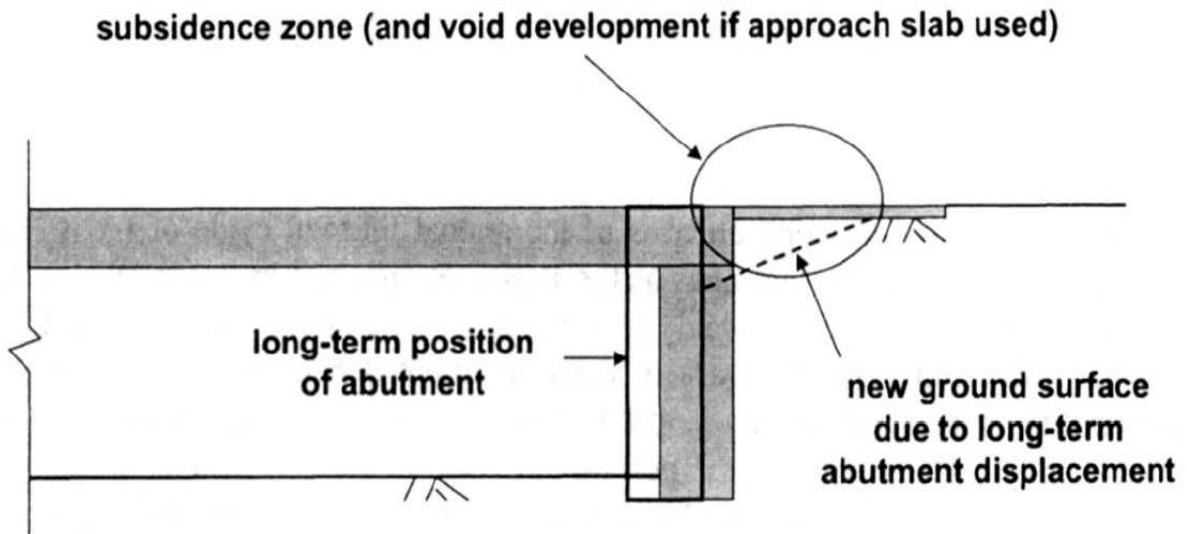
Figure 17. Development of void due to bridge movement (Horvath 2005)

Huntley and Valsangkar (2013) reported field test results that also did not show a linear trend earth pressures with depth because of temperature related wall rotations. They reported that in most cases, the maximum earth pressure occurred in hot summer (July) which corresponded to the maximum rotation observed on the abutment wall due to expansion of the bridge. Sensors located on the upper portion of the abutment showed horizontal to vertical stress ratios greater

than the Rankine coefficient for passive earth pressures. The sensors located in the bottom portion of the abutment showed lower ratios. Figure 18 shows the results from Huntley and Valsangkar (2013) in comparison with results reported by other researchers (Barker and Carder 2001; Civjan et al. 2004; Darley et al. 1998; Elgaaly et al. 1992; Hassiotis et al. 2005). Most studies showed that maximum earth pressures were found to occur during summer months.
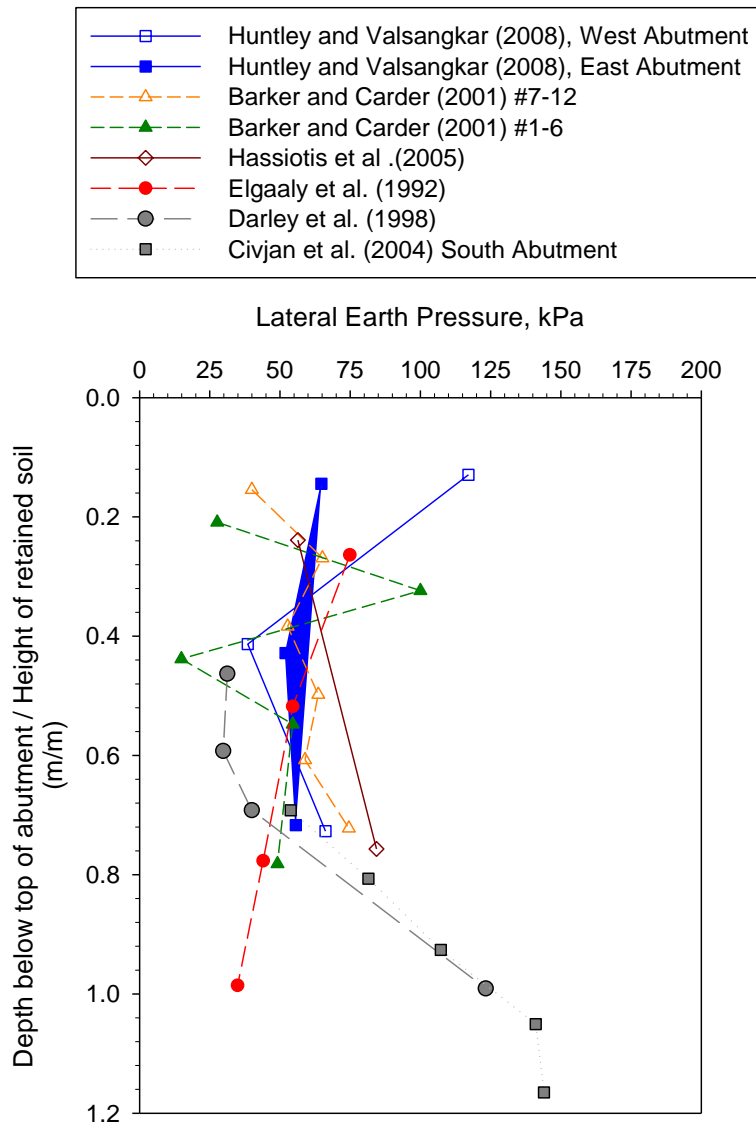
Figure 18. Comparison of maximum earth pressure behind various abutments (Reproduced from Huntley and Valsangkar 2013)

Lateral Earth Pressure Calculations by WisDOT

The Wisconsin DOT Bridge Manual (WisDOT 2014) specifies the use of full-retaining, semi-retaining, sill, spill-through or open, pile encased and special designs to resist horizontal stresses and transfer vertical stresses to the foundation. Full retaining abutments are designed to retain the entire roadway embankment and are the most expensive type (Figure 19). Semi-retaining abutments provide better horizontal clearance and sight distance than a full-retaining abutment. The semi-retaining abutments are located on the embankment slope and provides less of a collision hazard for an out of control vehicle. Sill abutments are constructed at the top of the slope after the embankment is close to final grade, eliminating the difficulties of obtaining adequate compaction adjacent to the relatively high walls of closed abutments (Figure 21). These abutments are the least expensive abutment type, but result in high costs for the superstructure. Spill-through or open abutments are constructed when a bridge is expected to have an expansion. The abutment is situated on columns or stems that extend upward from the natural ground and is essentially a pier being used as an abutment. Pile encased abutments are used when sill abutments are less economical. Special design abutments are used in addition to any of other types. These abutments can be required for aesthetic appeal, unique soil conditions, or for structural reasons.

Lateral earth pressures behind abutments are designed per Load and Resistance Factor Design (LRFD) procedure developed by AASHTO (2012). The backfill is designed assuming an active case. Table 5 shows the equivalent fluid pressures used for calculating earth pressures based on the pressure state and slope of the backfill.
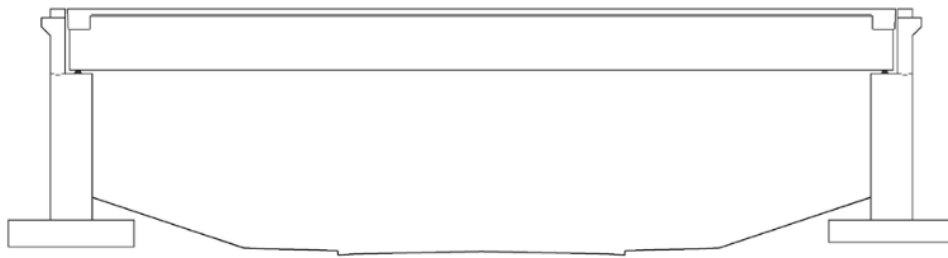
Figure 19. Full retaining abutment (WisDOT 2014)
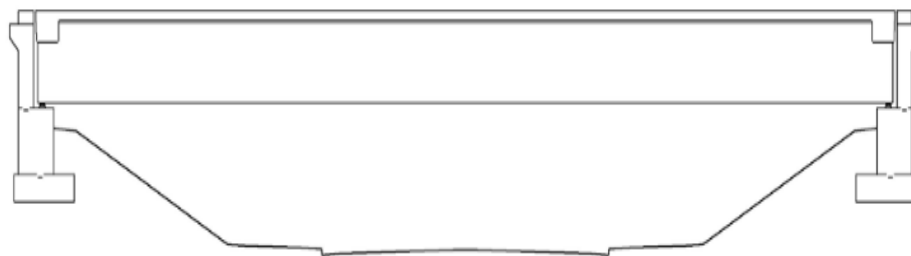
Figure 20. Semi-retaining abutment (WisDOT 2014)
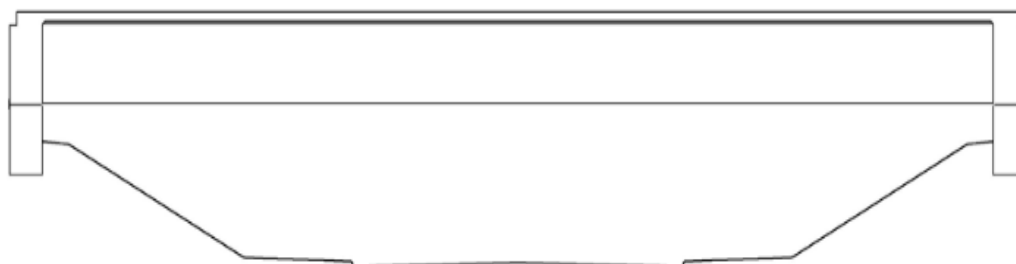
Figure 21. Sill abutment (WisDOT 2014)

Table 5. Values used for calculating lateral earth pressure (reproduced from

AASHTO 2012)

Soil Type	Level Backfill		Backfill with slope of 25°	
	At rest γ_{eq} (pcf)	Active $\Delta/H = 1/240$ γ_{eq} (pcf)	At rest γ_{eq} (pcf)	Active $\Delta/H = 1/240$ γ_{eq} (pcf)
Loose sand or gravel	55	40	65	50
Medium dense sand or gravel	50	35	60	45
Dense sand or gravel	45	30	55	40

The WisDOT Bridge Manual states that hydrostatic pressures, including both soil and water, can increase the equivalent fluid unit weight to 85 pcf. These unwanted pressures on the walls can potentially lead to damage and movement of abutments. Therefore, the manual recommends use of backfill material that is "free-draining" and assumes that they are "free-draining" in the design.

The WisDOT Bridge Manual lists settlement of approach slab, uplift of approach slab, backfill settlement under flexible pavement, approach slab not adequately supported at the

abutment, and erosion of backfill from infiltrated water as typical bridge problems associated with inadequate drainage. To mitigate these problems, the following recommendations are provided therein:

- Use select materials
- Place relatively thin 4-6 in. layers
- Strictly control moisture and density
- Properly compact backfill materials.
- Install moisture barriers.

CHAPTER 3. TESTING AND ANALYSIS METHODS

This chapter explains the laboratory and in situ test methods used to determine soil classification, compaction, shear strength, drainage, and collapse characteristics of backfill materials, and the analysis procedures used to assess drainage characteristics.

The following laboratory tests were performed: soil gradation and classification, Proctor and vibratory compaction, falling head permeability, direct shear, and oedometer collapse tests. A scaled bridge abutment model fabricated at Iowa State University was used assess drainage/infiltration characteristics of the backfill material. Three in situ tests, air permeability tests (APT); corehole permeameter (CHP) tests; and dynamic cone penetrometer (DCP) tests, were used in this study. Earth pressure cells (EPCs) and piezometers were installed to monitor lateral earth pressures and pore pressures, respectively, behind abutment walls.A finite element analysis software was used to analyze pore pressure dissipation in the backfill material. Data from the scaled bridge abutment model tests were used to calibrate the parameters used in the numerical analysis.

LABORATORY TEST METHODS

The test standards and references used in laboratory testing are summarized in Table 6. Details of each test method are provided in the flowing subsections of this chapter.

Particle Size Analysis

Two methods were used for particle size analysis, ASTM D6913-04 "*Standard test methods for particle-size distribution (gradation) of soils using sieve analysis*" and ASTM D1140-00 "*Standard test methods for amount of material in soils finer than no. 200 (75-μm) sieve.*"

Oven-dried samples were weighed and washed over a #200 sieve to remove the fine particles following ASTM D1140-00. The washed material was then oven dried for 24 hours. The resulting material was then separated through a set of sieves.

Table 6. Laboratory test standards and methods

Standard/Reference	Test
Soil classification tests	
ASTM D6913–04	Grain size analysis test
ASTM D1140-00	Percent fines content (finer than #200 sieve) test
ASTM D2487-06	Unified soil classification system
ASTM D3282-09	AASHTO soil classification system
Compaction tests	
ASTM D698-12e1	Standard Proctor test
ASTM D4253-00, 4254-00	Vibratory compaction or relative density test
Permeability tests	
ASTM D5856-95, Vennapusa (2004)	Falling head permeability test
Strength test	
ASTM D3080-98	Direct shear test
Collapse test	
See text for details	Collapse test
Abutment model tests	
See text for details	Pore pressure dissipation test

Soil Classification

The results from the particle size analysis were used to classify the material following ASTM D2487-06 *"Standard practice for classification of soils for engineering purposes (unified soil classification system)"* and ASTM D3282-09 *"Standard practice for classification of soils and soil-aggregate mixtures for highway construction purposes (AASHTO classification system)."*

Compaction Tests

Proctor compaction tests were conducted according to ASTM D698 "*Standard test methods for laboratory compaction characteristic of soil using standard effort (12,400 ft- lbf/ft^3 (600 kn-m/m^3))*" to determine the relationship between water content and dry unit weight. Each material was placed in plastic bags and water was added to achieve the desired moisture content. The Proctor molds used in this study were 10.16 cm (4 in.) and 15.24 cm (6 in) diameters depending method used based on the gradation properties. An automated mechanical hammer was used in this study.

Vibratory compaction tests were conducted to determine the minimum and maximum dry densities following ASTM D4253 *"Standard test methods for maximum index density and unit weight of soils using a vibratory table"* and ASTM D4254 *"Standard test methods for minimum index density and unit weight of soils and calculation of relative density."* An electromagnetic vibrating table was used in this study (Figure 22).

Figure 22. Vibrating table for relative density tests

The ASTM standards specify using a mold size of 15.24 cm (6 in.) or 27.94 cm (11 in.), based on the maximum particle size. The 15.24 cm (6 in.) diameter mold was used in this study. The standard requires conducting tests on oven dried material. In addition to this, tests were conducted at various moisture contents to determine the moisture-density relationship.

Permeability Tests

Falling head permeability tests were performed to determine the saturated hydraulic conductivity (K_{sat}) according to ASTM D5856 "*Standard Test Method for Measurement of Hydraulic Conductivity of Porous Material Using a Rigid-Wall, Compaction-Mold Permeameter.*" The tests were conducted in a material was placed in a 10.16 cm (4 in.) Proctor mold (Figure 23a) and compacted at in situ moisture content following using standard Proctor compaction effort (ASTM D698). The falling head permeameter uses a piezometer with marking ever 1 cm. The time it took for the water head to drop 10 cm (3.9 in.) was recorded.

(a)   (b)

Figure 23. Compaction mold permeameter setups used in this study: (a) 10.16 cm diameter mold compaction mold permeameter and (b) 30.28 cm diameter mold large scale compaction mold permeameter

The ASTM standard falling head permeability test setup involves using a porous stone that was determined to have lower drainage/infiltration capacity than the material that was being tested. Therefore, the porous stone was removed and replaced with a similar size non-woven geotextile fabric material. For some materials tested in this study, the modified setup also did not provide enough drainage capacity. In those cases, a large scale aggregate compaction mold permeameter fabricated at Iowa State University (Vennapusa 2004) was also used to conduct falling head tests (Figure 23b). In that testing, a compaction mold with dimensions of 30 cm height x 30 cm diameter was used. The bottom of the mold is outfitted with a porous stone with large openings to ensure rapid drainage. The compaction test procedure followed in this testing was similar to that the procedure followed for small scale testing. The water reservoir consisted

of a stand pipe with markings located every 10 cm. The time it took for each drop in head of 10 cm was recorded.

Pea gravel was used in the bottom half of the compaction mold and backfill material was placed and compacted in the upper half of the compaction mold. A non-woven geotextile fabric was used at the interface of backfill material and pea gravel (Figure 24). Permeability tests were performed on pea gravel with the geosynthetic fabric to ensure that it had a higher permeability than the geomaterial.

Figure 24. Geosynthetic fabric used in permeability testing

Collapse Index Tests

Collapse index tests were performed using a consolidometer/oedometer in this study in general accordance with ASTM D5333-03 "*Standard Test Method for Measurement of Collapse Potential of Soils*". Some deviations were made from the standard test procedure. Brief overview of the test procedures followed, deviations from the test standard, and justification for the deviations are described below.

Two slightly different methods (referred to as Methods A and B) were followed in this study. In both methods, the material was compacted to 100% standard Proctor dry density (not to be confused with standard Proctor maximum dry density) at that moisture content. Tests were conducted at various moisture contents to assess the influence of compaction moisture content on collapse after wetting. The material was placed in two lifts and was compacted with the wooden spacer placed on the material and using a rubber mallet for one to three times (Figure 25). Trial

tests were initially conducted to determine the compaction effort needed to achieve the desired compaction and the same procedure was followed on the remaining samples. The oedometer test setup with and without water are shown in Figure 26 and Figure 27, respectively.

Method A involved applying a seating stress of 6.9 kPa (1 psi) for 2 minutes or until 100% consolidation was achieved. After that, a vertical stress of 28 or 55 or 110 kPa (4, 8, 16 psi) was then applied for at least 2 minutes or until 100% consolidation was achieved. Tests were conducted separately for each vertical stress applied. After consolidation, water was added to the sample and the corresponding vertical deformation was measured to determine the collapse index using Eq. (15).

$$I_c(\%) = \frac{\Delta h}{h_o} \times 100 \tag{17}$$

where I_c = collapse index (%);

Δh = change in sample height after adding water (i.e., difference between height reading before and after wetting);

h_o = initial sample height.

The ASTM D5333 standard requires applying seating load of 5 kPa for about 5 minutes and then applying load increments each hour using 12, 23, 50, 100, 200 kPa. This was not followed here. A seating stress of 6.9 kPa (1 psi) was selected instead to simulate approximately 0.3 to 0.4 m thick fill layer. The load was only applied for 2 minutes or waited until primary consolidation was completed, instead of constant 5 minutes per standard. Most of the materials consolidated within 1 minute, while some consolidated within 3 to 4 minutes. For load increments, 27.6 kPa (4 psi), 55.2 kPa (8 psi), and 110.3 kPa (16 psi) were selected to simulate 1.4 to 1.6 m, 3.0 to 3.2 m, and 6.2 to 6.4 m backfill material height, based on review of backfill heights on field projects. The load increments were also maintained for a minimum of 2 minutes or until primary consolidation was achieved, instead of 24 hours per standard (which is primarily applicable to silt or clay type soils and not granular materials). Most of the materials consolidated within < 5 minutes.

Figure 25. Setup for compaction of backfill material in oedometer
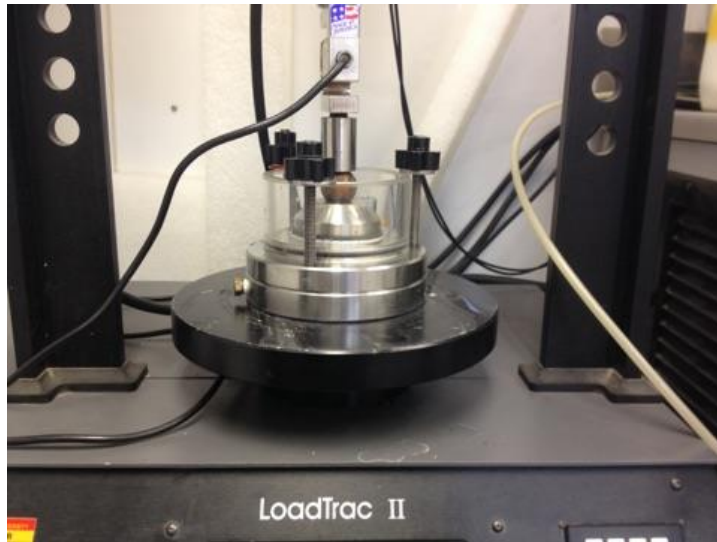
Figure 26. Oedometer test setup without water
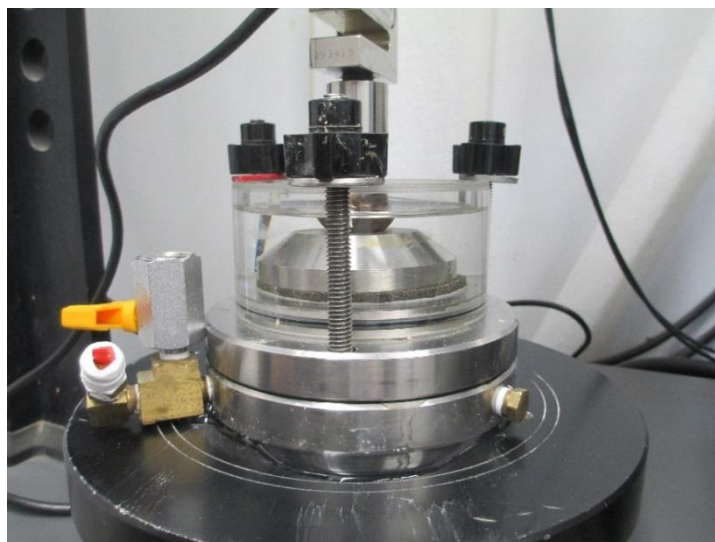
Figure 27. Oedometer test setup without water

Method B was used on the RAP and RAS materials assessed in this project to account for the particle crushing and creep behavior of the materials. This method involved performing double oedometer tests, i.e., one test without wetting and one test with wetting. A seating stress of 6.9 kPa (1 psi) was applied for two hours. After two hours, the stress was increased to 28, 55, 110 kPa (4, 8, 16 psi) consecutively, in 12 hour increments. Primary consolidation was not completed for most of these materials even after 12 hours because of the creep behavior. The difference in vertical heights or strains between the two tests (with and without wetting) was calculated as I_c of the material.

According to ASTM D5333, the classification for degree of collapse is as follows:

- $Ic = 0\%$ — Degree of Collapse: None
- $Ic = 0.1$ to 2% — Degree of Collapse: Slight
- $Ic = 2.1$ to 6.0% — Degree of Collapse: Moderate
- $Ic = 6.1$ to 10.0% — Degree of Collapse: Moderately Severe
- $Ic = > 10\%$ — Degree of Collapse: Severe

Direct Shear Test

Direct shear tests were performed to determine consolidated-drained shear strength parameters (i.e., drained cohesion *c'* and drained friction angle *ϕ'*) according to ASTM D3080M "*Standard test method for direct shear test of soils under consolidated drained conditions.*" The

material was compacted to 100% standard Proctor dry density and was saturated by adding water during the consolidation stage. The direct shear test apparatus is shown in Figure 28.

Figure 28. Direct shear test device

Abutment Model Tests

The abutment model was designed and fabricated at Iowa State University in 2005 for testing of bridge abutment backfill materials (White et al., 2005). In this study, the model was used to study the drainage properties of the backfill materials. The model is scaled to approximately one-fourth the dimensions of an Iowa DOT standard bridge abutment, except for the drain tile (Figure 29). A 4 in. drain tile wrapped with Wisconsin DOT specified sock was used in this study. This drain sock had an apparent opening size of 0.425 mm (No. 40 sieve) and a permittivity of 5 s^{-1}.

Geokon 3400 dynamic pore pressure sensors (PPs) were installed in the model to measure the pore pressure dissipation. Dynamic PP sensors were placed right behind the drain tile near the bottom of the backfill and at the back end of the abutment at the same elevation (Figure 30).

All materials were compacted at their natural moisture content, which is similar to what was used in the field during placement. For all tests, the material was compacted to achieve a minimum 95% of standard Proctor dry density at that moisture content (not to be confused with 95% standard Proctor maximum dry density), by compacting it in 7.6 cm (3 in.) thick lifts using a hand tamper (Figure 31). Based on the measured weight of the material, moisture content of the material, and the volume of the abutment model, the actual dry unit weight of the material was determined.
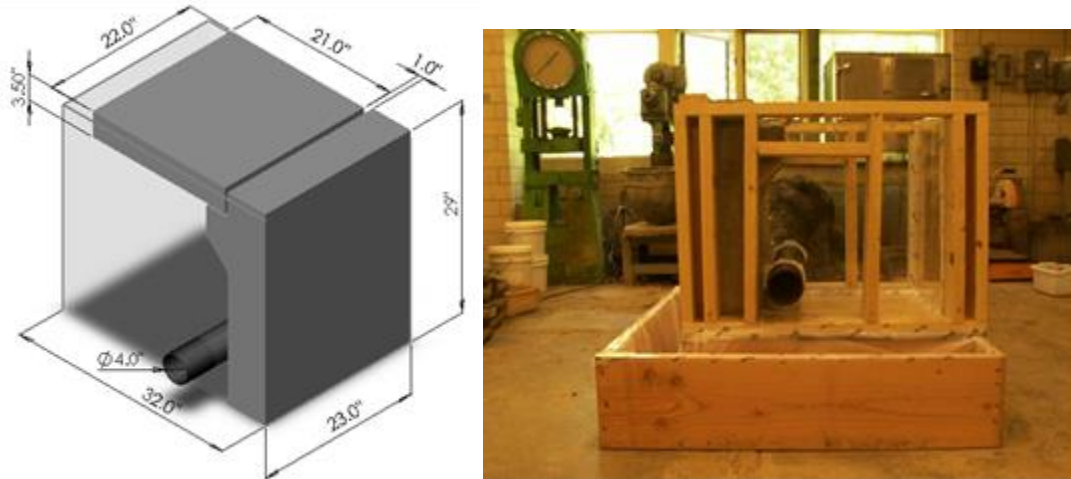
Figure 29. Schematic (left) and photograph of the ISU Water Management Bridge Approach Model (White et al. 2005)

100 mm dia. (4 in.) drain tile with sock

Dynamic Pore Pressure (PP) Sensors

36 cm
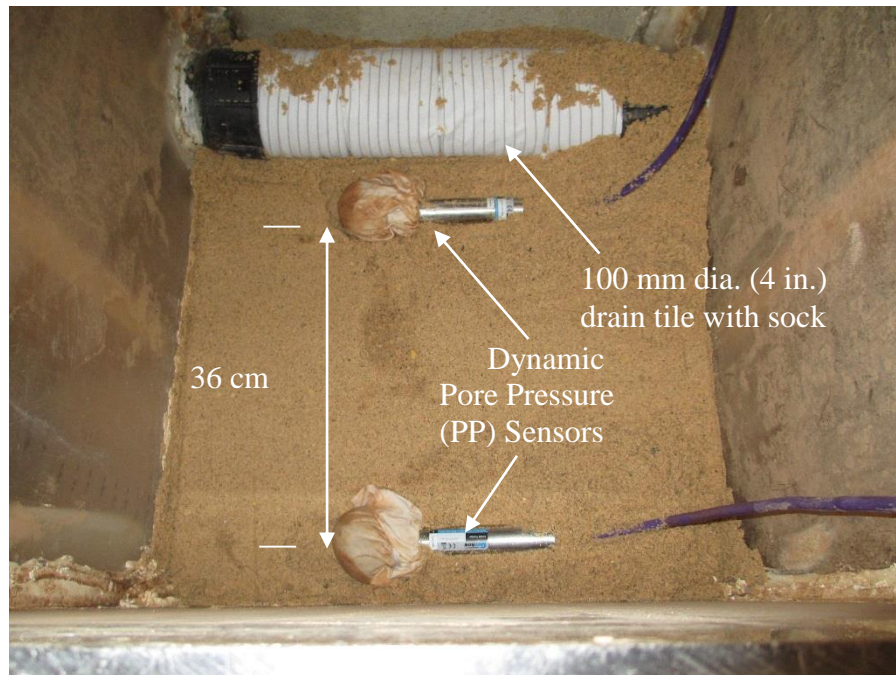
Figure 30. PP sensor locations in the abutment model

Figure 31. Compaction of fill material using a hand tamper

After filling the material to the desired elevation in the abutment model, APT and CHP tests (in that order) were conducted. Details of APT and CHP test procedures are provided in the Field Test Methods section of this chapter. A light-weight plexi-glass base plate was fabricated for CHP tests to fit in the abutment model. The base plate was placed over compressible foam. Weights were placed on the baseplate to prevent leakage between the foam and the material (Figure 32).

After APT and CHP tests, the model was filled with water by plugging the drain tile to saturate the material (Figure 33). An expandable drain plug was used to plug the drain tile. Pore pressure readings from both sensors were monitored to ensure the material was fully saturated. After saturation, drain plugs were removed (Figure 34) and pore pressure dissipation (i.e., drainage) with time were monitored by collecting data at 50Hz (i.e., 50 readings per sec), until about 95% of drainage is occurred or until no significant reduction in pore pressures was observed over a 24 hour period.

Figure 32. APT test setup (left) and CHP test setup (right)

Figure 33. Drain tile plugged for saturation

Figure 34. Water draining through the drain tile during dissipation test

FIELD TESTING METHODS

Dynamic Cone Penetrometer

Dynamic Cone Penetrometer (DCP) tests were performed according to ASTM D6951, "*Standard Test Method for Use of the Dynamic Cone Penetrometer in Shallow Pavement Applications.*" (Figure 35). DCP results were used to calculate California Bearing Ratio (CBR) values of the granular backfill. Loose layers of granular backfill can be identified when cumulative number of blows and CBR with depth profiles are plotted. DCP tests were performed to depths of about 1 m (39 in) to 2 m (78 in) using extension rods, below the testing surface. The DCP test was primarily used to identify any loose layers within the compacted backfill material.
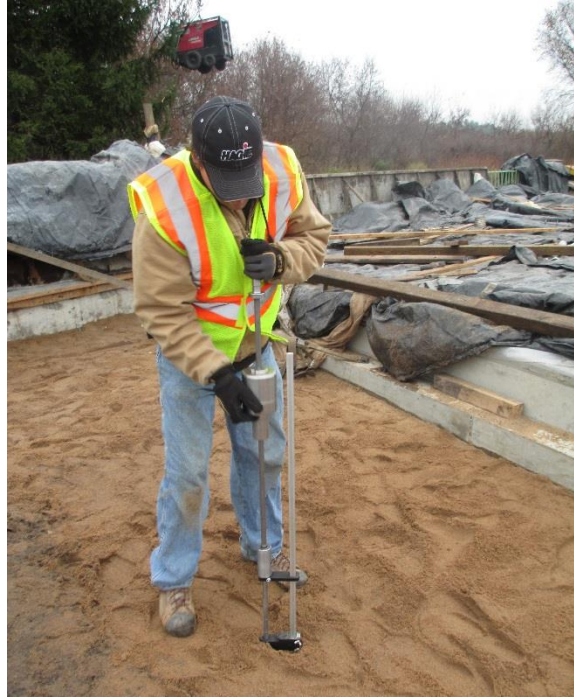
Figure 35. DCP tests at Slovak Valley Creek Bridge

Air Permeameter Test

The air permeameter test (APT) device (Figure 36) developed at Iowa State University (White et al. 2013) was used to rapidly (in < 30 seconds) determine the saturated hydraulic conductivity of the backfill materials in situ. Compressed CO_2 gas was used as the permeating fluid in this field study. The APT consists of a self-contained pressurized gas system with a self-sealing base plate and a theoretical algorithm to rapidly determine the K_{sat}. The gas flow is controlled using a regulator and a precision orifice. The inlet pressure and flow rate values are recorded and used in K_{sat} calculations using Equation 18.

$$K_{sat} = \left[\frac{2\mu_{gas}QP_1}{rG_o(P_1^2 - P_2^2)} \right] \text{ x } \frac{\rho g}{\mu_{water}(1-S_e)^2\left(1-S_e^{((2+\lambda)/\lambda)}\right)} \qquad (18)$$

where:

K_{sat} = saturated hydraulic conductivity (cm/s);

μ_{gas} = kinematic viscosity of the gas (PaS);

Q = volumetric flow rate (cm^3/s);

P_1 = absolute gas pressure on the soil surface (P_a) = $P_{o(g)}$ x 9.81 + 101325;

$P_{o(g)}$ = gauge pressure at the orifice outlet (mm of H_2O);

P_2 = atmospheric pressure (Pa);

r = radius at the outlet (4.45 cm);

G_o = Geometric factor (constant based on geometry of the device and test area; White et al. 2007),

S_e = effective water saturation [$S_e = (S–S_r)/(1-S_r)$];

λ = Brooks-Corey pore size distribution index;

S_r = residual water saturation;

S = water saturation;

ρ = density of water (g/m^3);

g = acceleration due to gravity (cm/s^2); and

μ_{water} = absolute viscosity of water (gm/cm-s).

Figure 36. Air permeability testing at Slovak Valley Creek Bridge

More details on the test device and K_{sat} calculation procedure are provided in White et al. (2007, 2013). The degree of saturation (S) values were obtained by assuming a 95% standard Proctor dry unit weight and measured in situ moisture content measurements. The S_r and λ parameters can be obtained by determining the soil-water retention properties (also known as soil water characteristic curves (SWCC) of the materials). Tests to determine the SWCC parameters can be time-consuming and require precise calibration of test equipment. As an alternative, empirical relationships from material gradation properties can be used (Zapata and Houston 2008). A summary of these relationships and the procedure to estimate S_r and λ parameters are summarized in White et al. (2013).

Core Hole Permeability Test

The core hole permeameter (CHP) is a test device that was recently developed at Iowa State University. The test was originally developed for testing base materials under pavements by coring a 150 mm (6 in.) diameter hole in the pavement. The setup was modified in this study to test the backfill materials in situ (Figure 37).

The setup involved placing a base plate on a compressible closed-cell foam over the backfill material, to prevent water leakage between the base plate and the material. A core hole sleeve was then attached to the plate. CHP was then inserted in the core hole and was sealed at the bottom of the device and against the interior of the hole. To seal the bottom of the CHP, an open cell foam ring is compressed under the CHP. By inflating a rubber tube between the outside of the CHP ring and the hole wall, the perimeter of the CHP is sealed against the hole wall. About 20 to 25 psi air pressure was used to inflate the rubber tube.

Figure 37. Corehole permeability test setup

Tests are performed by filling the permeameter with water and recording the head loss with time at different time intervals. Test readings are taken intermittently over a period of about 30 to 60 minutes or until the readings stabilize. Determination of the hydraulic conductivity was based on concepts from ASM D6391-06 "*Standard for Field Measurement of Hydraulic Conductivity Limits of Porous Materials Using Two Stages of Infiltration from a Borehole.*" For each set of readings, the water temperature was measured to correct for the viscosity of the water. The

following equations were used to calculate the in situ hydraulic conductivity using the CHP (K_{CHP}).

$$K_{CHP} = \frac{R_t G_1}{t_2 - t_1} \ln\left(\frac{H_1}{H_2}\right) \qquad (19)$$

$$R_t = \frac{2.2902(0.9842^T)}{T^{0.1702}} \qquad (20)$$

$$G_1 = \frac{\pi d^2}{11 D_1}\left[1 + \frac{a_1 d_1}{4 b_1}\right] \qquad (21)$$

where: R_t = ratio of kinematic viscosity of permeant at temperature during time increment t_1 to t_2 to that of water at temperature (T) 20°C (68°F);

T = Temperature,

H_1 = effective head at time t_1;

H_2 = effective head at time t_2;

d = effective inside diameter of standpipe = 3.461 cm (1.363 in.) at top and 32.9816 cm (12.985 in.) at middle;

d_1 = inside diameter of bottom casing = 12.700 cm (5 in.);

a_1 = +1 for impermeable base with thickness b_1, 0 for infinite (i.e., 20 times D_1) depth of tested material, and -1 for permeable base with thickness b_1 and;

b_1 = thickness of tested layer between bottom of device and top of underlying stratum.

CHP tests were conducted by taking measurements at different time intervals up to about 30 to 60 minutes. Generally, measurements showed decreasing permeability with time, indicating increasing saturation in the material. For comparison of K_{CHP} values between the test sites, the lowest permeability value is reported in this report.

INSTRUMENTATION

Vibrating wire type Geokon sensors were used in this study. The sensors included Geokon 4800 earth pressure cells (EPCs) and Geokon 4500 piezometers. Campbell Scientific data acquisition (DAQ) system consisting of CR1000 or CR5000 data loggers, multiplexers, and vibrating wire readers, were used to record the readings on-site (Figure 38 and Figure 39). The DAQ system was placed in a sealed enclosure and was battery powered through a solar panel (Figure 40).

EPCs and piezometers require temperature corrections to adjust the sensor readings. Temperature readings are recorded using thermistors attached to the sensors. The raw frequency values are converted to digits which are then used to calculate the corrected sensor readings (Equation 22 and 23):

$$R = \frac{f^2}{1000} \tag{22}$$

where, R = digit value and f = vibrating wire sensor frequency;

$$P = \left((R_1 - R_0) * G\right) + \left((T_1 - T_0) * T'\right) \tag{23}$$

where P = reading;

R_1 = current reading in digits;

R_0 = initial calibration reading;

G = linear gauge factor;

T_1 = current sensor temperature (°C)

T_0 = initial calibration temperature (°C); and

T' = temperature correction factor.

Geokon 4800 (Figure 41) EPCs consist of two flat plates welded together and separated by a small gap filled with hydraulic fluid. Increasing earth pressure squeezes the two plates together and builds up pressure in the fluid. The hydraulic fluid flows into the pressure transducer where the vibrating wire is located. The change in tension due to pressure, results in a change in frequency which is used to calculate the earth pressure.

Geokon 4500 (Figure 42) piezometers use a wire connected to a diaphragm in the device. Water passes through a porous stone in the front of the device. The diaphragm then adjusts to the water pressure by either slacking or tightening the wire. The change in tension results in a change in frequency which is then used to calculate the water pressure.
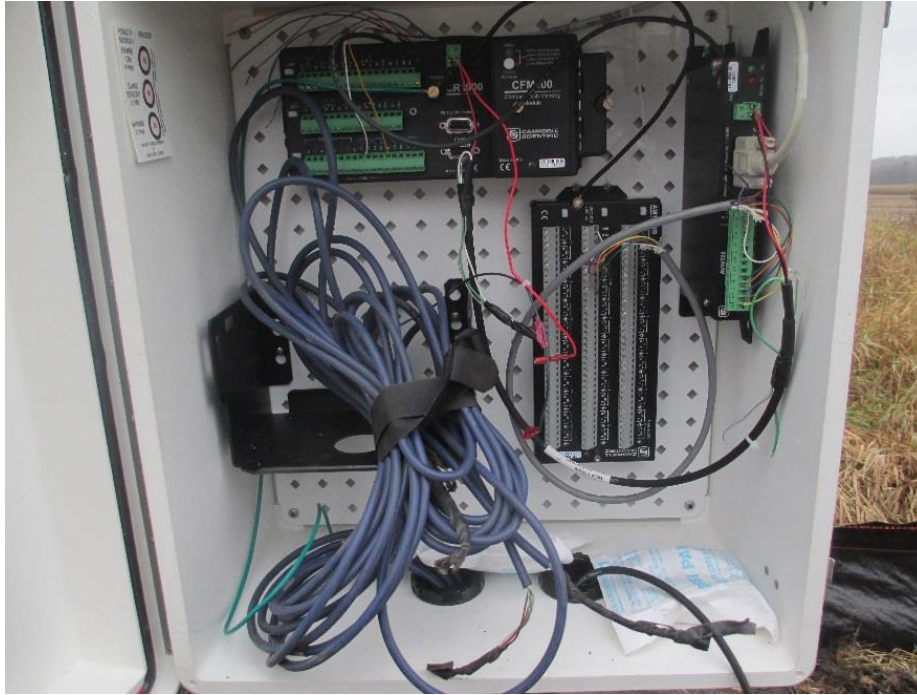
Figure 38. CR 1000 DAQ system
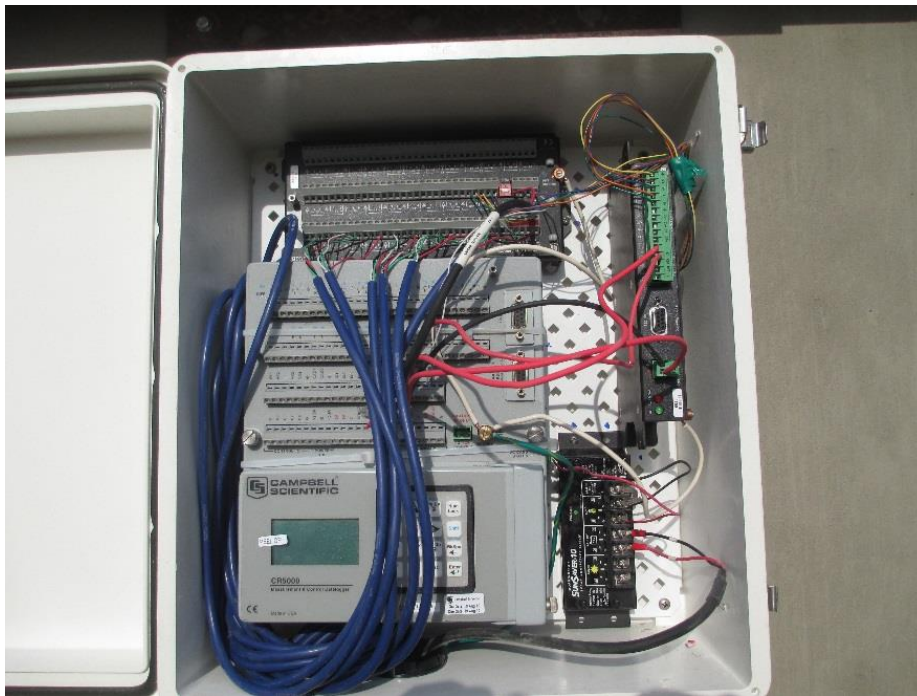
Figure 39. CR 5000 DAQ system

Figure 40. Sealed enclosure and solar panel used for the DAQ system
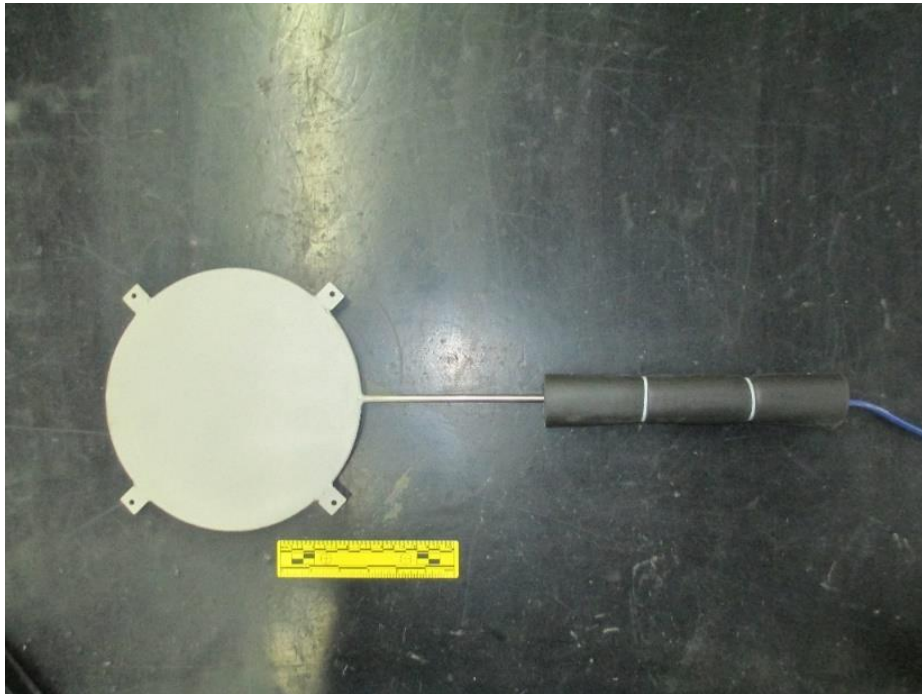
Figure 41. Geokon 4800 earth pressure cell

Figure 42. Geokon 4500 piezometer

Geokon 3400 dynamic piezometers were used in the bridge abutment model used in laboratory testing (Figure 43). In this dynamic sensors, pressure is applied on the transducer as water enters the piezometer. The pressure from the water causes the voltage to change, which is used to calculate pressure. Eq. 24 is used to calculate pressure:

$$P = \left((R_1 - R_0) * G\right) \tag{24}$$

where: R_1 = voltage reading after water pressure is applied;

R_0 = initial voltage reading; and

G = gage factor.
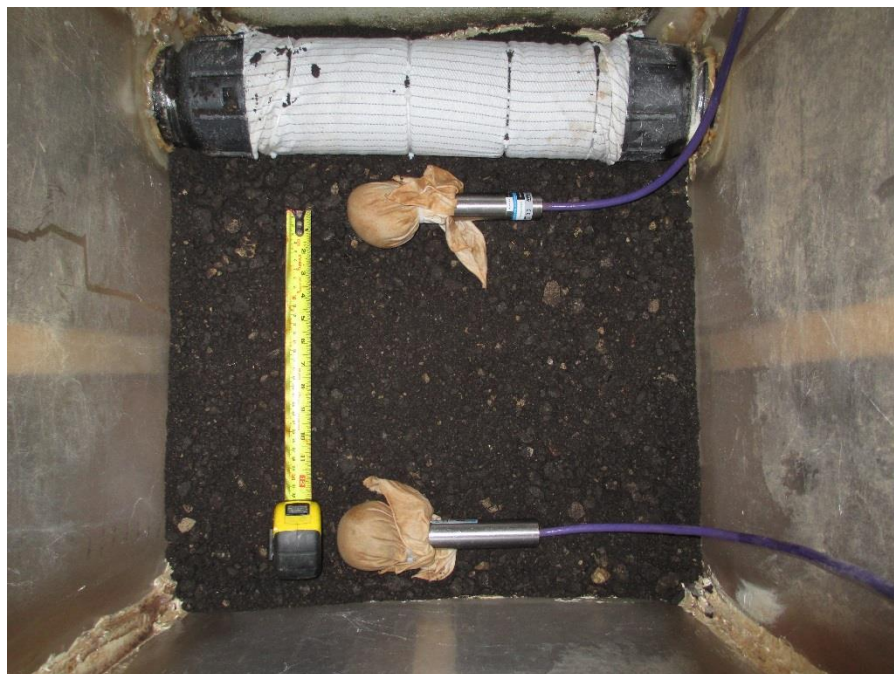
Figure 43. Geokon 3400 dynamic piezometers inside abutment model

NUMERICAL ANALYSIS

Geostudio Seep/W™ finite element modelling (FEM) program was used in this study to analyze the transient flow conditions in the backfill material. FEM analysis can take into account complex boundary conditions and geometrics to better understand the stress state in the soil and simulate the transient flow conditions (Fredlund et al. 1987). Soils in transient flow transition from a saturated to an unsaturated state, which affects the flow rate.

In this study, results obtained from the laboratory abutment scaled model tests were used to calibrate the input parameters used in the FEM models, and the calibrated values for the different materials were used to assess field conditions. The primary goal of the numerical analysis was to determine the rate of change in pore pressures with time (i.e., time for drainage). In the following discussion, the input parameters used in the FEM model, the methods followed to determine those parameters, and results of a parametric study that was conducted to assess the influence of the different input parameters are presented. The abutment model setup is shown in Figure 44. The FEM model was setup with an average mesh size of 15 mm with 1542 elements and 1628 nodes.
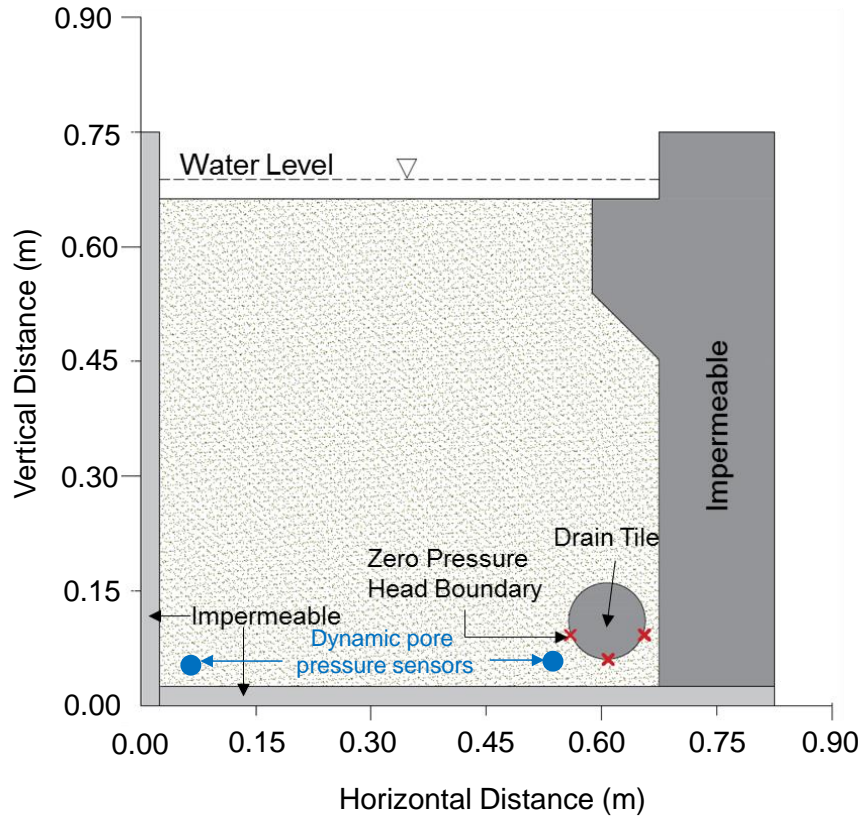
Figure 44. Abutment model setup in FEM analysis

Input Parameters in the FEM Model

The following are the input parameters used to model the granular backfill and the pipe underdrain system in the FEM model:

- Saturated hydraulic conductivity, K_{sat};
- Soil suction curve fitting parameters: *a*, *n*, and *m*;
- Volumetric moisture content at saturation, θ_s
- Coefficient of volumetric compressibility, m_v

The K_{sat} value was determined from CHP tests conducted on the material, both in situ and in laboratory (in abutment model tests).

Soil suction parameters are defined in the FEM model based on Fredlund and Xing (1994) model for suction versus volumetric moisture content:

$$\theta(\psi, a, n, m) = C(\psi) * \frac{\theta_s}{((\ln(e + (\frac{\psi}{a})^n)^m}$$
(25)

As an alternative to time-consuming laboratory testing to determine the curve fitting parameters *a*, *n*, and *m,* in this study, they were estimated using relationships developed by Zapata and Houston (2008) with soil gradation parameters:

$$a = \frac{0.8627(D_{60})^{-0.751}}{6.895} \tag{26}$$

$$n = 7.5 \tag{27}$$

$$m = 0.1772 * \ln(D_{60}) + 0.7734 \tag{28}$$

where D_{60} = diameter corresponding to 60% finer from sieve analysis in mm.

The θ_s is the volume of water in the saturated soil. This value was determined based on soil weight-volume relationships, for assumed (for field conditions) or measured (lab abutment model tests) unit weight of the material and measured gravimentric moisture content.

The m_v value can be determined from laboratory oedometer tests and is defined as the ratio of volumetric strain over change in effective stress as defined in Equation 29.

$$m_V = \frac{\Delta e}{(1+e_o)\Delta\sigma_v'} \tag{29}$$

where e_o = initial void ratio;

Δe = change in void ratio with application of vertical effective stress; and

$\Delta\sigma_v'$ = change in vertical effective stress.

The m_v value depends on the stress range over which it is calculated. For this study, an initial value of 1.05E-5/kPa is assumed as the m_v value, per GeoStudio Manual, and the value was modified to calibrate with laboratory measured values.

In the FEM model setup, the pipe underdrain system was modeled using a zero head pressure point boundary condition. The abutment walls and the layers beneath the abutment backfill were modeled as impermeable layers where no flow could occur for laboratory scaled model setup. For analysis on field bridge abutments, foundation layers were not assumed as impermeable layers.

Parametric Study

A parameteric study was performed to assess the influence of the input parameters in calculating the pore pressure dissipation times. Results are presented in Figure 45 to Figure 50, wherein one parameter was modified while all other parameters were held constant.

The results indicated that parameters K_{sat}, m_v, θ_s, and a had the most effect on the dissipation results near the drain tile. Parameter n had negligible effect and parameter m had some effect after about 70% of dissipation.

For the analysis performed in this study, the critical parameters K_{sat} and θ_s were directly obtained from laboratory or field testing. The initial values for parameters a, m, and m_v were determined as described above, but were modified to match the numerical analysis results with the measured values. The parameter n was held constant at 7.5.
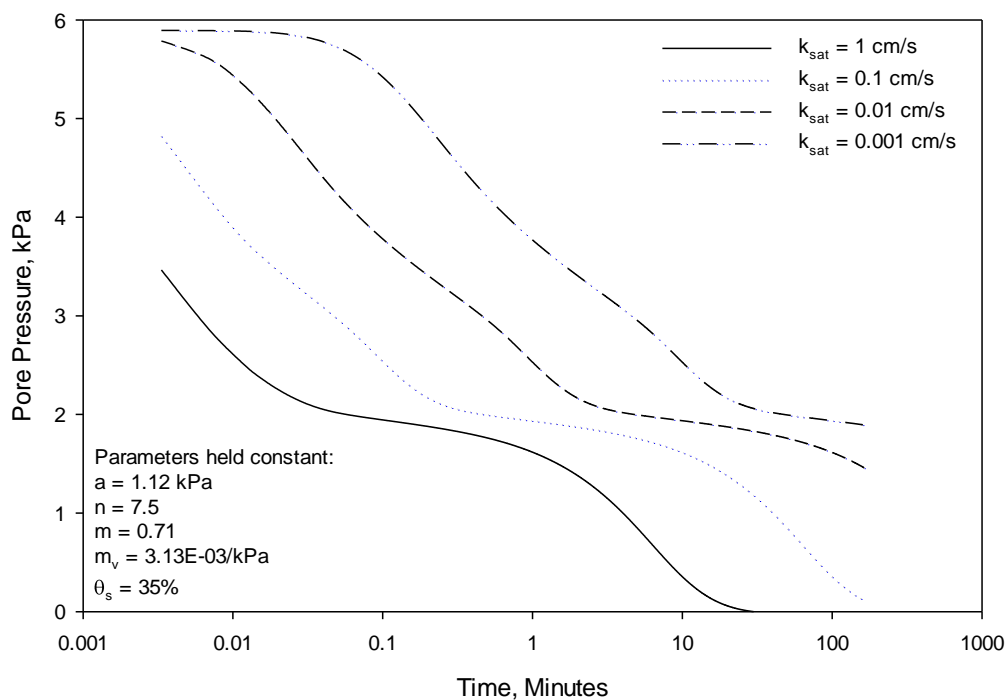
Figure 45. Effects of changing parameter K_{sat}
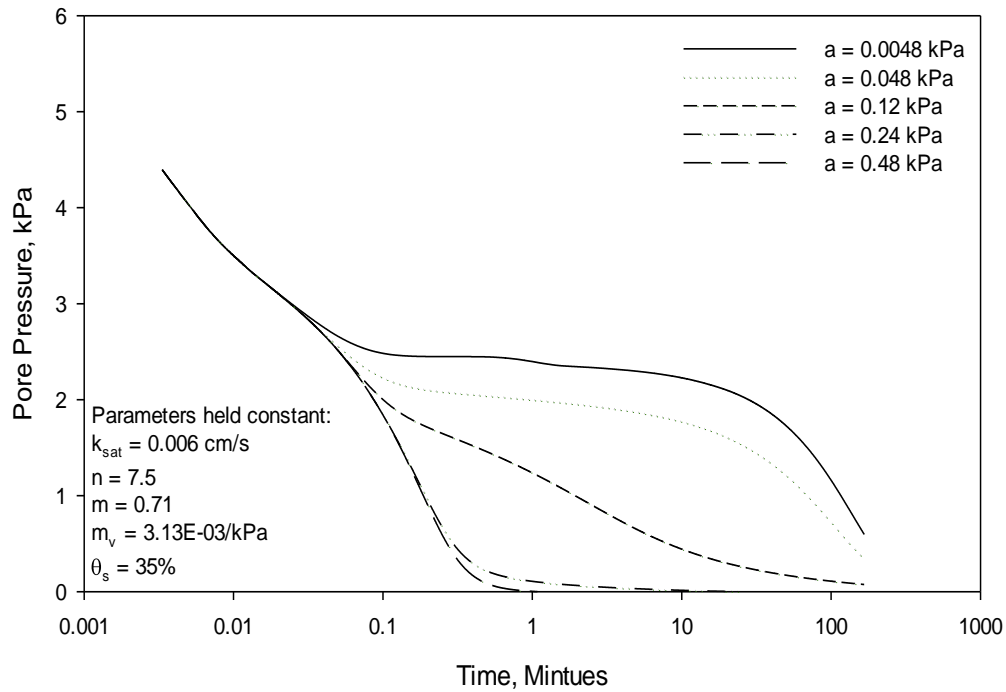
Figure 46. Effects of changing parameter *a*
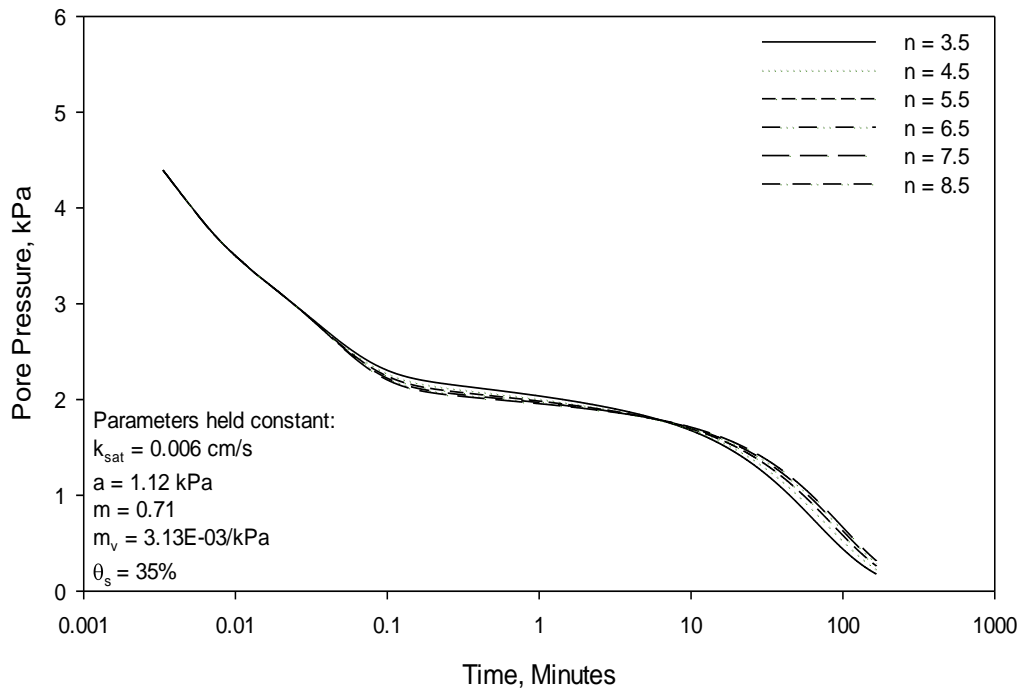
Figure 47. Effects of changing parameter *n*
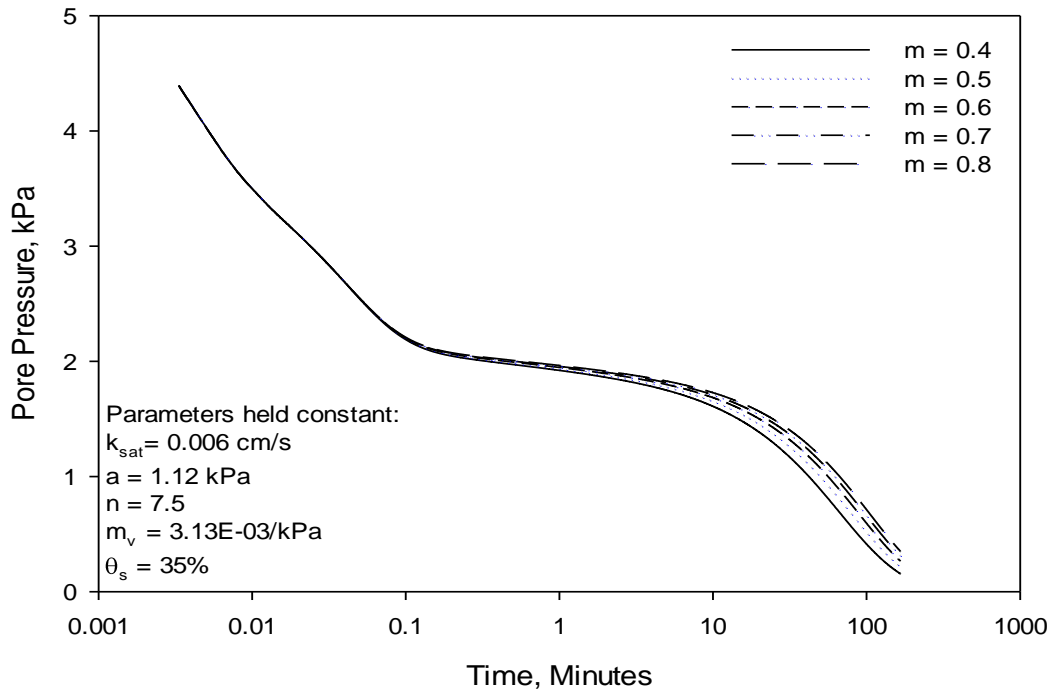
Figure 48. Effects of changing parameter *m*
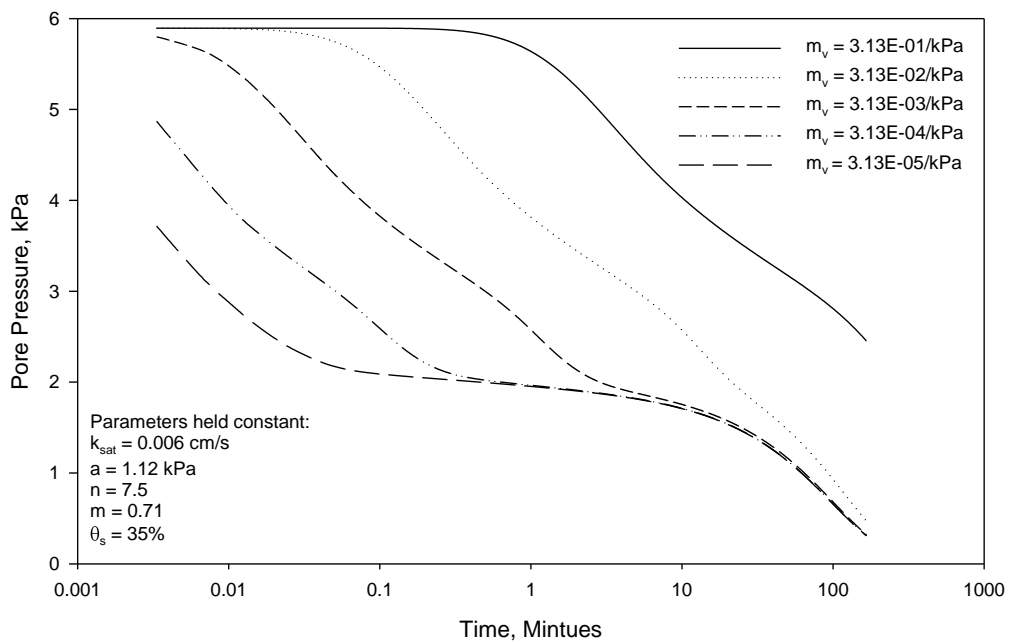
Figure 49. Effects of changing parameter *m_v*
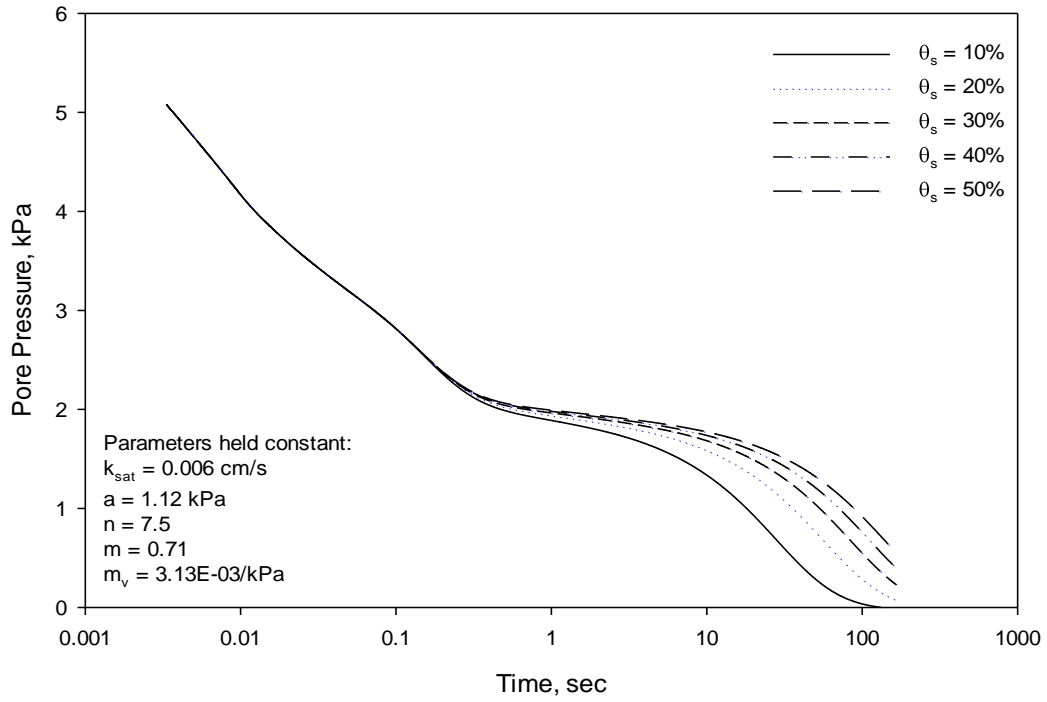
Figure 50. Effects of changing parameter θ_s

CHAPTER 4. LABORATORY TEST RESULTS AND ANALYSIS

This chapter summarizes the laboratory test results of the materials used in this study (Table 7). Four of the materials were obtained from bridge construction sites in WI. RAP and RAS materials were obtained from stockpiles at Mathy Construction Company in Onalaska, WI. The RAP and RAS materials were evaluated to determine whether these types of materials are suited for bridge abutment backfill.

This chapter is organized by the characteristics of the materials that were obtained by conducting particle-size analysis and classification tests, standard Proctor and relative density, permeability, direct shear, and oedometer collapse tests. After discussing the material properties, results of laboratory scaled abutment model test results are provided. At the end of this chapter, a summary of key findings from laboratory testing are provided.

Table 7. Materials and source locations

Material	Source location
Structure backfill	Slovak Valley Creek Bridge, Dunn County, WI
Structure backfill	Schwartz Road Bridge, Oconto County, WI
Structure backfill	Hobbles Creek Bridge, Price County, WI
Grade 1 granular backfill	Badger Road Bridge, Grant County, WI
Recycled asphalt pavement (RAP)	Mathy Construction Company, Onalaska, WI
Recycled asphalt shingles (RAS)	Mathy Construction Company, Onalaska, WI

Gradation Properties and Soil Classification

Figure 51 shows the particle-size analysis results for all materials with gradation limits proposed for erodible materials by Briaud et al. (1997). Results of particle-size analysis and soil classification tests are summarized in Table 8.
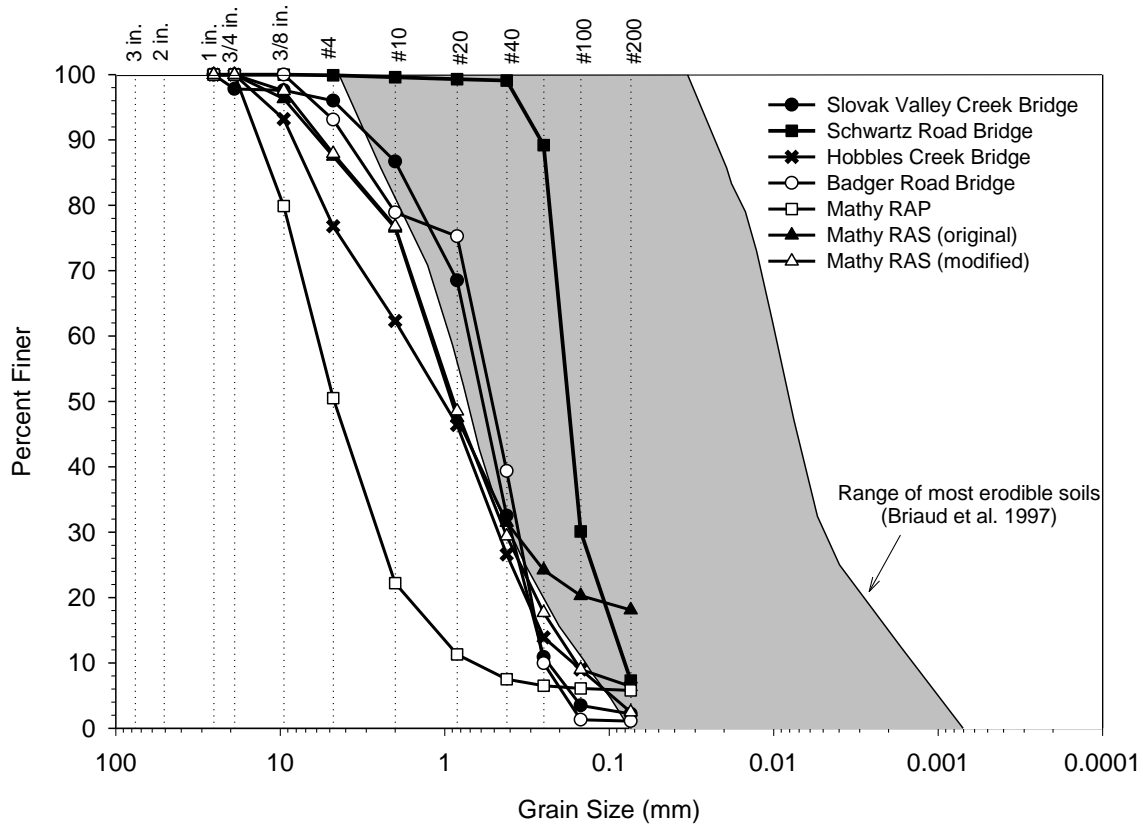
Figure 51. Particle size analysis results for all materials with Briaud et al. (1997) proposed range for most erodible soils

Mathy RAS material consisted of 18% fines passing the No. 200 sieve (shown as Mathy RAS original in Table 2). Since the material did not meet the WisDOT structure backfill or grade 1 granular backfill gradation limits, the fines were sieved out and the material gradation properties are presented in Table 2 as Mathy RAS modified. All remaining tests were performed only on Mathy RAS modified material.

With the exception of RAP, all other materials classified as sandy materials (SP, SP-SM, SM, and SW). RAP classified as a gravelly material (GW-GM). Schwartz Road Bridge material fell fully within the range of most erodible soils. Backfill materials from Slovak Valley Creek Bridge and Badger Road Bridge fell partially within the band, while the remaining materials did not.

Table 8. Results of particle-size analysis and soil classification tests

Property	Slovak Valley Creek Bridge	Schwartz Road Bridge	Hobbles Creek Bridge	Badger Road Bridge	Mathy RAP	Mathy RAS (Original)	Mathy RAS (Modified)
USCS classification	SP	SP-SM	SP-SM	SP	GW-GM	SM	SW
USCS classification description	Poorly graded sand	Poorly graded sand to silty sand	Poorly graded sand to silty sand	Poorly graded sand	Well graded sand to silty gravel	Silty sand	Well graded sand
AASHTO classification	A-1-b	A-3	A-1-b	A-1-b	A-1-a	A-1-b	A-1-b
Coefficient of uniformity	2.92	1.83	9.71	2.38	8.45	Not Applicable	7.29
Coefficient of curvature	0.96	1.11	0.75	0.90	1.72		1.00
D_{10} (mm)	0.2414	0.1052	0.1773	0.2504	0.7054		0.1611
D_{30} (mm)	0.4046	0.1499	0.4782	0.3672	2.6890	0.3876	0.4359
D_{60} (mm)	0.7057	0.1923	1.7212	0.5949	5.9632	1.2088	1.1746
Gravel % (>4.75 mm)	4.0	0.1	23.2	6.9	50.5	12.5	12.1
Sand % (4.75-0.074 mm)	93.8	92.6	70.4	92.4	43.7	69.4	85.4
Silt+Clay % (<0.074 mm)	2.2	7.3	6.4	0.7	5.8	18.1	2.5

Compaction Properties

Standard Proctor and relative density tests were performed on all of the materials. Results of maximum dry unit (γ_{dmax}) and optimum moisture content (w_{opt}) from standard Proctor tests and maximum index density (at oven-dried moisture content) from vibratory compaction test, and

bulking moisture contents (w_B) from Proctor and vibratory compaction tests are summarized in Table 9.

Of the materials obtained from the four bridge sites, Badger Road Bridge material had the highest maximum dry unit weight and Schwartz Road Bridge material had the lowest dry density. All four materials indicated bulking moisture contents between 1.5% and 4.1%. Vibratory compaction tests and Proctor compaction tests showed slightly different bulking moisture contents.

RAS (modified) material produced the lower maximum dry unit weight of all materials, and were similar to values reported by Soleimanbeigi et al. (2011). Both RAP and RAS did not show a bulking moisture content.

Table 9. Summary of Proctor and vibratory compaction test results

Property	Slovak Valley Creek Bridge	Schwartz Road Bridge	Hobbles Creek Bridge	Badger Road Bridge	Mathy RAP	Mathy RAS (modified)
γ_{dmax} (kN/m^3), standard Proctor	17.5	15.4	18.2	18.3	16.5	11.5
w_{opt} (%) standard Proctor	7.5	9.3	8.3	5.8	12.5	6.5
w_B (%) standard Proctor	3.0	1.5	3.9	1.9	—*	—*
γ_{dmax} (kN/m^3), Vibratory Compaction at oven-dried w	16.7	14.6	17.8	18.8	14.8	10.0
w_B (%)Vibratory Compaction	4.1	—*	1.8	3.6	—*	—*

* Not indicated
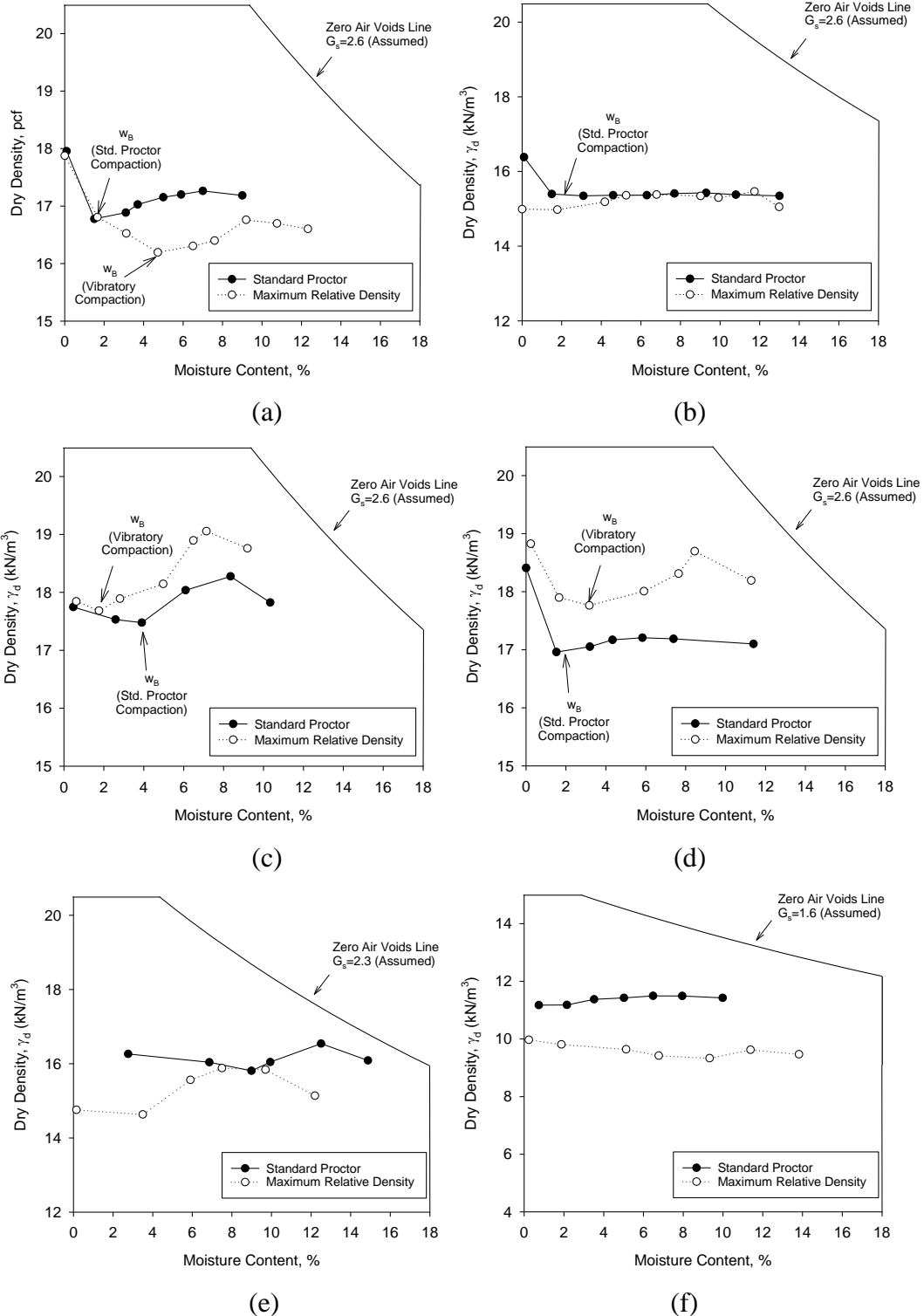
Figure 52. Compaction results for: (a) Slovak Valley Creek Bridge, (b) Schwartz Road Bridge, (c) Hobbles Creek Bridge, (d) Badger Road Bridge, (e) RAP, and (f) RAS

Drainage Properties

Falling head permeability tests were conducted at multiple times after saturating the material. All results are presented in Appendix B. K_{sat} after 30 minutes and 24 hours of saturation are presented in Figure 53. These results presented are for a head change from about 40 to 30 cm.
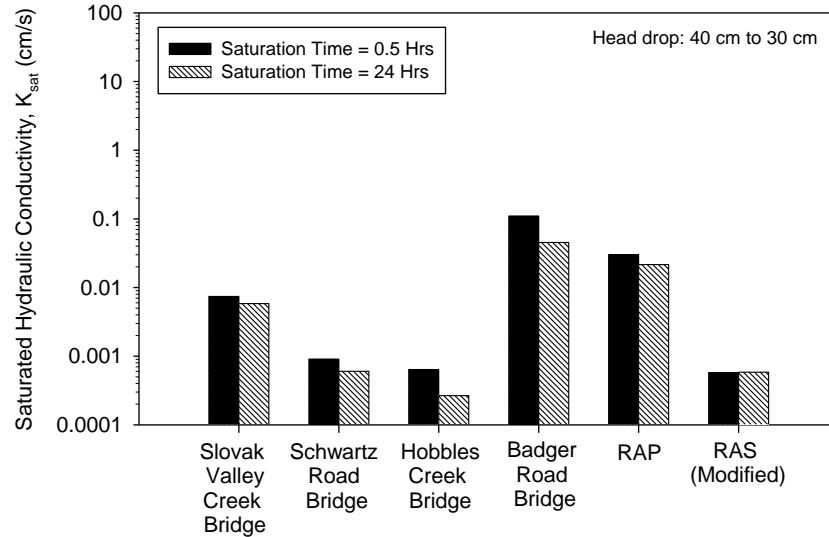
Figure 53. K_{sat} values from falling head permeability tests after 30 minutes and 24 hours of saturation time

The K_{sat} values of the four materials from the bridge sites varied by nearly three orders of magnitude (0.0002 to 0.11 cm/sec). Badger Road Bridge material had the highest K_{sat} and the Hobbles Creek Bridge had the lowest K_{sat}. The K_{sat} values reduced by 20% to 60% after 24 hours of saturation for the four materials, when compared to values obtained after 30 minutes of saturation time. The decrease in K_{sat} with time can be attributed to migration or settling of fine particles to the bottom of the sample.

Of the two recycled materials, RAP material showed the highest K_{sat} (about 0.03 cm/sec). RAS material showed $K_{sat} = 0.0006$ cm/sec which was similar to the Hobbles Creek material. The K_{sat} reduced by about 28% after 24 hours of saturation for RAP material, but did not show any difference for RAS material, when compared to 30 minutes saturation time.

The K_{sat} values for the RAS material were similar to the values reported by Soleimanbeigi et al. (2011). During laboratory testing, it was observed that the cellulose particles within the RAS material were floating in the water.

The K_{sat} values obtained from laboratory testing were compared with estimated values using different empirical relationships in Figure 54.

$$\begin{array}{ll} \text{Hazen (1930):} & K_{sat}(cm/s) = cD_{10}^2 \\[2mm] \text{Moulton (1980):} & K_{sat}(cm/s) = 1.2C_u^{0.735}D_{10}^{0.89}\left(\dfrac{e^3}{1+e}\right) \\[2mm] \text{Cedergren (1974):} & K_{sat}(cm/s) = 0.001D_{100}^{1.4} \\[2mm] \text{Shahabi et al. (1984):} & K_{sat}(cm/s) = \dfrac{6.214\times10^5 D_{10}^{1.478}n^{6.654}}{P_{200}^{0.597}}\times 0.000353 \end{array}$$
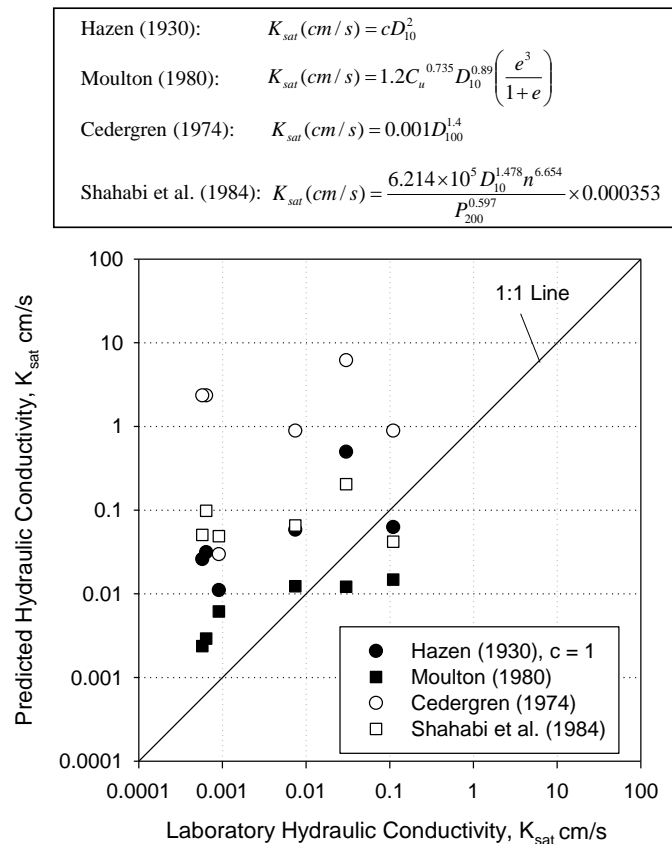
Figure 54. Comparison of measured and predicted hydraulic conductivities using different empirical relationships

The empirical equations proposed by Hazen (1930), Moulton (1980), Cedergren (1974), and Shahabi et al. (1984) were used for this comparison and are shown in Figure 54. Moulton and Cedergren equations were developed for aggregates while Hazen and Shahabi et al. equations were developed for sands.

With the exception of few cases, the empirical equations generally were higher than the measured values. K_{sat} values predicted using Moulton's equations were comparatively closer to the measured values than other relationships.

Shear Strength Properties

Drained friction angles (ϕ') and apparent cohesion (*c*') values from the direct shear tests are summarized in Table 10 and the Mohr-Coulomb failure envelopes are shown in Figure 55. All

materials were compacted to a target 100% standard Proctor maximum dry unit weight at in-situ moisture content.

Table 10. Direct shear test results

Material	Drained Friction Angle, φ' (degrees)	Apparent Cohesion, c' kPa
Slovak Valley Creek Bridge	29.7°	12.11
Schwartz Road Bridge	30.1°	3.52
Hobbles Creek Bridge	27.0°	6.35
Badger Road Bridge	31.8°	4.76
Mathy RAP	—*	—*
Mathy RAS	—*	—*

*could not be determined due to creep behavior, see text for details

The ϕ' values of the four bridge materials ranged from about 27 to 33 degrees with an apparent cohesion (c') of 4 to 12 kPa. Results of shear stress and vertical strain versus horizontal strain plots for these materials are provided in Appendix B.

The ϕ' values for RAP and RAS could not be calculated because of the secondary compression or creep behavior of the materials (Figure 56 and Figure 57), with increasing shear stresses even at 15% horizontal strain. This behavior was also noted previously by Rathje et al. (2006) and Soleimanbeigi et al. (2011).
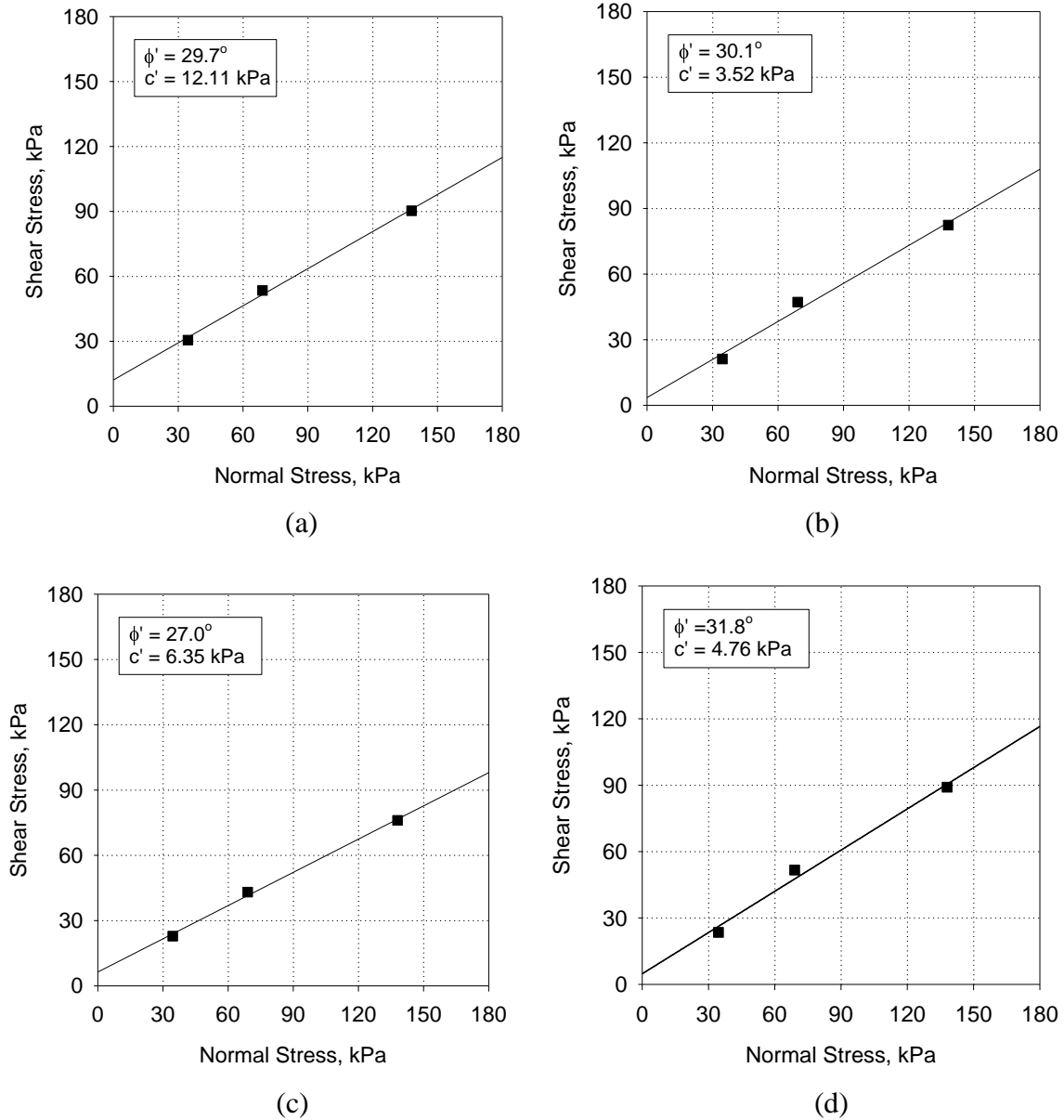
Figure 55. Direct Shear results for: (a) Slovak Valley Creek Bridge, (b) Schwartz Road Bridge, (c) Hobbles Creek Bridge, (d) Badger Road Bridge
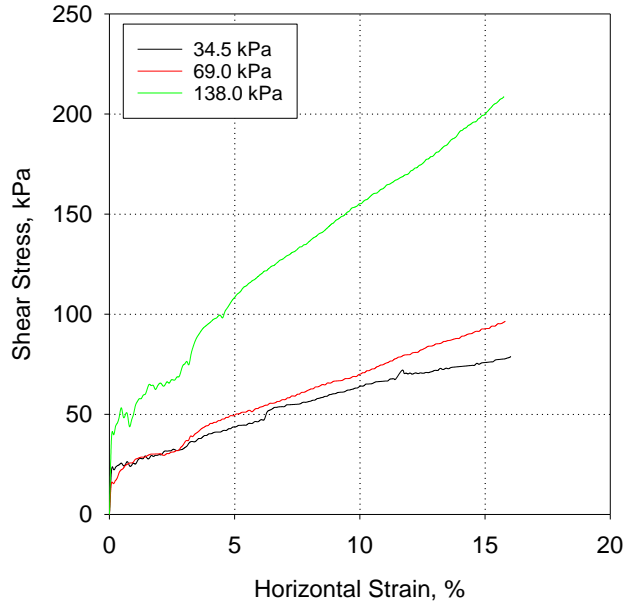
Figure 56. Creep behavior of RAP during direct shear test
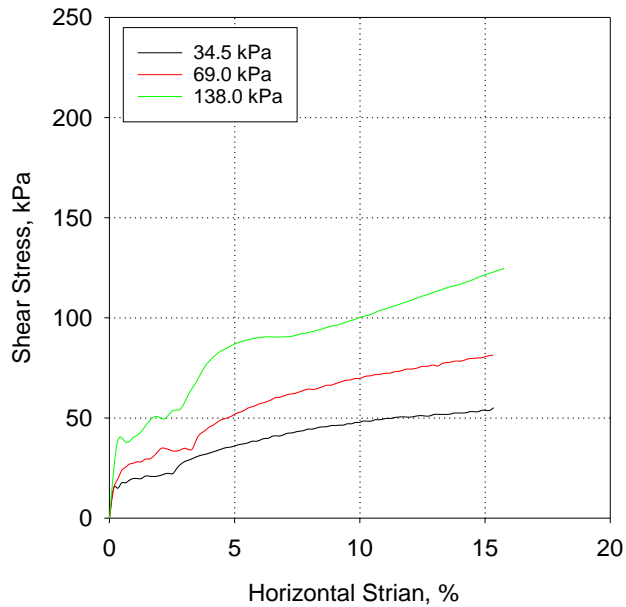
Figure 57. Creep behavior of RAS during direct shear test

Collapse Test Results

Collapse index (I_c) values versus moisture content for the four materials obtained from bridge sites are provided in Figure 55. Of the four materials, I_c was higher at about 3.5% for the Hobbles Creek material which classifies as moderate degree of collapse per ASTM D5333, followed by about 0.8% for Slovak Valley Creek material which classifies as slight degree of

collapse per ASTM D5333. The materials from the remaining two projects showed collapse < 0.2% which also classifies as slight degree of collapse per ASTM D5333.

For both Hobbles Creek and Slovak Valley Creek materials, I_c values were higher near bulking moisture contents (ranging between 2 and 4%). This indicates the importance of placing material at moisture contents away from the bulking moisture content.

All materials, except the Hobbles Creek material, showed decreasing I_c with increasing overburden stress. This decreasing trend means that the overburden stress is overcoming some of the capillary tension between the particles and reducing the collapse after wetting.

Collapse test results for RAP at four different moisture contents are presented in Figure 59 to Figure 61. At the end of each load increment (after 12 hours), the strain continued to increase which is further evidence of the creep behavior exhibited by the RAP material. At the three moisture contents tested (0% to 4.5%), the material showed negligible I_c values up to 55.2 kPa overburden stress, but showed a collapse strain of 1.4 to 2.4% when 110.3 kPa overburden stress was applied. At 3% moisture content, the material exhibited I_c = 1.9 to 3.8% at the three overburden stresses applied, which classifies as slight to moderate degree of collapse per ASTM D5333. These collapse values were similar to the values reported for RAP by Rathje et al. (2005).

Collapse tests were performed on RAS material at its natural moisture content (2%) (Figure 62). The material exhibited I_c values ranging from 4% to 5% at the three overburden stresses applied, which classifies as moderate degree of collapse per ASTM D5333.

Table 11 summarizes gradation parameters, bulking moisture contents, and the I_c test results for these materials. Although the degree of collapse according to ASTM D5333 was classified as slight to moderate of the materials tested in this study, a 1% collapse on a 3 m (10 ft) of backfill material can lead to about 30 mm (> 1 in.) of settlement. In that regard, any post-construction settlement related to collapse can be problematic and should be avoided. Based on the laboratory test results, placing material away from the bulking moisture content (i.e., in wet condition) can help avoid collapse related settlements upon wetting.
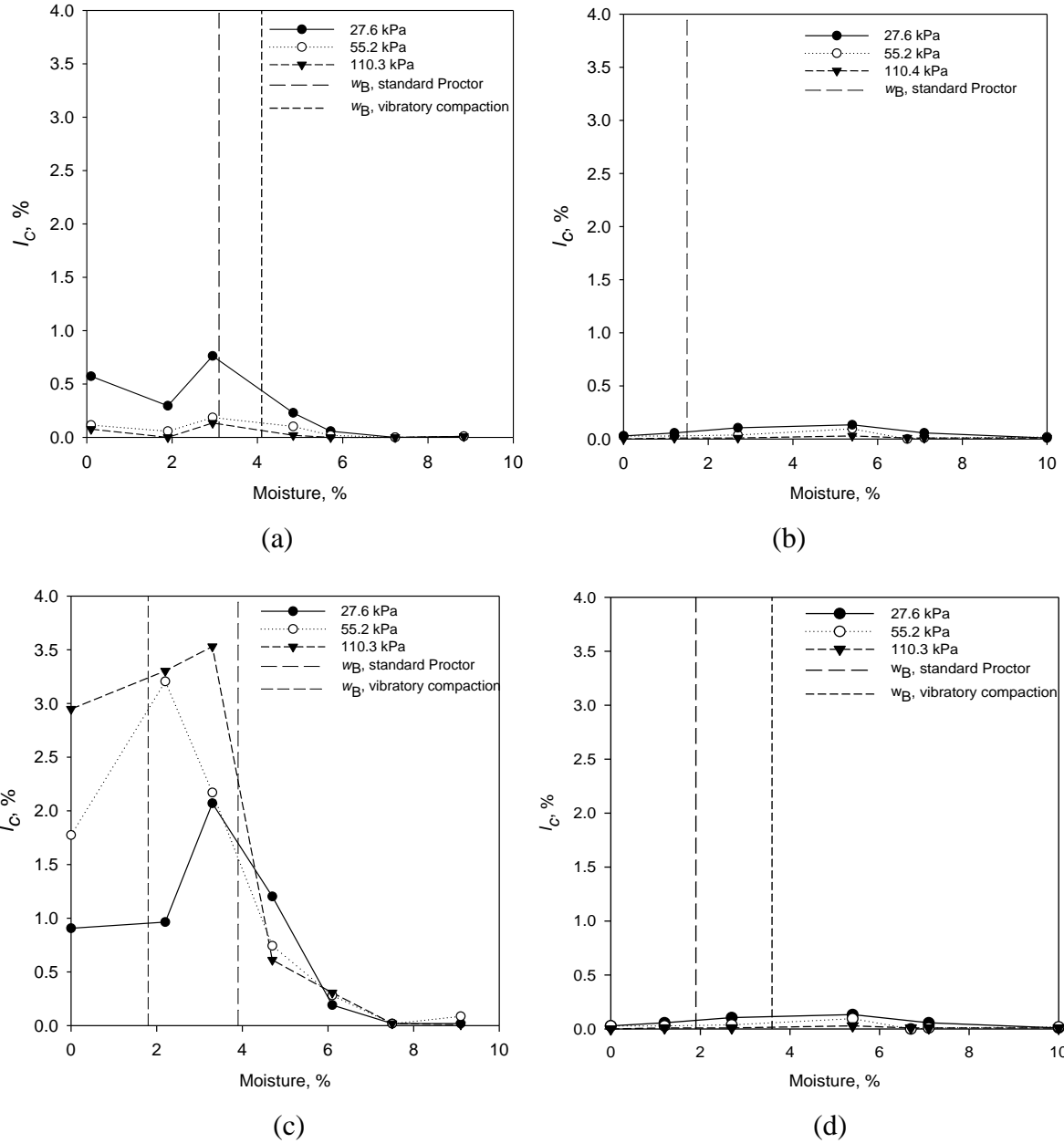
Figure 58. Collapse strains versus compacted moisture content of the material: (a) Slovak Valley Creek Bridge, (b) Schwartz Road Bridge, (c) Hobbles Creek Bridge, and (d) Badger Road Bridge
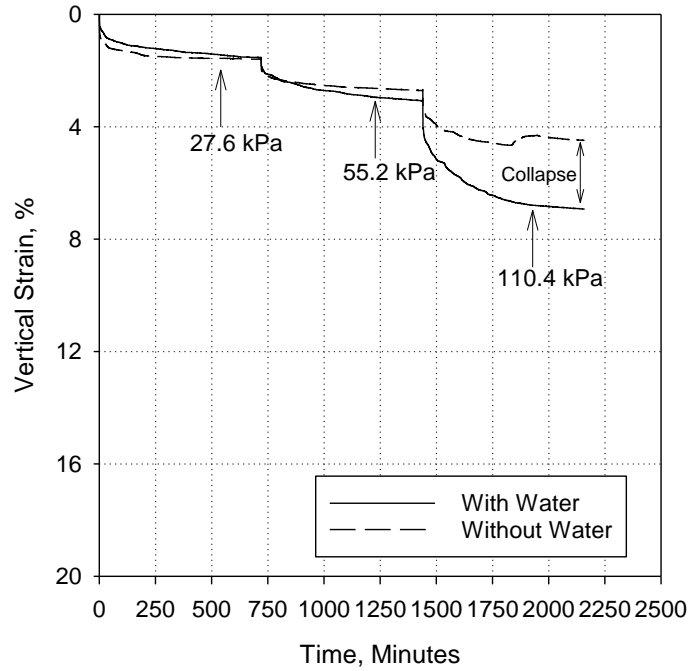
Figure 59. Collapse results for RAP at 0% moisture content
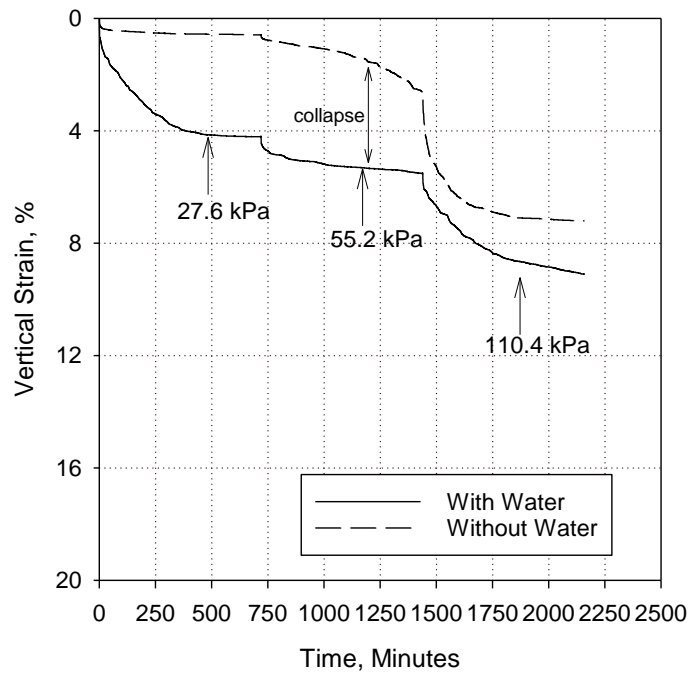
Figure 60. Collapse results for RAP at 3% moisture content
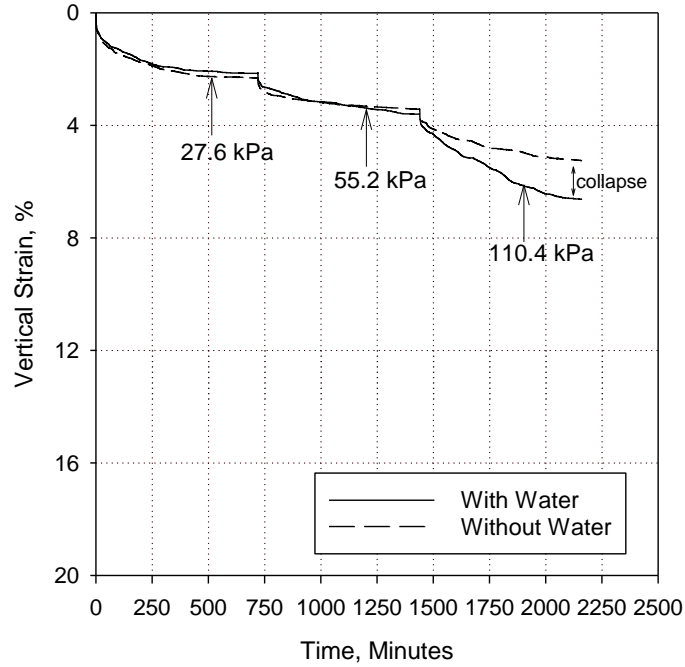
Figure 61. Collapse results for RAP at 4.5% moisture content
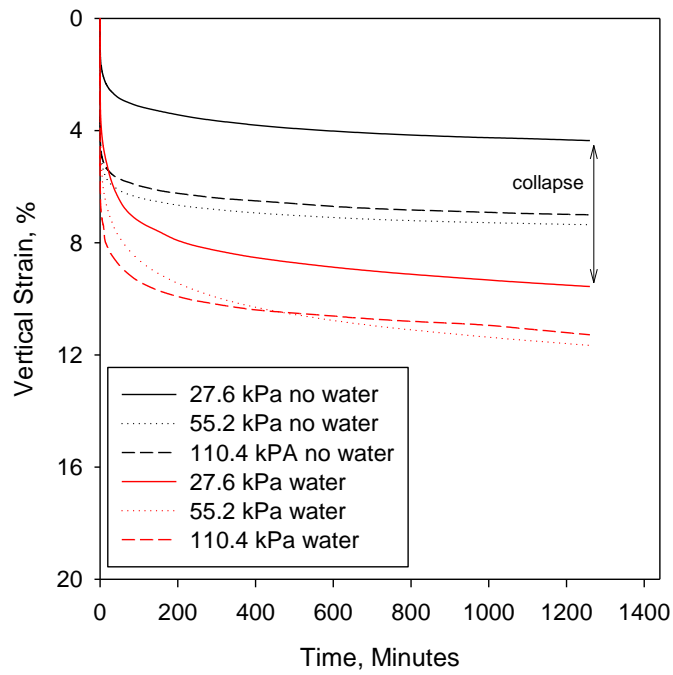
Figure 62**. Collapse results of RAS at 2% moisture**

Table 11. Summary of gradation parameters and collapse index results

Material	D_{60} (mm)	D_{30} (mm)	D_{10} (mm)	C_u	C_c	P_{200}, %	w_B,%[a]	Maximum Collapse, I_c, %[c]	Degree of Collapse per ASTM D5333
Slovak Valley Creek Bridge	0.70	0.40	0.24	2.92	0.96	2.2	3 - 4.1	0.1 - 0.8	Slight
Schwartz Road Bridge	0.19	0.15	0.10	1.83	1.11	7.3	9.3	< 0.1 - 0.10	Moderate
Hobble Creek Bridges	1.72	0.48	0.18	9.71	0.75	6.4	1.8 - 3.9	2.1 - 3.5	Slight
Badger Road Bridge	0.59	0.37	0.25	2.38	0.9	0.7	1.9 - 3.6	< 0.1 - 0.1	Slight
RAP	5.96	2.69	0.71	8.45	1.72	5.8	—[b]	3.8 - 4.3	Slight to Moderate
RAS	1.17	0.43	0.16	7.29	1	2.5	—[b]	4.3 - 5.2	Moderate

[a] Bulking moisture contents observed from Proctor and vibratory compaction methods
[b] not present
[c] I_c range from different overburden stresses at or near bulking moisture contents

Abutment Model Test Results and Analysis

Scaled abutment model tests were performed on all materials except RAS. Tests were not attempted on RAS material because of the time it consumed to prepare large quantities of the modified gradation material to meet with Wisconsin DOT gradation specifications.

After placing and compacting the materials to desired unit weight, the abutment model was sealed and flooded. Pore pressure sensor readings were monitored to ensure saturation. After that, the drain tiles were opened for drainage and pore pressure dissipations were monitored near the drain tile and near the back face of the abutment model wall. FEM numerical analysis was conducted to calibrate the input parameters. Results obtained from the sensor located near the drain tile were used in the calibration process.

In the following subsections results of abutment model testing and numerical analysis are organized for each material type. The results include moisture content and dry unit weight

measurements of the material compacted in the abutment model, APT and CHP test results after compaction, measured pore pressure dissipations, and results from numerical analysis and Casagrande and Shannon (1952) methods in comparison with the measured values.

The Casagrande and Shannon method did not produce similar shaped curves for pore pressure dissipation versus time as produced by the numerical method or by the measured values. Therefore, the shape factor c value in the Casagrande and Shanon method was adjusted to match the measured 95% and 50% pore pressure dissipation results. This produced two different curves and are shown for comparison.

Predicted times for a given amount of pore pressure dissipations from numerical analysis and Casagrande and Shannon methods are compared with the measured values by calculating the standard errors of the estimations. The standard error value was determined relative to the measured values by calculating the difference between the measured and the predicted values, squaring the difference, calculating the sum of the difference's, and determining the square root of the sum.

Slovak Valley Creek Bridge Material

The material moisture content ranged from about 3% to 5%, similar to what was measured in situ (discussed later in Chapter 5). The relative compaction achieved was about 98% standard Proctor dry density at an average of about 4% moisture content. APT and CHP tests indicated K_{sat} of 0.57 cm/s (1616 ft/day) and 0.07 cm/s (198 ft/day), respectively. APT K_{sat} was about an order of magnitude higher than the CHP K_{sat}.

The measured pore pressure dissipations with time over a 4 hour period for the two sensors is presented in Figure 63. Predicted pore pressure dissipations from numerical analysis and Casagrande and Shannon (1952) method are also presented in Figure 63 for comparison with the measurement values. Input parameters used in the numerical analysis and the shape factor values used in the Casagrande and Shannon method are also shown in Figure 63.

Figure 63. Measured and predicted drainage times for Slovak Valley Creek Bridge backfill material: (a) near drain tile and (b) 36 cm away from drain tile near the backwall of the abutment

The measured (near drain tile) and predicted times of different percentages pore pressure dissipation (from 5% to 95% in 5% increments) are compared in Figure 64, which showed a standard error in prediction of about 28 minutes for the numerical analysis method, 66 minutes using the Casagrande and Shannon method with c = 6.2, and 215 minutes using Casagrande and Shannon method with c = 0.02.

The abutment model tests indicated time for 50% drainage (t_{50}) < 2 seconds and for 95% drainage (t_{95}) ~ 3 hours near the drain tile. The numerical analysis results also indicated very similar results near the drain tile. The numerical analysis results near the back face of the abutment wall, however, indicated longer times than the measured values.

The Casagrande and Shannon method on the other hand was sensitive to the shape factor c value used and indicated 3 to 9 times higher standard errors in the predicted values.
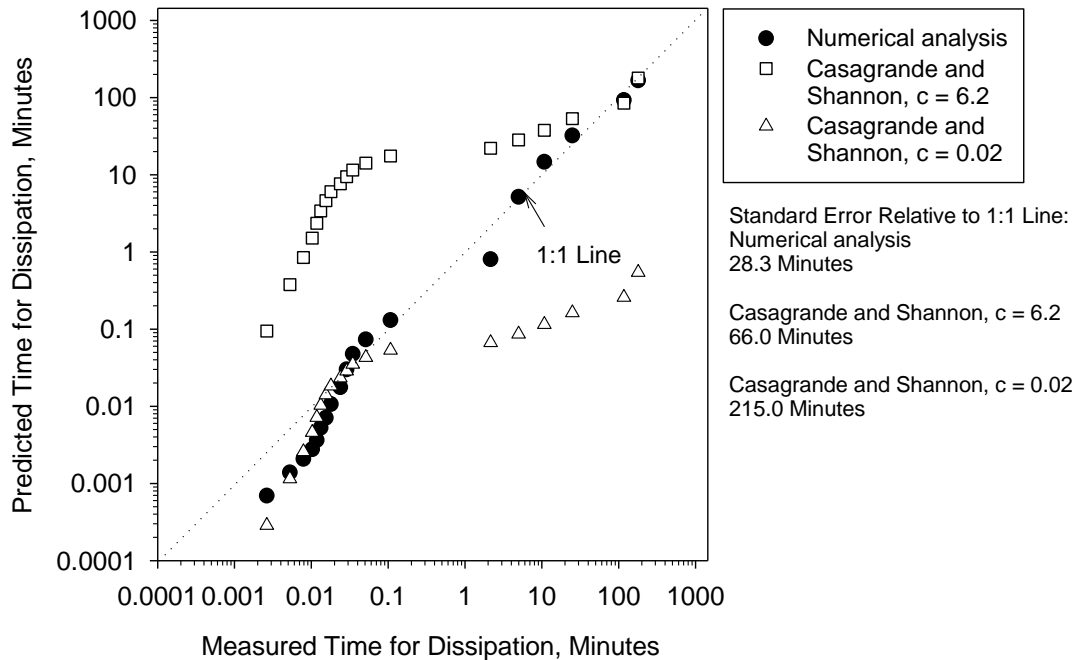
Figure 64. Linear regression analysis between measured and predicted dissipation times for different percentages of drainage for Slovak Valley Creek Bridge backfill

Schwartz Road Bridge Backfill Material

The material moisture content ranged from about 2% to 8%, similar to what was measured in situ (discussed later in Chapter 5). The relative compaction achieved was about 96% standard Proctor dry unit weight at 6% moisture content. APT and CHP tests indicated K_{sat} =

0.54 cm/s (1531 ft/day) and 0.04 cm/s (113 ft/day), respectively. APT K_{sat} was about an order of magnitude higher than the CHP K_{sat}.

Observations during testing indicated that as the water started draining, the backfill material started eroding into the drain tile. Pictures of drain tile at three different times after water started draining are provided in Figure 65. The erosion resulted in a depression at the top of the backfill (Figure 65d). The sock opening size was 0.425 mm (#40 sieve size) and the percent passing the #40 sieve on this material is 99%, which contributed to the erosion of the material.

(a)   (b)

(c)   (d)
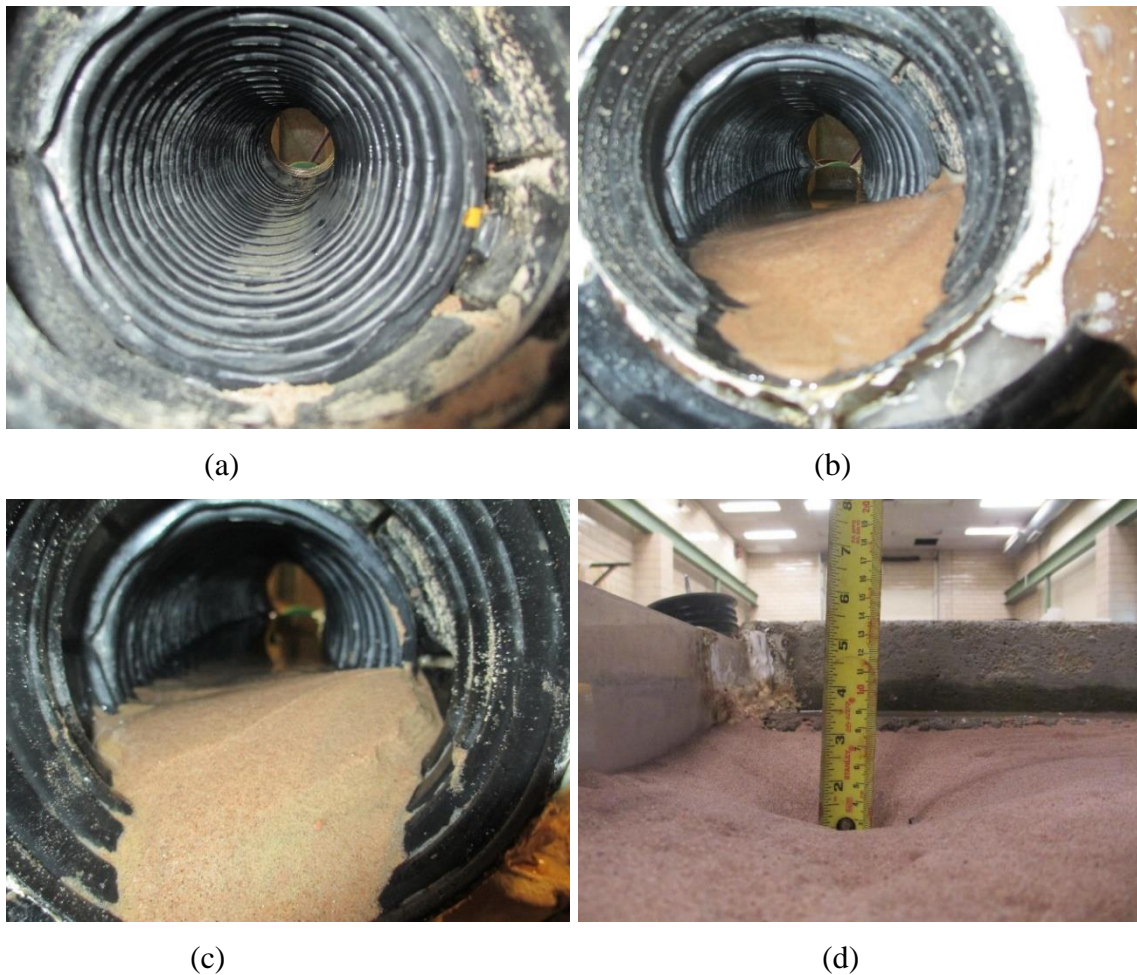
Figure 65. Drain tile at different times: (a) t = 0 min, (b) t = 3 min, and (c) t = 3.5 hours, and (d) depression at the surface because of material erosion at t = 24 hours
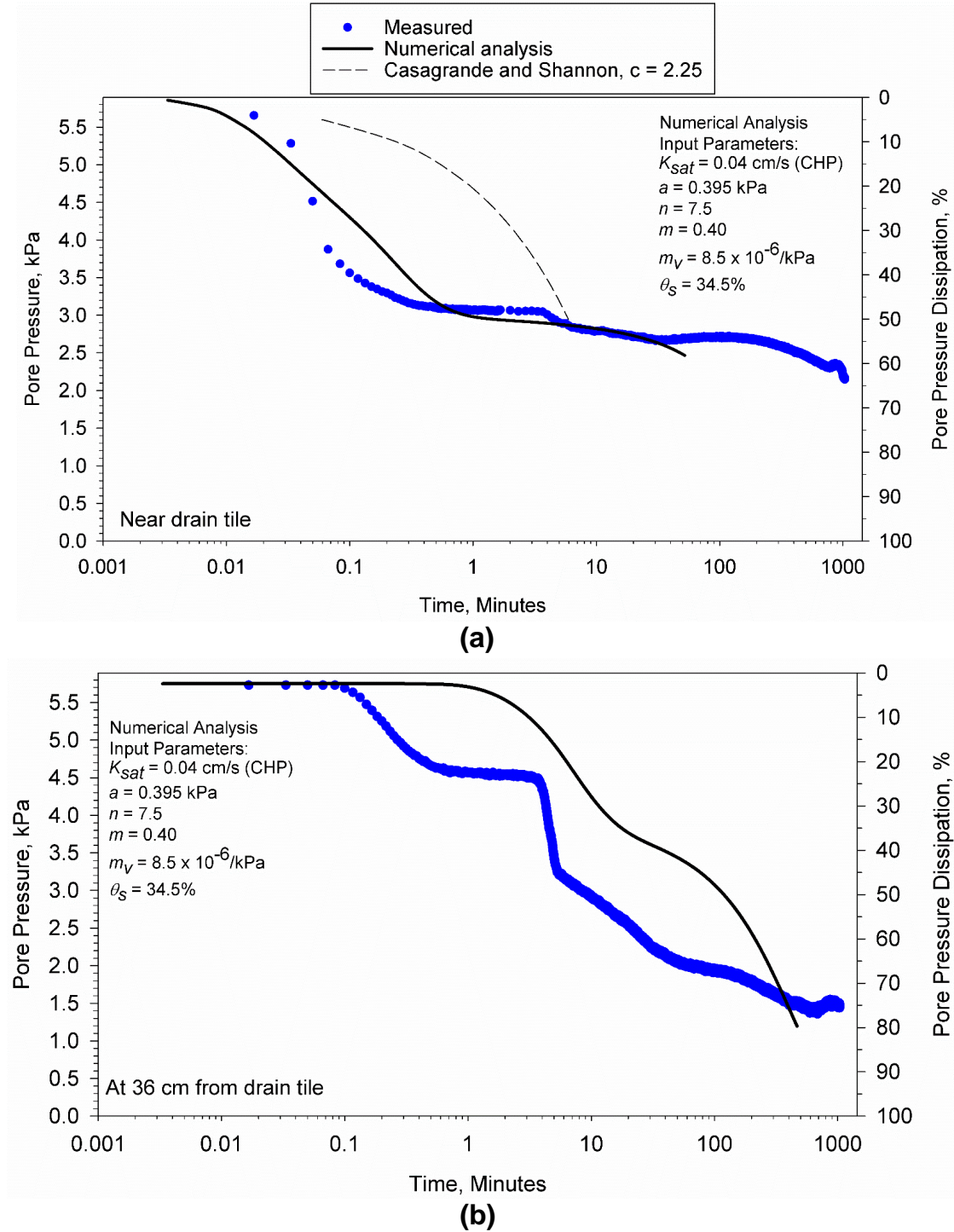
Figure 66. Measured and predicted drainage times for Schwartz Road Bridge

backfill material: (a) near drain tile and (b) 36 cm away from drain tile near the backwall

of the abutment

The measured pore pressure dissipation with time over a 24 hour period for the two sensors are presented in Figure 66. The predicted values from the numerical analysis and Casagrande and Shannon methods are also provided in Figure 66, for comparison with the measured values. Input parameters used in the numerical analysis are also shown in Figure 66. Casagrande and Shannon method was not used to calibrate for t_{95} as the material did not achieve 95% dissipation.

Results indicated that the rate of dissipation reduced substantially after about 50% dissipation at about 5 minutes, due to material erosion and clogging in the drain tile. The measured (near drain tile) and predicted times of different percentages pore pressure dissipation (from 5% to 50% in 5% increments) are compared in Figure 67, which showed a standard error in prediction of about 1 minute for the numerical analysis and 9 minutes for the Casagrande and Shannon method with c = 2.25. The numerical analysis results near the back face of the abutment wall, however, indicated longer times than the measured values.
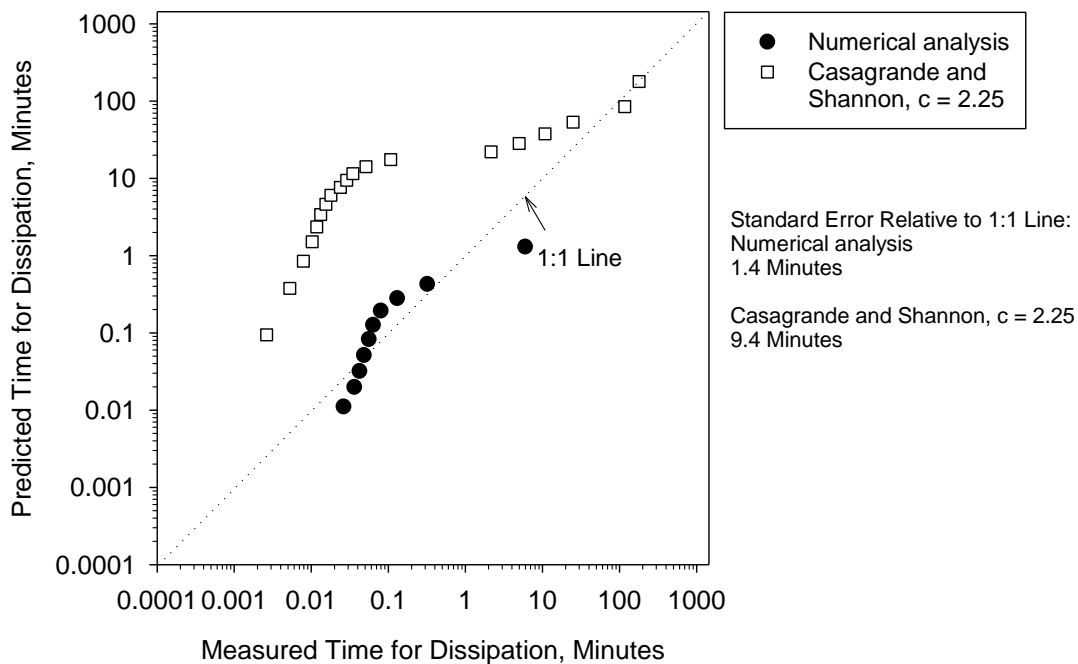
Figure 67. Linear regression analysis between measured and predicted dissipation times for different percentages of drainage for Schwartz Road Bridge backfill

Hobbles Creek Bridge Backfill Material

The material moisture content ranged from about 6% to 12%, similar to what was measured in situ (discussed later in Chapter 5). The relative compaction achieved was about 97% standard Proctor dry density at 9% moisture content. CHP tests indicated a K_{sat} of 0.004 cm/s (11 ft/day),

respectively. APT tests indicated a K_{sat} of about 0.052 cm/s (147 ft/day), which is about an order of magnitude higher than CHP K_{sat}.

The material was saturated for a period of 2 days and the pore pressure readings indicate < 50% saturation. Backsaturation was likely required to achive full saturation on this material, which was not possible for the testing conditions. The test was therefore terminated.

Badger Road Bridge Backfill Material

The material moisture content ranged from about 3% to 8%, similar to what was measured in situ (discussed later in Chapter 5). The relative compaction achieved was about 97% standard Proctor dry density at an average 5% moisture content. APT and CHP tests indicated K_{sat} of 0.74 cm/s (2098 ft/day) and 0.07 cm/s (198 ft/day), respectively. APT K_{sat} values were about an order of magnitude higher than that CHP K_{sat}.

The measured pore pressure dissipations with time over a 5 hour period for the front and back sensors are presented in Figure 68. The predicted values from the numerical analysis and Casagrande and Shannon methods are compared with the measured results in Figure 68. Input parameters used in the numerical analysis and the shape factor values used in the Casagrande and Shannon method are also shown in Figure 68.

The measured (near drain tile) and predicted times of different percentages pore pressure dissipation (from 5% to 95% in 5% increments) are compared in Figure 69, which showed a standard error in prediction of about 19 minutes for the numerical analysis method, 19 minutes using the Casagrande and Shannon method with c = 2.15, and 76 minutes using Casagrande and Shannon method with c = 0.02. The numerical analysis results near the back face of the abutment wall, however, indicated shorter than the measured values.
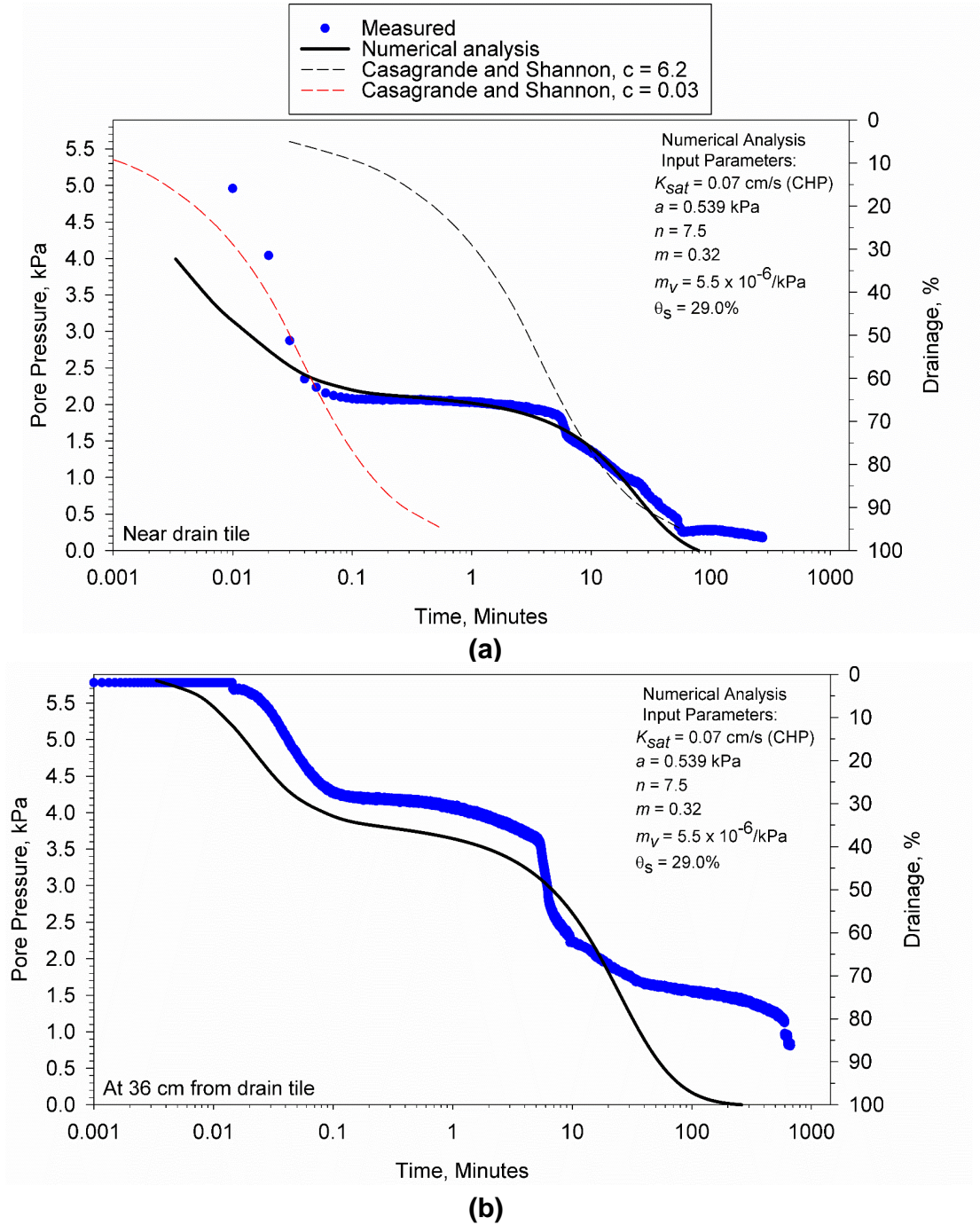
Figure 68. Measured and predicted drainage times for Badger Road Bridge backfill material: (a) near drain tile and (b) 36 cm away from drain tile near the backwall of the abutment
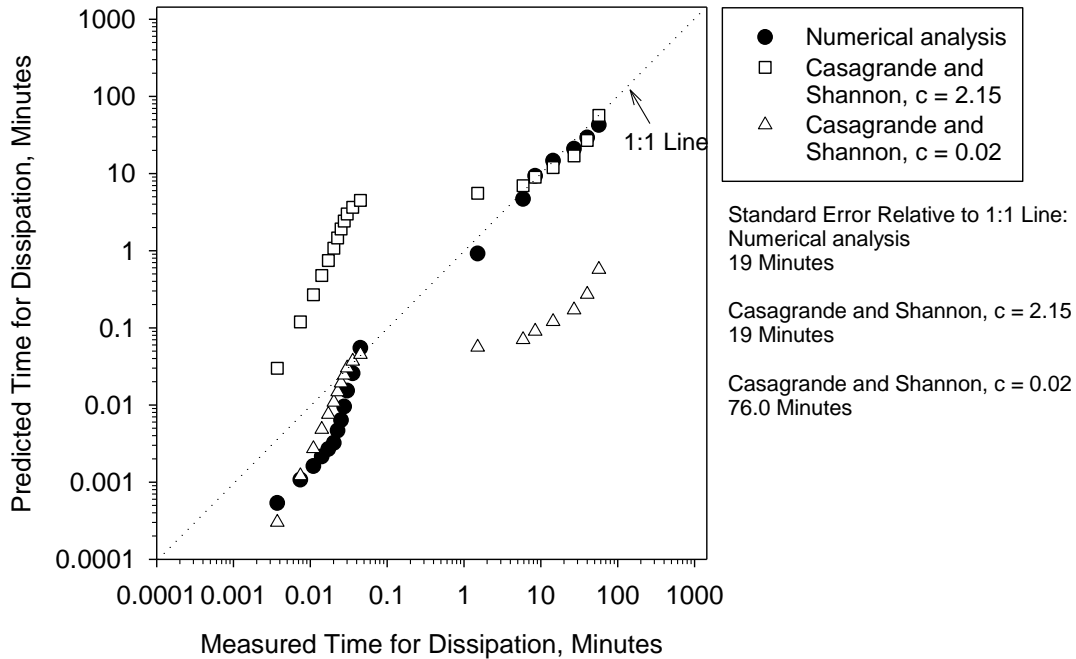
Figure 69. Linear regression analysis between measured and predicted dissipation times for different percentages of drainage for Badger Road Bridge backfill

The abutment model tests indicated $t_{50} < 2$ seconds and $t_{95} = 57$ minutes. The numerical analysis results were close to the measured values, with standard error of 19 minutes. The Casagrande and Shannon method also showed standard error of 19 minutes for $c = 2.15$, but the error was sensitive to the c value used.

RAP Material

The material moisture content ranged from about 2% to 7%. The relative compaction achieved was about 96% standard Proctor dry density at 5% moisture content. APT tests indicated K_{sat} values of 10.2 cm/s (28,792 ft/day). CHP tests indicated K_{sat} values of 1.22 cm/s (3456 ft/day).

The measured pore pressure dissipations with time over a 24 hour period for the front and back sensors are presented in Figure 70.
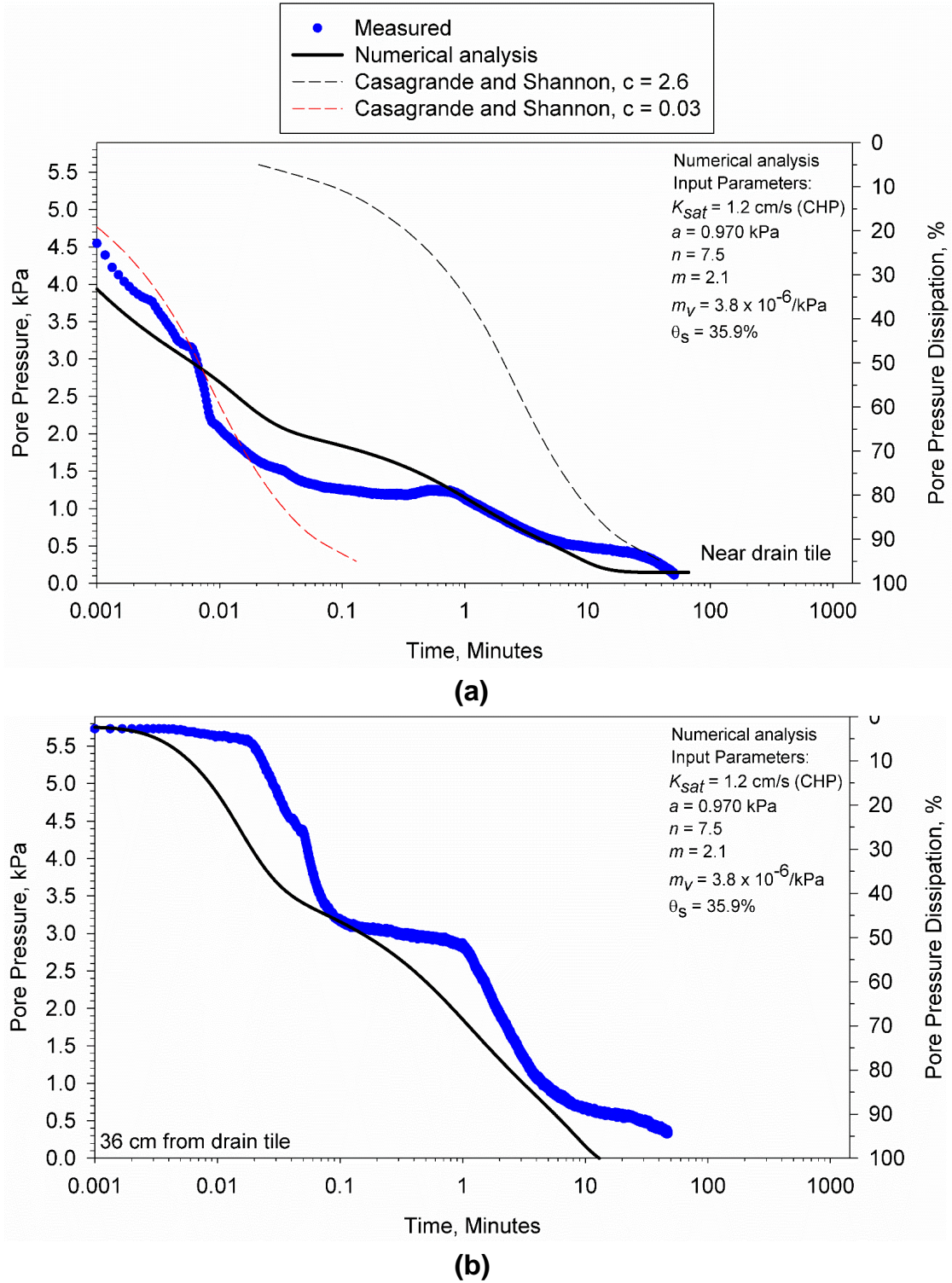
Figure 70. Measured and predicted drainage times for RAP: (a) near drain tile and (b) 36 cm away from drain tile near the backwall of the abutment

The predicted dissipation values from the numerical analysis and Casagrande and Shannon methods are compared with the measured values in Figure 70. Input parameters used in the numerical analysis and the shape factor value used in the Casagrande and Shannon method are also shown in Figure 70.
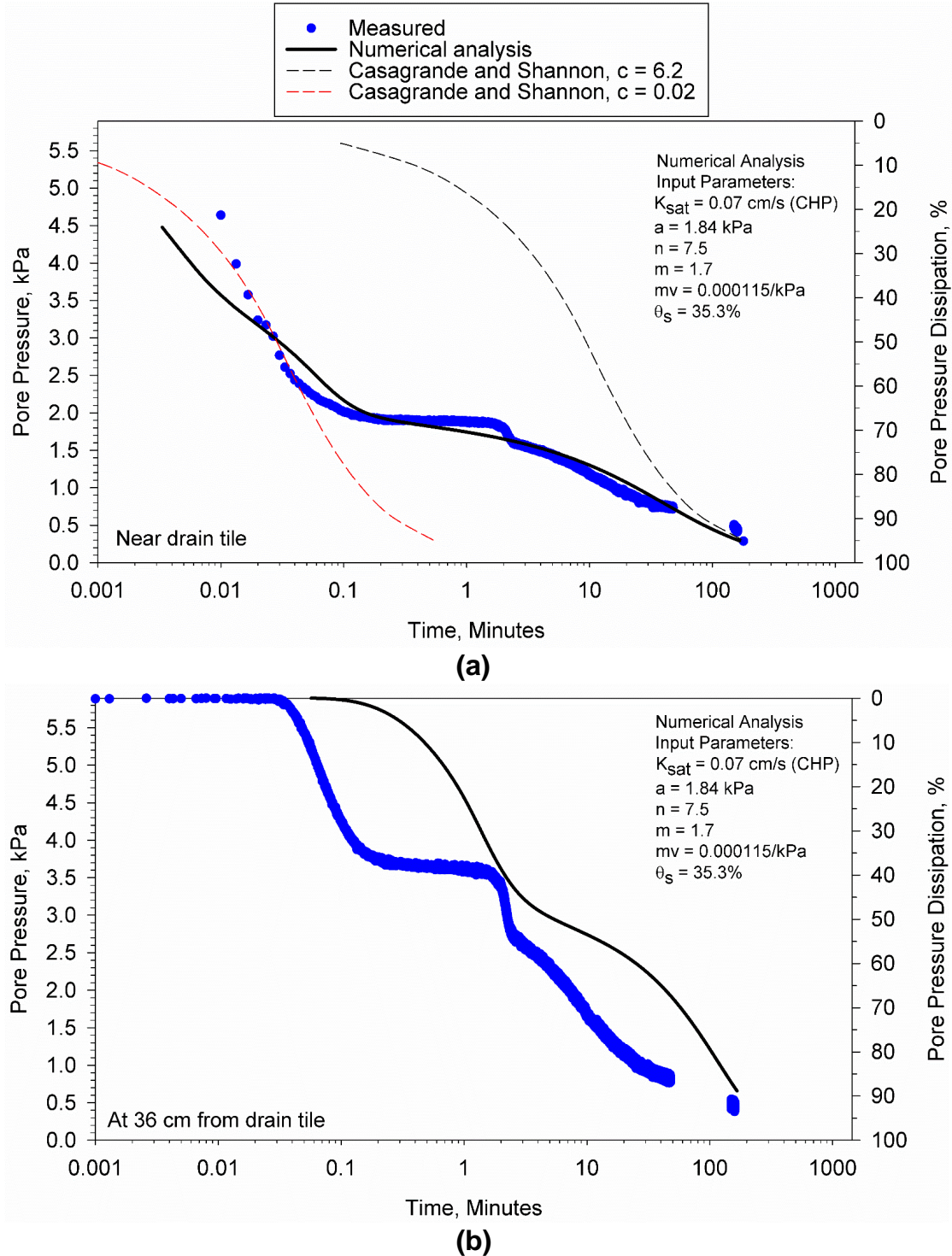
The measured (near drain tile) and predicted times of different percentages pore pressure dissipation (from 5% to 95% in 5% increments) are compared in Figure 70, which showed a standard error in prediction of about 35 minutes for the numerical analysis method, 21 minutes using the Casagrande and Shannon method with $c = 27$, and 40 minutes using Casagrande and Shannon method with $c = 0.08$. The abutment model tests indicated $t_{50} < 1$ second and $t_{95} = 40$ min. The numerical analysis results also resulted in similar values. The predicted values from the Cassagrnade and Shannon method were sensitive to the c values assumed.
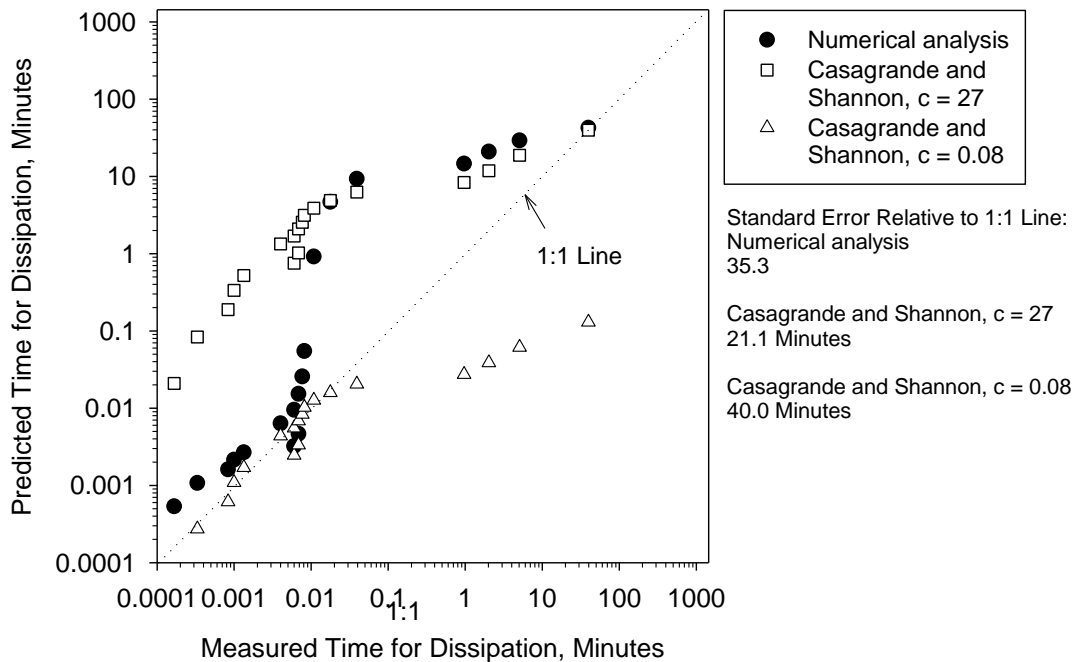
Figure 71. Linear regression analysis between measured and predicted dissipation times for different percentages of drainage for RAP

Geocomposite Drain

Of all the backfill materials tested above, Schwartz Road Bridge material showed poor drainage characteristics with material erosion through the drain tile. Therefore, tests were conducted on the same material by placing a Roadrain T5 geocomposite drain (Figure 72) along

the abutment wall/backfill interface to assess if drainage characteristics can be improved. The geocomposite was wrapped around the drain tile (Figure 73).

Figure 72. Roadrain T5 geocomposite drain

Figure 73. Geocomposite wrapped drain tile (top view)

The geocomposite drain is a synthetic tri-planar drain system manufactured by Syntec Corp, which consists of an active drainage system sandwiched between non-woven geosynthetic fabric layers. The properties of the geocomposite material are provided in Appendix C.

The relative compaction achieved was about 97% standard Proctor dry unit weight at 7% moisture content, which was similar to tests performed above for the Schwartz material without the geocomposite drain. APT and CHP tests indicated K_{sat} values of 0.57 cm/s (1616 ft/day) and 0.18 cm/s (510 ft/day). The APT K_{sat} value is similar to the one obtained in the model setup without the geocomposite drain system. CHP tests, however, showed higher K_{sat} values, which is attributed to the addition of the geocomposite drain.

The measured pore pressure dissipations with and without the geocomposite vertical drain are compared in Figure 74, which clearly shows that the addition of geocomposite drain increased the dissipation rates substantially with nearly 100% dissipation occurring within 10 minutes (as compared to < 65% dissipation occurring after 24 hours without the geocomposite). In addition, the addition of geocomposite also prevented erosion of backfill material (Figure 75).
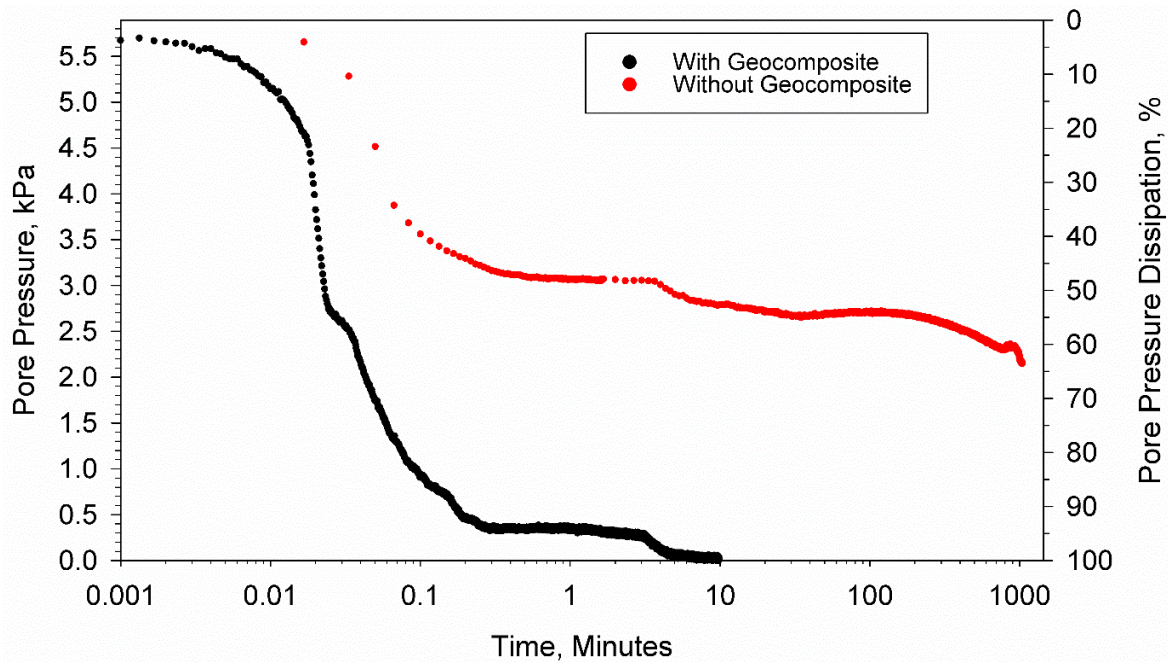
Figure 74. Dissipation times with and without geocomposite drain on Schwartz Road backfill material

Figure 75. Top of backfill after testing Schwartz road backfill material with geocomposite vertical drain (top view)

The predicted dissipation values from the numerical analysis and Casagrande and Shannon methods are compared with the measured results in Figure 76. Input parameters used in the numerical analysis and the shape factor value used in the Casagrande and Shannon method are also shown in Figure 76.

The pore pressure dissipation curves for this condition produced using the Casagrande and Shannon method matched well with the measured values, which was not the case for the results presented above without the geocomposite vertical drain. This is because the Casagrande and Shannon method assumes that the full vertical face of the drainage layer is open to drainage, which is true with the geocomposite drain. Without the vertical drain, the water only exits through the drain tile.

The abutment model tests indicated $t_{50} = 14$ seconds (as compared to 6 minutes without the geocomposite) and $t_{95} = 2$ minutes, which was unachievable without the geocomposite because of material erosion into drain tile and clogging.
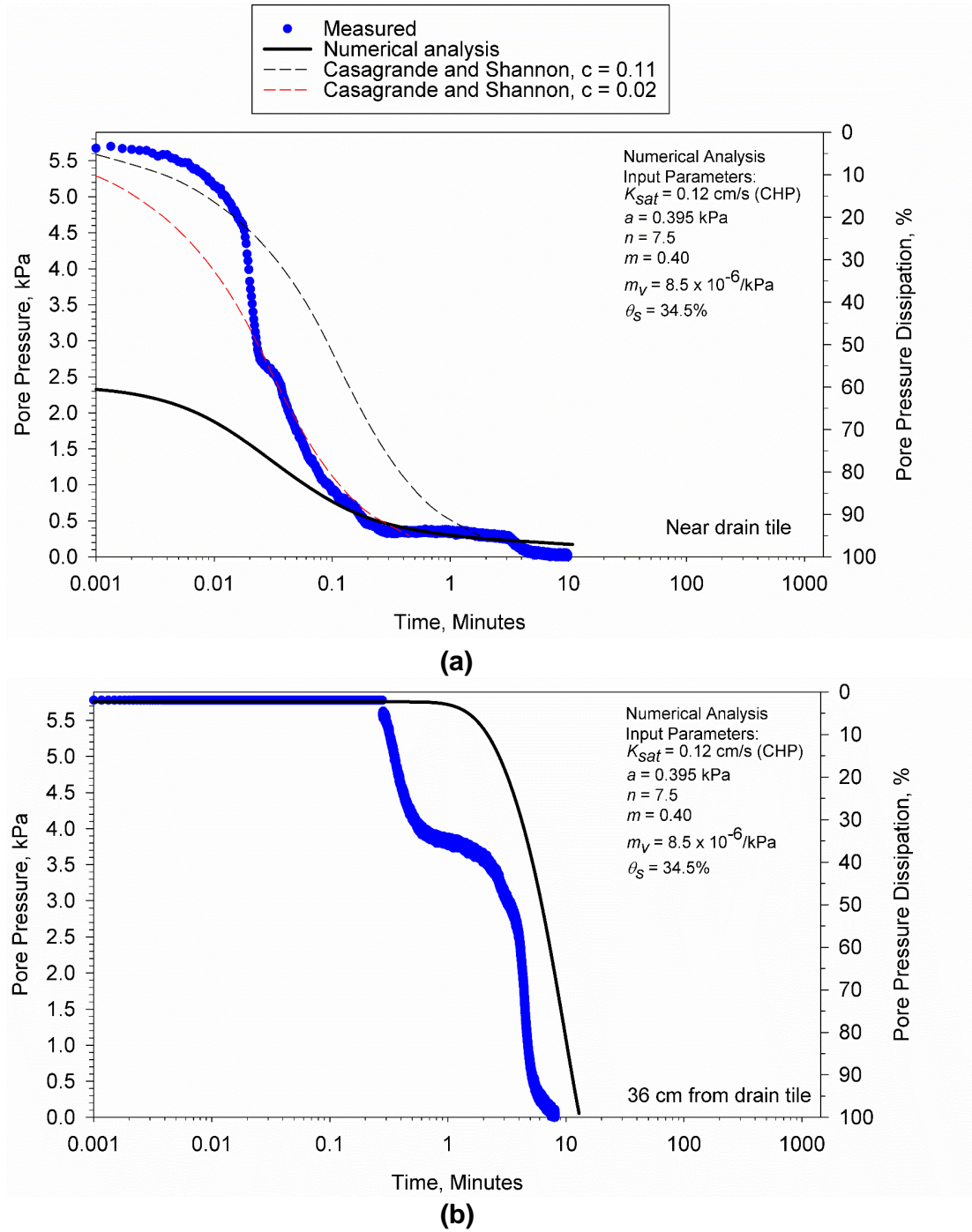
Figure 76. Measured and predicted drainage times for Schwartz Road Bridge backfill material with vertical geocomposite drain: (a) near drain tile and (b) 36 cm away from drain tile near the backwall of the abutment

The measured and predicted times of different percentages of pore pressure dissipations (from 5% to 95% in 5% increments) are compared using a linear regression model in Figure 77,

which showed a standard error in prediction of about 0.07 minutes for the numerical analysis.
Casagrande and Shannon method had a standard error of 0.9 minutes when $c = 0.11$ and 1.3
minutes when $c = 0.02$.
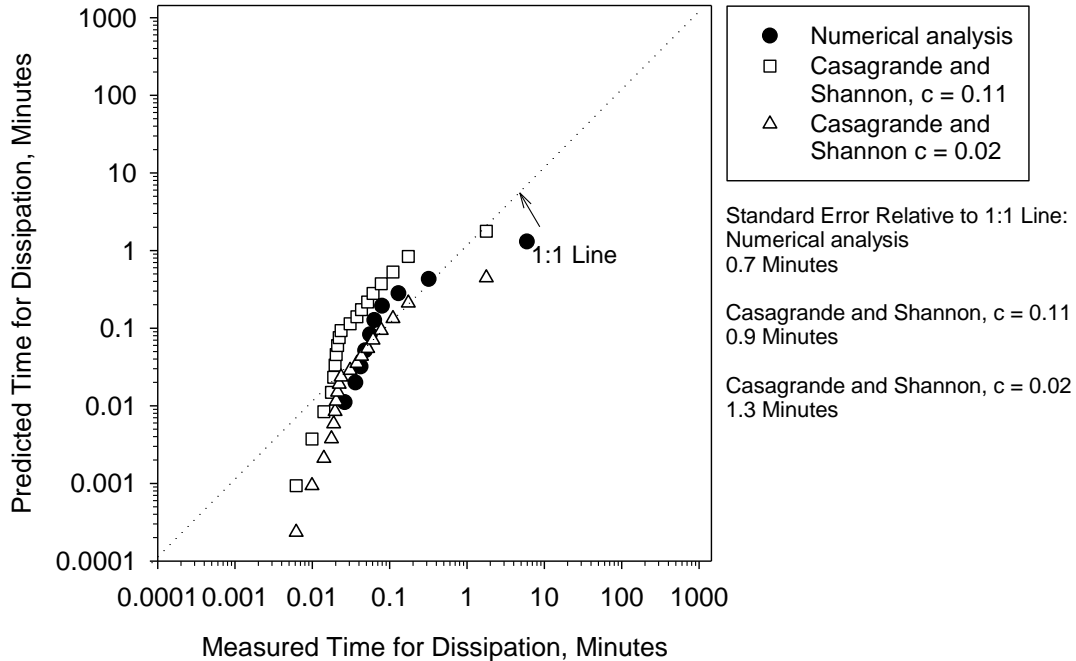
**Figure 77. Measured and predicted values for Schwartz Road Bridge with vertical
geocomposite drain**

In summary, addition of geocomposite drain substantially reduced the time required for pore
pressure dissipation in the backfill material (from > 1 day to < 10 minutes). It also reduced the
potential to erosion of the material into the backfill.

Summary of Abutment Model Test Results

Table 12 compares the material gradation parameters, K_{sat} values, and times for 50% and
95% dissipation from the model tests and numerical analysis.

Generally, increasing K_{sat} decreased the dissipation times, but addition of geocomposite
vertical drain substantially reduced the drainage time, although the material K_{sat} was not
relatively high. A statistical significant correlation between the various gradation parameters and
dissipation times was not evident for this dataset.

Table 12. Gradation parameters, hydraulic conductivity, and drainage times for abutment model and numerical analysis

Material	D_{10}, mm	D_{30}, mm	D_{60}, mm	D_{90}, mm	C_u	C_c	P_{200}, %	APT K_{sat}, cm/s	CHP K_{sat}, cm/s	t_{50}	t_{95}
Slovak Valley Creek Bridge	0.241	0.405	0.585	0.706	2.92	0.96	2.2	0.57	0.07	<2 s[a] <2 s[b]	3 h[a] 3 h[b]
Schwartz Road Bridge	0.105	0.150	0.192	0.258	1.83	1.11	7.3	0.54	0.04	6 min[a] < 2 min[b]	
Schwartz Road Bridge with Geocomposite Drain	0.105	0.150	0.192	0.258	1.83	1.11	7.3	0.57	0.18	14 s[a] <2 s[b]	2 min[a] 1 min[b]
Hobbles Creek Bridge	0.177	0.478	1.721	8.193	9.71	0.75	6.4	0.052	0.0004	—	—
Badger Road Bridge	0.250	0.367	0.595	4.033	0.7	0.9	0.7	0.74	0.07	< 2 s[a] < 2 s[b]	57 min[a] 43 min[b]
RAP	0.705	2.689	5.963	10.81	8.45	1.72	5.8	10.2	1.22	< 1 s[a] < 1 s[b]	42 min[a] 28 min[b]

— not obtained

a = measured values form abutment model

b = numerical analysis

Summary Key Findings

Material Properties

Particle size analysis tests indicated that the Schwartz Road Bridge backfill fell within the erosion bands specified by Briaud et al. (1997). Slovak Valley Creek Bridge and Badger Road Bridge fell partially within the erosion bands, while the remaining materials were outside the erosion bands.

Laboratory compaction tests reveal a definable bulking moisture content range for natural materials whereby the density is low due to partially saturated conditions resulting in suction that inhibits compaction. Bulking moisture content was not evident for RAP and RAS materials. The implication of bulking moisture content is that the materials placed and compacted at or near that moisture content can exhibit collapse upon wetting. Laboratory collapse tests on the backfill materials showed vertical strains ranging between < 0.2% and 4%, when compacted at bulking moisture contents. RAP and RAS produced vertical strains of about 4% to 5% under constant

loading. These vertical strains are not believed to be related to partially saturated bulking condition, but rather an indication of the composition of the materials. For reference a 1% collapse on a 3 m (10 ft) of backfill l can lead to about 30 mm (> 1 in.) of settlement. Therefore, any post-construction settlement related to collapse can be problematic and should be avoided.

The K_{sat} values of the four bridge site materials varied from 0.0002 to 0.11 cm/sec. Badger Road Bridge material had the highest K_{sat} and the Hobbles Creek Bridge had the lowest K_{sat}. The K_{sat} values reduced by 20% to 60% after 24 hours of saturation for the four materials, when compared to values obtained after 30 minutes of saturation time. Of the two recycled materials, RAP material showed the highest K_{sat} (about 0.03 cm/sec). RAS material showed $K_{sat} = 0.0006$ cm/sec which was similar to Hobbles Creek material. The K_{sat} reduced by about 28% after 24 hours of saturation for RAP material, but did not show any difference for RAS material, when compared to 30 minutes saturation time.

The empirical equations used to predict K_{sat} from gradation and compaction properties, generally produced higher than the measured values. K_{sat} values predicted using Moulton's equation were comparatively closer to the measured values than other relationships.

Direct shear tests indicated friction angles of the four bridge site backfill materials ranging between 27 and 33 degrees, with apparent cohesion values ranging between 4 and 12 kPa (0.6 to 1.7 psi). Shear strength parameters could not be determined for the RAP and RAS materials due to its secondary compression or creep behavior with increasing shear stresses even after 15% horizontal strain.

Scaled Abutment Model Testing and Numerical Analysis

One-fourth scaled abutment model was used to calibrate the FEM input parameters, by measuring pore pressure dissipation during free drainage tests. The FEA results demonstrated that numerical analysis can be used to predict pore pressure dissipation rates with high accuracy (drainage times ± few minutes), provided the input parameters are properly calibrated through laboratory testing. The main input parameters that needed calibration were coefficient of volume compressibility m_v, and soil suction curve fitting parameters. For comparison a simple analytical solution proposed by Casagrande and Shannon was evaluated to predict pore pressure dissipation times. Although the method was relatively simple, it was found to be very sensitive to the shape factor values used in the calculations, but can be determined from laboratory testing.

The bridge abutment model tests were used to calibrate the FEM parameters revealed that that the drainage times to achieve 95% drainage varied between 28 minutes and 3 hours for three materials (two obtained from bridge sites and RAP). On one of the backfill materials obtained from the bridge sites, fine particles eroded through the drain tile sock during free drainage causing clogging and only 60% of pore pressure dissipation at 24 hours. Erosion occurred because the material contained 99% passing the No. 40 sieve, and the drain tile sock had an aperture opening size of No. 40 sieve. By adding a geocomposite vertical drain along the face of the wall for this material, nearly 100% of drainage occurred within 10 minutes without any erosion.

Results indicated that as the permeability of the backfill material increased the pore pressure dissipation rates increased. A statistical significant correlation between the various gradation parameters and dissipation times was not evident for the data obtained from this study.

CHAPTER 5. FIELD TEST RESULTS AND ANALYSIS

Four newly constructed bridge sites were selected for field testing and instrumentation by the WisDOT. The geographic locations of the bridges are shown in Figure 78. Table 13 summarizes the locations of the bridges with brief information about the bridge and abutment backfill materials.
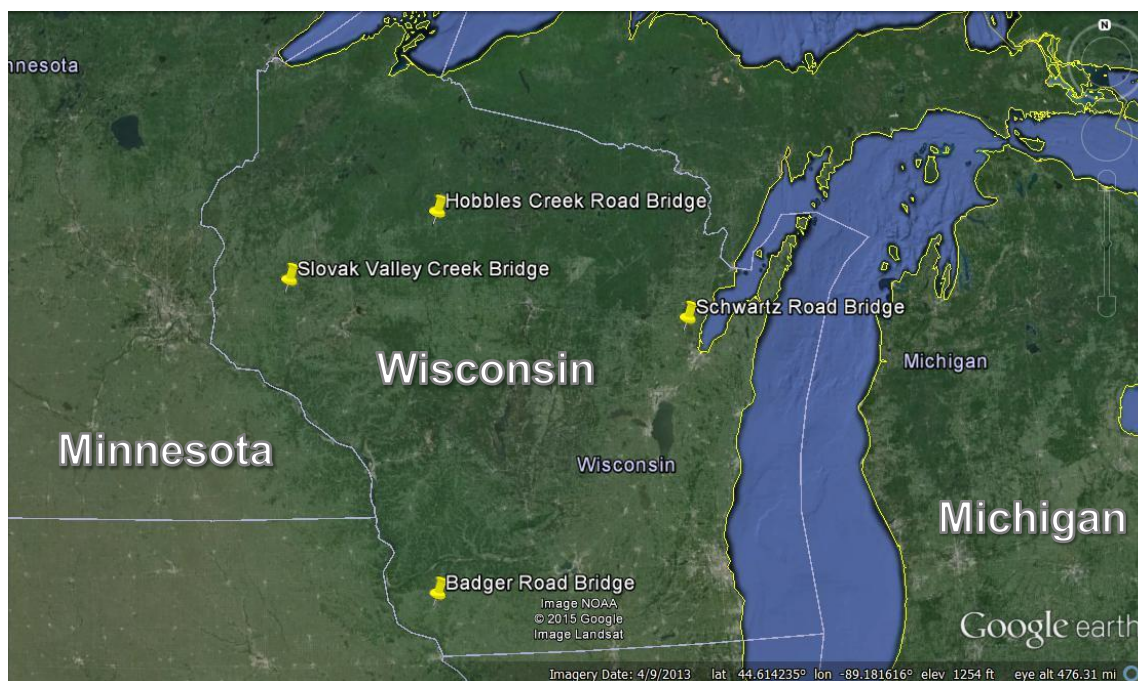
Figure 78. Geographic locations of the field project locations

Table 13. Summary of bridge project locations in Wisconsin

Bridge Name	Structure Number	Location	Bridge Description	Specified Backfill
Slovak Valley Creek Bridge	B-17-364	State Highway 79 over Slovak Valley Creek, Dunn County, WI	10.7 m (35 ft) long concrete bridge supported on CIP concrete abutment and piling	Structure Backfill Section 210
Schwartz Road Bridge	B-42-127	Schwartz Road over Little Suamco River, Oconto County, WI	25.1 m (82.5 ft) long concrete bridge supported on CIP concrete abutment and steel piling	Structure Backfill Section 210
Hobbles Creek Road Bridge	B-50-86	Hobbles Creek Road over Hobbles Creek, Price County, WI	13.6 m (44.5 ft) long concrete bridge supported on CIP abutment and steel piling	Structure Backfill Section 210
Badger Road Bridge	B-22-0283	Badger Road over Branch Martin Branch, Grant County, WI	17.3 m (56.7 ft) long concrete bridge supported on CIP abutment and steel piling	Granular Backfill Section 209

Due to a snow storm occurred early November of 2014 at the Hobbles Creek and Schwartz Road bridge sites, snow covered the solar panel resulting in a drained battery. No data was collected between early November 2014 and late February 2015 at these sites. New batteries were installed at the end of February 2015 and the data is currently being collected.

In the following sections of this chapter, brief information about the bridge, details of field testing and instrumentation performed by ISU, results of field testing and instrumentation, and data analysis, are presented separately for each project. At the end of this chapter, a summary of key findings from the field investigations are presented.

Slovak Valley Creek Bridge

The Slovak Valley Creek Bridge is a 10.7 m (35 ft) long two-lane concrete bridge located on State Highway 79 (S.H. 79) north of Boyceville in Dunn County, WI. The bridge is supported on a 10.5 m (34.7 ft) wide x 1.5 m (5.1 ft) tall cast in place concrete abutment founded on cast in place concrete piling installed to a depth of about 21.3 m (70 ft). Plan and cross-sectional views of the bridge are provided in Figure 79 and Figure 80, respectively.
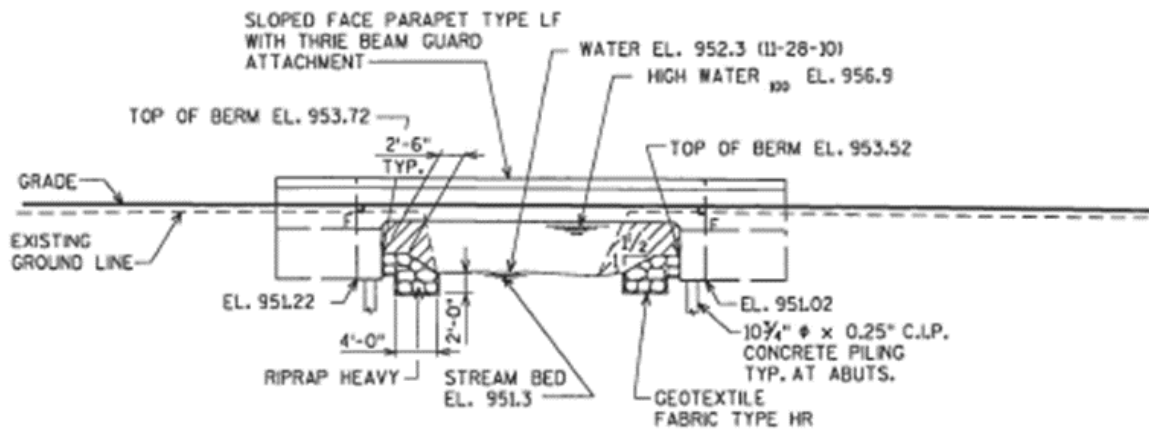
Figure 79. Slovak Valley Creek Bridge cross section (from project plans)
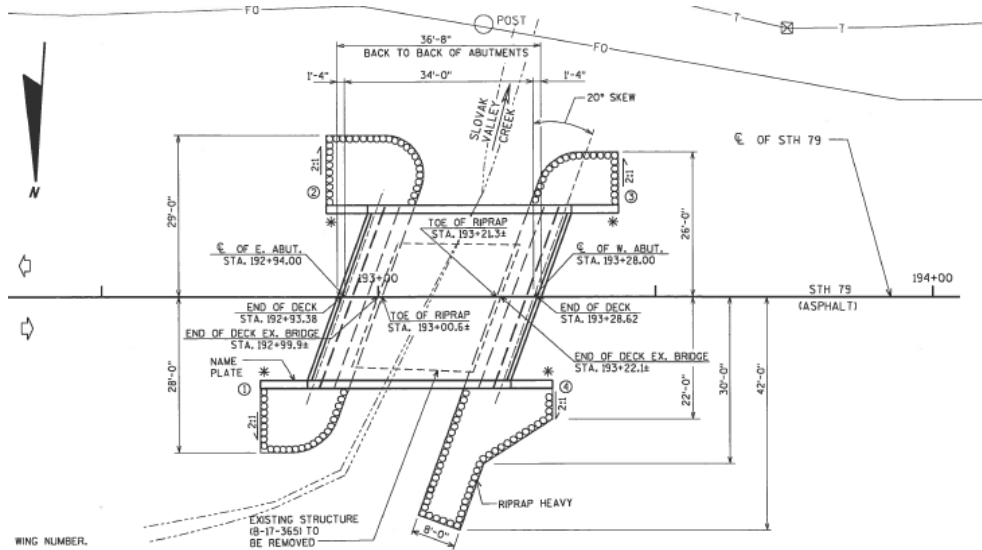
Figure 80. Slovak Valley Creek Bridge plan view (from project plans)

According to the subsurface soil information included in the bridge plans, the foundation soils consisted of sandy gravel to sand soils with occasional cobbles and gravel down to depths of about 30 to 35 m below grade. The project plans specified use of structure backfill per WisDOT Standard Specifications Section 210. The drain specifications called for a 0.15 m (6 in.) geotextile wrapped drain tile installed at a depth of about 0.46 m (1.5 ft) above the bottom of the structure backfill with a 0.5% slope to a suitable drainage location.

Construction

The ISU research team arrived on-site on October 31, 2013, shortly after the backfill material was placed and compacted to about 50 mm (2 in.) below its final elevation on the west abutment (Figure 81). Reportedly, a hand-held vibratory compactor was used for compacting the material in 0.3 m (1 ft) thick lifts.

The particle-size distribution curve of the material in comparison with the WisDOT Structure Backfill specifications is provided in Figure 82. The backfill material used on this site met the specified gradation limits.

Figure 81. Slovak Valley Creek Bridge west abutment near its final elevation
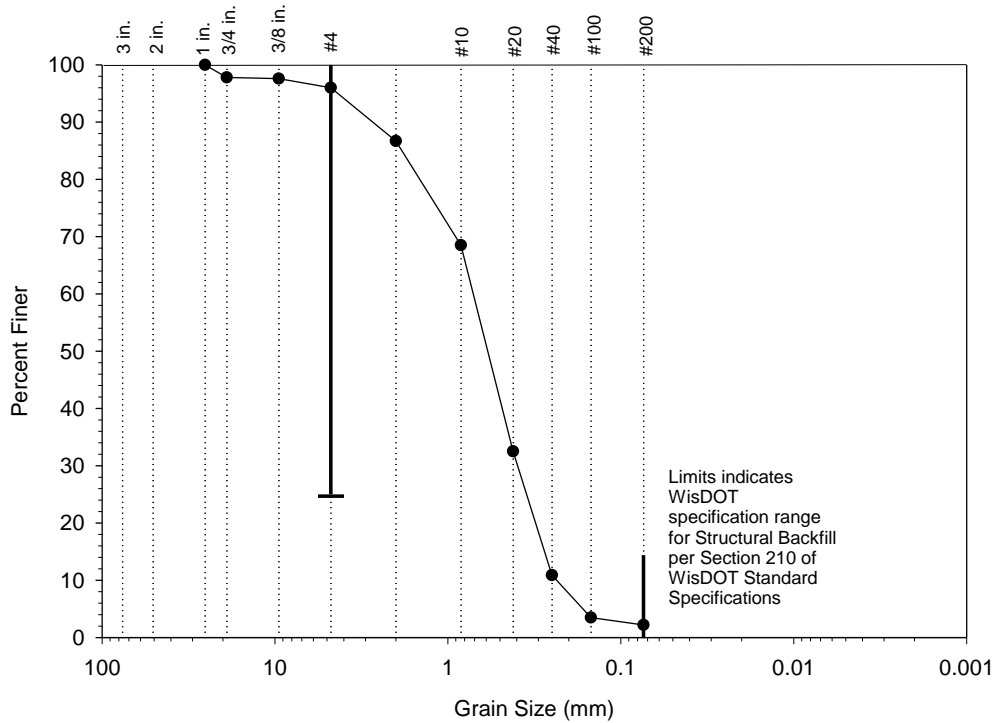
Figure 82. Slovak Valley Creek backfill material gradation in comparison with structure backfill gradation limits per WisDOT specifications

Samples from the structure backfill from various depths and from on-site stockpile were collected and tested for moisture content. The field moisture contents varied from about 3% to 5% and is compared with laboratory compaction and collapse index test results in Figure 83. The field moistures were slightly higher than the bulking moisture content identified with Proctor testing and were close to the bulking moisture content identified with vibratory compaction testing. The collapse index test results indicated a collapse strain of about 0.8% near bulking moisture content, which equals to about 12 mm (1 in.) of settlement after wetting for 1.5 m of backfill material at this site.

Field Testing

Five dynamic cone penetrometers (DCP) tests, three air permeability tests (APT), and three corehole permeability tests (CHP) tests were conducted on the backfill material. The test locations are identified in Figure 84 and Figure 85. Five DCP tests were performed along the centerline of the abutment with four in the granular backfill and one in the natural subgrade for comparison. APT and CHP tests were performed at about 1.0 m (3.3 ft) away from the face of the abutment in the granular backfill at three locations along the width of the abutment.

APT K_{sat} values showed an average of about 0.8 cm/s, and CHP K_{sat} values showed an average of about 0.1 cm/s.

DCP-CBR with depth and cumulative blows with depth profiles are shown in Figure 86. DCP-CBR profiles showed that CBR generally increased with depth, which is an effect of confinement on cohesionless materials. DCP #4 showed layers of loosely compacted fill at depths of about 1.3 to 1.5 m, and DCP #1 showed a similar loose layer at a depths of about 0.7 to 1.0 m.

(a)

(b)
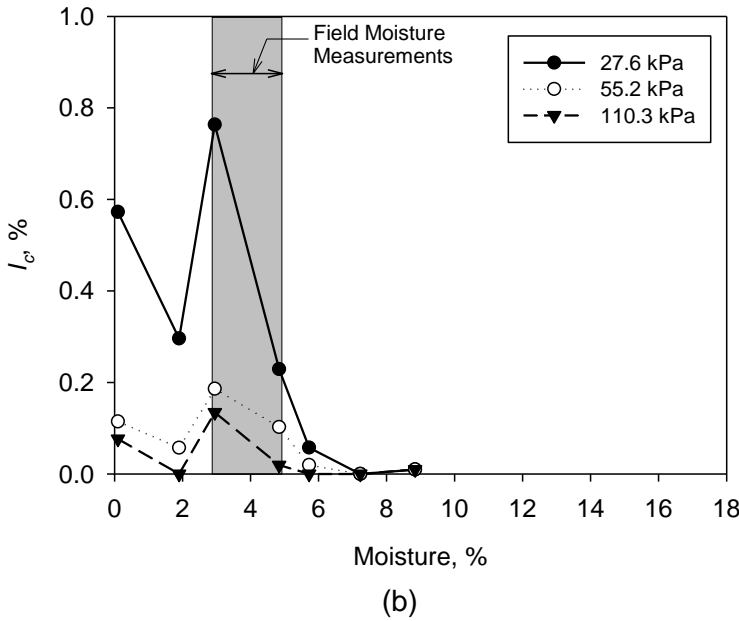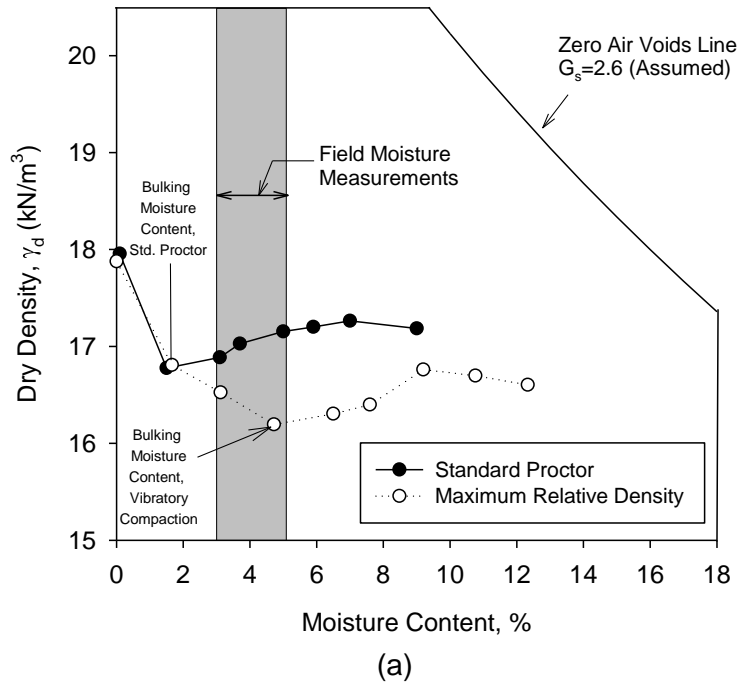
Figure 83. Field moisture results compared to: (a) laboratory compaction results; and (b) laboratory collapse index test results
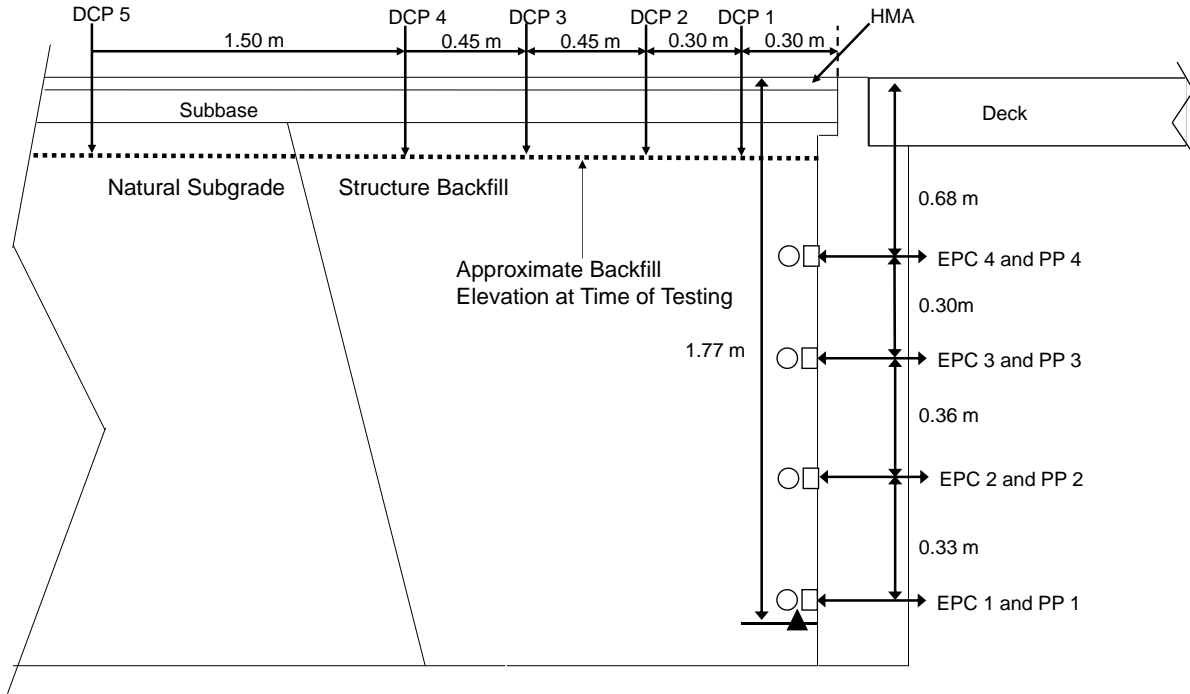
Figure 84. Cross-sectional view of the bridge abutment showing EPC and PP sensor locations and DCP test locations at Slovak Valley Creek Bridge
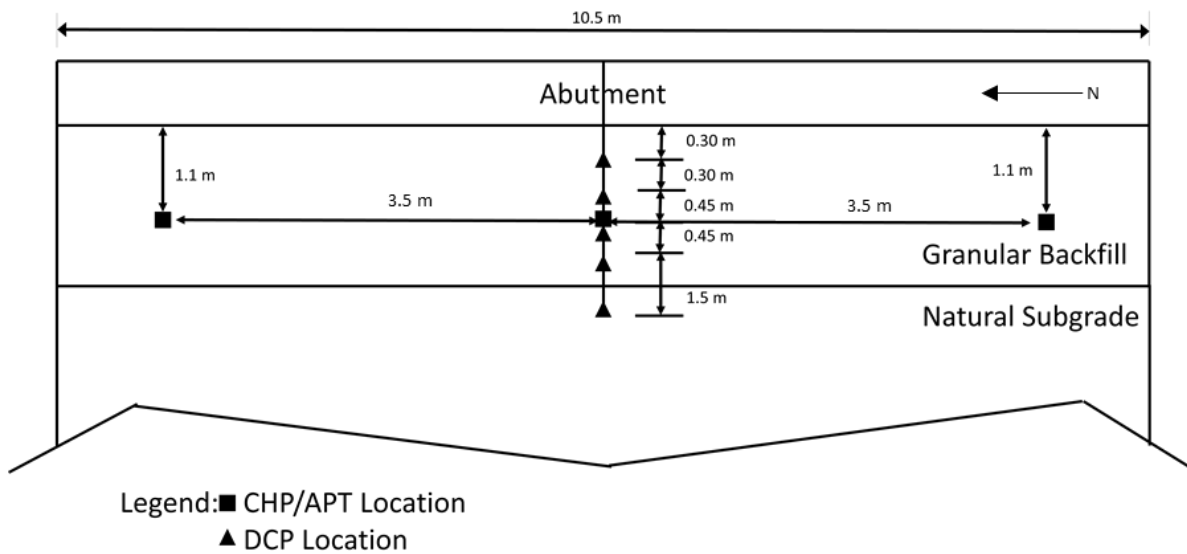
Figure 85. Plan view of the bridge abutment showing APT, CHP, and DCP test locations at Slovak Valley Creek Bridge
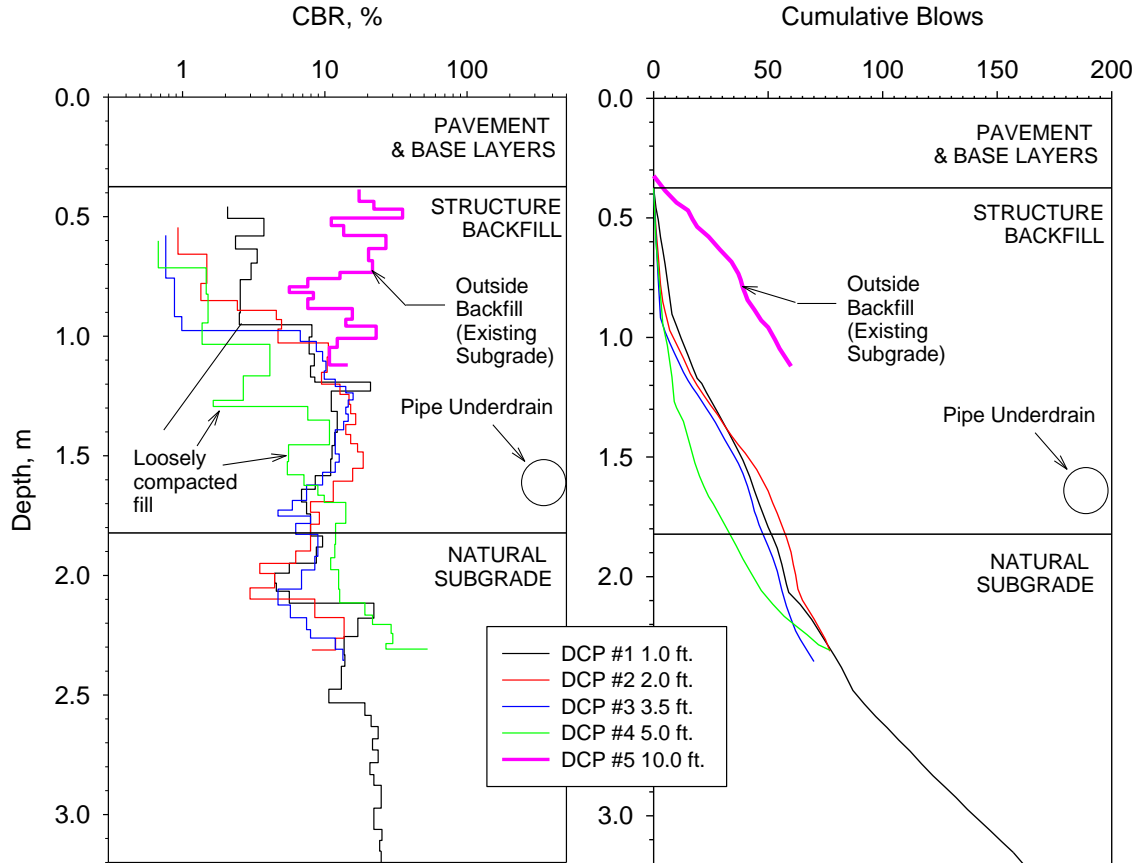
Figure 86. DCP results for Slovak Valley Creek Bridge

Instrumentation

Four EPC and four PP sensors were installed at various depths down to near the drain tile along the face of the abutment wall as shown in (Figure 84). A picture of EPC and PP sensor installed against the wall is shown in Figure 87.

The backfill material was carefully excavated to place the sensors at desired elevations, and was hand then compacted in relatively thin lifts (about 25 to 50 mm thick) to fill the excavation. The sensors were connected to on-site DAQ system, which was initially set to collect data every 1 minute and was then changed to 5 minutes.

Figure 89 shows the measured lateral stresses with the ambient and sensor temperature readings. Figure 90 shows the measured pore water pressure with the ambient and sensor temperature readings. One of the data logger components failed during a period of very cold temperatures in early January 2014. This resulted in data loss as indicated in the figures. Also, up to about mid-March 2014, temperature readings were not correctly recorded due to a calibration

error, therefore the readings were not corrected for temperature up to that time. After mid-march 2014, all readings were corrected for temperature.

Figure 87. Photograph of an installed PP (left) and EPC (right) sensors

Figure 88. Compaction of backfill material in thin layers after installing PP and EPC sensors at multiple depths
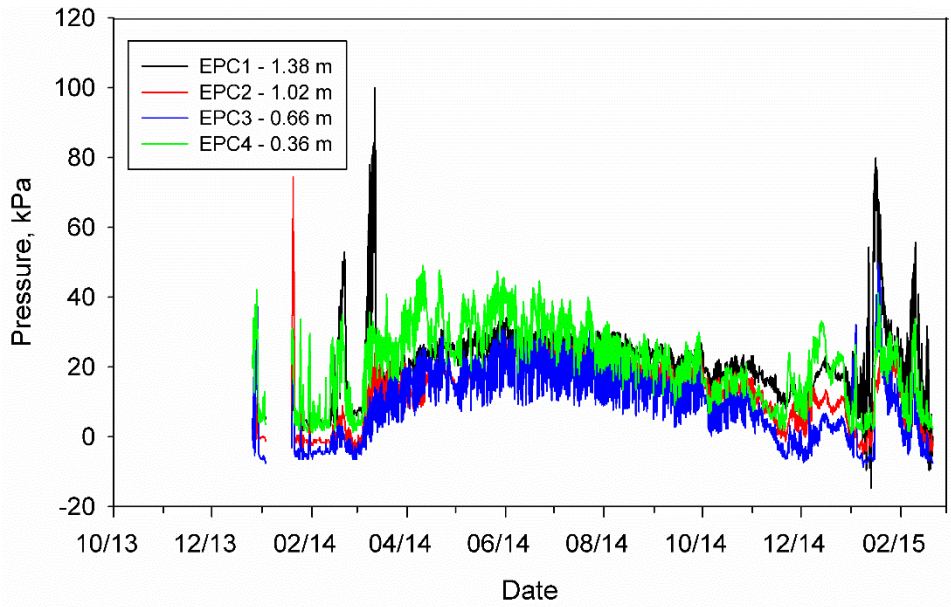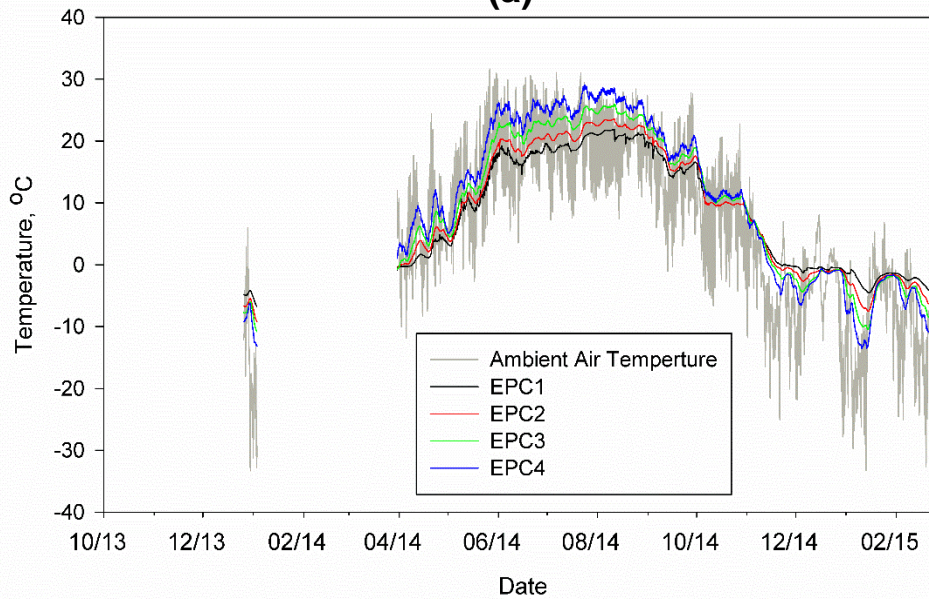
Figure 89. EPC lateral earth pressure (total) readings from Slovak Valley Creek Bridge: (a) total lateral earth pressure readings with time, and (b) ambient and EPC temperature readings with time
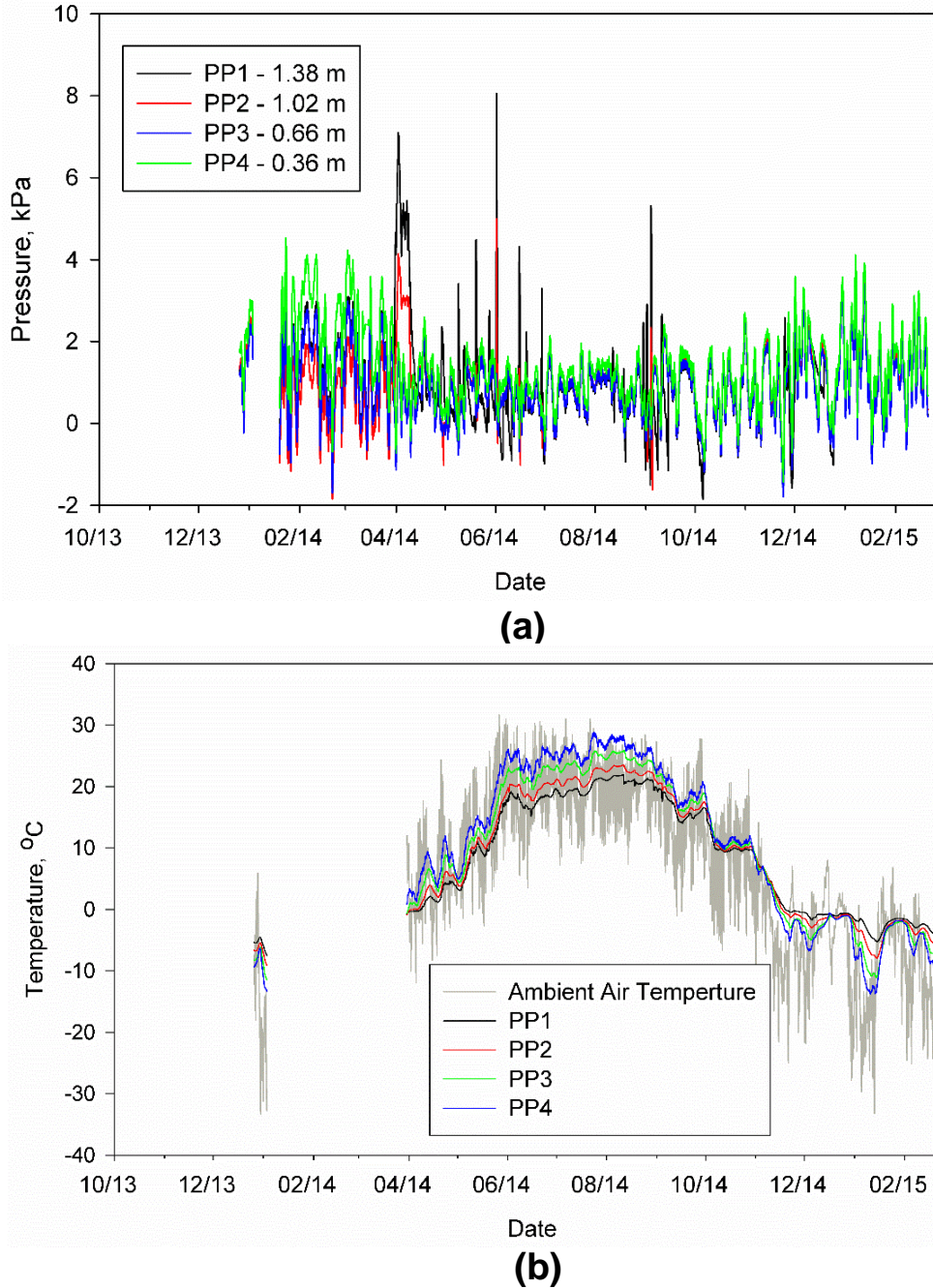
Figure 90. PP readings from Slovak Valley Creek Bridge: (a) pore water pressure readings with time, and (b) ambient and PP temperature readings with time

Field visits indicated ponding at the bridge site on April 7, 2014 (Figure 91), and a water depth of about 0.76 m (2.5 ft) was measured at the center of the creek.

The lateral earth pressure values from the following four days were selected to compare with the theoretical values:

(a) December 31, 2013 representing the coldest day (air temperature = -33ºC);

(b) May 26, 2014 representing the hottest day (air temperature = +33ºC);

(c) April 2, 2014 representing the day when the highest pore water pressures were recorded behind the abutment wall; and

(d) March 12, 2014 representing the day when highest lateral stresses were recorded behind the abutment wall (at the bottom).

Figure 91. Water ponding on April 7, 2014

The measured lateral earth pressures with depth in comparison with the theoretical Rankine active and passive earth pressures and Coulomb passive earth pressures are presented in Figure 92. The theoretical values were calculated using $\phi' = 29.7º$ from laboratory direct shear testing, and wall friction $\delta = 2/3 \, \phi'$ (for Coulomb passive pressure calculations) and assuming a total unit weight of 17.68 kN/m^3 (based on 95% standard Proctor maximum density and 4% moisture content). A surcharge load of 17.13 kPa was used in the calculations to account for weight of backfill material above the top of the abutment, and the weight of the pavement and base layers. These theoretical values assume no pore pressures behind the wall, as considered in the design. The lateral earth pressures used in design by the Wisconsin DOT are close to the Rankine active case.

In Figure 93, measured lateral stresses at various depths are compared with the assumed design values per Wisconsin DOT Bridge Design Manual for loose and dense sands.
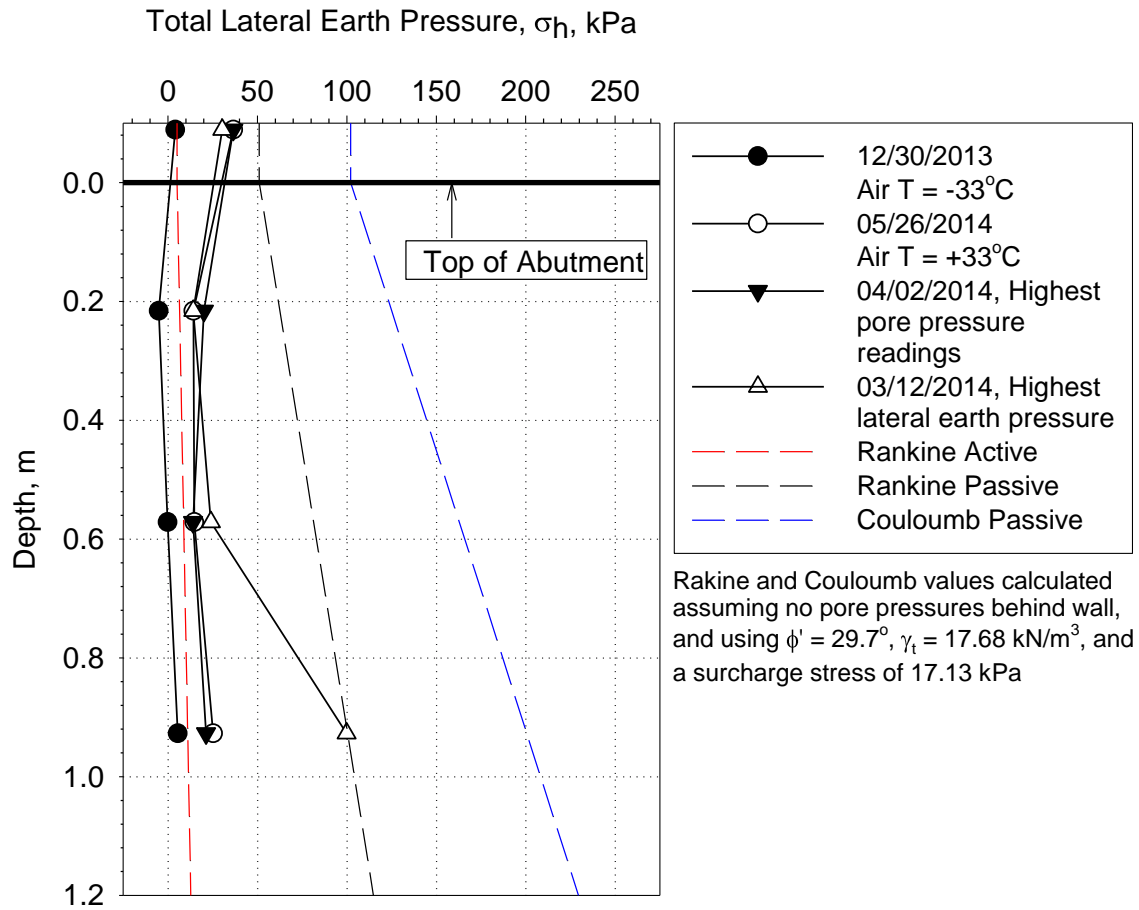
Figure 92. Measured and theoretical distribution of lateral earth pressures

The results indicate that the in situ lateral stresses did not follow a linear trend with depth as shown in the theoretical values, and also changed with time. On the coldest day, the values were close to or lower than the active earth pressures, which can be attributed to contraction of the bridge and abutment wall moving away from the backfill. On the hottest day, the values in the upper sensor (located 0.1 m above the top of the abutment) measured values close to Rankine passive pressures, while in the lower sensors, the values were close to and higher than active pressures. This increase in pressure near the top can be attributed to expansion of the bridge structure and abutment wall moving towards the backfill material. This was also previous observed by other researchers as documented in Chapter 2 (Broms and Ingelson 1971; Huntley and Valsangkar 2013).
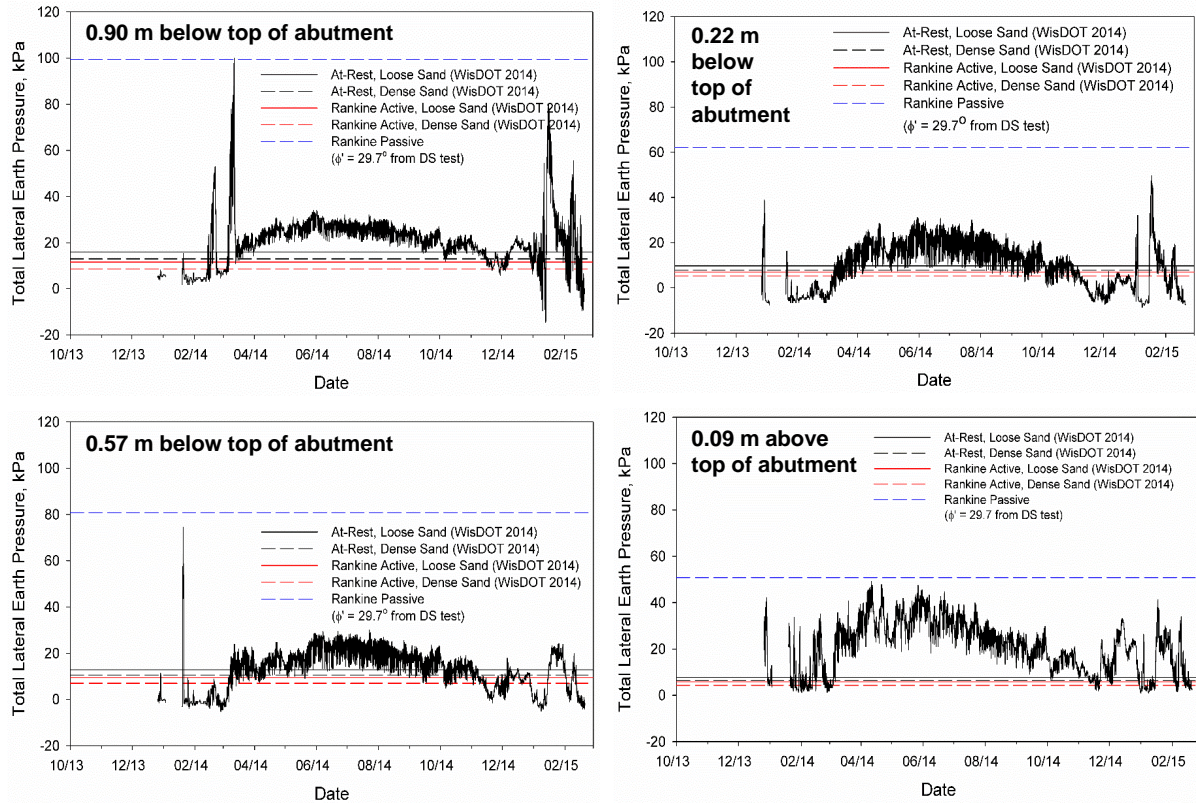
Figure 93. Measured lateral earth pressures with time at different times in comparison with the design assumed values for loose and dense sand conditions per Wis DOT Bridge Design Manual

Surprisingly, the highest lateral stresses were recorded near the bottom of the wall on March 12, 2014, even when the temperatures were relatively cold (T = 5°C). This behavior can be attributed to (although cannot be adequately verified) frozen undrained water in or near the drain tile with temperature fluctuations occurred during that time. Similar peaks in EPC1 readings near the bottom of the wall were also noticed during January 2015 when the temperatures were below freezing.

A close review of pore pressure changes with time and field observations indicated that drainage from the backfill material occurred from April 7 to 12, 2014, following a flooding period associated with snow melting in the creek. This data was used to compare with predictions from numerical analysis and Casagrande and Shannon methods, based on calibrated input parameter values from laboratory scaled abutment model testing. K_{sat} value obtained from field CHP testing was used in the analysis.

The boundary conditions setup for the field conditions are shown in Figure 95. In the FEM model setup, the bridge backfill material was modeled to have negative pressure head above the phreatic line. The location of the phreatic line was determined based on the pore pressure reading, which was located near about the mid-height of the backfill. Numerical analysis was performed assuming impermeable foundation layers (forcing all the drained water to go through the drain tile) and also assuming permeable foundation layers (with K_{sat} = 0.001 cm/s). The c values obtained for Casagrande and Shannon method matching with t_{95} from laboratory testing (c = 6.2) was used for comparison.
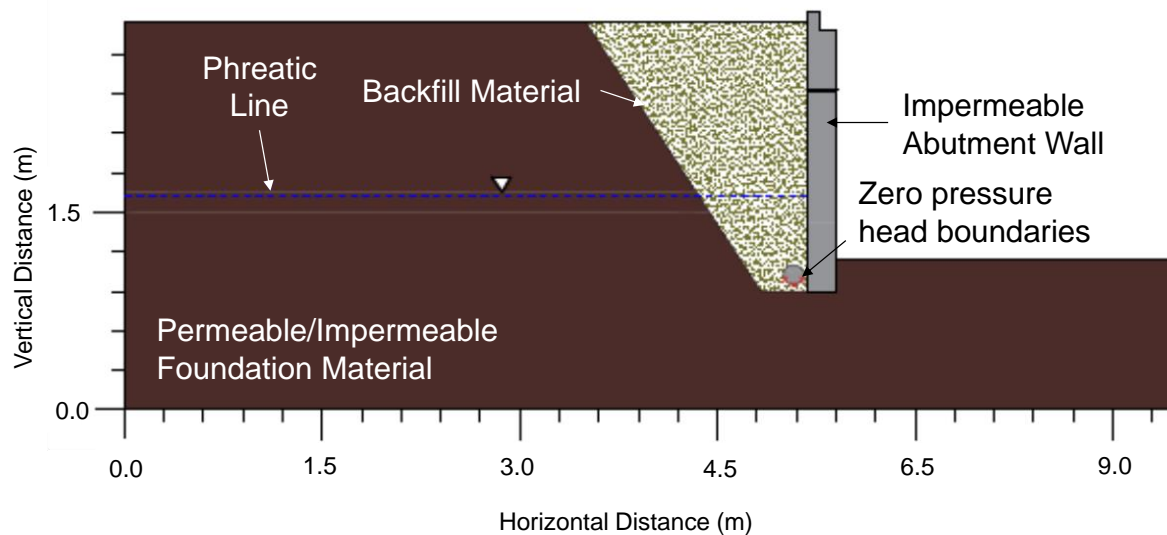
Figure 94. Numerical model and boundary conditions setup for field drainage analysis

The measured pore pressure dissipation are compared with the predicted values in Figure 95 and Figure 96. The measured values showed frequent fluctuations with increasing and decreasing values, likely because of how the water was drawn into and drained out of the abutment. This was not accounted for in the numerical analysis.

113
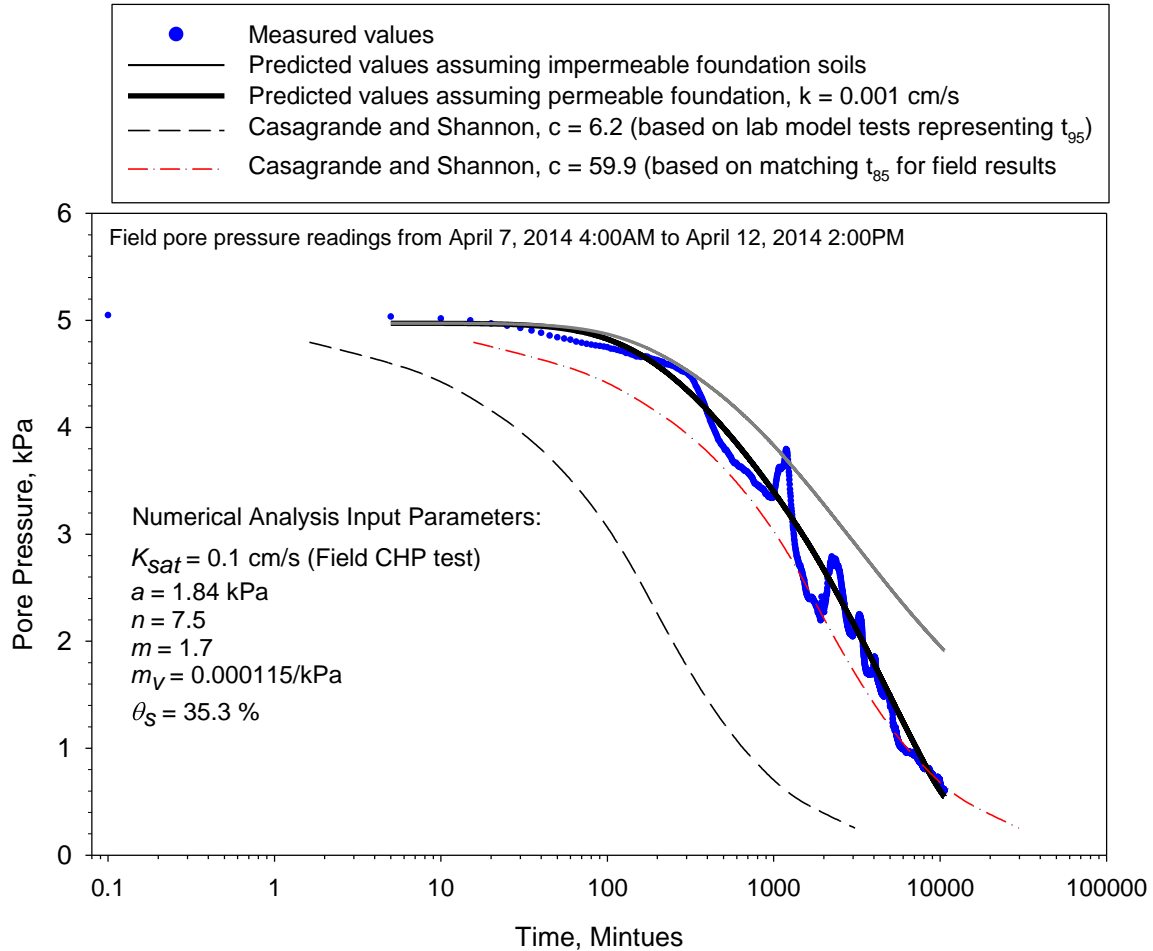
Figure 95. Measured and predicted pore pressure dissipations from April 7, 2014 to April 12, 2014

The measured values indicated $t_{50} \sim 26$ hours, while numerical analysis with impermeable layers indicated $t_{50} \sim 57$ hours and with permeable layers indicated $t_{50} \sim 39$ hours. Standard error for the numerical analysis was calculated as about 87 hours for impermeable foundation, and about 42 hours for permeable foundation. The predicted values from numerical analysis were conservative but followed the same trend observed in the measured values.

Casagrande and Shannon method with $c = 6.2$ indicated $t_{50} \sim 162$ minutes with a standard error of about 236 hours. By modifying the c value to match with the t_{85} measured in the field, which resulted in $c = 59.9$, reduced the standard error to about 32 hours.

114
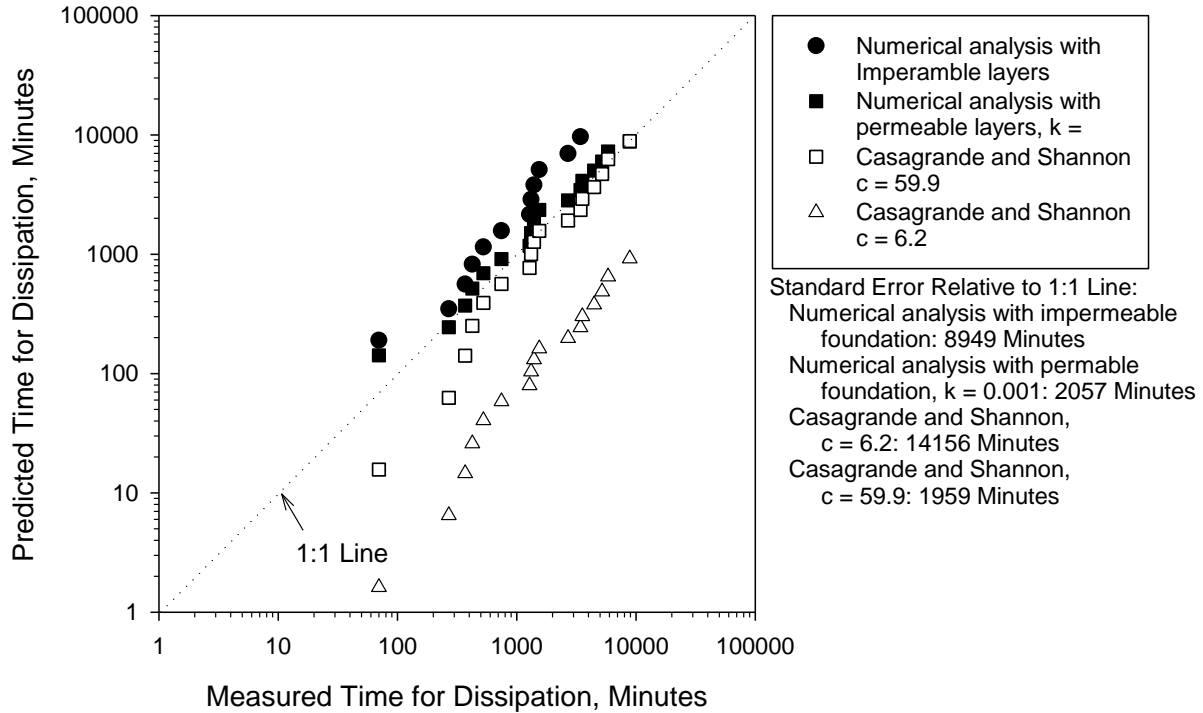
Figure 96. Linear comparison of measured and predicted values

Schwartz Road Bridge

The Schwartz Road Bridge is a 25.1 m (82.5 ft) long two-lane concrete bridge located on Schwartz Road over Little Suamco River near Pulaski in Oconto County, WI. The bridge is supported on a 9.3 m (30.5 ft) wide x 1.5 m (5 ft) tall cast in place concrete abutment founded on HP 10x42 steel piling installed to a depth of about 10.7 m (35 ft). Plan and cross-sectional views of the bridge are provided in Figure 97 and Figure 98, respectively.

According to the subsurface soil information included in the bridge plans, the foundation soils consisted of sandy gravel to gravelly sand deposits down to depths of about 4.5 to 6.1 m (15 to 20 ft), silt soils with intermittent sand layers up to depths of about 7.3 to 7.6 m (24 to 25 ft), and sand and gravel deposits down to bedrock at depths of about 35 to 37 ft below existing grade.
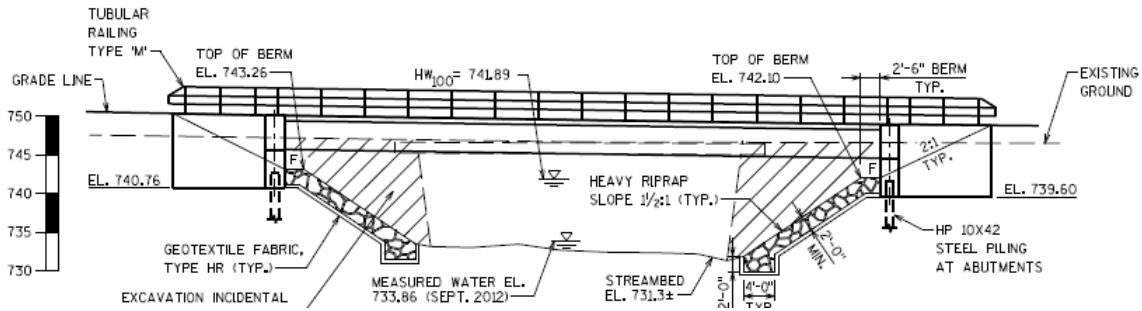
Figure 97. Schwartz Road Bridge cross section (from project plans)
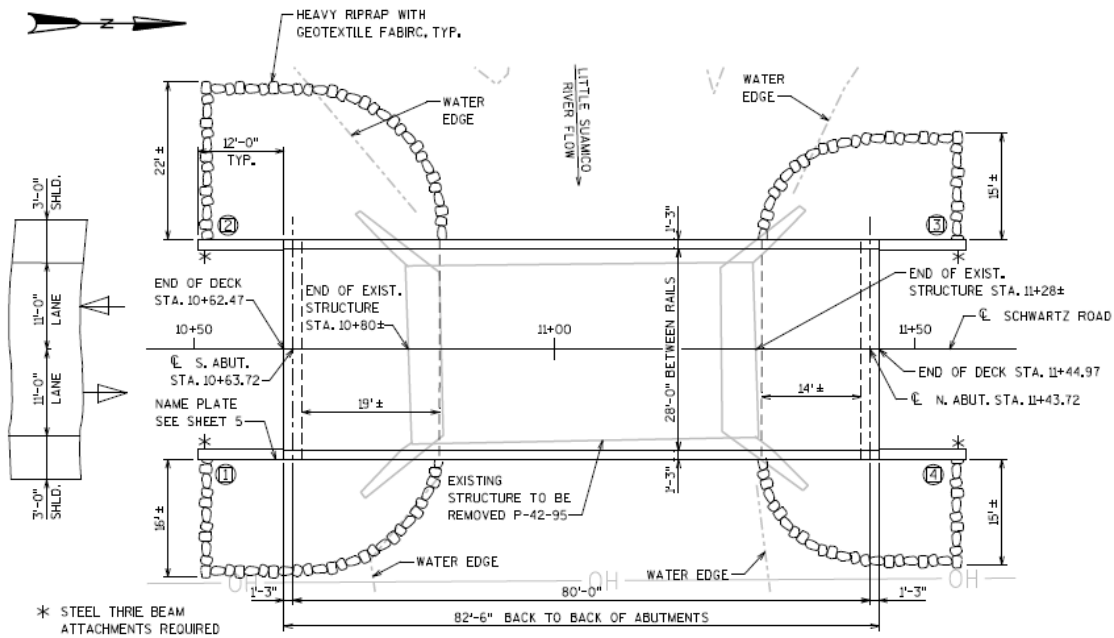
Figure 98. Schwartz Road Bridge plan view (from project plans)

The project plans specified use of structure backfill per WisDOT Standard Specifications Section 210. The drain specifications called for a 0.15 m (6 in.) geotextile wrapped drain tile installed at the bottom of the abutment with a 0.5% slope to the east slopes.

Construction

The ISU research team arrived on-site on September 6, 2014, before the backfill material was placed. The project site reportedly received about 10 cm (4 in.) of rain prior to our arrival and the creek was near its maximum water level (Figure 99). The water level was below the bottom of the backfill elevation, however.

Figure 99. Creek level at Schwartz Road Bridge on 9/6/14 at 9:00 am

Figure 100. Ponded water in the abutment excavation at Schwartz Road Bridge

The abutment backfill excavation was flooded with 0.6 m to 0.9 m (2 to 3 ft) of ponded

water, despite the presence of drain tile at the bottom of the excavation. About 0.3 m to 0.5 m of

backfill was placed over the drain tile prior to our arrival. Pictures at the bottom of the excavation near the drain tile after the ponded water was drained out are shown in Figure 101. Field observations indicated that the drain sock was clogged with fines (as evidenced in laboratory abutment model testing described in Chapter 5) and was not draining the water. The bottom of the excavation was very soft.

The contractor pumped the water out and excavated some of the soft material out of the excavation. New backfill material was placed in 0.3 m (1 ft) thick lifts and compacted using a hand-held vibratory compactor (Figure 102).

The particle-size distribution curve of the material in comparison with the WisDOT Structure Backfill specifications is provided in Figure 103. The backfill material used on this site met the specified gradation limits.

Samples from the structure backfill and from on-site stockpile were collected and tested to determine in place moisture content. The material moisture contents varied from about 2% to 8% and is compared with laboratory compaction and collapse index test results in Figure 104.

The field moistures were higher than the bulking moisture content identified with Proctor testing. The collapse test results indicated a maximum collapse strain of about 0.13% at 5.4% moisture content, which was within the field moisture content range. This collapse equals to about 2 mm (0.08 in.) of settlement after wetting for the 1.5 m of backfill material at this site.

Figure 101. Bottom of the excavation near the drain tile on the south abutment after pumping out the ponded water

Figure 102. Compaction of backfill at Schwartz Road Bridge

Figure 103. Schwartz Road Bridge backfill material gradation in comparison with structure backfill gradation limits per WisDOT specifications
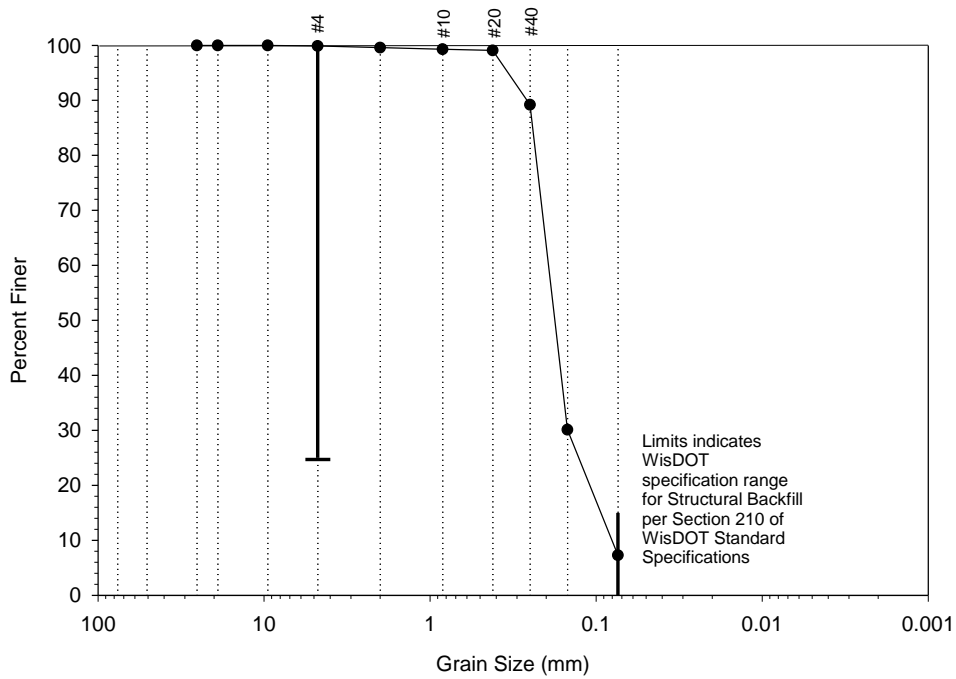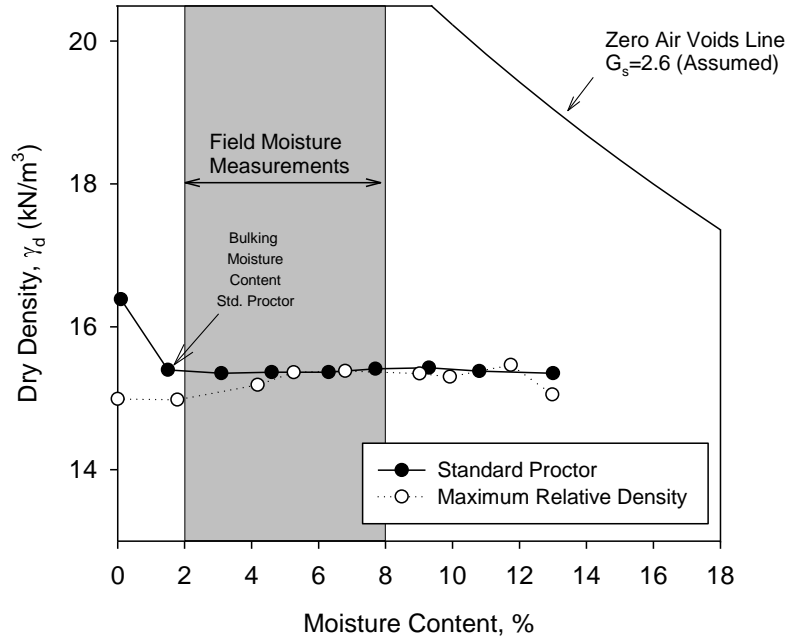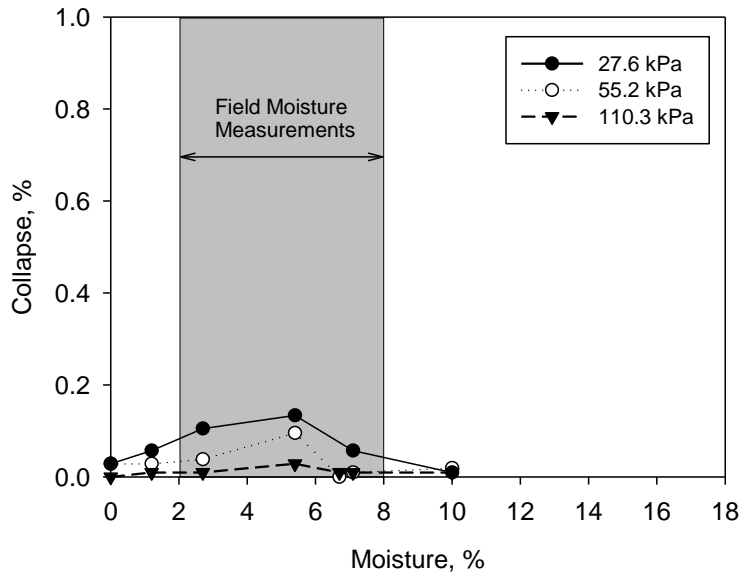
Figure 104. Field moisture results compared to: (a) laboratory compaction results; and (b) laboratory collapse index test results

Field Testing

Six DCP tests and three APT tests were conducted on the backfill material. CHP tests were attempted but could not be conducted at this site due to water leakage issues. DCP and APT locations are shown in (Figure 105). Two DCP tests were performed in the bottom of the

excavation, and four DCP tests were performed at the top of the backfill after all lifts were placed and compacted.

DCP-CBR with depth and cumulative blows with depth profiles are shown in Figure 106. DCP tests at the bottom of the excavation indicated very soft conditions with CBR ranging from <1.0 to 3.0 up to about 0.3 to 0.5 m below the bottom of the excavation. DCP-CBR values at the surface indicated that values generally increased with depth, which is typical for cohesionless materials due to the effect of confinement.

APT tests indicated a K_{sat} of 0.1 cm/s to 0.16 cm/s (283 ft/day to 454 ft/day) in the three tests performed.
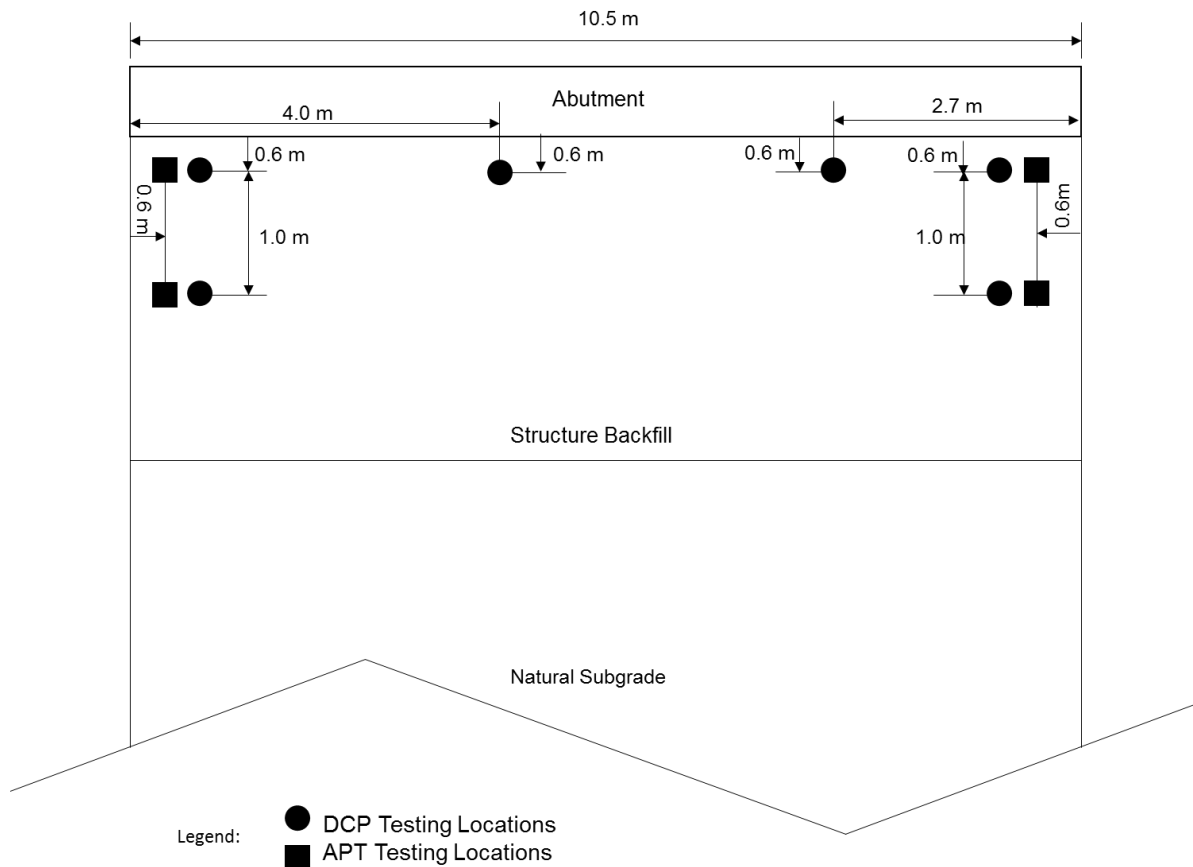
Figure 105. Plan view of the bridge abutment showing APT and DCP test locations at Schwartz Road Bridge
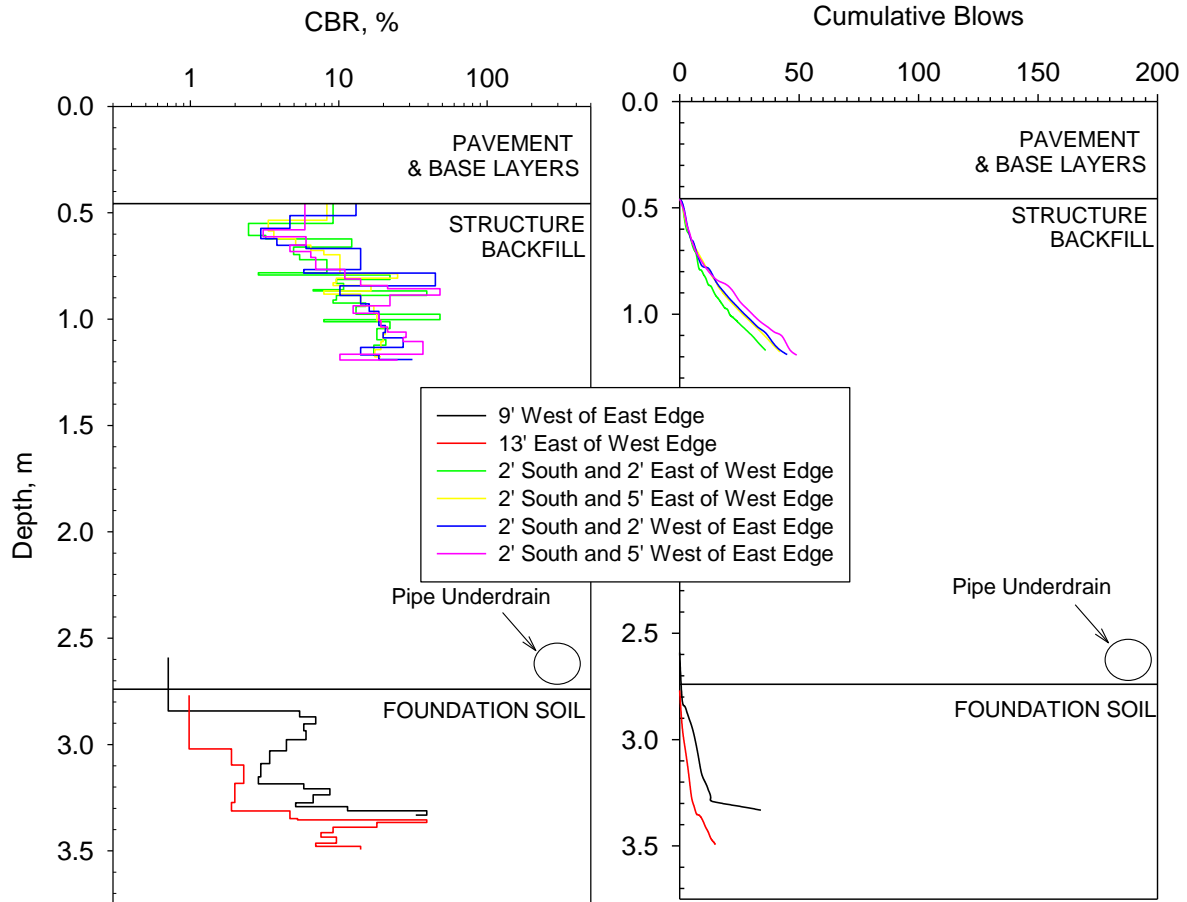
Figure 106. DCP results for Schwartz Road Bridge

Instrumentation

Three EPCs and two PP sensors were installed behind the abutment (Figure 107). EPC1 was installed slightly above the drain tile to measure lateral stress and EPC2 measuring vertical stress was installed next to the drain tile (Figure 108 and Figure 109). PP1 sensor was installed at the bottom of the drain tile. EPC3 measuring lateral stress and a PP2 sensor was installed near the top of the abutment. The EPCs and pore pressure sensors were installed as backfill was being compacted. A third pore pressure (PP3) sensor was installed at 3.0 m (9.8 ft) below the top of the deck near the creek, to monitor water level changes in the creek (Figure 110).

Figure 107. Cross-sectional view of the bridge abutment showing EPC and PP sensor locations at Schwartz Road Bridge

Figure 108. Installation of lateral EPC at drain tile at Schwartz Road Bridge

Figure 109. Installation of vertical EPC at drain tile at Schwartz Road Bridge

Location of creek
pore pressure
sensor

Figure 110. Location of creek pore pressure sensor at Schwartz Road Bridge

Figure 111 shows the measured lateral stresses with the ambient and sensor temperatures.

Figure 112 shows the measured pore pressures and the ambient and sensor temperature data.

Results indicated that lateral pressures at the top of the abutment (EPC3) were either similar are greater than the lateral pressures measured at the bottom (EPC2). Pore pressure data in the creek (PP3) showed 2.5 kPa at the time of sensor installation and rapidly dropped down to below zero, indicating water level decrease in the creek. Negative pore pressures indicate capillary saturation. Interestingly, the fluctuations observed in pore pressure readings in all three sensors followed the same trend.

Using the highest lateral stresses recorded on September 6, 2014, stresses with depth are presented in Figure 113. The theoretical Rankine active and passive earth pressures and Coulomb passive earth pressures are also shown in Figure 113 for comparison. The theoretical values were calculated using $\phi' = 30.1°$ from laboratory direct shear testing, and wall friction $\delta = 2/3\ \phi'$ (for Coulomb passive pressure calculations) and assuming a total unit weight of 15.25 kN/m^3 (based on 95% standard Proctor maximum density and 4.5% moisture content). A surcharge load of 41.1 kPa determined from the vertical EPC was used in the calculations to account for weight of backfill material above the top of the abutment height and the weight of pavement and base layers. These theoretical values assume no pore pressures behind the wall, as considered in the design.

The measured values were close to the Rankine active case values. Additional data is being collected for comparison and the results will be updated for the final report.

Figure 111. EPC readings from Schwartz Road Bridge: (a) total lateral earth pressure readings with time, and (b) ambient and EPC temperature readings with time

Figure 112. PP readings from Schwartz Road Bridge: (a) pore water pressure readings with time, and (b) ambient and PP temperature readings with time

Figure 113. Measured and theoretical distribution of lateral earth pressures

Hobbles Creek Bridge

The Hobbles Creek Bridge is a 13.6 m (44.5 ft) long sloping two-lane concrete bridge located on Hobbles Creek Road over Hobbles Creek in Price County, WI. The bridge is supported on a 9.5 m (31.2 ft) wide x 2.3 m (7.7 ft) tall cast in place concrete abutment founded on HP 10x42 steel piling installed to a depth of about 15.2 m (50 ft). Plan and cross-sectional views of the bridge are provided in Figure 114 and Figure 115, respectively.

According to the subsurface soil information included in the bridge plans, the foundation soils consisted sandy gravel to sand soils with occasional cobbles and gravel down to depths of about 45 ft to 60 ft below existing grade.

The project plans specified use of Structure Backfill per WisDOT Standard Specifications Section 210. The drain specifications called for a 0.15 m (6 in.) geotextile wrapped drain tile installed at a depth of about 0.66 m (2.2 ft) above the bottom of the structure backfill with a 0.5% slope to a suitable drainage location.
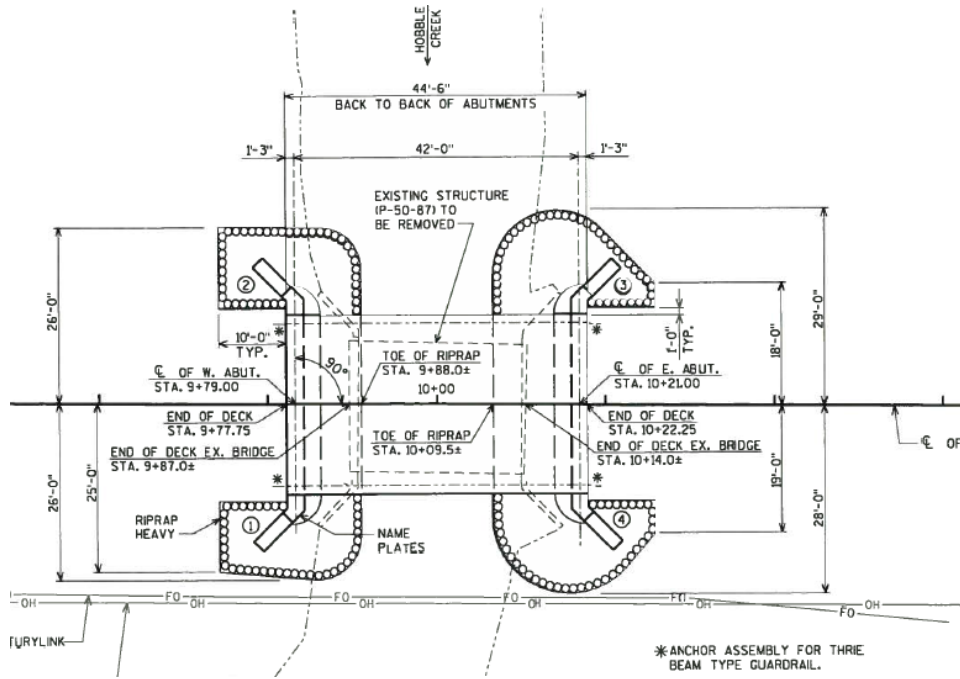
Figure 114. Hobbles Creek Bridge plan view (from project plans)
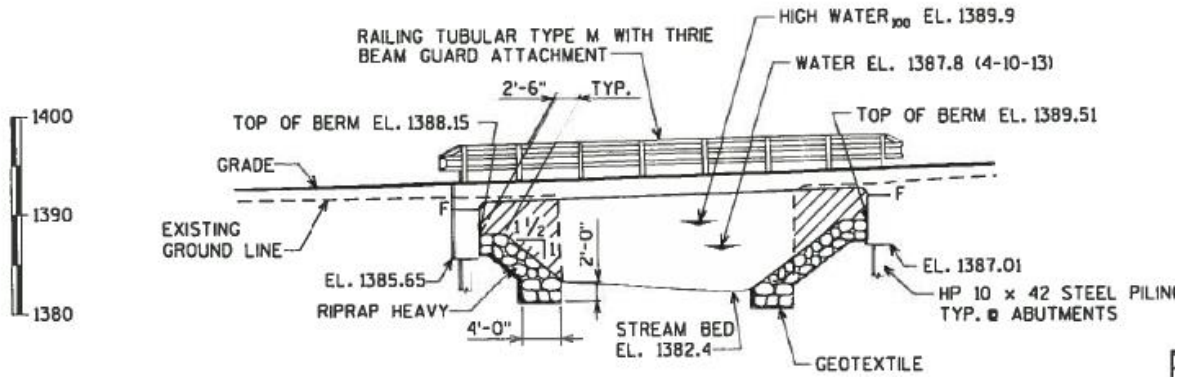
Figure 115. Hobbles Creek Bridge cross section (from project plans)

Construction

The ISU research team arrived on-site on October 6, 2014, before the backfill material was placed (Figure 116). Some standing water was observed in the west abutment excavation (Figure 117). The backfill was compacted with a hand-held vibratory compactor and compacted in 0.3 m (1 ft) thick lifts (Figure 118).

Figure 116. Hobbles Creek Bridge west abutment before backfilling

Figure 117. West abutment excavation at Hobbles Creek with standing water

Figure 118. Hobbles Creek Bridge after backfilling

The particle-size distribution curve of the material in comparison with the WisDOT Structure Backfill specifications is provided in Figure 119. The backfill material used on this site met the specified gradation limits.

Samples from the structure backfill from on-site stockpile were collected and tested for in place moisture content. The moisture contents varied from about 6% to 12% and is compared with laboratory compaction and collapse index test results in Figure 120. The field moistures were higher than the bulking moisture contents identified with Proctor and vibratory compaction testing. The collapse test results indicated a potential collapse strain of about 3.5% at 3.3% moisture content, which the outside the field moisture range.

Field Testing

APT tests were conducted at three location on top of the backfill and CHP test was conducted at one location. DCP tests were performed at three locations near the bottom, mid-depth, and top of the backfill. The locations are shown in Figure 121.

APT tests indicated K_{sat} values with an average of about 0.08 cm/s (226 ft/day) at the three locations. Figure 122 shows the results for CHP tests. K_{sat} values started at 0.0058 cm/s (16 ft/day) and decreased to 0.0047 (13 ft/day) after about 90 minutes. APT tests indicated hydraulic conductivities one magnitude higher than CHP.

DCP-CBR with depth and cumulative blows with depth profiles are shown in Figure 123. DCP-CBR profiles generally increased with depth.

Figure 119. Hobbles Creek Bridge backfill material gradation in comparison with structure backfill gradation limits per WisDOT specifications

(a)

(b)

Figure 120. Field moisture results compared to: (a) laboratory compaction results; and (b) laboratory collapse index test results

134
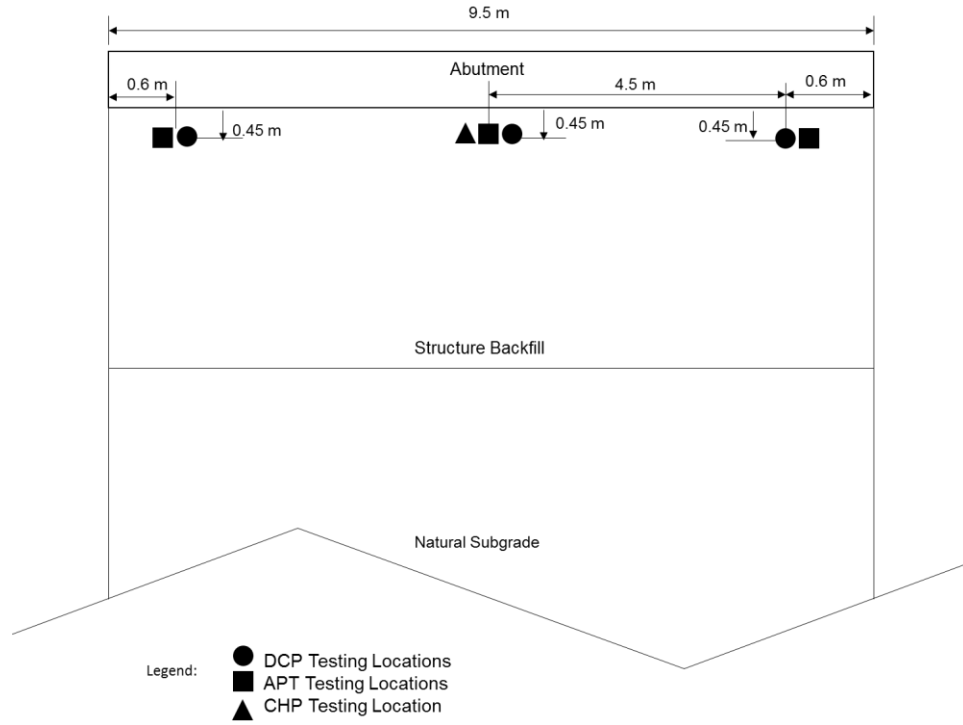
Figure 121. Plan view of the bridge abutment showing APT and DCP test locations at Hobbles Creek Bridge
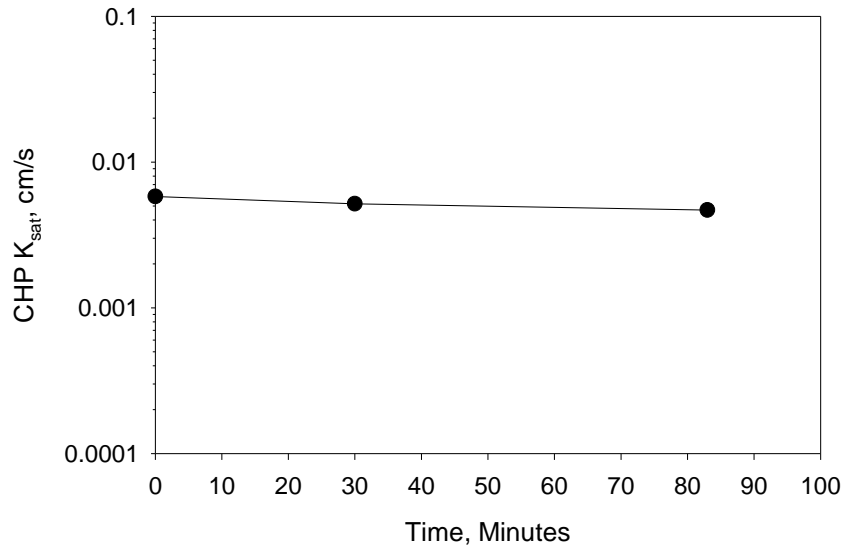
Figure 122. CHP results for Hobbles Creek Bridge

Figure 123. DCP test results for Hobbles Creek Bridge

Instrumentation

Three EPCs and two PP sensors were installed behind the abutment (Figure 124). EPC1 measuring lateral stress, EPC2 measuring vertical stress and PP1 were installed against the abutment wall next to the drain tile. EPC3 measuring lateral stress and PP2 were installed near the top of the abutment. The EPCs and pore pressure sensors were installed as backfill was being compacted. Pictures from EPC and PP installation in the backfill are shown in Figure 125 and Figure 126. A third pore pressure (PP3) sensor was installed at a depth of about 2.3 m (7.5 ft) below the top of the deck near the creek to monitor water level changes in the creek.
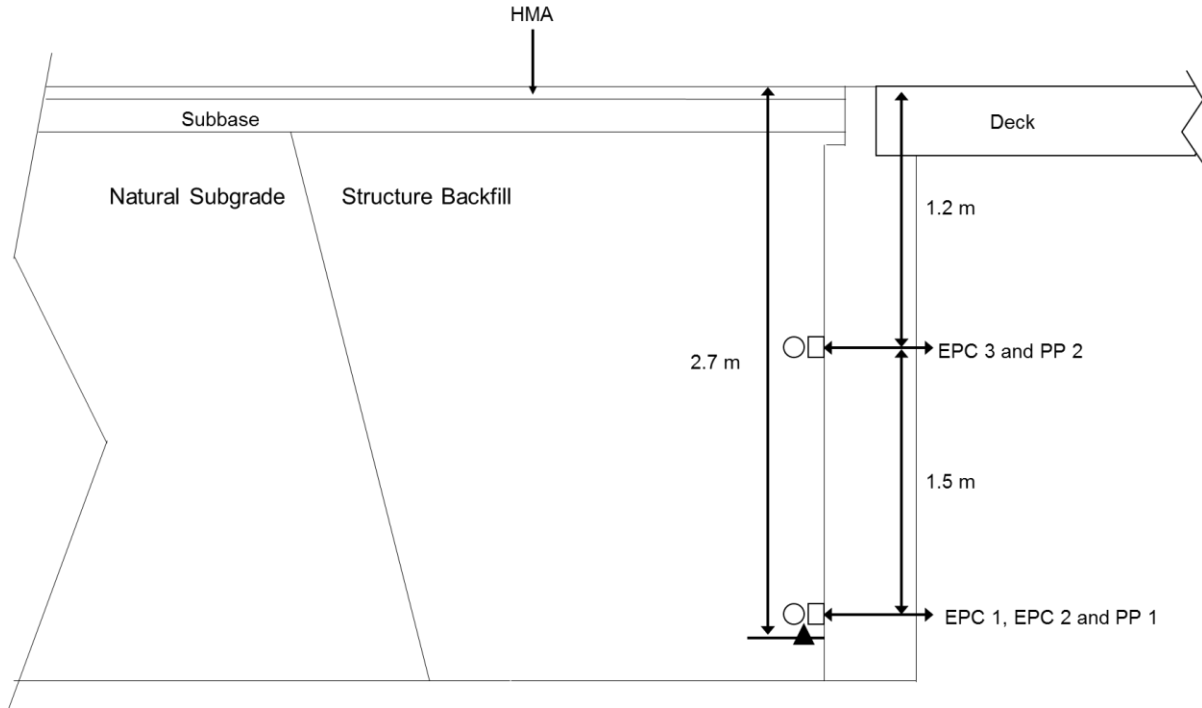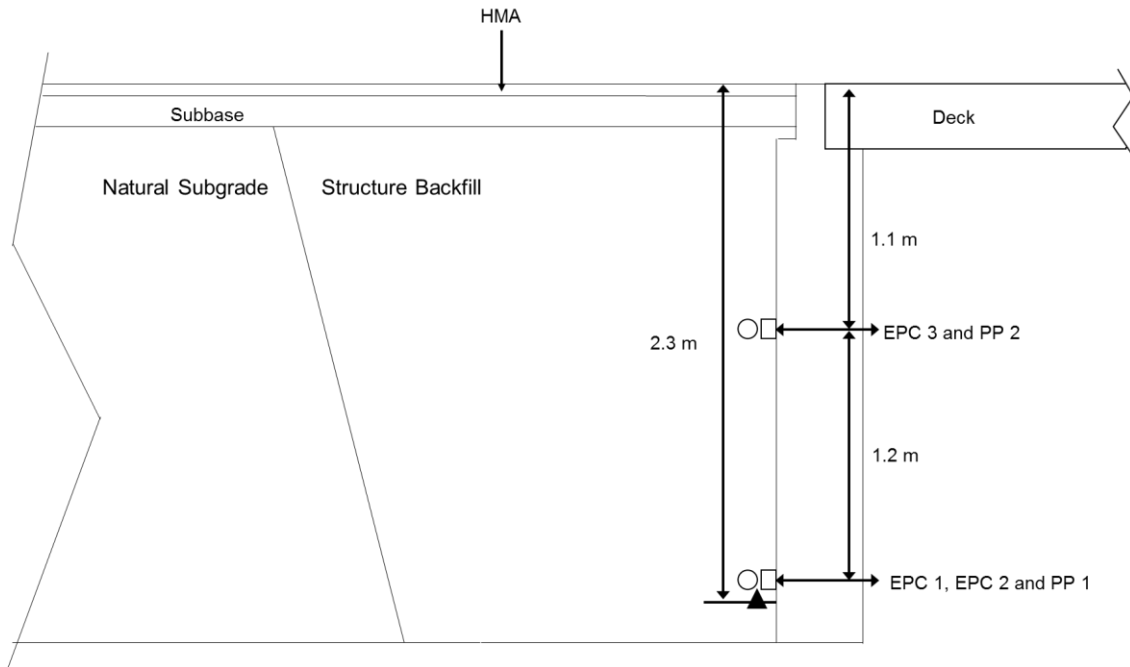
Figure 124. Cross-sectional view of the bridge abutment showing EPC and PP sensor locations at Hobbles Creek Bridge

Figure 125. Vertical EPC and pore pressure sensor installation at Hobbles Creek Bridge

Figure 126. Lateral EPC installation at Hobbles Creek Bridge

Figure 127 shows the measured lateral stresses with the ambient and sensor temperatures. Lateral stresses at the bottom of the abutment, near the drain tile, were greater than the stresses measured near the top of the abutment.

Figure 128 shows the measured pore water pressures with the ambient and sensor temperature data. Negative pore pressures indicating capillary saturation was observed in all the sensors.

The measured maximum lateral pressures with depth in comparison with theoretical Rankine active and passive earth pressures and Coulomb passive earth pressures are presented in Figure 113. The theoretical values were calculated using $\phi' = 30.1°$ from laboratory direct shear testing, and wall friction $\delta = 2/3\ \phi'$ (for Coulomb passive pressure calculations) and assuming a total unit weight of 19.44 kN/m^3 (based on 95% standard Proctor maximum density and 8% moisture content). A surcharge load of 8.12 kPa calculated from the vertical EPC was used in the calculations to account for weight of backfill material above the top of the abutment height and the weight of pavement and base layers. These theoretical values assume no pore pressures behind the wall, as considered in the design. The measured values were between the Rankine

active and passive case values. Additional data is being collected and will be updated for the final report.
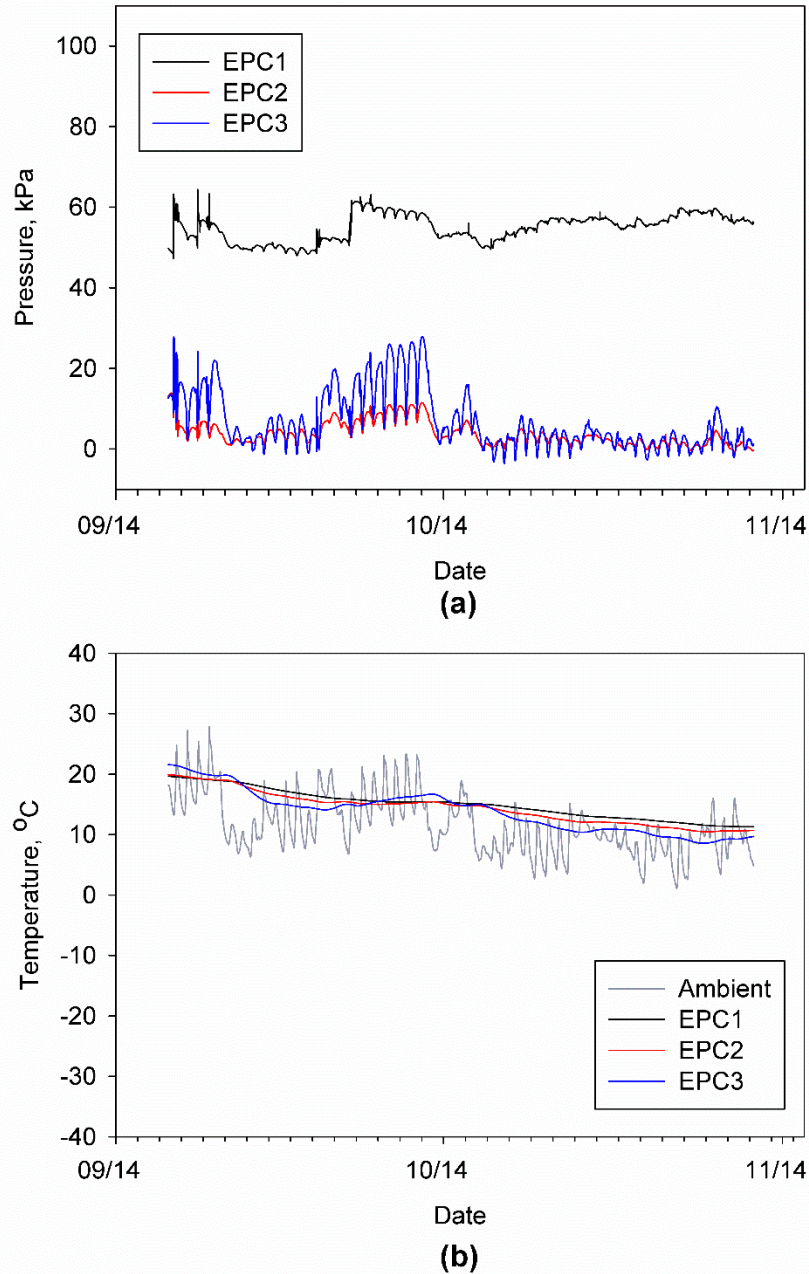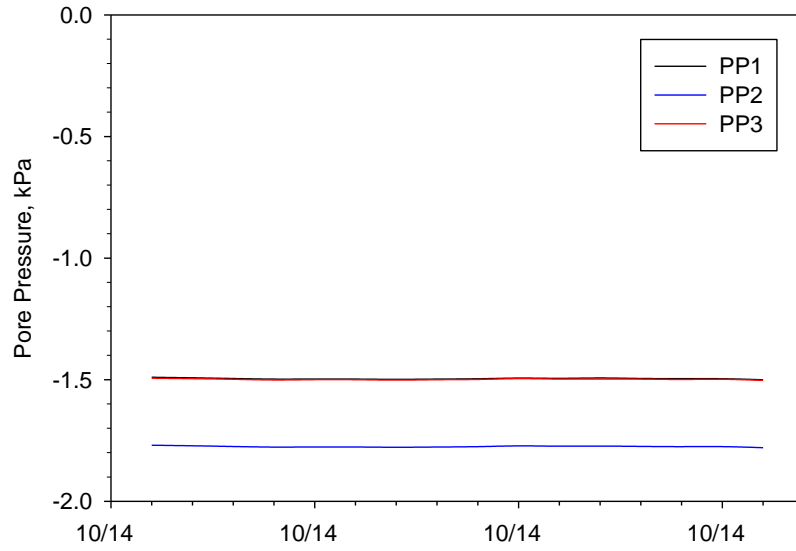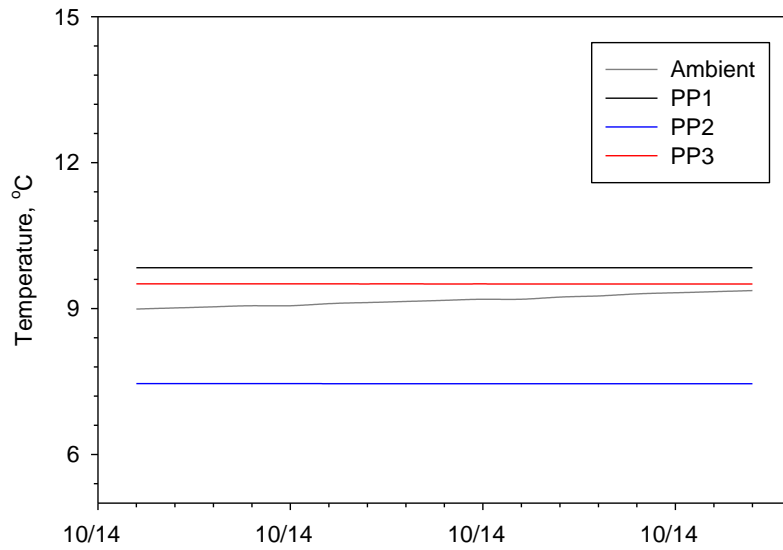

Figure 127. EPC readings from Hobbles Creek Bridge: (a) total lateral earth pressure readings with time, and (b) ambient and EPC temperature readings with time
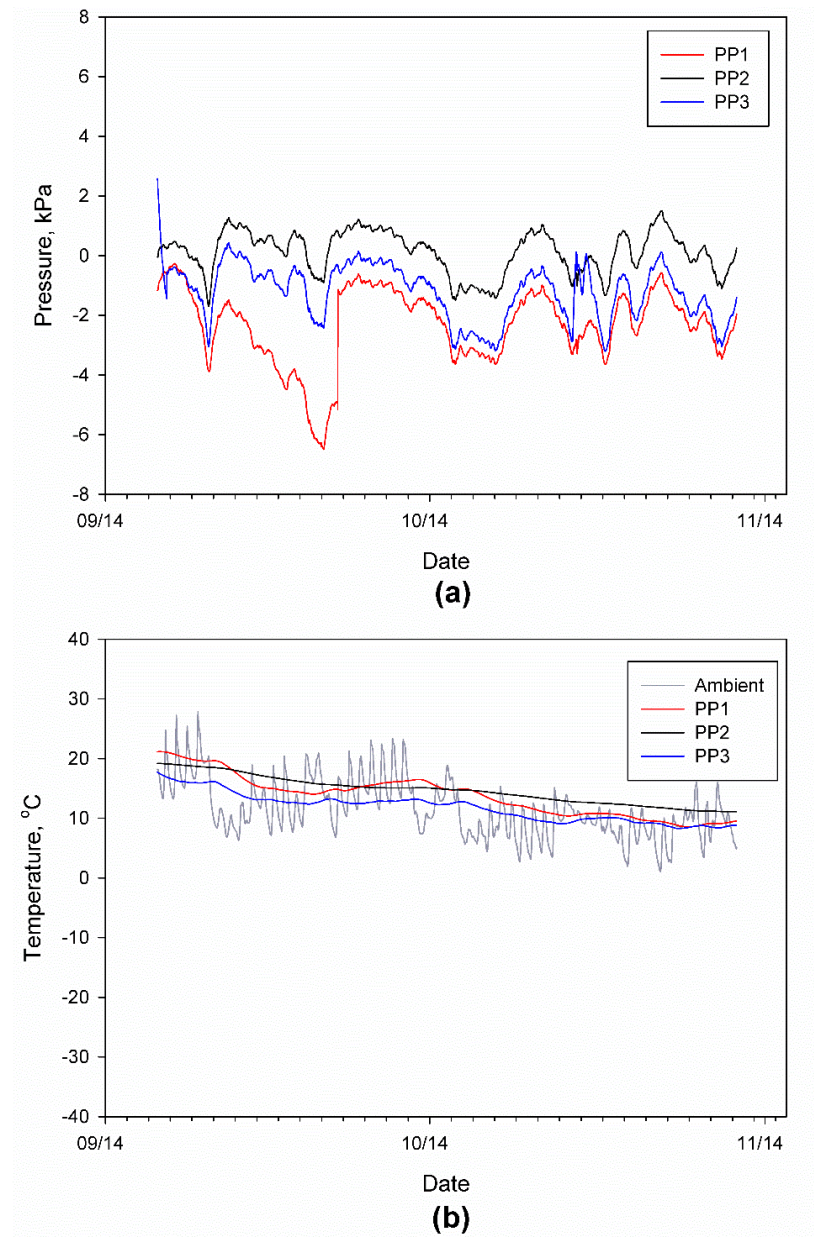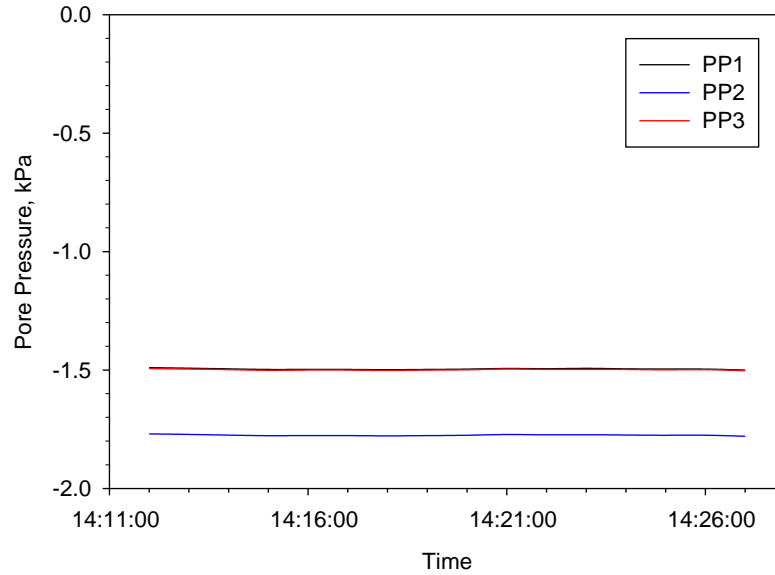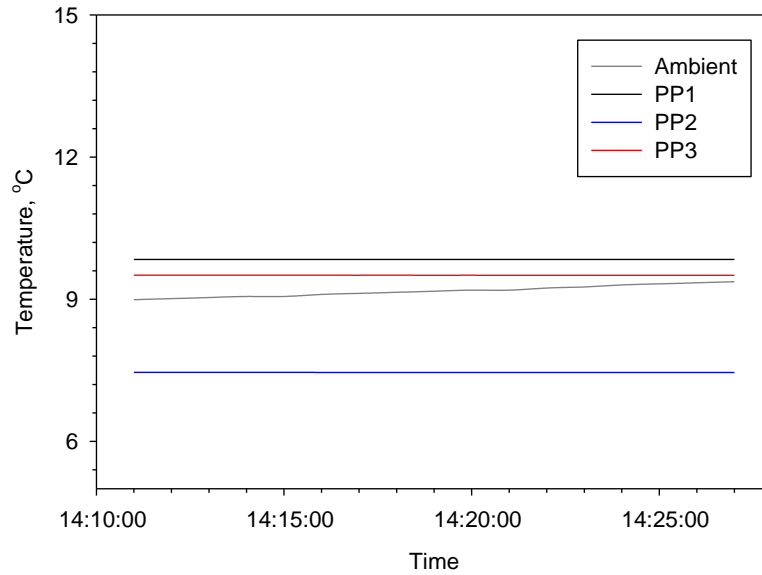
Figure 128. PP readings from Hobbles Creek Bridge: (a) pore water pressure readings with time, and (b) ambient and PP temperature readings with time
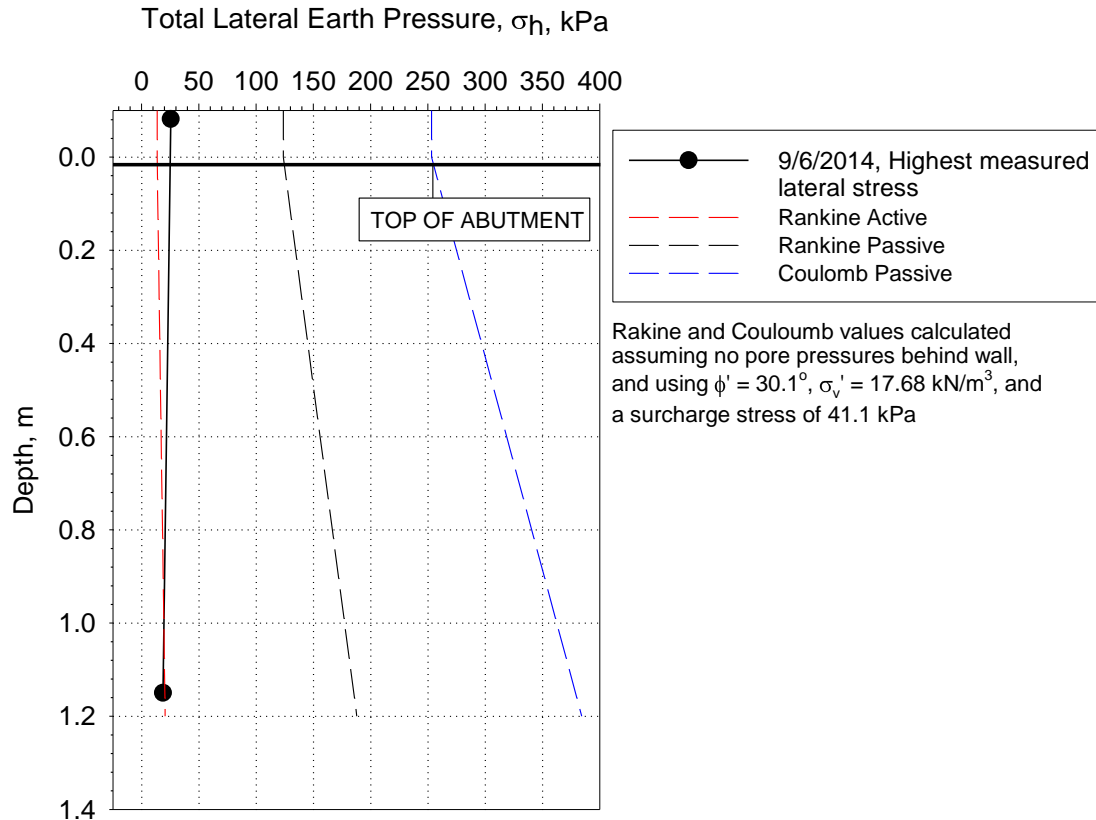
Total Lateral Earth Pressure, σ_h, kPa
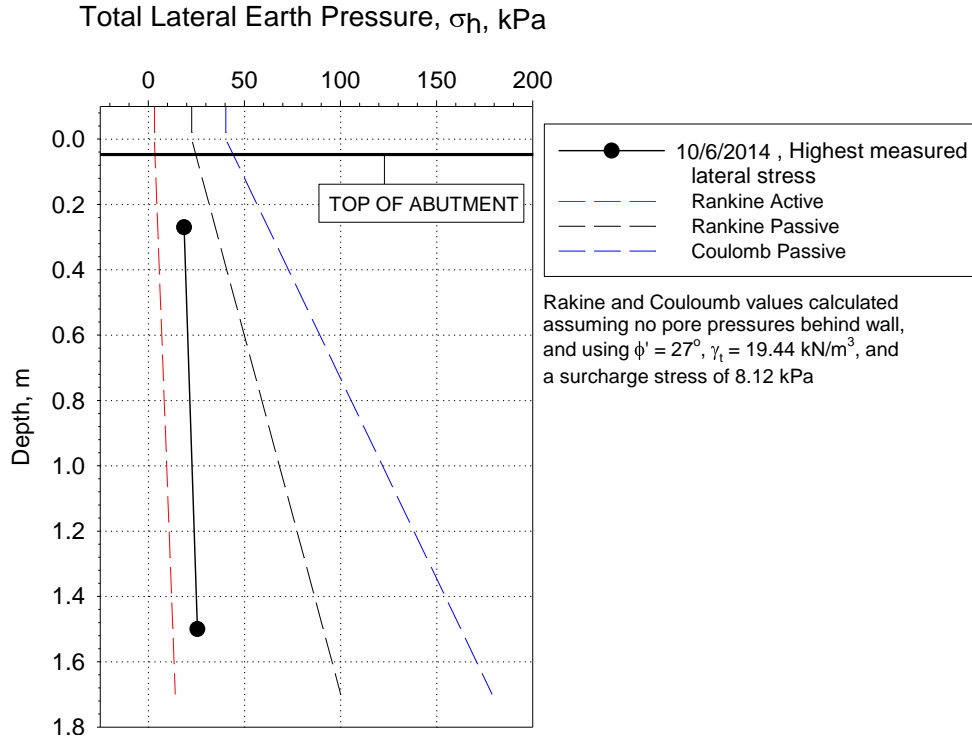
Figure 129. Measured and theoretical distribution of lateral earth pressure

Badger Road Bridge

The Badger Road Bridge is a 17.3 m (56.7 ft) long two-lane concrete bridge located on Badger Road over Branch Marin Brach near North Lancaster in Grant County, WI. The bridge is supported on a 8.6 m (28.2 ft) wide x 1.5 m (5 ft) tall cast in place concrete abutment founded on HP 10x42 steel piling installed to a depth of about 7.0 m (23 ft). Cross-sectional and plan views of the bridge are provided in Figure 130 and Figure 131, respectively. According to the subsurface soil information included in the bridge plans, the foundation soils consisted of silty clays down to about 5.2 m (17 ft) underlain by sandy soils with gravel and cobbles down to the bottom of the boring depths of about 8.2 to 8.5m (27 to 28 ft).

The project plans specified use of Grade 1 Granular Backfill per WisDOT Standard Specifications Section 209. The drain specifications called for a 0.15 m (6 in.) geotextile wrapped drain tile installed at the bottom of the abutment with a 0.5% slope to a suitable drainage location.
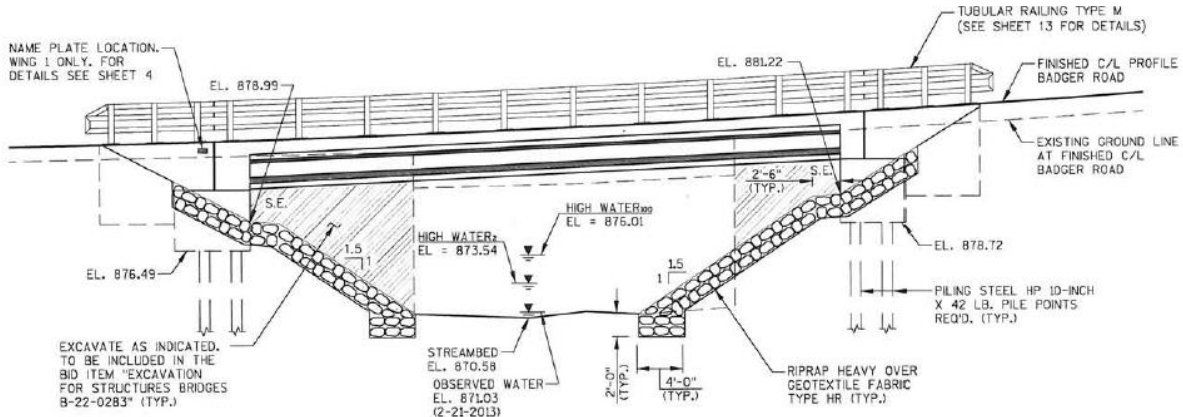
Figure 130. Badger Road Bridge cross section (from bridge plans)
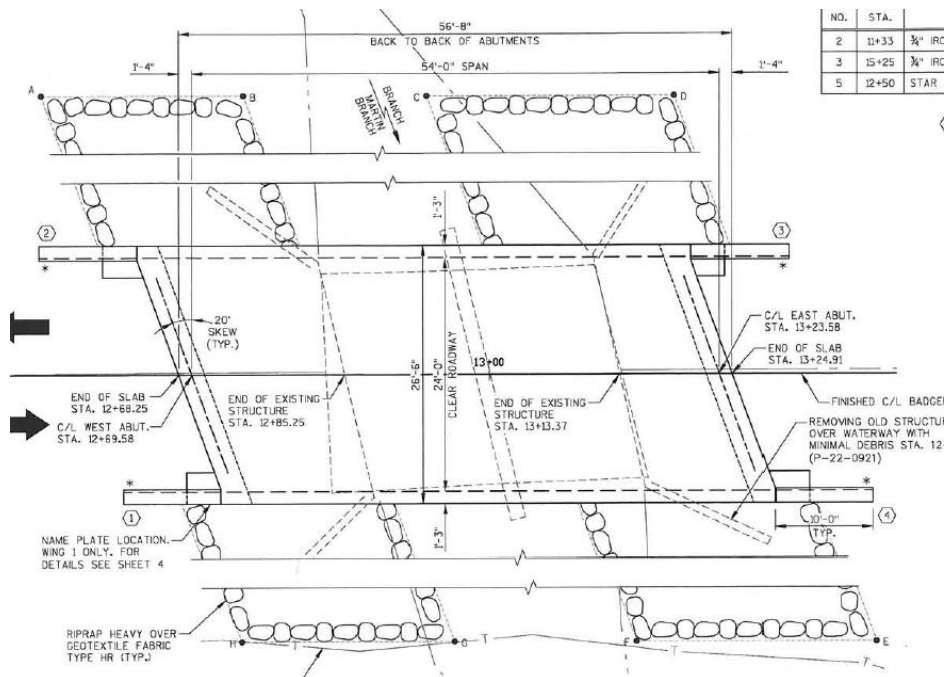
Figure 131. Badger Road Bridge plan view (from project plans)

Construction

The ISU research team arrived on-site on November 11, 2014, before the backfill material was placed (Figure 132). The backfill was compacted with a vibratory compactor attached to an excavator and compacted in 0.3 m (1 ft) thick lifts (Figure 133 to Figure 134).

The particle-size distribution curve of the material in comparison with the WisDOT Class 1 Granular Backfill specifications is provided in Figure 135. The backfill material used on this site met the specified gradation limits.

Figure 132. Badger Road Bridge before backfilling on west abutment

Figure 133. Compaction with vibratory compactor attached to an excavator

Figure 134. Badger Road Bridge after backfilling abutment
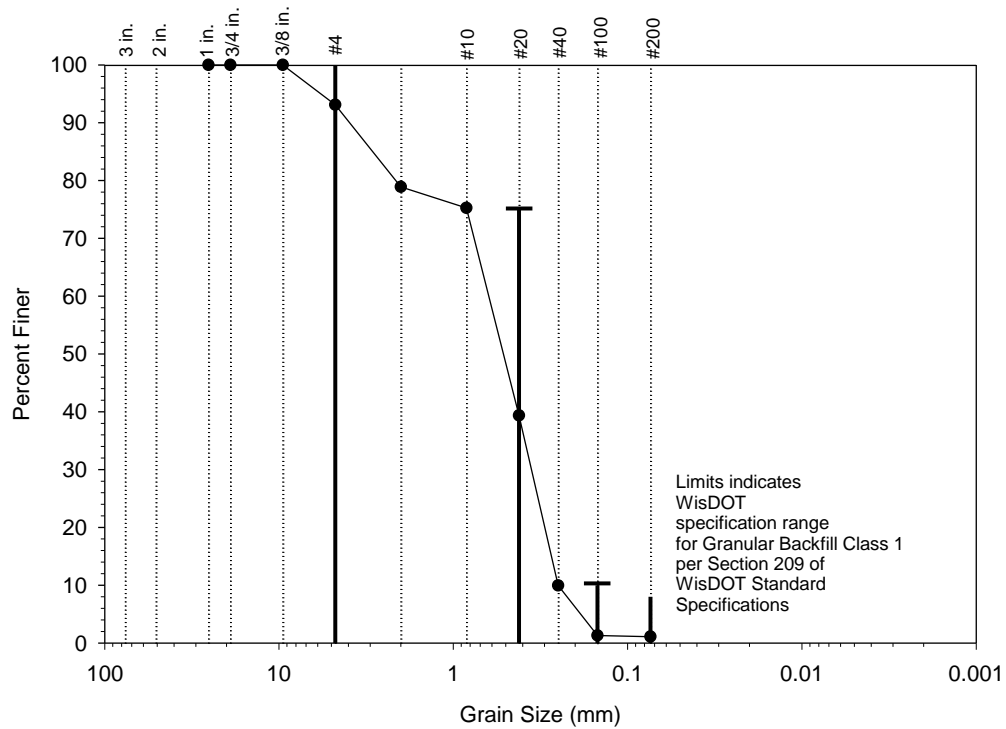
Figure 135. Badger Road Bridge backfill material gradation in comparison with Class 1 granular backfill gradation limits per WisDOT specifications

144
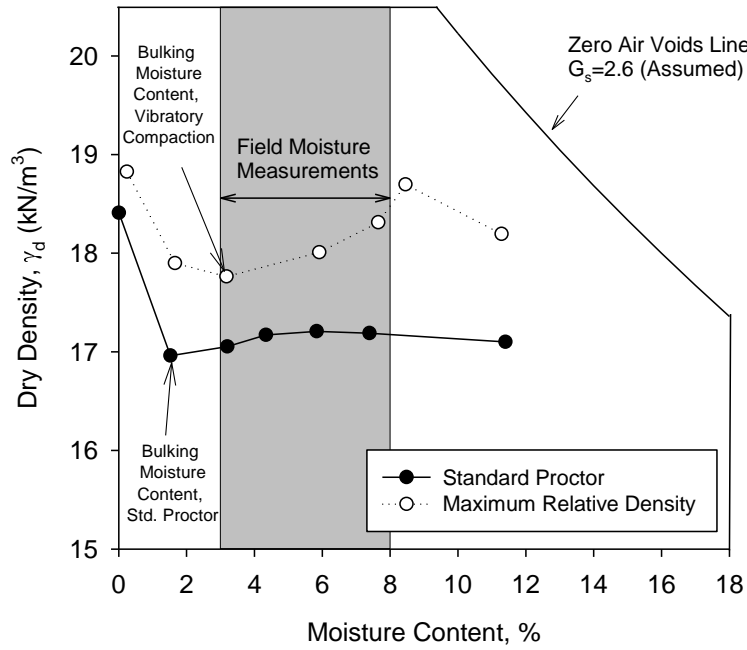
(a)
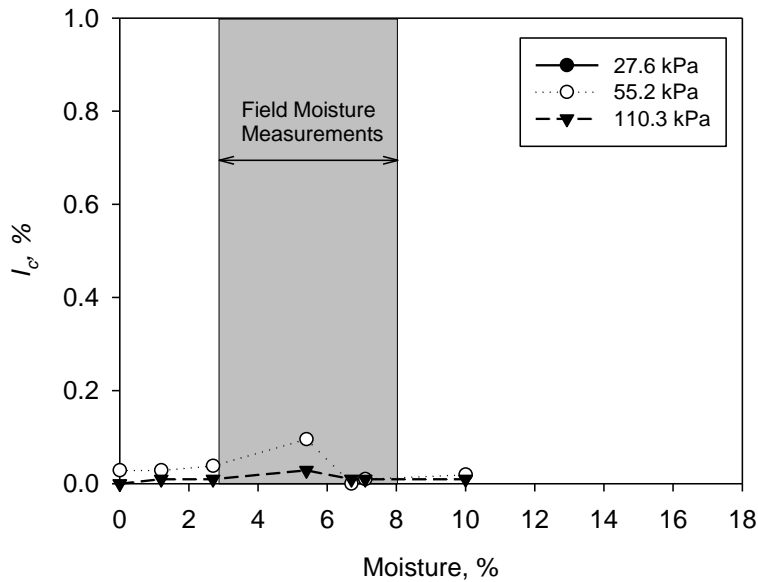
(b)

Figure 136. Field moisture results compared to: (a) laboratory compaction results; and (b) laboratory collapse index test results

Samples from the structure backfill from on-site stockpile were collected and tested for in place moisture content. The moisture contents varied from about 3% to 8% and is compared with laboratory compaction and collapse index test results in Figure 136. The field moistures were

higher than the bulking moisture content identified with Proctor testing. The collapse test results indicated a maximum collapse strain of about 0.13% at 5.4% moisture content.

Field Testing

Three DCP and APT tests, and one CHP test were conducted on the backfill material. The locations are shown in Figure 137. The DCP tests were performed at the bottom of the excavation, at mid depth in the backfill, and at the top of the backfill. APT tests were performed at 0.6 m (2 ft) from each wing wall and one in the center of the abutment. The CHP test was performed for 30 minutes. APT and CHP tests were performed about 0.45 m (1.5 ft) away from the face of the abutment in the granular backfill.
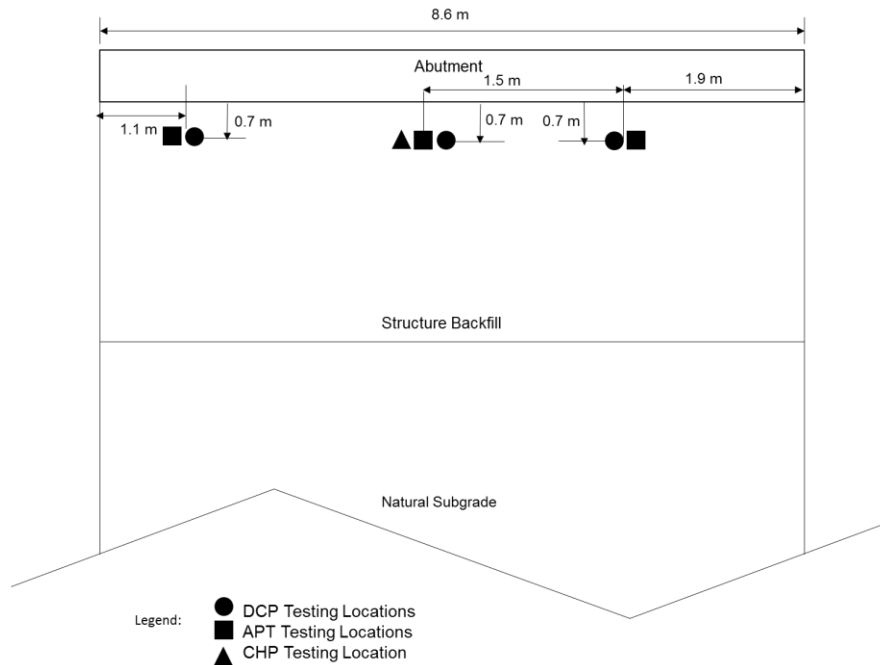
Figure 137. Plan view of the bridge abutment showing APT and DCP test locations at Badger Road Bridge

APT tests indicated an average K_{sat} value of about 0.5 cm/s (1417 ft/day). CHP test showed a K_{sat} of about 0.06 cm/s (170 ft/day). APT tests indicated hydraulic conductivities one magnitude higher than CHP.

DCP-CBR with depth and cumulative blows with depth profiles are shown in Figure 138. DCP-CBR profiles indicated low CBR values (0.5 to 3) at surface but generally increased with depth, which is an effect of confinement.
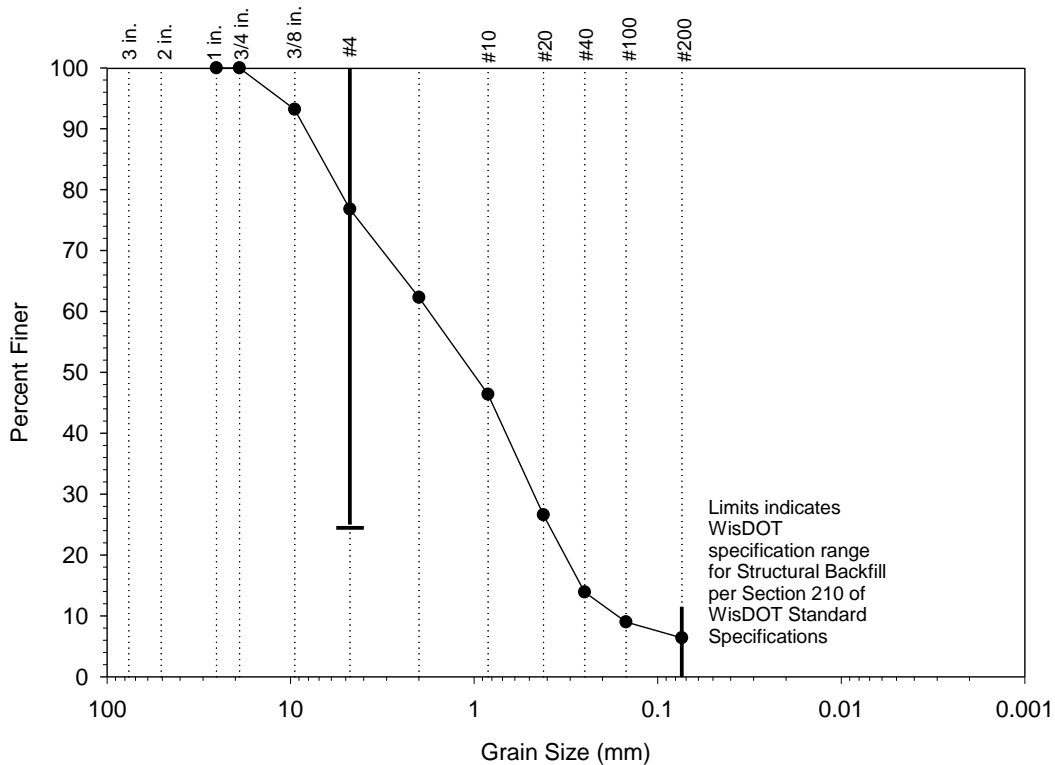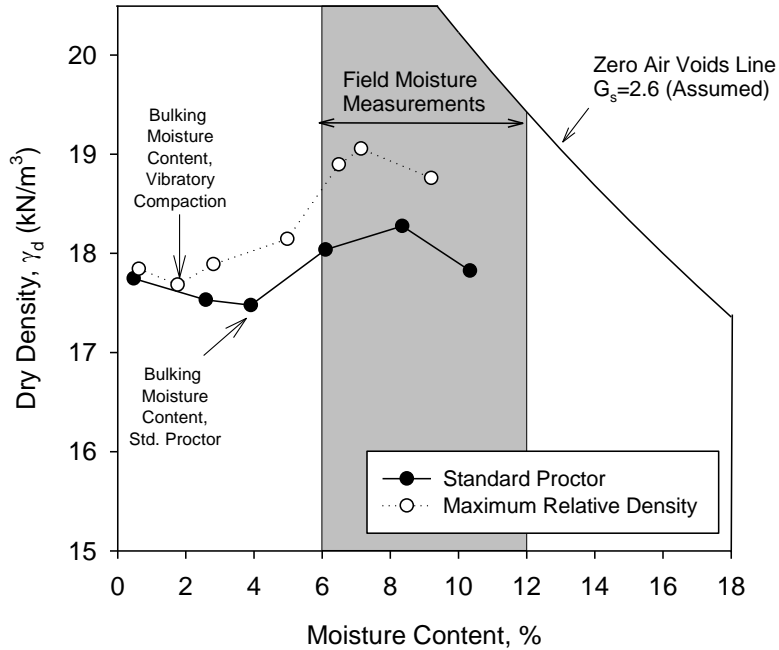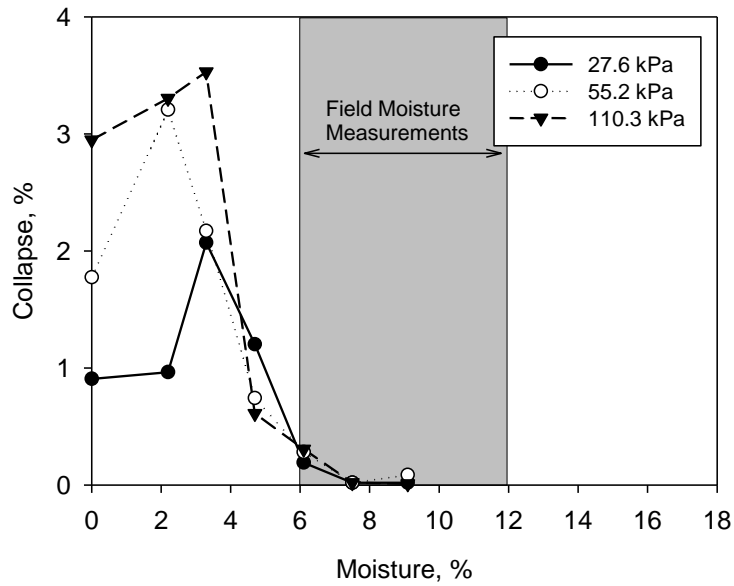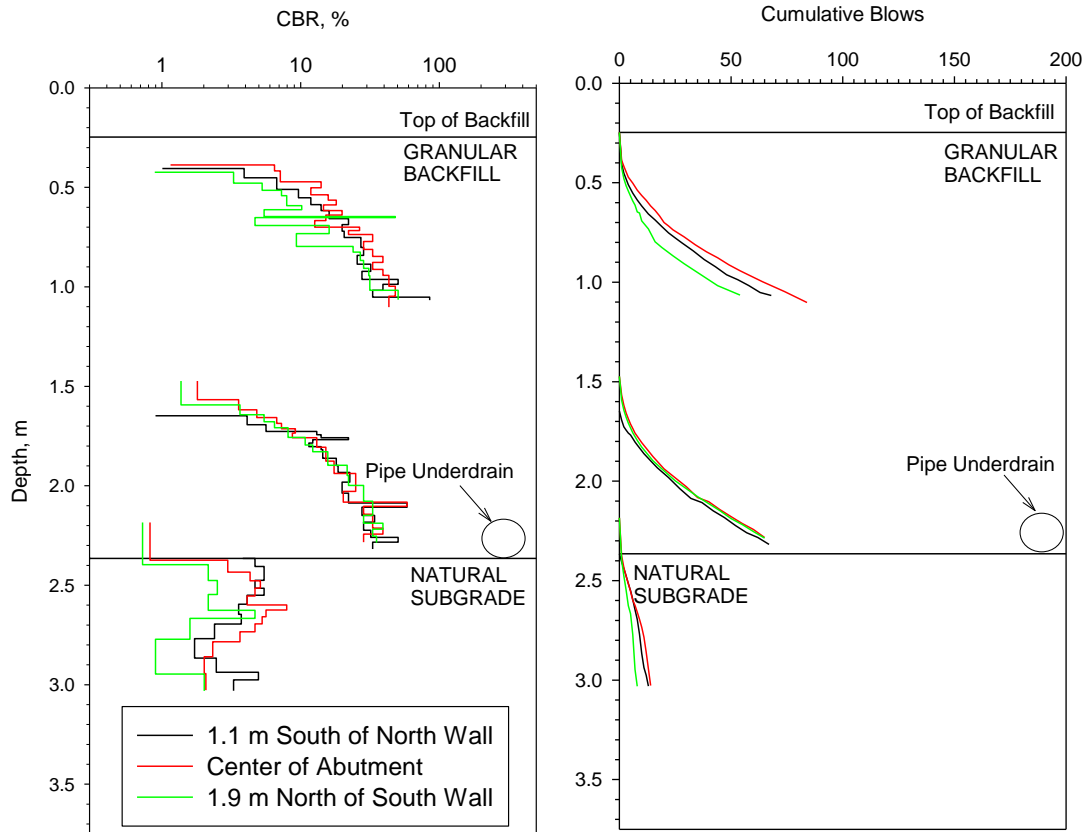
Figure 138. DCP results for Badger Road Bridge

Instrumentation

Three EPCs and two PP sensors were installed behind the abutment (Figure 139). EPC1 measuring vertical stresses and EPC2 measuring lateral stress and a pore pressure (PP1) sensor was installed against the abutmen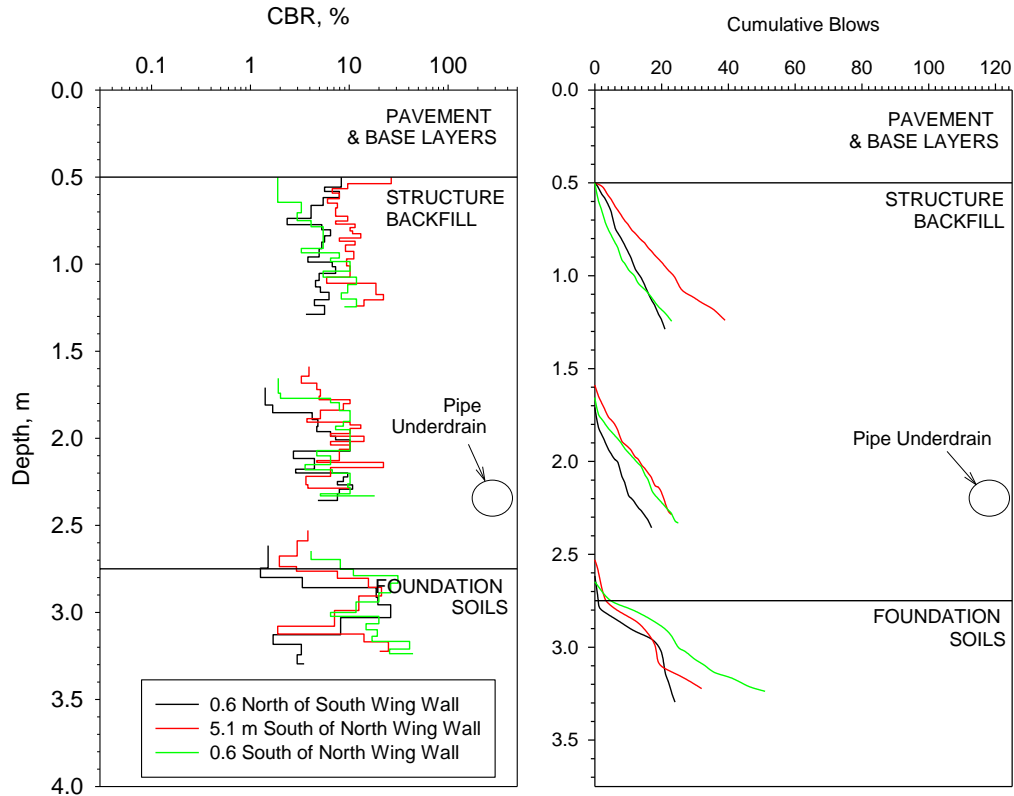t next to the drain tile (Figure 139). EPC3 measuring lateral stress and a PP2 sensor were installed near the top of the abutment. The EPCs and pore pressure sensors were installed as backfill was being compacted. PP3 was installed at a depth of about 5.6 m (18.3 ft) below the top of the deck in the creek to monitor water level changes in the creek. No water was present in the creek at the time of installation.

Figure 141 shows the measured lateral stresses with the ambient and sensor temperatures. Lateral stresses at the bottom of the abutment (near the drain tile) were greater than the stresses measured near the top of the abutment. Figure 142 shows the measured pore water pressure with the ambient and sensor temperature data. Negative pore pressures indicating capillary saturation was observed in all the sensors.
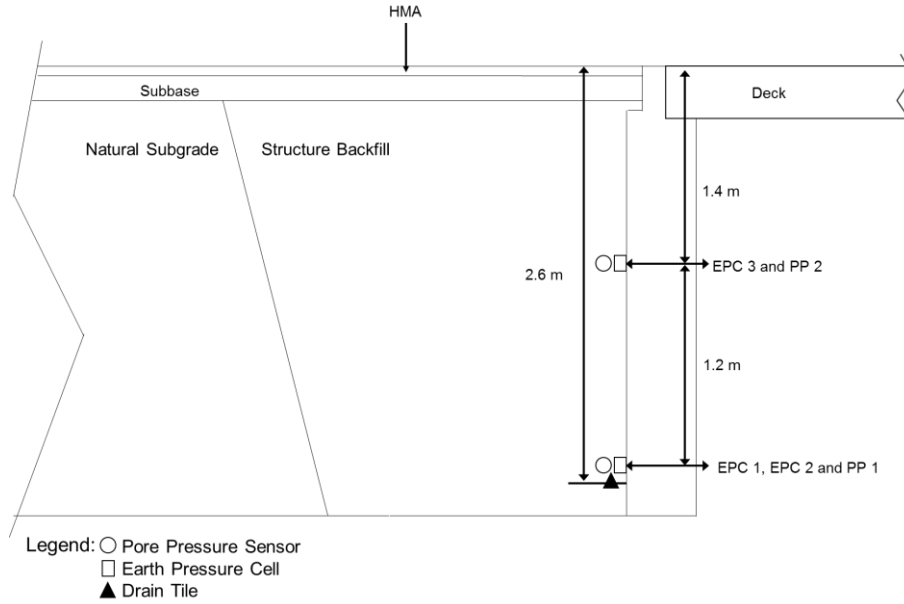
Figure 139. Cross-sectional view of the bridge abutment showing EPC and PP sensor locations at Badger Road Bridge

Figure 140. Sensor installation behind Badger Road Bridge
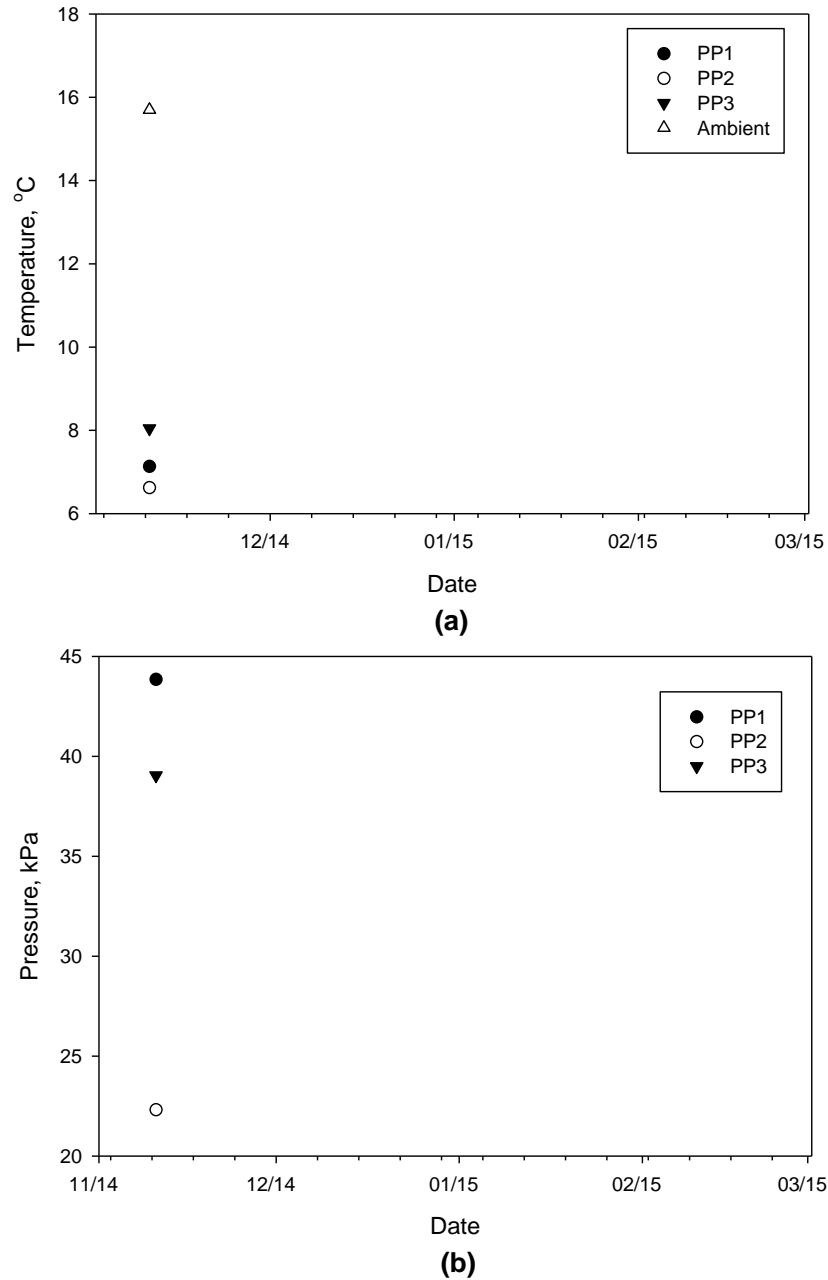
Figure 141. EPC readings from Hobbles Creek Bridge: (a) total lateral earth pressure readings with time, and (b) ambient and EPC temperature readings with time
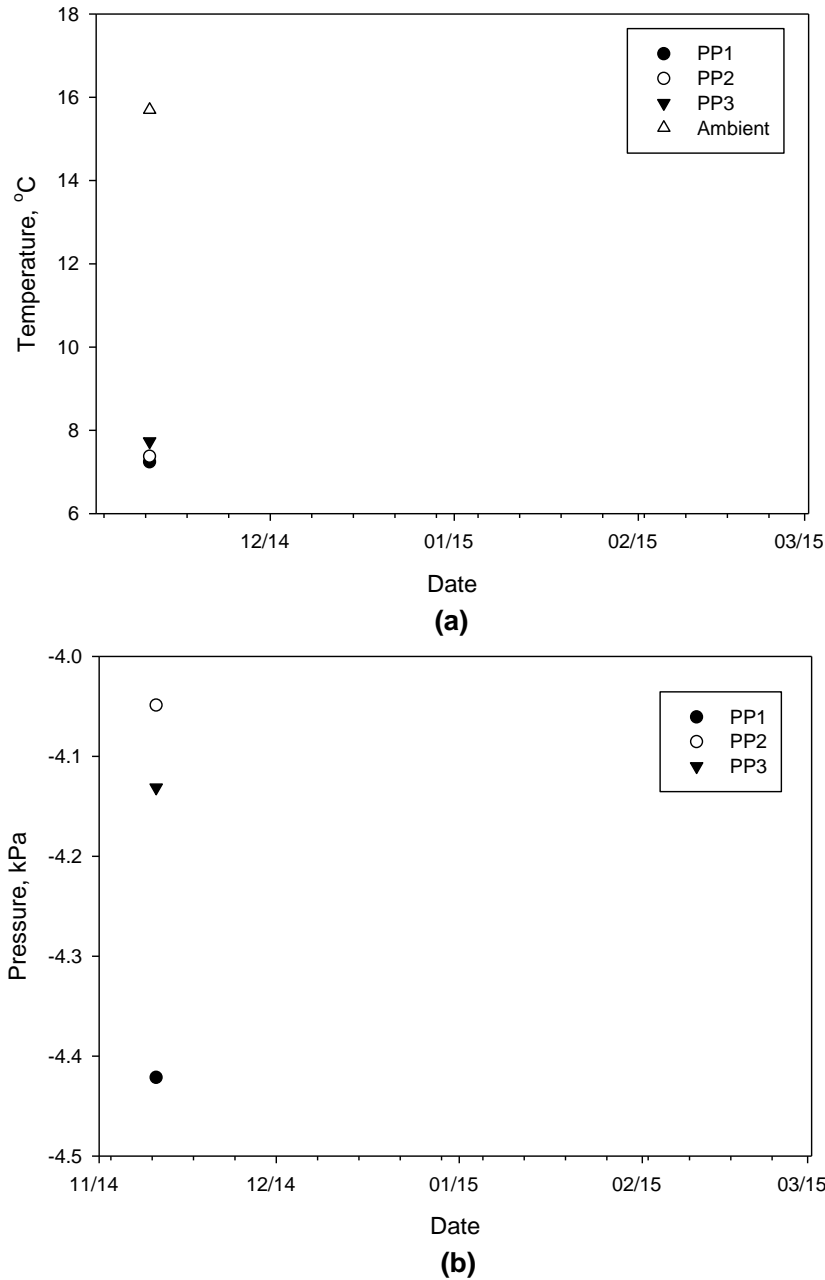
Figure 142. PP readings from Badger Road Bridge: (a) pore water pressure readings with time, and (b) ambient and PP temperature readings with time

The measured lateral stresses with depth in comparison with theoretical Rankine active and passive earth pressures and Coulomb passive earth pressures are presented in Figure 113. The theoretical values were calculated using $\phi' = 30.1°$ from laboratory direct shear testing, and wall friction $\delta = 2/3 \; \phi'$ (for Coulomb passive pressure calculations) and assuming a total unit weight

of 17.29 kN/m^3 (based on 95% standard Proctor maximum density and 8% moisture content). A surcharge load of 25.42 kPa calculated from the vertical EPC was used in the calculations to account for weight of backfill material above the top of the abutment and the weight of pavement and base layers. These theoretical values assume no pore pressures behind the wall, as considered in the design. Additional data is being collected and will be updated for the final report.
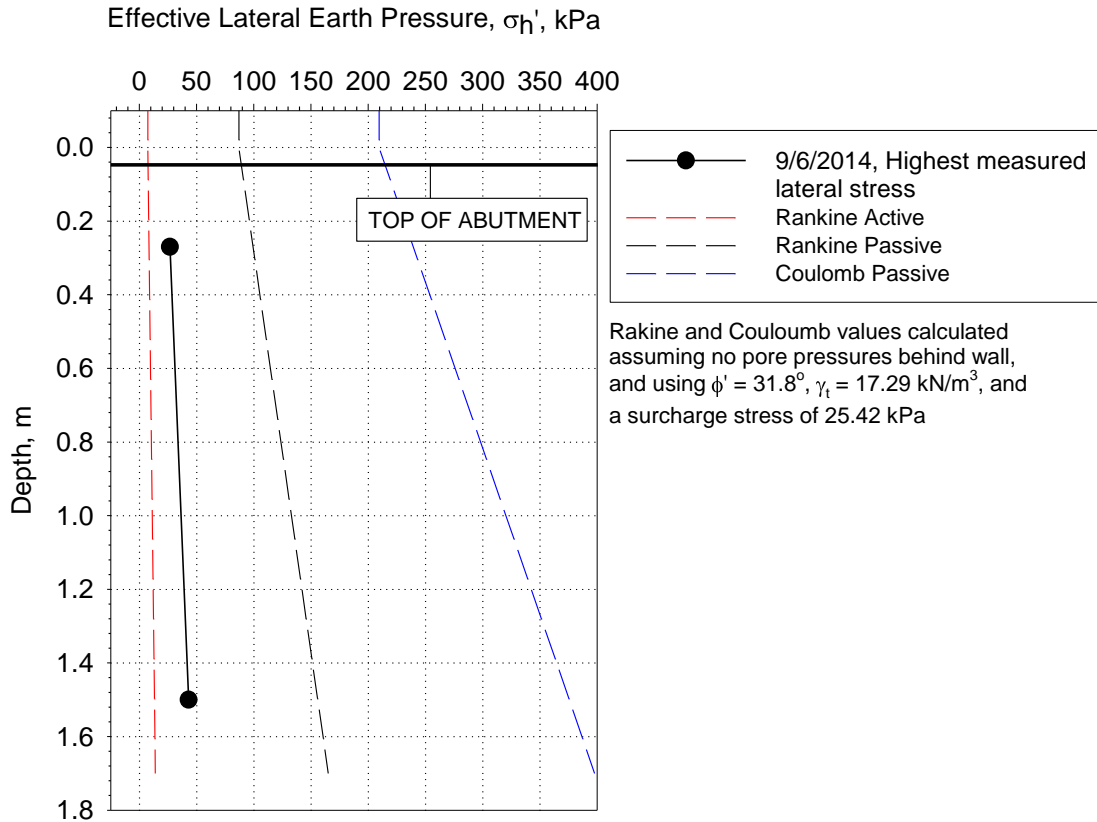
Figure 143. Measured and theoretical distribution of lateral earth pressures

Summary Key Findings

Key findings from field testing and observations are as follows:

- Backfill materials were placed at or near bulking moisture contents at three out of the four project sites.

- Lift thicknesses varied from about 200 mm (8 in) to 300 mm (12 in.) at the four sites and DCP testing at one bridge site indicated loose layers within the compacted backfill.

- At one of the bridge sites, it was observed that ponded water in the backfill excavation (because of rain occurred after the excavation) did not drain because of clogged sock around the perforated drain tile.

- The APT K_{sat} values varied from 0.08 to 0.8 cm/s and the CHP K_{sat} values from 0.005 to 0.1 cm/s, for the four backfill materials. The CHP results represent a larger volume of soil compared to the APT.

Key findings from in-ground instrumentation monitoring are as follows:

- Lateral earth pressure measurements indicated that the field condition is more complex than the simple linear stress distribution assumed for design. During summer months at one project site, lateral stresses near the top of the abutment were close to the Rankine passive pressure while at the bottom of the abutment lateral stresses were close to the Rankine active pressures.

- Over a majority of the monitoring period of this study, lateral stress measurements were greater than the values assumed in the design according to the Wisconsin DOT Bridge Manual.

- Pore pressure readings following a flooding period at one bridge site were used to determine that the abutment backfill was saturated to about its mid height and then drainage occurred over a period of 7 days.

- FEA was conducted using calibrated input parameters from the physical scaled abutment model were used to predict dissipation values in the field. Results from FEA compared well with the measured dissipation values in the field. The Casagrande and Shannon method, however, over-estimated the pore pressure dissipation times.

CHAPTER 6. CONCLUSIONS AND RECOMMENDATIONS

Key findings and conclusions from the detailed literature review conducted on this research topic, laboratory testing and analysis of bridge abutment backfill materials and alternative RAP and RAS materials, and field investigation of the drainage performance of the backfill materials, are presented below. Based on the findings from this research, recommendations are provided at the end of this chapter.

Literature Review

Poor water management has been documented in the literature as a major problem of erosion and damage around bridge abutments (Helwany et al. 2007; Jayawickrama et al. 2005; White et al. 2005). Drainage performance can be increased and erosion problems can be mitigated by compacting granular material at moisture contents wet of optimum, using coarser gradation materials, using geotextile around porous backfill to prevent fines infiltration, and/or using a geocomposite vertical drain (White et al. 2007b). This topic is of significant national interest.

Results documented in the literature on RAP and RAS recycled materials indicated that those materials exhibit severe creep behavior (Rathje et al. 2006; Soleimanbeigi et al. 2011). Some of the creep behavior can be mitigated by treating the materials with fly ash, but the permeability of the materials are reduced.

Construction specifications for bridge abutment backfill materials varied significantly among the 51 agencies reviewed (48 U.S. State DOTs and 3 Canadian Provinces). Key findings from this review are as follows:

- The maximum allowable fines content varied between 5% and 25%.
- Although most agencies specify a maximum allowable lift thickness, none of the agencies specify QC/QA for lift thickness control during construction. 35 out of the 51 agencies do not have QC/QA testing requirements for moisture or density control during backfill placement.
- Currently, 3 out of the 51 agencies reviewed recommend flooding or wet of optimum conditions during backfill placement and compaction as a method to avoid post-construction backfill collapse.
- 39 agencies follow a standard drainage design of porous backfill around the drain tile. 20 agencies allow use of geosynthetic wrap around the porous backfill material, and 6

agencies allow use of geocomposite vertical drain design. 15 agencies use a combination of two or more of these design alternatives.

To the author's knowledge, only limited studies (Evans et al. 2012 and Gomez 2013) reported field assessment of drainage in terms of long-term monitoring of pore pressures in the backfill materials.

Laboratory Test Results and Analysis

Material Properties

Gradation analysis shows that some of tested backfill materials fall within the range of most erodible soils. The upper gradation limits of the current Wisconsin DOT backfill material specifications also fall within this range.

The permeability of the backfill materials collected varied from 0.0002 to 0.11 cm/s. Further, using empirical equations for estimate permeability can result in over-estimation of the permeability of the materials.

Laboratory compaction tests reveal a definable bulking moisture content range for natural materials whereby the density is low due to partially saturated conditions resulting in suction that inhibits compaction. Bulking moisture content was not evident for RAP and RAS materials. The implication of bulking moisture content is that the materials placed and compacted at or near that moisture content can exhibit collapse upon wetting. Laboratory collapse tests on the backfill materials showed vertical strains ranging between < 0.2% and 4%, when compacted at bulking moisture contents.

RAP and RAS produced vertical strains of about 4% to 5% under constant loading. These vertical strains are not believed to be related to the partially saturated bulking condition, but rather an indication of the composition of the materials. For reference a 1% collapse on a 3 m (10 ft) of backfill l can lead to about 30 mm (> 1 in.) of settlement. Therefore, any post-construction settlement related to collapse can be problematic and should be avoided.

Direct shear tests indicated drained friction angles of the four bridge site backfill materials ranging between 27 and 33 degrees, with apparent cohesion ranging between 4 and 12 kPa (0.6 and 1.7 psi). RAP and RAS materials exhibited significant secondary compression or creep with increasing shear stresses even after 15% horizontal strain.

Scaled Abutment Model Testing and Numerical Analysis

One-fourth scaled abutment model was used to calibrate the FEM input parameters, by measuring pore pressure dissipation during free drainage tests. The FEA results demonstrated that numerical analysis can be used to predict pore pressure dissipation rates with high accuracy (drainage times ± few minutes), provided the input parameters are properly calibrated through laboratory testing. The main input parameters that needed calibration were coefficient of volume compressibility m_v, and soil suction curve fitting parameters *a,* and *m*. For comparison a simple analytical solution proposed by Casagrande and Shannon was evaluated to predict pore pressure dissipation times, but the method was found to be very sensitive to the shape factor values used in the calculations, but can be determined from laboratory testing.

The bridge abutment model tests were used to calibrate the FEM parameters revealed that that the drainage times to achieve 95% drainage varied between 28 minutes and 3 hours for three materials (two obtained from bridge sites and RAP). On one of the backfill materials obtained from the bridge sites, fine particles eroded through the drain tile sock during free drainage causing clogging and only 60% of pore pressure dissipation at 24 hours. Erosion occurred because the material contained 99% passing the No. 40 sieve, and the drain tile sock had an aperture opening size of No. 40 sieve. By adding a geocomposite vertical drain along the face of the wall for this material, nearly 100% of drainage occurred within 10 minutes without any erosion.

Results indicated that as the permeability of the backfill material increased the pore pressure dissipation rates increased. A statistical significant correlation between the various gradation parameters and dissipation times was not evident for the data obtained from this study.

<div align="center">

Field Test Results and Analysis

</div>

Field Test Results and Observations

- Backfill materials were placed at or near bulking moisture contents at three out of the four project sites.
- Lift thicknesses varied from about 200 mm (8 in) to 300 mm (12 in.) at the four sites and DCP testing at one bridge site indicated loose layers within the compacted backfill.

- At one of the bridge sites, it was observed that ponded water in the backfill excavation (because of rain occurred after the excavation) did not drain because of clogged sock around the perforated drain tile.

- The APT K_{sat} values varied from 0.08 to 0.8 cm/s and the CHP K_{sat} values from 0.005 to 0.1 cm/s, for the four backfill materials. The CHP results represent a larger volume of soil compared to the APT.

Lateral Loads behind Abutment Wall

- Lateral earth pressure measurements indicated that the field condition is more complex than the simple linear stress distribution assumed for design. During summer months at one project site, lateral stresses near the top of the abutment were close to the Rankine passive pressure while at the bottom of the abutment lateral stresses were close to the Rankine active pressures.

- Over a majority of the monitoring period of this study, lateral stress measurements were greater than the values assumed in the design according to the Wisconsin DOT Bridge Manual.

- Pore pressure readings following a flooding period at one bridge site were used to determine that the abutment backfill was saturated to about its mid height and then drainage occurred over a period of 7 days.

- FEA was conducted using calibrated input parameters from the physical scaled abutment model were used to predict dissipation values in the field. Results from FEA compared well with the measured dissipation values in the field. The Casagrande and Shannon method, however, over-estimated the pore pressure dissipation times.

<div align="center">

Recommendations

</div>

Based on the findings from this research the following recommendations are made for material and construction specifications, QC/QA, drainage design, and abutment design:

- To improve drainage performance, material erosion and post-construction wetting-induced collapse should be minimized ad materials with higher permeability characteristics must be selected. The particle size limits of the structure backfill and grade 1 granular backfill should be modified by limiting sand and silt size contents. Proposed gradation limits are summarized in Table 14.

- A drainage design that involves addition of an active geocomposite vertical drain system along the face of the wall along with geotextile wrapped around the drain tile is recommended. The vertical drainage system can substantially increase drainage times. Several state DOTs (e.g., KS, SD, VA, AZ, IL) have developed standard specifications for using geocomposite vertical drains behind abutment wall, which can be used as reference to develop specifications for WI.

- Addition of QC/QA guidelines to project specifications are suggested to better control lift thickness and backfill moisture. Based on the type of construction equipment observed on projects, it is suggested that the lift thicknesses should be limited to 150 mm (6 in.). Further, extensive wetting of the placed material is recommended to reduce post-construction wetting-induced collapse.

- Instrumentation monitoring results were obtained from two freeze-thaw periods at one of the sites, but limited data was obtained from the remaining four sites. It is recommended that these bridge sites be monitored for an additional 3 to -5 year period and the data be analyzed to assess the lateral stress and drainage performance of the abutments and backfill materials. This long-term study will provide an invaluable dataset that is virtually non-existent in the literature, particularly with monitoring pore pressures behind the abutment wall.

- Field demonstration projects comparing the performance of bridge abutment backfills with and without the proposed recommendations should be planned to adequately assess the long-term performance improvements and associated changes in construction costs.

- QC/QA testing and observation is recommended for new construction. The DCP device is recommended to measure the penetration resistance of the fill materials and determine lift thicknesses and uniformity. The APT device is recommended as a rapid method for in situ permeability. Field observations should include material placement conditions and construction equipment used.

- RAP and RAS materials exhibited collapse upon wetting and creep under constant applied load in the laboratory. These can result unwanted post-construction settlements in the backfill material and therefore are not recommended for use as abutment backfill materials.

Table 14. Proposed gradation limits for bridge backfill materials in comparison with the existing WisDOT specifications

Sieve size	Section 210 Structure Backfill (% passing)	Section 209 Grade 1 Granular Backfill (% passing)	Proposed Limits
3"	100	—	100
No. 4	25-100	0-100	0-80
No. 40	—	0-75	0-15
No. 100	—	0-15	0-5
No. 200	0-3.75* 0-15*	0-8	0

Notes: — not specified, * percent passing is based on material passing No. 4 sieve (i.e., if percent passing No. 4 is 25%, the maximum percent passing No. 200 will be 3.75%; similarly, if percent passing No. 4 is 100%, the maximum percent passing No. 200 will be 15%)

REFERENCES

AASHTO (1993). *AASHTO Guide for Design of Pavement Structures 1993*, American Association of State Highway and Transportation Officials, Washington, D.C.

AASHTO (2012). *AASHTO LRFD Bridge Design Specifications*, American Association of State Highway and Transportation Officials, Washington, D.C.

Alabama Department of Transportation (2012). www.dot.state.al.us. Accessed May 2014.

Alaska Department of Transportation (2012). www.dot.state.ak.us. Accessed May 2014.

Alberta Ministry of Transportation (2014). www.transportation.alberta.ca. Accessed May 2014

Arizona Department of Transportation (2013). www.azdot.gov. Accessed May 2014.

Arkansas Department of Transportation (2007). www.arkansashighways.com Accessed May 2014.

ASTM. (2007a). "Standard Test Method for Particle-Size Analysis of Soils." *Annual book of ASTM standards*, ASTM D422, West Conshohocken, PA.

ASTM. (2007b). "Standard Test Methods for Laboratory Compaction Characteristics of Soil Using Standard Effort (12400 ft-lb/ft^3 (600 kN-m/m^3))." *Annual book of ASTM standards*, ASTM D698, West Conshohocken, PA.

ASTM. (2007c). "Standard Test Methods for Maximum Index Density and Unit Weight of Soils Using a Vibratory Table." *Annual book of ASTM standards*, ASTM D4253, Conshohocken, PA.

Abu-Hejleh, N., Hanneman, D., White, D. J., and Wang, T. l. K., I. (2006). "Flow fill and MSE Bridge Approaches Performance, Cost, and Recommendations for Improvements." Colorado Department of Transportation, Denver, CO.

Ardani, A. (1987). "Bridge Approach Settlement." Colorado Dept. of Highways, Denver.

Barker, K. J., and Carder, D. R. (2001). "Performance of an integral bridge over the M1-A1 link road at Branham Crossroads." TRL Report 521, UK.

Barksdale, R. D. (1996). *The Aggregate Handbook*, National Stone Association, Washington, D.C.

Briaud, J.-L. (2008). "Case Histories in Soil and Rock Erosion: Woodrow Wilson Bridge, Brazos River Meander, Normandy Cliffs, and New Orleans Levees." *Journal of Geotechnical and Geoenvironmental Engineering*, 134(10), 22.

Briaud, J.-L., Maher, S. F., and James, R. W. (1997). "Bump At the End of the Bridge." *Civil Engineering*, ASCE, 67(5), 68-69.

Broms, B. B., and Ingelson, I. (1971). "Earth Pressure against the Abutments of a Rigid Frame Bridge." *Geotechnique*, 21(1), 15-28.

California Department of Transportation (2014). www.dot.ca.gov. Accessed May 2014.

Caquot, A., and Kersiel, J. (1948). *Tables for the Calculation of Passive Pressure*, Gauthier-Villars, Paris.

Casagrande, A., and Shannon, W. L. (1952). "Base Course Drainage for Airport Pavements." *Transactions of the American Society of Civil Engineers*, 117(1), 22.

Cedergren, H. R. (1974). *Drainage of highway and airfield pavements*, Wiley, New York.

Cedergren, H. R. (1994). "America's Pavements: World's Longest Bathtubs." *Civil Engineering*, ASCE, 64(9), 56-58.

Civjan, S., Brena, S. F., Butler, D. A., and Crovo, D. S. (2004). "Field Monitoring of Integral Abutment Bridge in Massachusetts." *Transportation Research Record*, 1892(1), 9.

Colorado Department of Transportation (2012). www.coloradodot.info. Accessed May 2014.

Connecticut Department of Transportation (2014). www.ct.gov/dot/site. Accessed May 2014.

Darley, P., Carder, D. R., and Barker, K. J. (1998). "Seasonal thermal effects over three years on the shallow abutment of an integral bridge in Glasgow." TRL Report 344, UK.

Das, B. (2010). *Principals of Geotechnical Engineering*, Cengage Learning, Stamford, CT.

Das, B. M. (1990). *Principles of Geotechnical Engineering*, PWS-KENT Publishing Compacny, Boston.

Delaware Department of Transportation (2013). www.deldot.gov. Accessed May 2014.

Duncan, J., and Mokwa, R. (2001). "Passive Earth Pressures: Theories and Tests." *Journal of Geotechnical and Geoenvironmental Engineering*, 127(3), 9.

Elgaaly, M., Sandford, T. C., and Colby, C. (1992). "Testing an integral steel frame Bridge." *Transportation Research Record*, 1371, 7.

England, G., and Tsang, N. (2001). "Towards the design of soil loading for integral bridges." Concrete Bridge Development Group, Cambridge, United Kingdom, 17.

Florida Department of Transportation (2014). www.dot.state.fl.us. Accessed May 2014.

Fredlund, D. G., Lam, L., and Barbour, S. L. (1987). "Transient seepage model for saturated-unsaturated soil systems - A geotechnical engineering approach", *Canadian Geotechnical Journal*, 24(4), 15.

Georgia Department of Transportation (2012). www.dot.ga.gov. Accessed May 2014.

Gomez, B., W. (2013). "Evaluation of Design Assumptions for Structural Backfill of Abutments and retaining Walls." Ph.D Dissertation, University of Vermont, Burlington, Vermont.

Hassiotis, S., Khodair, Y., and Wallace, L. F. "Data from full-scale testing of integral abutment bridge." *Proc., Transportation Research Board 84th Annual Meeting*, Transportation Research Board, Washington, D.C.

Hawaii Department of Transportation (2014). www.hidot.hawaii.gov. Accessed May 2014.

Hazen, A. (1930). "Water Supply." American Civil Engineering Handbook, Wiley, New York.

Helwany, S., Koutnik, T. E., and Ghorbanpoor, A. (2007). "Evaluation of Bridge Approach Settlement Mitigation Methods." WHRP Final Report 07-14, Wisconsin Department of Transportation, Madison, WI.

Horvath, J. (2005). "Integral-Abutment Bridges: A Complex Soil-Structure Interaction Challenge (ASCE)." *Geotechnical Engineering for Transportation Projects*, American Society of Civil Engineers, 460-469.

Huntley, S. A., and Valsangkar, A. J. (2013). "Field monitoring of earth pressures on integral bridge abutments." *Canadian Geotechnical Journal*, 50(8), 841-857.

Idaho Department of Transportation (2012). www.itd.idaho.gov. Accessed May 2014.

Illinois Department of Transportation (2014). www.dot.state.il.us. Accessed May 2014.

Indiana Department of Transportation (2013). www.in.gov/indot. Accessed May 2014.

Iowa Department of Transportation (2014). www.iowadot.gov/. Accessed May 2014.

Jayawickrama, P., Nash, P., Leaverton, M., and Mishra, D. (2005). "Water Intrusion in Base/Subgrade Materials at Bridge Ends." Texas Tech Uniersity, Austin, TX, 173.

Kansas Department of Transportation (2013). www.ksdot.org. Accessed May 2014.

Kenney, T. C., Lau, D., and Ofoegbu, G. I. (1984). "Permeability of compacted granular materials." *Canadian Geotechnical Journal*, 21(4), 3.

Kentucky Department of Transportation (2014). www.transportation.ky.gov. Accessed May 2014.

Louisiana Department of Transportation (2014). wwwsp.dotd.la.gov. Accessed May 2014.

Maine Department of Transportation (2014). www.maine.gov/mdot. Accessed May 2014.

Massachusetts Department of Transportation (2014). www.massdot.state.ma.us. Accessed May 2014.

Michigan Department of Transportation (2014). www.michigan.gov/mdot. Accessed May 2014.

Minnesota Department of Transportation (2013). www.dot.state.mn.us. Accessed May 2014.

Mississippi Department of Transportation (2014). www.mdot.ms.gov. Accessed May 2014.

Missouri Department of Transportation (2013). www.modot.org. Accessed May 2014.

Montana Department of Transportation (2014). www.mdt.mt.gov. Accessed May 2014.

Moulton, L. K. (1980). "Highway Subdrainage Design." Federal Highway Administration, Washington, D.C.

NAVFAC (1986). "Foundations and Earth Structures." Navy, ed., Naval Facilities Engineering Command, Alexandria, VA.

Nebraska Department of Transportation (2014). www.transportation.nebraska.gov. Accessed May 2014.

Nevada Department of Transportation (2014). www.nevadadot.com. Accessed May 2014.

New Hampshire Department of Transportation (2014). www.nh.gov/dot. Accessed May 2014.

New Jersey Department of Transportation (2013). www.state.nj.us/transportation. Accessed May 2014.

New Mexico Department of Transportation (2012). www.dot.state.nm.us. Accessed May 2014.

New York Department of Transportation (2014). www.dot.ny.gov. Accessed May 2014.

North Carolina Department of Transportation (2012). www.ncdot.gov. Accessed May 2014.

North Dakota Department of Transportation (2010). www.dot.nd.gov. Accessed May 2014.

Nova Scotia Ministry of Transportation (2013). www.novascotia.ca/TRAN. Accessed May 2014.

Ohio Department of Transportation (2014). www.dot.state.oh.us. Accessed May 2014.

Oklahoma Department of Transportation (2014). www.okladot.state.ok.us. Accessed May 2014.

Oregon Department of Transportation (2014). www.oregon.gov/ODOT. Accessed May 2014.

Phares, B., White, D., Bigelow, J., Berns, M., and Zhang, J. (2011). "Identification and Evaluation of Pavement-Bridge Interface Ride Quality Improvement and Corrective Strategies." Report Number FHWA/OH-2011/1, Ohio Department of Transportation, Columbus, OH.

Puppala, A. J., Sireesh, S., Archeewa, L. R., and Nazarian, S. (2009). "Recommendations for Design, Construction, and Maintenance of Bridge Approach Slabs: Synthesis Report." The University of Texas at Arlington, Arlington, Texas, 186.

Rathje, E. M., Rauch, A. F., Trejo, D., Folliard, K. J., Viyanant, C., Esfellar, M., Jain, A., and Ogalla, M. (2006). "Evaluation of Crushed Concrete and Recycled Asphalt Pavement as Backfill for Mechanically Stabilized Earth Walls." University of Texas, Austin, TX, 182.

Rhode Island Department of Transportation (2014). www.tmc.dot.ri.gov. Accessed May 2014.

Richardson, N. D. (1997). "Drainability Characteristics of Granular Pavement Base Material." *Journal of Transportation Engineering*, 123(5), 7.

Evans, R., White, D.J., and Klaiber, W. (2012). "Modified Sheet Pile Abutments for Low-Volume Road Bridges," IHRB Project TR-568, Iowa Department of Transportation, Ames, IA.

Saskatchewan Department of Highways and Transportation (2013). ww.highways.gov.sk.ca/. Accessed May 2014.

Shahabi, A. A., Das, B. M., and Tarquin, A. J. "An Empirical Relation for Coefficient of Permeability of Sand." *Proc., Fourth Australia-New Zealand Conference on Geomechanics*, 54-57.

South Carolina Department of Transportation (2014). www.dot.state.sc.us. Accessed May 2014.

South Dakota Department of Transportation (2014). www.sddot.com. Accessed May 2014.

Soleimanbeigi, A., Edil, T., and Benson, C. (2011). "Recycled Asphalt Shingles Mixed with Granular Byproducts as Structural Fills." Student Project Report, University of Wisconsin System Solid Waste Research Program, Univeristy of Wisconsin, Madison, WI.

Soleimanbeigi, A., Edil, T., and Benson, C. (2013). "Evaluation of Fly Ash Stabilization of Recycled Asphalt Shingles for Use in Structural Fills." *Journal of Materials in Civil Engineering*, 25(1).

Taylor, D. W. (1948). *Fundamentals of Soil Mechanics*, Wiley, New York.

Tennessee Department of Transportation (2014). www.tdot.state.tn.us. Accessed May 2014.

Terzaghi, K. (1943). *Theoretical Soil Mechanics*, John Wiley and Sons, INC., New York.

Texas Department of Transportation (2014). www.txdot.gov. Accessed May 2014.

Utah Department of Transportation (2014). www.udot.utah.gov. Accessed May 2014.

Vennapusa, P. (2004). "Determination of the Optimum Base Characteristics for Pavements." MS Thesis, Iowa State University of Science and Technology, Ames, IA.

Vennapusa, P., White, D. J., Klaiber, F. W., Wang, S., and Gieselman, H. (2012). "Geosynthetic Reinforced Soil for Low-Volume Bridge Abutments." IHRB Project TR-621, Center for Earthworks Engineering Research, Ames, IA.

Virginia Department of Transportation (2014). www.virginiadot.org. Accessed May 2014.

Wahls, H. E. (1990). "Design and construction of bridge approaches." NCHRP Synthesis of Highway Practice 159, 51.

Washington Department of Transportation (2014). www.wsdot.wa.gov. Accessed May 2014.

White, D., Sritharan, S., Suleiman, M., Mekkawy, M., and Chetlur, S. (2005). "Identification of the Best Practices for Design, Construction, and Repair of Bridge Approaches." Center for Earthworks Engineering Research, Institute for Transportation, Ames, IA.

White, D. J., Mekkawy, M., Sritharan, S., and Suleiman, M. (2007). ""Underlying" Causes for Settlement of Bridge Approach Pavement Systems." *Journal of Performance of Constructed Facilities*, 21(4), 9.

White, D. J., Mekkawy, M. M., Suleiman, M. T., Sritharan, S., (2007). "Performance of collapsible bridge approach backfill with geosynthetic drainage and reinforcement." *Geosynthetics International*, 14(2), 12.

White, D. J., Vennapusa, P., and Zhao, L. (2013). "Verification and Repeatability Analysis for the In Situ Air Permeameter Test." *Geotechnical Testing Journal*, 37(2), 11.

WisDOT (2015). "Standard Specifications." Wisconsin Department of Transportatoin, Madison, WI.

WisDOT (2014). "WisDOT Bridge Manual." Wisconsin Department of Transportatoin, Madison, WI.

Wyoming Department of Transportation (2013). www.dot.state.wy.us. Accessed May 2014.

APPENDIX A. BRIDGE ABUTMENT DRAINAGE DESIGN AND SPECIFICATION REVIEW

This appendix shows tables with the results from the specification review.

Table 15. Specifications for underdrain systems

State/Province	Drainage Type	State/Province	Drainage Type
AK	a	NC	b
AL	a,b	ND	b
AR	a,b	NE	a
AZ	a,b,c	NH	a
CA	a	NJ	a
CO	b	NM	a
CT	a,b	NV	a
DE	a	NY	a
FL	a	OH	a
GA	a	OK	a
HI	b	OR	a,b,c
IA	a	RI	a
ID	b	SC	a
IL	a,c	SD	a,b,c
IN	a	TN	a,b
KS	c	TX	b
KY	a	UT	—
LA	a,b,c	VA	a,b,c
MA	a	WA	a
ME	a	WI	a,b
MI	a,b	WV	a
MN	b	WY	a
MO	a,b,c	Alberta	b
MS	a	Nova Scotia	—
MT	a	Saskatchewan	a

Note: Drainage types a, b, c are identified in Figure 11.

.

Table 16. Gradation specifications from different U.S. and Canadian agencies for bridge abutment granular backfill

State/Province	4"	3"	2"	1.5"	1"	0.75"	0.5"	.375"	# 4	# 8	# 10	#16	# 30	# 40	#50	# 100	# 200
AK	—	100	—	—	—	—	—	—	20-55	—	—	—	—	—	—	—	0-6
AL	—	—	—	100	95-100	—	25-60	—	0-10	0-5	—	—	—	—	—	—	—
AR	—	—	—	—	—	—	—	—	—	—	—	—	—	—	—	—	—
AZ	—	100	—	—	—	60-100	—	—	—	35-80	—	—	—	—	—	—	0-12
CA	—	100	100	—	—	—	—	—	—	—	—	—	—	—	0-100	0-8	0-4
CO	—	—	100	—	—	—	—	—	30-100	—	—	—	—	—	10-60	—	5-20
CT	—	—	—	—	—	—	—	—	—	—	—	—	—	—	30-100	—	0-10
DE	—	—	—	—	85-100	—	—	—	—	—	—	—	—	—	—	—	0-25
FL	—	—	—	—	—	—	—	—	—	—	—	—	—	—	—	—	0-15
GA	—	—	—	—	—	—	—	—	—	—	—	—	—	—	—	—	0-25
HI	—	100	—	—	—	—	—	—	20-75	—	—	—	—	—	—	—	0-15
IA	—	100	—	—	—	—	—	—	—	20-100	—	—	—	—	—	—	0-10
ID	—	—	—	—	—	—	—	—	30-100	—	—	—	—	—	—	—	0-5
IL	—	—	—	—	—	—	—	—	50-100	—	—	—	—	—	—	—	0-4
IN	—	—	90-100	—	—	—	—	—	20-70	—	—	—	—	—	—	—	0-8
KS	100	—	—	—	—	—	—	—	50-100	—	—	—	—	—	—	—	0-4
KY	100	—	—	—	—	—	—	—	0-30	—	—	—	—	—	—	—	0-5
LA	—	—	—	—	100	—	—	—	—	—	—	—	—	—	—	—	0-10
MA	—	—	—	—	—	—	50-85	—	40-75	—	—	—	—	—	—	8-28	0-10
ME	—	100	—	—	—	—	—	—	—	—	—	—	—	0-70	—	—	0-20
MI	—	100	—	—	60-100	—	—	—	—	—	—	—	—	50-100	—	0-30	0-7
MN	—	—	—	—	0-100	—	—	—	—	—	—	—	—	—	—	—	0-12
MO	100	—	—	—	—	—	—	—	—	—	—	—	—	0-60	—	—	0-10
MS	—	—	—	—	100	—	80-100	—	—	35-100	—	25-90	—	—	5-50	0-8	0-2
MT	—	—	100	—	—	—	—	—	20-40	—	—	—	—	—	—	—	0-8
NC	—	—	—	—	—	—	—	—	—	—	—	—	—	—	—	—	—
ND	—	—	—	—	100	80-98	60-85	30-65	—	—	5-20	—	—	0-6	—	0-3	—
NE	—	—	—	—	100	—	90-98	—	0-40	—	0-20	—	—	—	0-10	—	0-6
NH	—	100	—	—	—	—	—	—	70-100	—	—	—	—	—	—	—	0-12
NJ	AASHTO Classification A-1 or A-2-4																
NM	—	—	—	—	—	—	—	100	80-100	—	65-95	—	—	25-55	—	—	0-20
NV	—	100	—	—	—	—	—	—	35-100	—	—	20-100	—	—	—	—	0-12
NY	100	—	—	—	—	—	—	—	0-70	—	—	—	—	—	—	—	0-15
OH	—	—	—	—	—	—	—	—	—	—	—	—	—	—	—	—	0-20
OK	—	100	—	—	90-100	—	—	—	—	—	—	—	—	0-45	—	—	0-10
OR	—	—	—	—	—	—	—	—	—	—	—	—	—	—	—	—	—
RI	—	100	—	—	—	—	—	—	30-100	—	—	—	—	—	—	—	0-8
SC	—	—	100	—	—	—	—	—	30-50	—	—	—	—	—	—	—	0-12
SD	—	—	—	—	—	—	—	100	95-100	—	—	45-85	—	—	10-30	—	0-2

Table 16. Continued

State/Province	4"	3"	2"	1.5"	1"	0.75"	0.5"	.375"	# 4	# 8	# 10	#16	# 30	# 40	#50	# 100	# 200
TN	—	—	—	100	—	—	—	—	35-55	—	—	—	—	—	—	—	4-15
TX	Not Specified																
UT	—	—	—	100	95-100	—	25-60	—	0-10	—	—	—	—	—	—	—	0-5
VA	—	100	95-100	—	—	—	—	—	—	—	25-55	—	—	16-30	—	—	4-14
VT	—	—	—	—	—	—	—	—	—	—	—	—	—	—	—	—	0-6
WA	—	—	75-100	—	—	—	—	—	22-66	—	—	—	—	—	—	—	0-5
WI	—	100	—	—	—	—	—	—	25-100	—	—	—	—	—	—	—	0-15
WV	100	—	—	—	—	—	—	—	—	—	—	—	—	0-60	—	—	0-15
WY	—	—	100	—	—	—	—	—	0-50	—	—	—	0-35	—	—	0-10	0-4
Alberta	—	100	—	100	70-94	—	—	44-74	32-62	—	—	17-43	12-34	—	8-26	5-18	2-10
Nova Scotia	100	—	—	60-85	—	—	—	—	25-50	—	—	—	—	—	25-50	—	2-7
Saskatchewan	—	—	—	—	100	55-100	25-100	—	—	—	15-85	—	—	0-25	—	—	0-5

— not specified

Table 17. Lift thickness and compaction requirements for bridge abutment backfill materials by state/province

State/Province	Lift Thickness (in.)	Target Compaction (%)	Moisture Control	Reference Laboratory Test	Quality control/Quality Assurance
AK	8	95	± 2% of optimum moisture content	AASHTO T 180	—
AL	8	Compact as directed by the engineer	Moisture control not require	AASHTO T 99	—
AR	6	95	Place at near optimum moisture content	AASHTO T 99	AASHTO T 310
AZ	8	95	Place at optimum or near optimum for compaction.	AASHTO T 99	—
CA	9	95	Place material and add enough moisture to make compaction.	California Test 216	—
CO	6	95	Place material and add enough moisture to make compaction.	AASHTO T 180	—
CT	12	95	Place at optimum moisture content	AASHTO T 180	—
DE	8	95	± 2% of optimum moisture content	AASHTO T 99	AASHTO T 191/T 238/T 239
FL	6	100	—	AASHTO T 99	Yes, but no specific test is listed
GA	12	Compact to specification on the plans	Compact to specification on the plans	AASHTO T 99	—
HI	8	95	Moisten until compaction is met	AASHTO T 180	HDOT TM 1/TM 2/TM 3
IA	8	95	Place at optimum to +4% of optimum.	AASHTO T 99	—
ID	8	95	Compact backfill to meet compaction.	AASHTO T 99	AASHTO T 310
IL	8	95	Place material at optimum, if the material is wetter than optimum allow to dry and then place.	AASHTO T 99	AASHTO T 310
IN	8	95	Place at specified moisture, which usually falls below optimum.	AASHTO T 99	AASHTO T 191/T 310
KS	8	Specified in contract documents	Provide material with enough moisture to allow compaction		—
KY	6	95	Place at optimum moisture content.	AASHTO T 99	—
LA	9	Compacted by approved methods to the satisfaction of the engineer.	—	—	—
MA	—	—	—	—	—
ME	8	Each layer [must be] thoroughly compacted by use of approved compactors before successive layers are placed.	Add water when needed to meet target compaction percentage.	—	—
MI	6	100	Place material at below saturations as determined from One Point Cone Chart.	AASHTO T 99	—
MN	8	Compact backfill in accordance with 2105, "Excavation and Embankment," to the specified density for adjacent and overlying embankment construction as shown the plans.	—	AASHTO T 99	Yes, but no specific test is listed
MO	12	90	—	AASHTO T 99	—
MS	8	98	—	AASHTO T 99	—
MT	8	95	Place material at ± 2% of optimum moisture content.	AASHTO T 99	MT-212/313
NC	12	95	Add or remove moisture until compaction has been met	AASHTO T 99	—

Table 18. Continued

ND	12	Specified in Plans	Specified in Plans	—	—
NE	6	100	Add water when needed to meet target compaction percentage.	AASHTO T 99	—
NH	8	98	—	AASHTO T 99	AASHTO T 191/T 204/T 310
NJ	12	95	—	AASHTO T 99	AASHTO T 310
NM	8	95	Place at near optimum moisture content	AASHTO T 180	AASHTO T 310
NV	8	95	Add water when needed to meet target compaction percentage.	Nev. T101G	Nev. T102/T103
NY	6	95	Place material at water content that can achieve target compaction percentage.	AASHTO T 99	—
OH	8	Compact all embankment materials, except for rock and hard shale, in horizontal lifts to a dry density greater than the percentage of maximum dry density in Table 203.07-1.	Add water when needed to meet target compaction percentage.	AASHTO T-99	—
OK	6	95	—	AASHTO T 99	—
OR	6	100	-4% to +2% of optimum moisture content	AASHTO T 99	—
RI	12	95	—	AASHTO T 180	—
SC	8	95	—	SC-T-29	—
SD	6	97	Place material at ± 4% of optimum moisture content.	AASHTO T 99	—
TN	6	100	—	AASHTO T 99	Yes, but no specific test is listed
TX	8	Specified in Plans	Place material at moisture content needed to achieve compaction	—	—
UT	6	Specified in Plans	Specified in Plans	AASHTO T 99	—
VA	6	95	Place material at optimum moisture content to +2% of optimum moisture content.	VTM-12	—
WA	6	95	Place material at a moisture content no greater than +3% of optimum moisture content.	AASHTO T 99/ AASHTO T 180	AASHTO T 310
WI	8	Compact each layer, before placing the next layer, by using engineer approved rollers or portable mechanical or pneumatic tampers or vibrators.	—	—	—
WV	4	95	—	AASHTO T 99	Yes, but no specific test is listed
WY	8	Compact it to the same density as adjacent material.	—	—	—
Alberta	6	95	Place at optimum moisture content.	ASTM D698	—
Nova Scotia	12	98	Place at ± 2% of optimum moisture content.	ASTM D698	—
Saskatchewan	6	95	Place at optimum moisture content	ASTM D698	—

— not specified
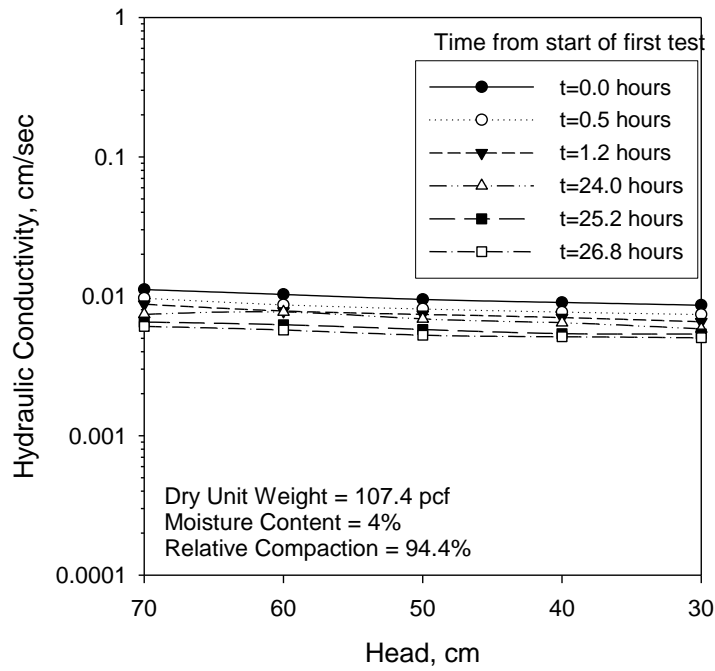
APPENDIX B. LABORATORY TEST RESULTS

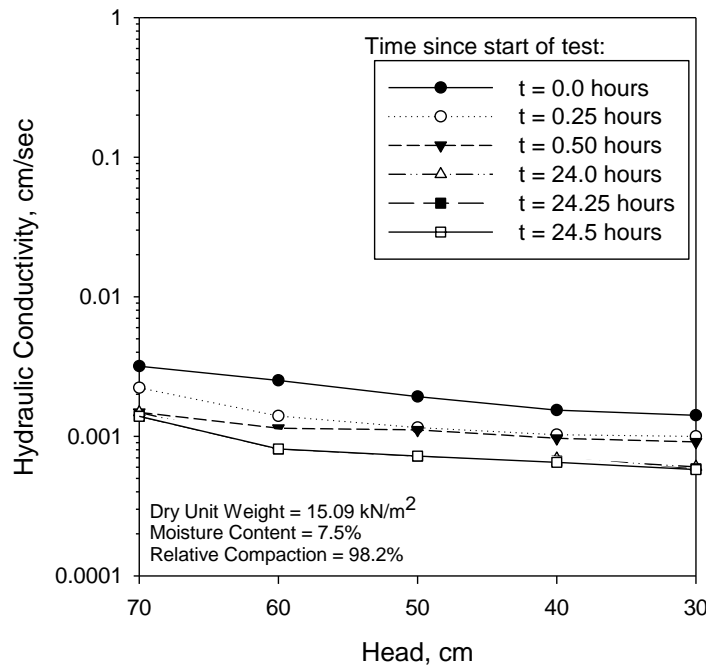**Figure 144. Falling head permeability results for Slovak Valley Creek Bridge backfill**

Figure 145. Falling head permeability results for Schwartz Road Bridge backfill
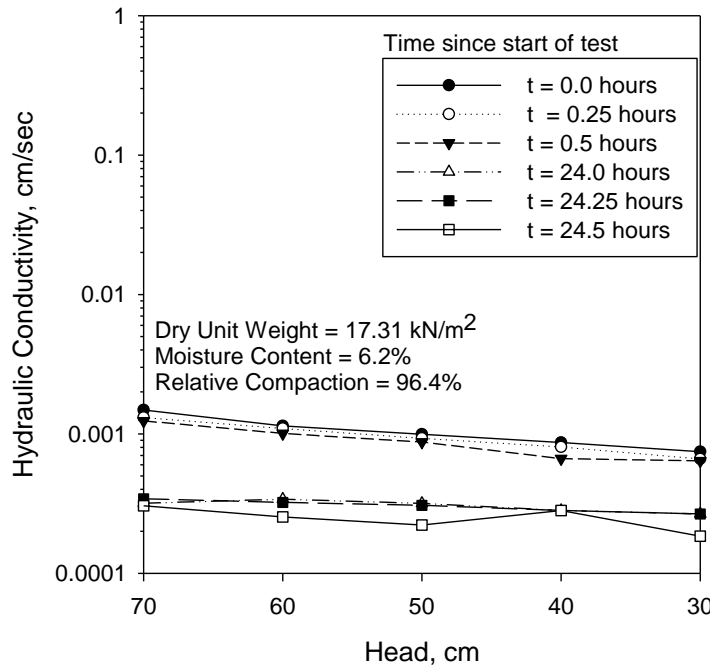
Figure 146. Falling head permeability results for Hobbles Creek Bridge backfill
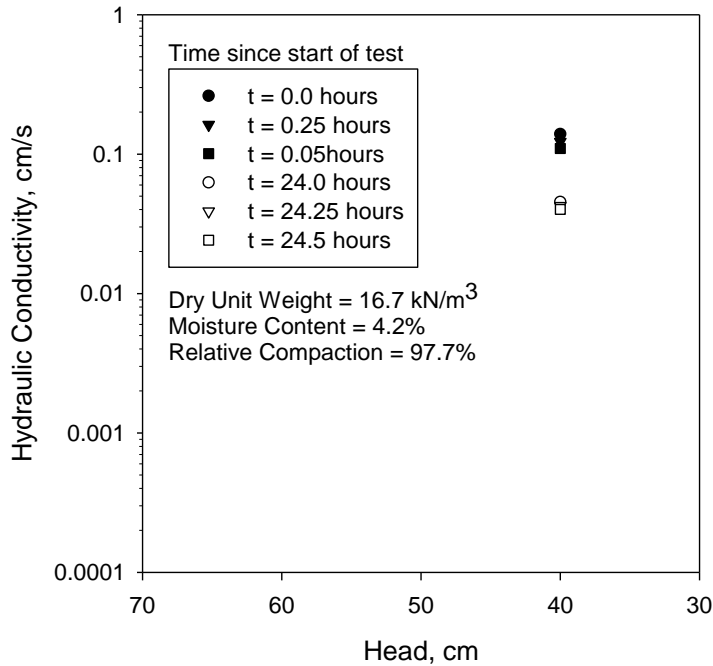
Figure 147. Falling head permeability results for Badger Road Bridge backfill

171

Figure 148. Falling head permeability results for RAP

Figure 149. Falling head permeability results for RAS

Figure 150. Direct shear results for Slovak Valley Creek Bridge backfill

Figure 151. Direct shear results for Schwartz Road Bridge backfill

Figure 152. Direct shear results for Hobbles Creek Bridge backfill

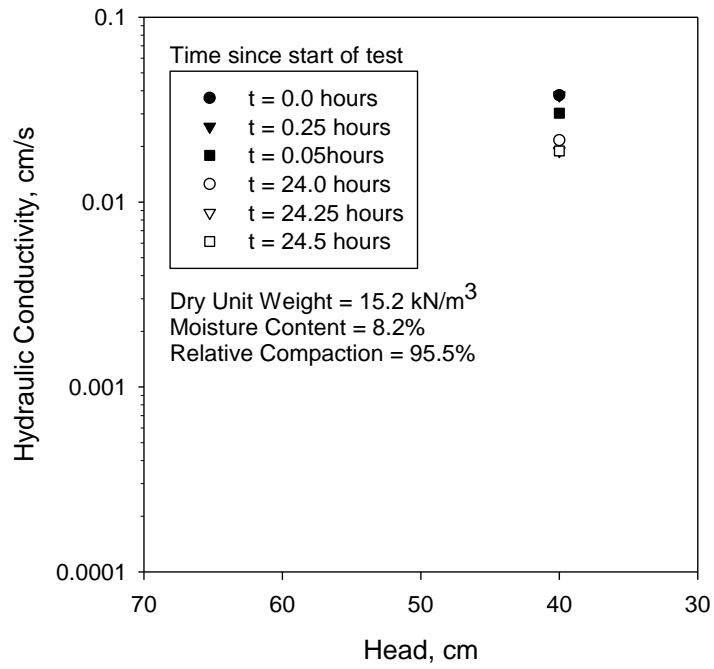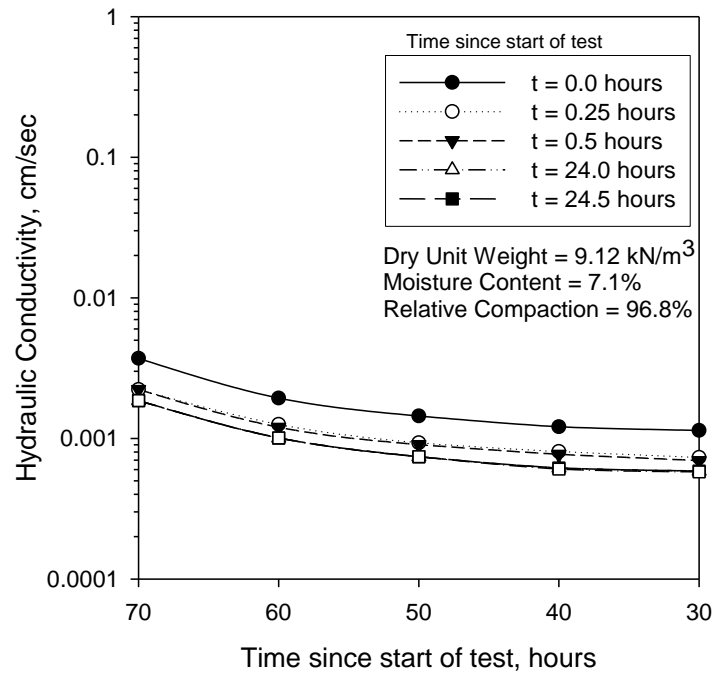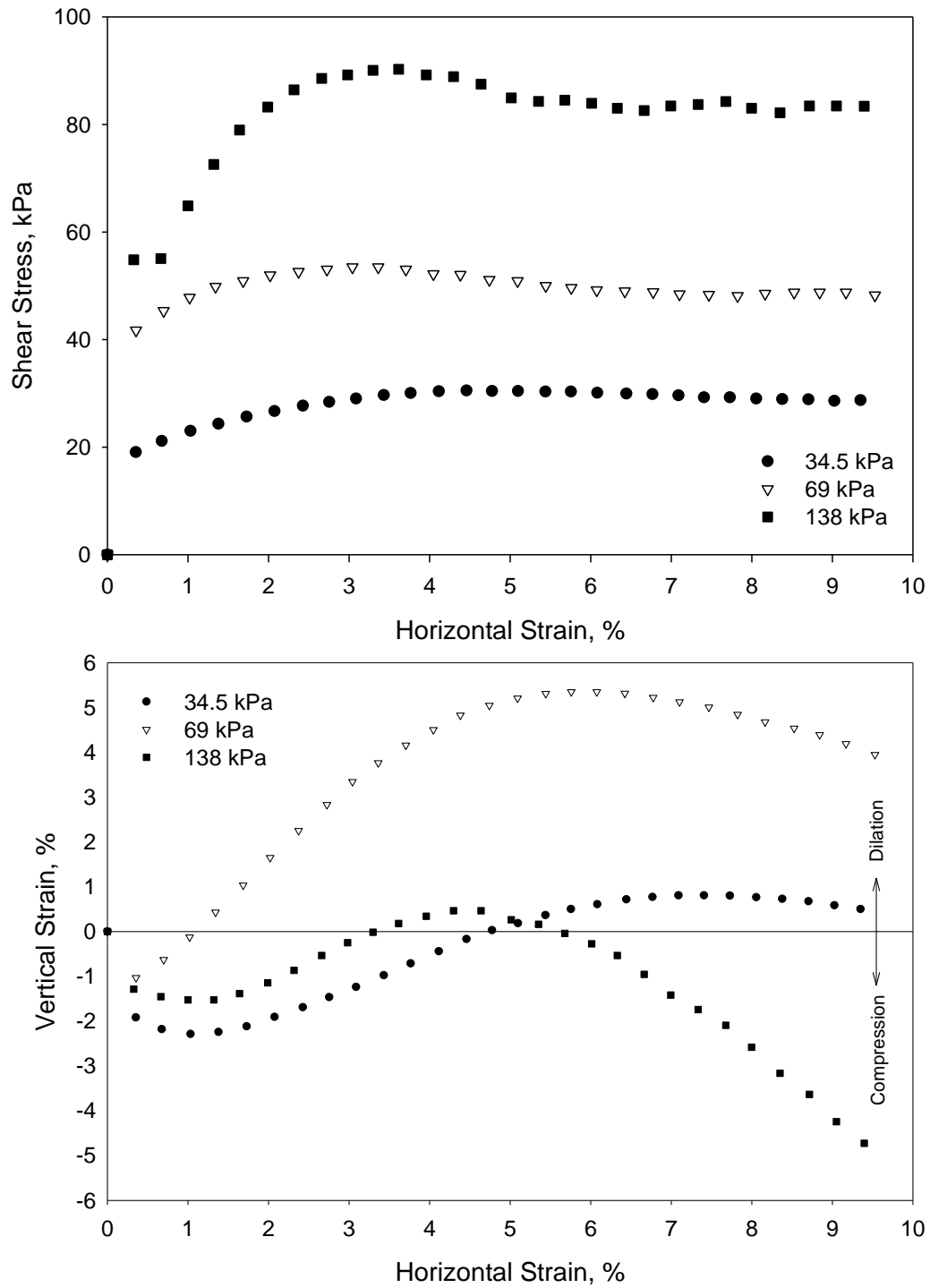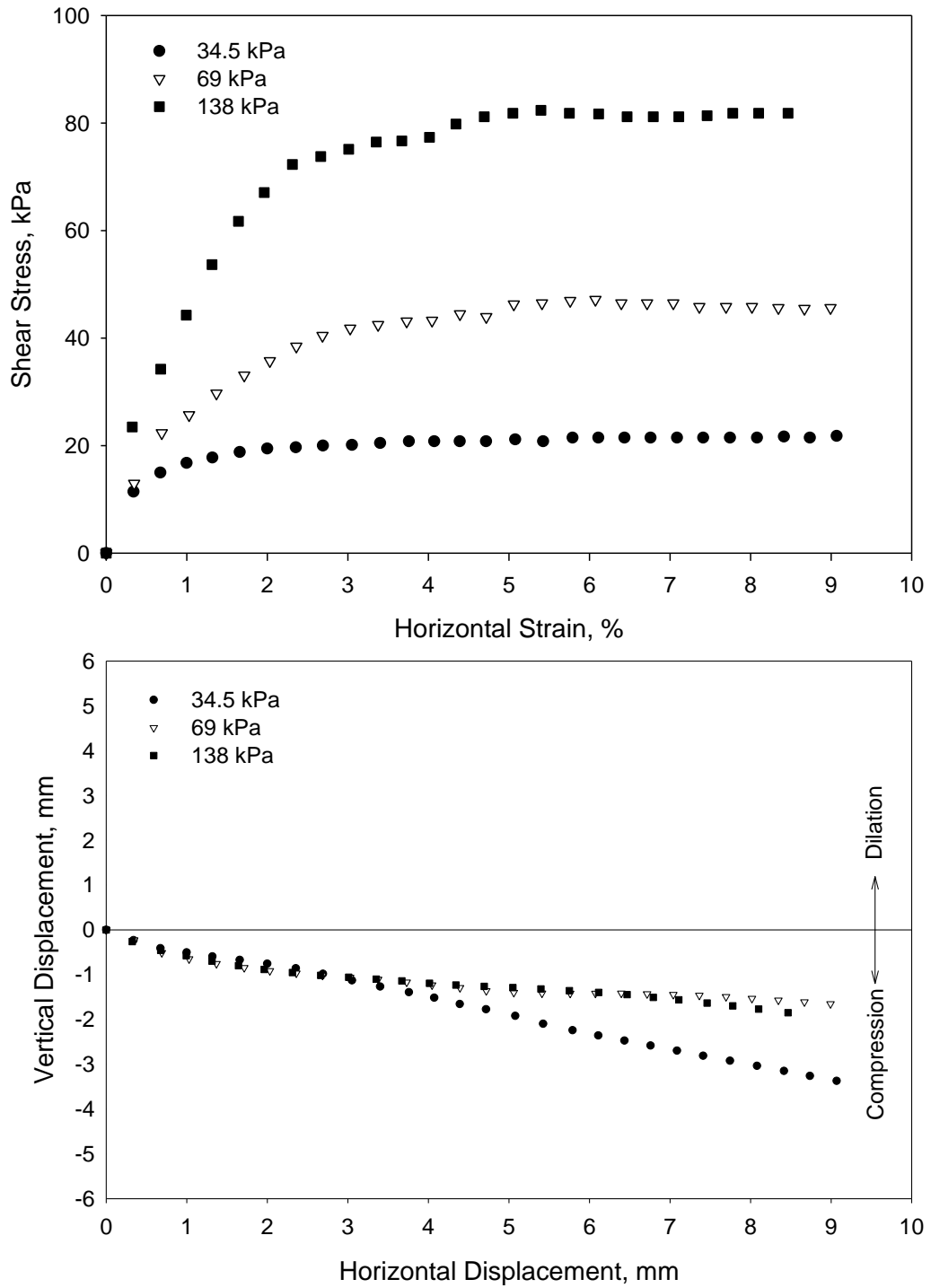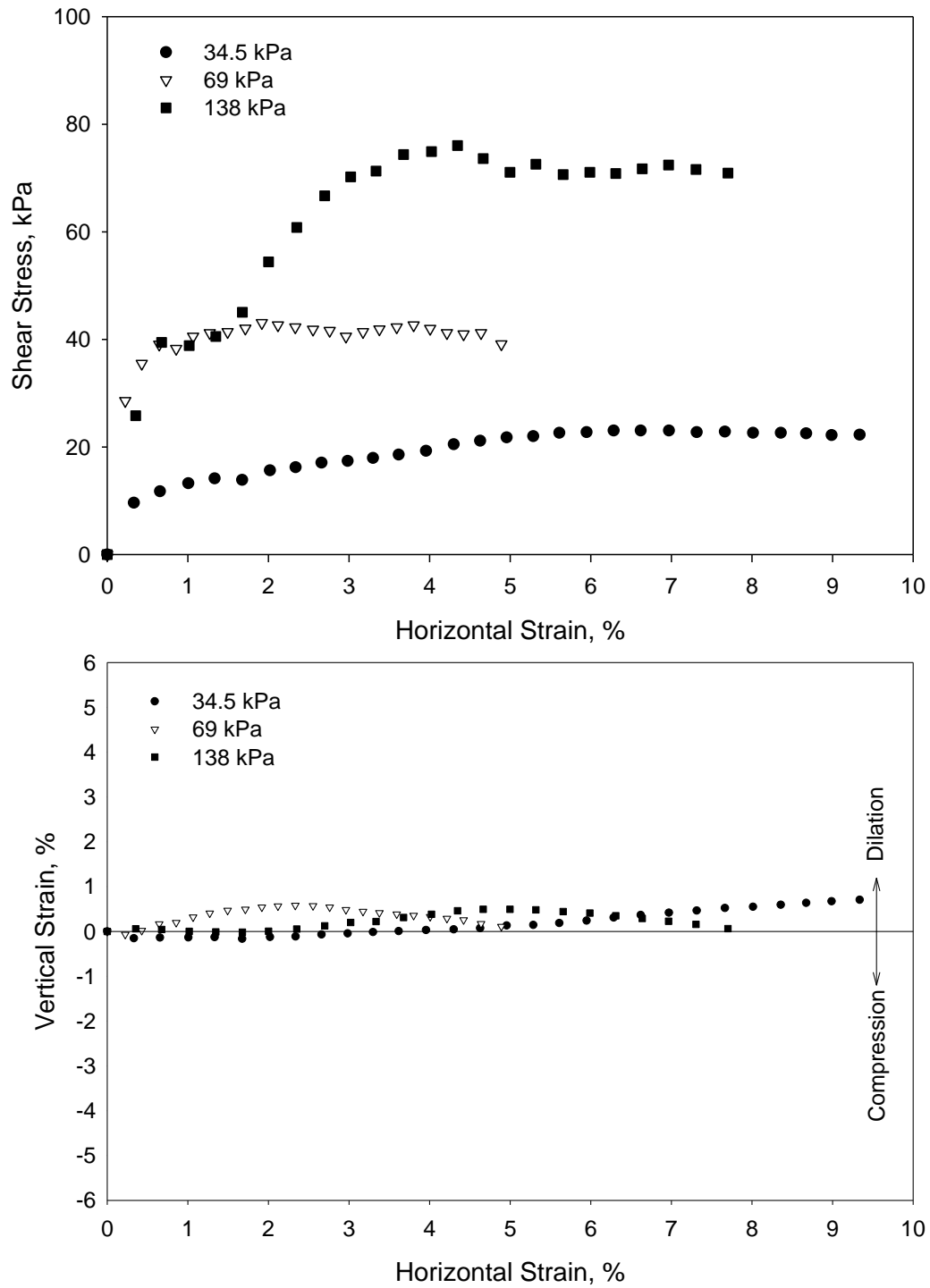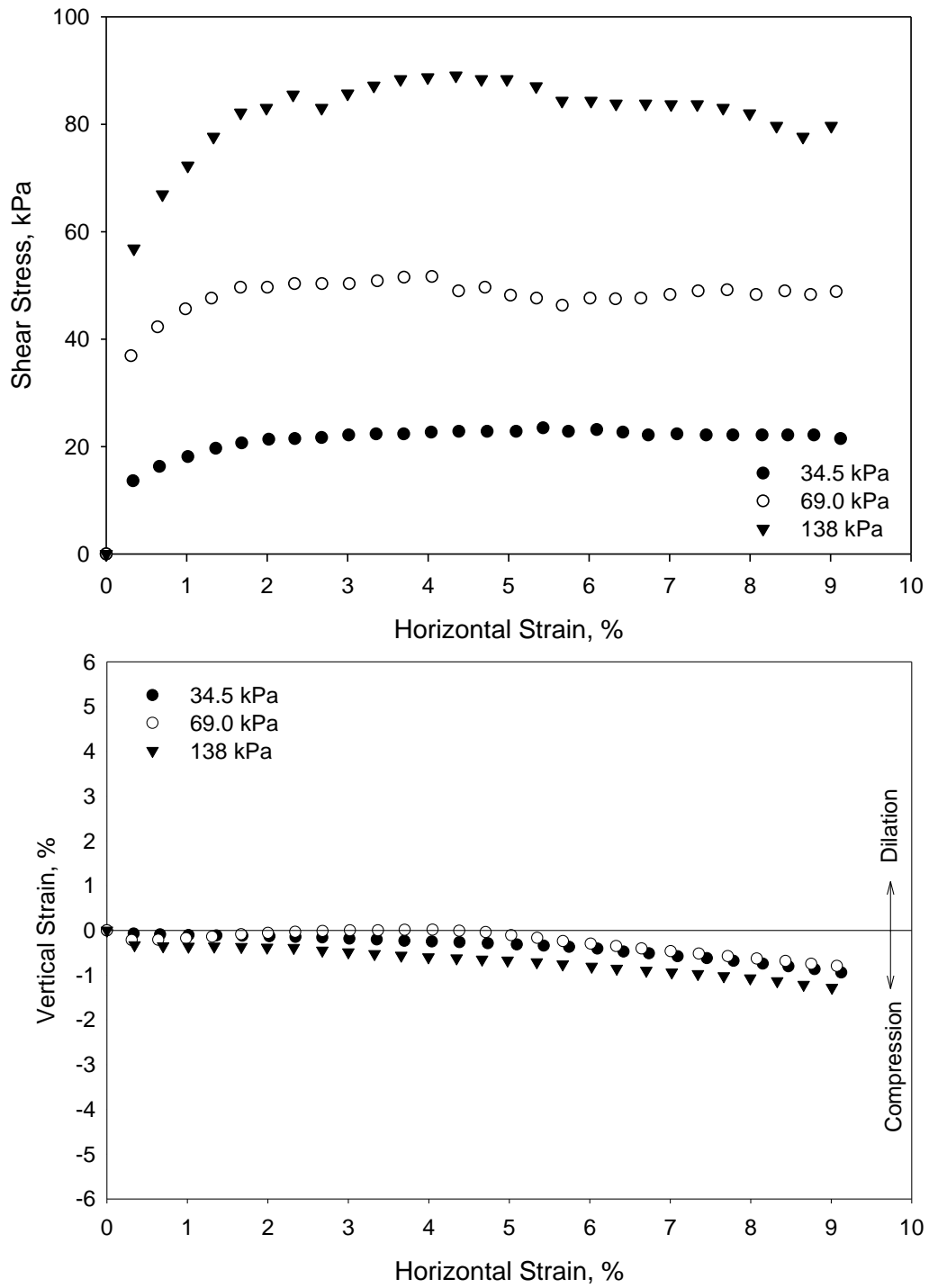**Figure 153. Direct shear results for Slovak Valley Creek Bridge backfill**

APPENDIX C. ROADRAIN T-5 SPECIFICATIONS

SYNTEC PRODUCT SPECIFICATION

SYNTEC, LLC
4800 Pulaski Highway
Baltimore, Maryland 21224 • USA
Phone: 410-327-1070 • Toll Free: 1-800-874-7437 Fax: 410-327-1078
www.synteccorp.com

SYNTEC
GEOSYNTHETICS EVOLVED

ROADRAIN T-5

ROADRAIN T-5 is a Synthetic Subsurface Drainage Layer (SSDL) comprised of a tri-planar structure with thermally bonded 6 oz. nonwoven geotextile filters on both sides. This product quickly removes subsurface water from pavement base and sub-base layers, while providing a void-maintaining system to work as a capillary break. ROADRAIN T-5 also works as a separation and base reinforcement layer. ROADRAIN T-5 has properties conforming to the values and test methods listed below:

PROPERTY	TEST METHODS	UNITS	VALUE	QUALIFIER
TRI-PLANAR CORE[1]				
Density	ASTM D 792	g/cm^3	0.94 – 0.96	Range
Melt Flow Index	ASTM D 1238	g/10 min	1.0	MAX
Carbon Black	ASTM D 4218	%	2-3	Range
Rib Spacing (top & bottom)	Callipered	inch (mm)	0.4 (10)	Typical
Central Rib Spacing	Callipered	inch (mm)	0.5 (12.5)	Typical
Unsupported Aperture Area	Callipered	inch^2 (mm$^{2)}$)	0.3 (195)	MAX
Thickness	ASTM D 5199	mil (mm)	280 (7.1)	±10 %
NONWOVEN GEOTEXTILE[1]				
Strength	AASHTO M 288	Exceeds Class 2		
U.V. Resistance (500 hrs)	ASTM D 4355	%	70	MARV
AOS	ASTM D 4751	US Std Sieve(mm)	70 (0.212)	MaxARV
Permittivity	ASTM D 4491	sec^{-1}	1.4	MARV
Water Flow Rate	ASTM D 4491	gpm/ft^2 (l/min/m^2)	110 (4481)	MARV
SSDL PERFORMANCE				
Capillary Barrier	ASTM 5918	Effective		Notes[2]
Coefficient of Permeability	ASTM D 4716	ft/day	56,700	Notes[3]
DIMENSIONS & FLOW ORIENTATION				
Roll Size	12.75 ft x 200 ft (3.89 m x 61 m)			
Direction of Primary Flow	Across the roll width @ approximately 45°			

Qualifiers: MARV=Minimum Average Roll Value (MARV), MAV=Minimum Average Value, MAX=Maximum Value, MaxARV=Maximum average roll value.

NOTES:
1. Geotextile and core properties listed are prior to lamination.
2. USACE Cold Regions Research and Engineering Laboratory (CRREL) "Freezing tests on lean clay with Tenax tri-planar geocomposite as capillary barrier"
3. Coefficient of permeability is calculated with the measured SSDL transmissivity and the nominal core thickness. SSDL transmissivity is tested along the primary flow direction with the boundary conditions as follows: steel plate/Ottawa sand/SSDL/Ottawa sand/steel plate, 1 hour seating period @ 5,000psf and gradient 2%.

APPENDIX D. LABORATORY/FIELD TEST RESULTS SUMMARY

Table 19. Laboratory and field parameters and drainage times from field, abutment model, and numerical analysis

Property	Parameter	Slovak Valley Creek Bridge	Schwartz Road Bridge		Hobbles Creek Bridge	Badger Road Bridge	RAP	Modified RAS
Gradation	D_{10}, mm	0.241	0.105		0.177	0.250	0.705	0.161
	D_{30}, mm	0.405	0.150		0.478	0.367	2.689	0.436
	D_{60}, mm	0.585	0.192		1.721	0.595	5.963	1.175
	D_{90}, mm	0.706	0.258		8.193	4.033	10.809	5.542
	D_{100}, mm	25.4	9.525		25.4	9.525	25.4	25.4
	P_{200}, %	2.2	7.3		6.4	0.7	5.8	2.5
	C_u	2.92	1.83		9.71	0.9	8.45	7.29
	C_c	0.96	1.11		0.75	2.38	1.72	1.00
	USCS	SP	SP-SM		SP-SM	SP	GW-GM	SW
	AASHTO Classification	A-1-b	A-3		A-1-b	A-1-b	A-1-a	A-1-b
Collapse	w_B*, %	3 - 4.1	9.3		1.8 - 3.9	1.9 – 3.6	—	—
	Collapse, I_c, %#	0.13 – 0.76	0.05 - 0.10		2.07 - 3.53	0.03 - 0.13	3.77 - 4.30	4.28 - 5.20
	Collapse Classification (ASTM D5333)	Slight	Moderate		Slight	Slight	Slight to Moderate	Moderate
Permeability	CHP, K_{sat}, cm/s (lab)	0.07	0.04	0.18	0.0004	0.07	1.22	—
	CHP, K_{sat}, cm/s (field)	0.1	—	—	0.005	0.06	—	—
	APT, K_{sat}, cm/s (lab)	0.57	0.54	0.57	—	0.74	10.2	—
	APT, K_{sat}, cm/s (field)	0.8	0.1-0.16	—	0.08	0.5	—	—
Drainage Times	t_{50}	<2 s[a] <2 s[b]	6 min[a] < 2 min[b]	14 s[a] <2 s[b]	—	< 2 s[a] < 2 s[b]	< 1 s[a] < 1 s[b]	—
	t_{95}	3 h[a] 3 h[b]		2 min[a] 1 min[b]	—	57 min[a] 43 min[b]	42 min[a] 28 min[b]	—
	t_{50}	25.8 h[c] 57.2 h[d] 39.0 h[e]	—		—	—	—	—
	t_{85}	148 h[a] 153 h[b] 111 h[c]	—		—	—	—	—

Note: shaded region with vertical geocomposite drain
— no value or not obtained
* = range indicate by standard Proctor and vibratory compaction test
# = range depending on overburden stress
a = abutment model

b = abutment model numerical analysis
c = In situ drainage
d = in situ numerical analysis with impermeable layers
e = in situ numerical analysis with permeable layers